A Posteriori Finite Element Bounds for Linear-Functional Outputs of Coercive Partial Differential Equations and of the Stokes Problem

by

Marius Paraschivoiu

B.S., Mechanical Engineering, École Polytechnique de Montréal (1991)
M.S., Mechanical Engineering, École Polytechnique de Montréal (1993)

Submitted to the Department of Mechanical Engineering
in partial fulfillment of the requirements for the degree of

Doctor of Philosophy

at the

MASSACHUSETTS INSTITUTE OF TECHNOLOGY

October 1997
[February 1998]

Author .....
Department of Mechanical Engineering
October 1, 1997

Certified by .....
Anthony T. Patera
Professor of Mechanical Engineering
Thesis Supervisor

Accepted by .....
Ain A. Sonin
Chairman, Departmental Committee on Graduate Students

A Posteriori Finite Element Bounds for Linear-Functional Outputs of Coercive Partial Differential Equations and of the Stokes Problem

by

Marius Paraschivoiu

Submitted to the Department of Mechanical Engineering
on October 1, 1997, in partial fulfillment of the
requirements for the degree of
Doctor of Philosophy

Abstract

Simulation–based engineering design and optimization are premised upon the accurate prediction of performance metrics such as flowrate, heat flux, and drag and lift forces. These metrics, which we will term "outputs," are functionals of the underlying field variables, such as velocity, temperature and pressure. We consider here the situation in which these functionals are linear, which includes many cases of practical interest.

There are two main problems that limit the use of simulations in engineering design: first, each appeal to the simulation is very expensive, which hinders interactivity in design; and second, evaluation of the reliability of the outputs is often unavailable, which precludes confident use of simulations in design. In this thesis we address these drawbacks in a new procedure focused on increasing the speed and reliability of simulation–based engineering design. The method exploits a fast "H–discretization" to compute bounds to the outputs that would have been obtained on a very fine mesh termed the "truth" mesh. These bounds inexpensively provide the desired assurance about the numerical error in the output.

The method is based upon the construction of an augmented Lagrangian, in which the objective is a quadratic "energy" reformulation of the desired output, and the constraints are the finite element equilibrium equations and the intersubdomain continuity requirements. Rigorous bounds are then obtained by application of quadratic–linear duality theory, in which the candidate Lagrange multipliers are obtained from the inexpensive H–discretization. The only computations required on the "truth" mesh are subdomain–decoupled symmetric local Neumann problems, which are very inexpensive to invert.

This technique is illustrated for the convection–diffusion equation both in one and two space dimensions. Outputs such as the flux, the pointwise value, and the average over a region are considered. Extension to the incompressible Stokes equations is then presented; for this problem, bounds for the lift force on an immersed body are calculated. The results indicate that this technique offers rigorous, quantitative, inexpensive, and relatively sharp bounds for "truth"–mesh engineering outputs, and thus provides for a fast and reliable design framework. Limitations and future work are briefly described.

Thesis Supervisor: Anthony T. Patera
Title: Professor of Mechanical Engineering

à Chantal
pour les années passées et pour celles a venir

à mes parents
Angela et Ion
pour leur encouragement

Acknowledgments

I want to extend my deepest gratitude to Professor Anthony T. Patera for his guidance, support and encouragement throughout my work at MIT. His unlimited energy and availability, along with his wisdom, will be warmly remembered.

I am also grateful to Professor Jaime Peraire, of the Department of Aeronautics and Astronautics of MIT, for his support and many useful discussions.

This work was supported by DARPA and ONR under Grant N00014-91-J-1889, AFOSR under Grant F49620-910052, NASA Langley Research Center under Grant NAG 1-1613 and NASA Lewis Research Center under Grant NCC 3-438.

I want to acknowledge Quebec's founding agency FCAR, *le Fonds pour la Formation de Chercheurs et l'Aide à la Recherche*, for the Aeronautical Fellowship that financially supported my studies at MIT for three years.

I want to thank my fiance Chantal Benoit–Barné for her love, support and understanding. This thesis is dedicated to her.

I am also grateful to Dr. Serhat Yeşilyurt, John Otto, Nicholas Hadjiconstantinou, Miltos Kambourides, and Jeremy Teichman for their assistance and their friendship.

I want to thank the students and the staff of the Fluid Mechanics Laboratory for providing me with a enjoyable working environment.

Contents

List of Figures

Chapter 1

Introduction

1.1 Motivation

A large variety of engineering and natural science applications, including fluid dynamics, thermodynamics and continuum mechanics, have benefited from numerical simulations. Over the past two decades, this field has evolved continuously, and has now reached a point where results are reasonably reliable for a wide range of conditions. It is important to understand that numerical simulations are not yet adequate to solve all problems and many improvements remain to be addressed. However, for an increasing number of problems, numerical simulations offer a relatively fast, flexible and inexpensive alternative to experiments.

As a result, computer simulations are becoming increasingly important as tools for engineering design and optimization, and much effort is spent to incorporate this technology in design. A design effort typically consists of exploring an input–output relationship between design variables and performance requirements (e.g., an objective function). In general, for one set of design variables, a numerical deterministic simulation obtains only one value of the objective function. This function serves to find the design variables that achieve a target performance; more commonly described as solving an optimization problem. It is important to understand that, in this context, the end goal of the numerical simulation is not the simulation but rather, to provide some quantitative information about some aspect of the simulation (termed outputs).

To fix ideas, drag and lift forces, flow rate, heat transfer, deformation, and stress may be the system outputs, s, of particular interest in pursuing design objectives. These system characteristics are typically functionals of field variables, $u(x)$, (velocity, temperature, and displacement) obtained from approximation schemes such as, in this thesis, the finite element method ($u_\delta \approx u(x)$). Note that the main parameter of an approximation method is the discretization size δ. For a given approximation space, the accuracy of the approximation of s, s_δ, is directly related to the discretization size. As we decrease the size of the

elements we increase the accuracy but we also increase the computation time. This latter increase is not linear for dimension spaces greater that one. The designer is then faced with a trade–off between accuracy and computational resources.

It is often the case, in addressing this trade–off, that engineering design is based upon a hierarchy of numerical approximations. The first discretization, characterized by an element size $\delta = H$, is a "working" coarse mesh approximation which is relatively inexpensive, but which generates solutions $u_H(x)$ and associated output $s_H(u_H)$ that are deemed sufficiently accurate for the purposes of "preliminary" analysis. The second discretization, characterized by element size $\delta = h(< H)$, is a "truth" mesh which produces a solution $u_h(x)$ and associated output $s_h(u_h)$ for which $|s_h - s|$ is assumed negligibly small. The h–discretization serves to verify the prediction of the H–discretization, either prior to design, as in a validated–surrogates framework [49], during design, as in the trust–region optimization techniques [6], or after design, as final confirmation of the anticipated performance. In any guise, validation or confirmation is a necessary precursor to the acceptance of numerical results as "admissible evidence" in the engineering design process, and must therefore provide predictive results for the particular output $s_h = \ell(u_h)$ of interest.

It is clear that the calculations on the "truth" mesh are very expensive and sometimes impossible to perform due to limited computational resources. The ideal situation in our validation or confirmation context would be to know (at very low cost) the value of the "truth" mesh output. Previous investigations [31, 5, 13], which measure the error in the energy norm, would not help us, as we are interested in the output. The *a priori* estimation applied to linear functionals only gives rough information about the convergence but does not provide a quantitative prediction of the "truth" mesh output. Therefore, at present, the choice the designer has is to be patient and run the expensive simulation — if resources permit — or qualify the error of the output based on experience or from heuristic or approximate arguments. In this thesis we address these shortcomings.

1.2 Objectives of this Thesis

Our goal is to develop a fast method to evaluate or approximate the "truth" mesh output and thereby provide the "truth" validation. The proposed technique should provide precise reliability information at a cost that does not overwhelm the output calculation cost on the "working" mesh. One approach to estimate the "truth" mesh output is to calculate rigorous, inexpensive and quantitative bounds to s_h.

In this thesis, we develop a method to construct precise bounds for s_h,

$$(s_h)_{LB}(H) \leq s_h \leq (s_h)_{UB}(H), \tag{1.1}$$

inexpensively. From the bounds (1.1) we can also derive a predictor for s_h,

$$(s_h)_{pre}(H) = \frac{1}{2}((s_h)_{LB}(H) + (s_h)_{UB}(H)), \tag{1.2}$$

which will satisfy

$$|(s_h)_{pre}(H) - s_h| \leq \Delta(H), \tag{1.3}$$

where

$$\Delta(H) = \frac{1}{2}|(s_h)_{LB}(H) + (s_h)_{UB}(H)|. \tag{1.4}$$

The final objective of this research is to obtain a technique to bound outputs of the Navier–Stokes equations. However, many specific points need to be addressed beforehand. At present, this technique is developed and illustrated for boundary values problems of second order, self-adjoint, linear coercive partial differential equations and for the classical Stokes problem. Among the vast variety of problems where these equations have been successfully applied, we think of applications in composite materials, phase transitions, optimal shape design, polyphased fluids, permeability of porous medias and low Reynolds number sedimentation [21, 26, 40]

In particular, the goals of this thesis are:

- The development in variational and algebraic formulation of our bound procedure for outputs of boundary value problem ODEs.
- The illustration of the performance of the bound procedure for output of ODEs such as pointvalue and flux outputs.
- The extension of the bound procedure to coercive elliptic PDEs with emphasis on different hybrid flux calculation approaches.
- The extension of the bounds procedure to the Stokes problem with illustration of the bounds for outputs such as the flowrate and lift force.
- Optimization of the bounds by the introduction of a scalarization procedure.

The remainder of the thesis is as follows. In Chapter 2 we review some of the key mathematical ingredients required for this work. In Chapter 3 we introduce our bound procedure for ODEs. We extend our bound procedure in Chapter 4 and Chapter 5, first, to the convection–diffusion problem in two space dimensions, second, to the Stokes problem. In Chapter 6, we examine different approaches to the hybrid flux approximation. In Chapter 7 we introduce the Optimal Stabilization Parameter to maximize out lower bound and to minimize our upper bound. Results for the convection–diffusion equation in one–dimension and two–dimensions, results for the Poisson problem for higher spatial discretization and results for the Stokes problem are presented in Chapter 8. To conclude, in Chapter 9, we

discuss some limitations of the present approach and future extensions needed to ultimately bound outputs of the Navier–Stokes equation. In addition, we prove in Appendix A that for some special outputs the lower bound is equal to the H–mesh solution. We call the latter situation *compliance*. In Appendix B we cover preliminary work for the bounds formulation of a nonuniform velocity field for the convection–diffusion equations. In Appendix C we describe the reference Crouzeix–Raviart elements.

Chapter 2

Mathematical Background

2.1 Hilbert Spaces

Hilbert spaces are of fundamental importance in studying elliptic boundary value problems as well as to understanding linear functionals. Therefore, we need to briefly introduced the basic concepts such as the definitions of the spaces, the associated norms, and some important theorems. For a complete description see [1, 34, 38].

Let Ω be an open subset of $\mathbf{R}^d$ with boundary Γ where d is the dimension of the problem of interest. We first define one special case of the Hilbert spaces; the Lebesgue space. The Hilbert spaces are themselves special cases of the Sobolev spaces. Let $L^2(\Omega)$ be the Lebesgue space defined as

$$L^2(\Omega) = \left\{ v | \int_\Omega v^2 \, \mathrm{d}A < \infty \right\}. \tag{2.1}$$

In words, Lebesgue space are the set of all functions $v(x)$ such as the integral of $v^2(x)$ over Ω is finite. Associated with this space we define the inner product as

$$(u, v)_{L^2} = (u, v) = \int_\Omega uv \, \mathrm{d}A, \tag{2.2}$$

and the norm as

$$\|u\|_{L^2(\Omega)} = \left(\int_\Omega u^2 \, \mathrm{d}x \right)^{\frac{1}{2}}. \tag{2.3}$$

The Hilbert space $\mathcal{H}^1(\Omega)$ of functions, for which both the derivatives and the functions are in $L^2(\Omega)$, is of particular interest in the variational context. We define this space by

$$\mathcal{H}^1(\Omega) = \left\{ v | \, v \in L^2(\Omega), \; D^1 v \in (L^2(\Omega))^d \right\}, \tag{2.4}$$

where

$$D^\alpha = \frac{\partial^{|\alpha|}}{\partial x_1^{\alpha_1} ... x_d^{\alpha_d}}, \; \alpha = (\alpha_1, ..., \alpha_d), \; |\alpha| = \sum_{i=1}^{d} \alpha_i, \; \alpha_i \geq 0, \text{ integers.} \tag{2.5}$$

The inner product for this space is

$$(u,v)_{\mathcal{H}^1} = \int_\Omega \frac{\partial u}{\partial x_i}\frac{\partial v}{\partial x_i} + uv \, \mathrm{d}A. \tag{2.6}$$

In (2.6) we use the Einstein summation convention, in which all repeated indices (here i) are summed from $i = 1, ..., d$. We also introduce the associated seminorm

$$|u|_{\mathcal{H}^1(\Omega)} = \left(\int_\Omega \frac{\partial u}{\partial x_i}\frac{\partial u}{\partial x_i} \ \mathrm{d}x \right)^{\frac{1}{2}}, \tag{2.7}$$

and the norm

$$\|u\|_{\mathcal{H}^1(\Omega)} = \left(\int_\Omega \frac{\partial u}{\partial x_i}\frac{\partial u}{\partial x_i} + u^2 \ \mathrm{d}x \right)^{\frac{1}{2}}. \tag{2.8}$$

Some important proofs also require the set of functions in $\mathcal{H}^1(\Omega)$ that vanish on the boundary of Ω, which we define as the space $\mathcal{H}_0^1(\Omega)$,

$$\mathcal{H}_0^1(\Omega) = \left\{ v | \, v \in \mathcal{H}^1(\Omega), \ v|_{\partial\Omega} = 0 \right\}. \tag{2.9}$$

An important result is derived for functions in this space. Here, we only state this result without proof: Functions $u \in \mathcal{H}_0^1(\Omega)$ are bounded by their derivatives functions,

$$\|u\|_{\mathcal{H}^1} \leq C_0 |u|_{\mathcal{H}^1}, \tag{2.10}$$

where C_0 (> 1) is independent of u. In addition, $|u|_{\mathcal{H}^1}$ and $\|u\|_{\mathcal{H}^1}$ are said to be equivalent if

$$|u|_{\mathcal{H}^1} \leq \|u\|_{\mathcal{H}^1} \leq C_0 |u|_{\mathcal{H}^1}, \qquad \forall u \in \mathcal{H}_0^1(\Omega). \tag{2.11}$$

Extending our earlier definitions, we introduce the general Hilbert spaces $\mathcal{H}^m(\Omega)$ defined for any integer $m(\geq 1)$ such that

$$\mathcal{H}^m(\Omega) \ \left\{ v | \, v \in L^2(\Omega), ..., D^m \in (L^2(\Omega))^d \right\}, \tag{2.12}$$

under the norm

$$\|u\|^2_{\mathcal{H}^m(\Omega)} = \sum_{0 \leq |\alpha| \leq m} \|D^\alpha u\|^2_{L^2(\Omega)}. \tag{2.13}$$

We now define a space, $\mathcal{H}^{-m}(\Omega)$, called the dual space of $\mathcal{H}^m(\Omega)$, consisting of all bounded linear functionals $\ell : \mathcal{H}^m(\Omega) \to \mathbf{R}$. For $\ell \in \mathcal{H}^{-m}(\Omega)$ the associated norm is given by

$$\|\ell\|_{\mathcal{H}^{-m}(\Omega)} = \sup \frac{\langle \ell, v \rangle}{\|v\|_{\mathcal{H}^m(\Omega)}}, \tag{2.14}$$

which is, by definition, finite. For a bounded linear functionals of functions in $\mathcal{H}^m(\Omega)$ there

exists a constant C such that $|\ell(v)| \leq C\|v\|_{\mathcal{H}^m}$, where $\|\cdot\|_{\mathcal{H}^m}$ is the norm associated with $\mathcal{H}^m$. We now generalize the L^2–inner product by defining the duality pairing associated with these spaces: For a functional $\ell \in \mathcal{H}^{-m}(\Omega)$ and a function $v \in \mathcal{H}^m(\Omega)$, we obtain

$$\ell(v) = \langle \ell, v \rangle_{\mathcal{H}^m}. \tag{2.15}$$

To illustrate the use of dual spaces we show that the delta–distribution δ_{x_0} is bounded in $\mathcal{H}^1(\Omega)$ for $\Omega \in \mathbf{R}^1$. We first write

$$v(x_0) = \int_0^{x_0} \frac{\mathrm{d}v}{\mathrm{d}x}\, \mathrm{d}x, \tag{2.16}$$

and evoking the Cauchy–Schwarz inequality we obtain

$$\begin{aligned} |v(x_0)| &= \left(\int_0^{x_0} (1)^2\, \mathrm{d}x\right)^{\frac{1}{2}} \left(\int_0^{x_0} \left(\frac{\mathrm{d}v}{\mathrm{d}x}\right)^2 \mathrm{d}x\right)^{\frac{1}{2}} && (2.17)\\ &\leq \left(\int_0^{1} \left(\frac{\mathrm{d}v}{\mathrm{d}x}\right)^2 \mathrm{d}x\right)^{\frac{1}{2}} && (2.18)\\ &\leq |v|_{\mathcal{H}^1} && (2.19)\\ &\leq \|v\|_{\mathcal{H}^1}. && (2.20) \end{aligned}$$

By definition, because $v(x_0)$ is bounded in $\mathcal{H}^1$, it follows that the delta–distribution is in $\mathcal{H}^{-1}$. Note that for $\Omega \in \mathbf{R}^2$ this is not the case, as described in Section 4.1.2.

Finally, the space $\mathcal{H}^{1/2}(\partial\Omega)$ is introduced to specify the space of function associated with the boundary data g or associated with linear boundary functionals. This space is defined by the norm

$$\|u\|_{\mathcal{H}^{1/2}(\partial\Omega)} = \inf_{\{v \in \mathcal{H}^1(\Omega), v|_{\partial\Omega} = g\}} \|v\|_{\mathcal{H}^1(\Omega)}. \tag{2.21}$$

Note that, it indicates that the boundary data can be less regular that $\mathcal{H}^1(\partial\Omega)$ but more that $L^2(\partial\Omega)$.

The following Lax-Milgram theorem allows us to show well-posedness of certain elliptic problems. Let $a(w, v)$ be a bilinear form where v, w are each defined on a Hilbert space $\mathcal{H}_0^1(\Omega)$. Assume that a is continuous

$$|a(w, v)| \leq C\|w\|_{\mathcal{H}_0^1(\Omega)} \cdot \|v\|_{\mathcal{H}_0^1(\Omega)}, \qquad \forall w, v \in (\mathcal{H}_0^1(\Omega))^2, \tag{2.22}$$

and coercive, i.e. there exists a $C_1 > 0$ such that

$$a(v, v) \geq C_1 \|v\|^2_{\mathcal{H}_0^1(\Omega)}, \qquad \forall v \in \mathcal{H}_0^1(\Omega). \tag{2.23}$$

Then, for every bounded functional $\ell \in \mathcal{H}^{-1}(\Omega)$, there exists a unique element $u_\ell \in \mathcal{H}^1(\Omega)$

such that

$$a(u_\ell, v) = \ell(v), \qquad \forall v \in \mathcal{H}^1(\Omega), \tag{2.24}$$

and that satisfies the stability *a priori* estimate

$$\|u_\ell\|_{\mathcal{H}^1(\Omega)} \leq \frac{\|\ell\|_{\mathcal{H}^{-1}(\Omega)}}{C_1}. \tag{2.25}$$

Relatedly the Riesz representation theorem states that for every $\ell \in \mathcal{H}^{-1}(\Omega)$ there is a unique member of $\mathcal{H}^1(\Omega)$, u_ℓ such that $\ell(v) = (v, u_\ell)_{\mathcal{H}^1}$, $\forall v \in \mathcal{H}^1(\Omega)$.

2.2 PDEs and Outputs

The long term objective of this research is to bound outputs of the incompressible and compressible Navier-Stokes equations. Hence, to extend the bounds technique to the complexity level included in these equations we need to proceed step by step. The first step is the development of our technique for application to boundary value problems of ordinary differential equations presented in Chapter 3. The second step is the generalization of the bound technique to coercive partial differential equations which are covered in Chapter 4. To prepare the reader, we review here ingredients of the Partial Differential Equations and associated weak forms. We will also introduce the formal definition of the output linear functionals.

2.2.1 Governing Equations

Let $\Omega \in \mathbf{R}^2$ be a bounded domain with Lipschitz boundary $\partial\Omega$. First we consider the Poisson problem of finding the solution $u(x)$ to

$$-\frac{\partial^2 u}{\partial x_i \partial x_i} = f \quad \text{in } \Omega \quad i = 1...2, \tag{2.26}$$

with

$$u = g_D \quad \text{on } \Gamma_D = \partial\Omega, \tag{2.27}$$

where $f \in \mathcal{H}^{-1}(\Omega)$ and $g_D \in \mathcal{H}^{1/2}(\Gamma_D)$ and Γ_D is a Dirichlet domain boundary. The variational form of (2.26) is: Find $u \in \mathcal{H}^1_D(\Omega)$,

$$\int_\Omega \frac{\partial v}{\partial x_i}\frac{\partial u}{\partial x_i}\,\mathrm{d}A = \int_\Omega v f\,\mathrm{d}A, \qquad \forall v \in \mathcal{H}^1_0(\Omega), \tag{2.28}$$

where

$$\mathcal{H}^1_D(\Omega) = \left\{ v \in \mathcal{H}^1(\Omega) |\ v|_{\Gamma_D} = g_D \right\}. \tag{2.29}$$

We now introduce bilinear and linear forms as a useful notation in simplifying (2.28),

$$a(w,v) = \int_\Omega \frac{\partial w}{\partial x_i}\frac{\partial v}{\partial x_i}\,\mathrm{d}A, \qquad \forall (w,v) \in (\mathcal{H}^1(\Omega))^2, \tag{2.30}$$

and

$$\ell^N(v) = \int_\Omega fv\,\mathrm{d}A, \qquad \forall v \in \mathcal{H}^1(\Omega), \tag{2.31}$$

or equivalently (in fact, more properly defined)

$$\ell^N(v) =< f, v >_{\mathcal{H}^1(\Omega)}, \tag{2.32}$$

Inserting these definitions in (2.26) we obtain

$$a(v,u) = \ell^N(v), \qquad \forall v \in \mathcal{H}^1_0(\Omega). \tag{2.33}$$

Second, we consider the convection–diffusion problem, where we look for $u(x)$ that satisfies

$$-\frac{\partial}{\partial x_i}(\nu\frac{\partial u}{\partial x_i}) + U_i\frac{\partial u}{\partial x_i} = f \qquad \text{in } \Omega,\ i = 1, ..., 2\ , \tag{2.34}$$

with boundary conditions

$$u \;=\; 0 \qquad \text{on } \Gamma_D = \partial\Omega, \tag{2.35}$$

where ν is the positive viscosity, U a constant velocity field, and Γ_D is the Dirichlet boundary. For simplicity, in this section we only consider homogeneous Dirichlet problems. Dirichlet inhomogeneous and Neumann boundary problems will be treated in Chapter 4.

The variational form of (2.34) is: Find $u \in \mathcal{H}^1_D(\Omega)$ such that

$$\int_\Omega \nu\frac{\partial v}{\partial x_i}\frac{\partial u}{\partial x_i} + vU_i\frac{\partial u}{\partial x_i}\,\mathrm{d}A = \int_\Omega vf\,\mathrm{d}A, \qquad \forall v \in \mathcal{H}^1_0(\Omega), \tag{2.36}$$

where $\mathrm{d}A$ is a differential area element. We can also write (2.36) as

$$a(v,u) = \ell^N(v), \qquad \forall v \in \mathcal{H}^1_0(\Omega), \tag{2.37}$$

where

$$a(w,v) = \int_\Omega \nu\frac{\partial w}{\partial x_i}\frac{\partial v}{\partial x_i} + vU_i\frac{\partial u}{\partial x_i}\,\mathrm{d}A, \qquad \forall (w,v) \in (\mathcal{H}^1(\Omega))^2, \tag{2.38}$$

and ℓ^N is given by (2.31) or (2.32).

Finally, we consider the Stokes problem: Find $(u_1, u_2, p) \in (\mathcal{H}^1(\Omega))^2 \times L^2(\Omega)$ that

satisfies

$$-\frac{\partial^2 u_i}{\partial x_j x_j} + \frac{\partial p}{\partial x_i} = f_i, \quad \text{in} \quad \Omega, \qquad i = \{1,2\} \tag{2.39}$$

$$-\frac{\partial u_i}{\partial x_i} = 0 \quad \text{in} \quad \Omega, \tag{2.40}$$

$$u_i = 0 \quad \text{on} \quad \Gamma_D = \partial\Omega, \qquad i = \{1,2\} \tag{2.41}$$

with homogeneous Dirichlet boundary conditions. The variational form follows as

$$\int_\Omega \frac{\partial v_i}{\partial x_j}\frac{\partial u_i}{\partial x_j} - \frac{\partial v_i}{\partial x_i}p - v_i f_i \, \mathrm{d}A = 0, \qquad \forall (v_1, v_2) \in (\mathcal{H}_0^1(\Omega))^2, \tag{2.42}$$

$$-\int_\Omega \frac{\partial u_i}{\partial x_i} q \, \mathrm{d}A = 0, \qquad \forall q \in L_0^2(\Omega), \tag{2.43}$$

where $\mathrm{d}A$ is a differential area element. Here, we define

$$\mathcal{H}_0^1(\Omega) = \{v \in \mathcal{H}^1(\Omega) |\ v|_{\Gamma_D} = 0\}, \tag{2.44}$$

$$L_0^2(\Omega) = \{q \in L^2(\Omega) |\ \int_\Omega q \, \mathrm{d}A = 0\}. \tag{2.45}$$

We now introduce the bilinear form,

$$d_i(w,q) = \int_\Omega q \frac{\partial w}{\partial x_i} \, \mathrm{d}A, \qquad \forall (w,q) \in \mathcal{H}^1(\Omega) \times L^2(\Omega). \tag{2.46}$$

and write

$$a(v_i, u_i) - d_i(v_i, p) = \ell_i^N(v_i), \qquad \forall (v_1, v_2) \in (\mathcal{H}_0^1(\Omega))^2, \tag{2.47}$$

$$-d_i(u_i, q) = 0, \qquad \forall q \in L_0^2(\Omega). \tag{2.48}$$

Recall that we use the Einstein summation convention, in which all repeated indices are summed from $i = 1, ..., d$.

2.2.2 Output Linear Functionals

In this thesis we consider two types of field variables. The solution to (2.28) yields the field variable u and solution to (2.47)-(2.48) yields the field variables (u_1, u_2, p). Our goal is to calculate bounds to outputs which are linear functionals of these two types of field solutions. Clearly, a large number of outputs, s, of interest to the engineering community are expressed as linear functionals. Examples of such outputs include the average over a region of Ω (including a point), the average over a curve of Ω or a portion of Γ_N (Neumann boundary), and the integral of the flux over a portion of Γ_D (Dirichlet boundary). For the

solution to (2.28), u, we define our linear output functional $s = \ell(u)$, where

$$\ell : \mathcal{H}^1(\Omega) \to \mathbf{R}. \tag{2.49}$$

For the field solution (u_1, u_2, p) to (2.47)-(2.48), we define $s = \ell(u_1, u_2, p)$ where

$$\ell : (\mathcal{H}^1(\Omega))^2 \times L_0^2(\Omega) \to \mathbf{R}. \tag{2.50}$$

We have seen in (2.14) that the norm of bounded functionals is related to the norm of the field solution. This fact will allow *a priori* estimates to be developed for outputs, as well as to guarantee some basic well behaved properties. Hence, when possible we express the output functional (ℓ) in $\mathcal{H}^{-1}(\Omega)$ or $\mathcal{H}^{-1/2}(\partial\Omega)$. Nevertheless, if u is sufficiently regular, our technique can also generate sharp bounds for functionals, $\ell(v)$, which are not bounded.

2.3 Finite Element Methods

We now consider the finite element method for the Poisson problem just as an example. Suppose that $X_\delta \subset \mathcal{H}_0^1(\Omega)$ is a finite element subspace. The finite element approximation to the variational Poisson problem (2.28) is: Find $u_\delta \in X_\delta$ such that

$$a^s(v, u_\delta) = \ell^N(v), \qquad \forall v \in X_\delta. \tag{2.51}$$

From (2.33) and (2.51) we express

$$a^s(v, u - u_\delta) = 0, \qquad \forall v \in X_\delta, \tag{2.52}$$

which leads to the usual finite element result that u_δ is the best possible fit to u in X_δ in the $\mathcal{H}^1$-seminorm. The well-posedness of problem (2.51) follows from the Lax–Milgram theorem. The discrete output of interest, is calculated from u_δ using a linear functional, $s_\delta = \ell(u_\delta)$. In this section we discuss three approximation spaces, X_δ, associated with a triangular partitioning of our domain.

2.3.1 Triangulation

Two different types of triangulations are required for our "hierarchical" bound procedure. For standard finite element methods, however, one triangulations suffice. Nevertheless, we present both triangulations in this Section: the H–mesh and the h–mesh, where the latter is a refinement of the former. As our H–mesh discretization of Ω we take a geometrically

conforming regular triangulation $\mathcal{T}_H$ consisting of K triangles T_H such that

$$\overline{\Omega} = \bigcup_{T_H \in \mathcal{T}_H} \overline{T}_H. \tag{2.53}$$

We denote the set of all (open) edges γ of a triangulation as $\mathcal{E}(\mathcal{T}_H)$, and the set of three edges γ_{T_H} associated with each element T_H as $\mathcal{E}(T_H)$. We denote the set of interior edges as $\mathcal{E}_{int}(\mathcal{T}_H)$, and the sets of Dirichlet and Neumann edges — the edges that are part of Dirichlet and Neumann boundary segments — as $\mathcal{E}_D(\mathcal{T}_H)$ and $\mathcal{E}_N(\mathcal{T}_H)$. We denote the set of all the N nodes of the triangulation by $\mathcal{M}(\mathcal{T}_H)$.

The triangulation and elemental edges are, of course, related. In particular, given an edge γ_{T_H} in $\mathcal{E}(T_H)$, we shall indicate that coincident edges γ in $\mathcal{E}(\mathcal{T}_H)$ as $\gamma = E(\gamma_{T_H})$. We next associate with each edge γ in $\mathcal{E}(\mathcal{T}_H)$ a unique normal $\hat{n}^\gamma$ such that, if γ lies on $\partial\Omega$, $\hat{n}^\gamma$ coincides with the outward normal $\hat{n}$ on $\partial\Omega$. Then, for all T_H in $\mathcal{T}_H$, and all edges γ_{T_H} in $\mathcal{E}(T_H)$, we define

$$\sigma_{T_H}^{\gamma_{T_H}} = \hat{n}_i^{E(\gamma_{T_H})}\, \hat{n}_i^{\gamma_{T_H}}, \tag{2.54}$$

where $\hat{n}^{\gamma_{T_H}}$ is the outward normal on γ_{T_H} with respect to T_H. In essence, $\sigma_{T_H}^{\gamma_{T_H}}$ is ± 1 on the two "sides" of an edge γ in $\mathcal{E}(\mathcal{T}_H)$.

We next introduce the h–mesh triangulation $\mathcal{T}_h$, consisting of triangles T_h such that

$$\overline{\Omega} = \bigcup_{T_h \in \mathcal{T}_h} \overline{T}_h. \tag{2.55}$$

We shall require that $\mathcal{T}_h$ be a refinement of $\mathcal{T}_H$, in that we can express each T_H in $\mathcal{T}_H$ as

$$\overline{T}_H = \bigcup_{T_h \in \mathcal{R}_{T_H}} \overline{T}_h, \tag{2.56}$$

where $\mathcal{R}_{T_H}$ is thus the set of h–mesh elements which comprise T_H. A uniform R refinement will denote an h–mesh in which $\mathcal{R}_{T_H}$ consists of R^2 number of triangles T_h for each T_H.

2.3.2 Conforming Discretization

We first define the most common discretization in finite element methods. The finite–dimensional space X_δ is the projection of a infinite–dimensional space $\mathcal{H}_D^1(\Omega)$ defined as

$$X_\delta = \{v|_{T_H} \in \mathbf{P}_n(T_H)\} \bigcap \mathcal{H}_0^1(\Omega), \tag{2.57}$$

where $\mathbf{P}_n(T_H)$ is the space of all polynomials of degree less that or equal to n, defined over triangular elements T_H in $\mathcal{T}_H$. The discrete statement corresponding to (2.33) then takes

the form: Find $u_\delta \in X_\delta$ such that

$$a^s(v, u_\delta) = \ell^N(v), \qquad \forall v \in \mathcal{H}_0^1(\Omega). \tag{2.58}$$

For (2.36) the discrete statement is; Find $u_\delta \in X_\delta$ such that

$$a(v, u_\delta) = \ell^N(v), \qquad \forall v \in \mathcal{H}_0^1(\Omega). \tag{2.59}$$

Note that the operator in this last case is the nonsymmetric operator of the convection–diffusion problem. The orthogonality property presented for the Poisson problem in (2.52) also holds for the convection diffusion problem as well. In this case, however, the orthogonality property does not guarantee that u_δ is the best fit in X_δ for the $\mathcal{H}^1$–seminorm.

Our goal now is to expand our bases such as $X_\delta = \text{span}(\varphi_i, i = 1, ...N)$. Therefore, we construct a set of the n^{th}–order Lagrangian interpolants for the basis function, $\varphi_i(\Omega)$, $i = 1, ..., N$ such that

$$\varphi_i(x_j) = \delta_{i,j}, \qquad i, j = 1, ..., N, \tag{2.60}$$

where $x_j \in \Omega$ is a global node of $\mathcal{T}_H$ and $\delta_{i,j}$ is the Kronecker delta. We also define these bases elementally as the function $\varphi^j_{T_H}$, "conforming" basis function for $\mathbf{P}_1(T_H)$ associated with (global) node x_j of the triangulation $\mathcal{T}_H$: $\varphi^j_{T_H}(x)$ is $+1$ at $x = x_j$, and vanishes at the other two vertices of T_H.

The Galerkin method expands the solution u_δ and test function v_δ using these basis functions,

$$u_\delta(x) = \sum_{j=1}^{N} u_j \varphi_j(x), \tag{2.61}$$

$$v_\delta(x) = \sum_{j=1}^{N} v_j \varphi_j(x). \tag{2.62}$$

By replacing these expanded forms of u_δ and v_δ in (2.51) we finally obtain

$$\underline{v}_\delta^T \underline{L}_\delta \underline{u}_\delta = \underline{f}_\delta, \qquad \forall \underline{v}_\delta \in \mathbf{R}^N. \tag{2.63}$$

Here $\underline{L}_\delta$ is the global system matrix corresponding to the weak discrete operators and $\underline{f}_\delta$ is the vector of global nodes values corresponding to the inhomogeneities. We now take $(\underline{v}_\delta)_i = \underline{e}_i$ for $i = 1, ..., N$ where the $\underline{e}_i$ are the unit vectors in each of the N directions of R^N; therefore, for homogeneous Dirichlet problem our discrete linear system of equation becomes

$$\tilde{\underline{L}}_\delta \tilde{\underline{u}}_\delta = \tilde{\underline{f}}_\delta, \tag{2.64}$$

where $\tilde{\underline{u}}_\delta \in \mathbf{R}^{\tilde{N}}$, $\tilde{\underline{f}}_\delta \in \mathbf{R}^{\tilde{N}}$ are $\underline{u}_\delta$ and $\underline{f}_\delta$ with entries i for which $(\underline{x}_{1i}, \underline{x}_{2i}) \in \Gamma_D$ eliminated,

and $\tilde{\underline{L}}_\delta \in \mathbf{R}^{\tilde{N}\times\tilde{N}}$ is the $\underline{L}_\delta$ with rows and columns i for which $(\underline{x}_{1i}, \underline{x}_{2i}) \in \Gamma_D$ eliminated. Notice $\tilde{N}$ is the number of interior nodes.

2.3.3 Nonconforming Discretization

By conforming we mean that $X_\delta \subset X$; if $X_\delta \not\subset X$ then we have a nonconforming finite element space. We define a first order polynomial nonconforming space $\overline{X}_\delta$ as,

$$\overline{X}_\delta = \left\{ v|_{T_H} \in \mathbf{P}_1(T_H) | \int_{\gamma_{T_H}} [v]\, \mathrm{d}s = 0, \quad \forall \gamma_{T_H} \in \mathcal{E}(\mathcal{T}_H) \right\} \tag{2.65}$$

where the notation $[\cdot]$ denotes the jump in the values of functions v across element boundaries,

$$[v] = \begin{cases} \sigma_{T_H}^{\gamma_{T_H}} v_{T_H} + \sigma_{T'_H}^{\gamma_{T'_H}} v_{T'_H} & \text{on} \quad \gamma_{T_H} = \overline{T}_H \cap \overline{T}'_H \\ v & \text{on} \quad \gamma_{T_H} \subset \partial\Omega \end{cases} . \tag{2.66}$$

To fix ideas, we present for $\delta = H$ the "nonconforming" basis functions for $\mathbf{P}_1(T_H)$, $\zeta_{T_H}^{\gamma_{T_H}}$, where for all T_H in $\mathcal{T}_H$,

$$\zeta_{T_H}^{\gamma_{T_H}} \in \mathbf{P}_1(T_H), \quad \forall \gamma_{T_H} \in \mathcal{E}(T_H), \tag{2.67}$$

and

$$\int_{\gamma'_{T_H}} \zeta_{T_H}^{\gamma_{T_H}} \mathrm{d}s = \begin{cases} |\gamma_{T_H}| & \gamma'_{T_H} = \gamma_{T_H} \\ 0 & \gamma'_{T_H} \neq \gamma_{T_H} \end{cases}, \forall \gamma_{T_H}, \gamma'_{T_H} \in \mathcal{E}(T_H), \tag{2.68}$$

where $|\gamma_{T_H}|$ is the length of γ_{T_H}. The function $\zeta_{T_H}^{\gamma_{T_H}}$ is $+1$ at the two endpoints of γ_{T_H}, and -1 at the remaining vertex of T_H. Similarly to the conforming discretization of Section 2.3.3, we expand the solution u_δ and the test function v_δ using the above basis functions, chose the appropriate trial functions to obtain a system of equations, and apply the boundary condition to arrive at the discrete linear system corresponding to (2.51),

$$\tilde{\underline{L}}_H^* \tilde{\underline{u}}_H^* = \tilde{\underline{f}}_H^*, \tag{2.69}$$

where $\tilde{\underline{L}}_H^* \in \mathbf{R}^{\overline{N}\times\overline{N}}$, $\tilde{\underline{u}}_H^* \in \mathbf{R}^{\overline{N}}$ and $\tilde{\underline{f}}_H^* \in \mathbf{R}^{\overline{N}}$. The number of interior node of the nonconforming mesh is $\overline{N}$. To show well–posedness we refer the reader to [33]. In addition, this discretization satisfies similar stability results as for the conforming case.

2.3.4 The Crouzeix–Raviart Element

We present here the Crouzeix–Raviart element used for the discretization of the Stokes problem (2.47)-(2.48). This element is a $\mathbf{P}_2^+$ cubic bubble for the velocity and a $\mathbf{P}_1$ discontinuous for the pressure which satisfies the *inf sup* and the "efficiency" condition that the

pressure space be one degree lower that the velocity space [20]. The discontinuous pressure is ideal for two–fluid problems and for decoupling the pressure degrees of freedom. However, this element has a larger number of pressure degree of freedom compared to the usual Taylor–Hood element [38].

For components of velocity, we identify

$$X_\delta = \{v|_{T_\delta} \in \mathbf{P}_2^+(T_\delta),\ \forall T_\delta \in \mathcal{T}_\delta\} \bigcap \mathcal{H}_0^1(\Omega), \tag{2.70}$$

where $\mathbf{P}_2^+(T_\delta) = \{\mathbf{P}_2(T_\delta) + \alpha_{T_H}\xi_1\xi_2\xi_3,\ \alpha_{T_H} \in \mathbf{R}\}$ is the space of quadratic polynomials enhanced by a "bubble" function over T_δ. The barycentric coordinates (ξ_1, ξ_2, ξ_3) define the "bubble" function, i.e. a function that vanishes on the boundaries of the elements.

For pressure, we introduce

$$Y_\delta = \{q|_{T_\delta} \in \mathbf{P}_1(T_\delta),\ \forall T_\delta \in \mathcal{T}_\delta\} \bigcap L_0^2(\Omega). \tag{2.71}$$

Let ϕ^V and ϕ^P be the basis functions associated with $\mathbf{P}_2^+$ and $\mathbf{P}_1$ meshes respectively. The bases associated with the (2.70)-(2.71) spaces are chosen to be

$$X_\delta = \text{span}\{\phi^V,\ i = 1, ..., N\}, \tag{2.72}$$

and

$$Y_\delta = \text{span}\{\phi^P,\ i = 1, ..., M = 3K\}. \tag{2.73}$$

where N and M are the number of global velocity and pressure nodes respectively. In practice we work elementally where all the integrals and derivatives are performed on the reference element defined in Appendix C.

Proceeding with the discretization we arrive at the following linear system,

$$\begin{bmatrix} \underline{A}_\delta & 0 & -\underline{D}_{1\delta}^T \\ 0 & \underline{A}_\delta & -\underline{D}_{2\delta}^T \\ -\underline{D}_{1\delta}^T & -\underline{D}_{2\delta}^T & 0 \end{bmatrix} \begin{Bmatrix} \underline{u}_{1\delta} \\ \underline{u}_{2\delta} \\ \underline{p}_\delta \end{Bmatrix} = \begin{Bmatrix} \underline{f}_{1\delta} \\ \underline{f}_{2\delta} \\ 0 \end{Bmatrix}, \tag{2.74}$$

where $\underline{A}_\delta$ is the standard Laplacian, $\underline{D}_{i\delta}^T$ are the operators corresponding to (2.46) and $\underline{f}_{i\delta}$ are the forcing terms. We have not yet applied the boundary conditions but their implementation follows classical removing of rows and columns associated with boundary nodes.

2.3.5 The h–mesh problem

We review, in the context of coercive operators, some of the convergence properties of the finite element approximation schemes. We consider here only a standard Galerkin

approximation.

We define here the quantity for which we wish to obtain a bound. In particular, for our output of interest, s_h, we first look for a $u_h \in X_h^D$ such that

$$a(v, u_h) = \ell^N(v), \qquad \forall v \in X_h, \tag{2.75}$$

and then compute the output,

$$s_h = \ell^O(u_h). \tag{2.76}$$

To show the importance of bounded functionals, we write

$$|s - s_h| = |\ell^O(u) - \ell^O(u_h)| = |\ell(u - u_h)| \leq C\|u - u_h\|_{\mathcal{H}^1}, \tag{2.77}$$

based the definition of bounded linear functionals. As regards convergence rate, we expect $\|u-u_h\|_{\mathcal{H}^1} \leq Ch\|u\|_{\mathcal{H}^2}$ for $u \in \mathcal{H}^2(\Omega)$, where $C = C(\Omega)$, which suggests that $|s-s_h| \approx O(h)$ as $h \to 0$.

However, a sharper result can be obtained. We know that from the Riesz representation theorem (or Lax–Milgram) that we can identify a $u^\ell \in \mathcal{H}^2(\Omega) \cap \mathcal{H}_0^1(\Omega)$, such that $\ell^O(v) = a(v, u^\ell), \forall v \in \mathcal{H}_0^1(\Omega)$. We now set $v = u - u_h \in \mathcal{H}_0^1(\Omega)$ to write

$$\ell^O(u - u_h) = a(u - u_h, u^\ell). \tag{2.78}$$

By evoking orthogonality 2.52, we then obtain

$$\ell^O(u - u_h) = a(u - u_h, u^\ell - v) \leq C\|u - u_h\|\|u^\ell - v\|, \qquad \forall v \in \mathcal{H}_0^1(\Omega), \tag{2.79}$$

and finally

$$|s - s_h| \leq Ch^2\|u\|_{\mathcal{H}^2}\|u^\ell\|_{\mathcal{H}^2}. \tag{2.80}$$

For example, for a convex domain, smooth data, and a smooth functional, we expect $|s - s_h| \approx O(h^2)$ as $h \to 0$. Later, we will address similar types of procedures of *a posteriori* error analysis but first we review the constrained minimization problem used in our bound theory.

2.4 Constrained Minimization

In this section we consider the following constrained minimization problem,

$$c = \min_{\{z \in Z | \mathcal{R}(y,z)=0,\, \forall y \in Y\}} \mathcal{C}(z), \tag{2.81}$$

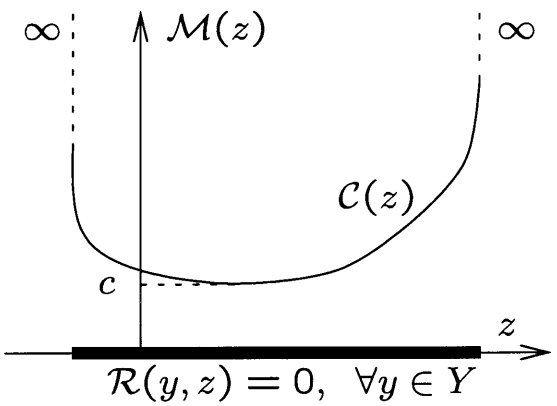

Figure 2-1: Representation of the constrained minimization problem.

where $\mathcal{C}(z)$ is a quadratic (or more general convex) functional and Z, Y are vector spaces of dimension N, M respectively. For example, as will be the case in this thesis, we can write $\mathcal{C}(z) = \mathcal{A}(z,z) - \mathcal{D}(z)$ where $\mathcal{A}(z,z')$ is a bilinear symmetric positive semi-definite form and $\mathcal{D}(z)$ is a linear form. We assume the constraints of this optimization problem to be linear equality constraints. Therefore, we can write $\mathcal{R}(y,z) = \mathcal{B}(y,z) - \mathcal{G}(y)$ as a summation of a bilinear form ($\mathcal{B}$) and a linear form ($\mathcal{G}$).

One approach to the solution to this constrained minimization problem leads to the construction of a Lagrangian,

$$\mathcal{L}(z,y) = \mathcal{C}(z) + \mathcal{R}(y,z), \tag{2.82}$$

where y is the Lagrange multiplier that imposes the linear equality constraints. The solution to the minimization problem is obtained by

$$c = \min_{z \in Z} \sup_{y \in Y} \mathcal{L}(z,y). \tag{2.83}$$

When removing y (Lagrange multiplier) we obtain the primal problem that is the constrained minimization of $\mathcal{C}(z)$. To show this, we define $\mathcal{M}(z)$ as $\sup_{y \in Y} \mathcal{L}(z,y)$ by

$$\mathcal{M}(z) = \begin{cases} \mathcal{C}(z) & \mathcal{R}(y,z) = 0, \ \forall y \in Y \\ \infty & \exists y \in Y \text{ s.t. } \mathcal{R}(y,z) \neq 0 \end{cases}. \tag{2.84}$$

We now look for the minimum of $\mathcal{M}(z)$ that is $\min_{z \in Z} \sup_{y \in Y} \mathcal{L}(z,y)$, and using the previous definition we obtain (2.81). In Figure 2-1 we depict graphically the constrained minimization problem. We observe that outside the region for which $\mathcal{R}(y,z) \neq 0$, $\mathcal{M}(z)$ is ∞ and c is the minimum of those finite values.

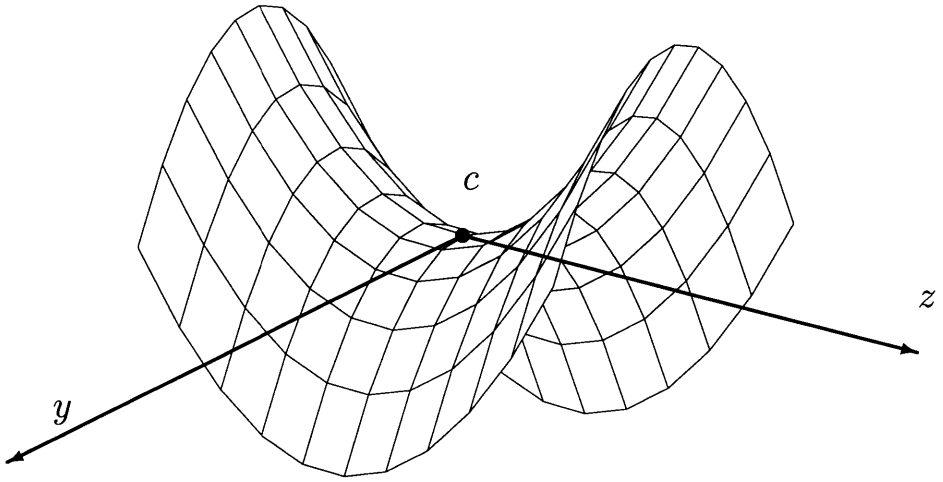

Figure 2-2: Saddle representation.

Introducing $\mathcal{P}(y)$ as the minimum function of $\mathcal{L}(z,y)$ over all z we can write

$$\mathcal{P}(y) = \min_{z \in Z} \mathcal{L}(z,y) \leq \mathcal{L}(z,y). \tag{2.85}$$

In addition, from (2.84) we recall that

$$\mathcal{M}(z) = \sup_{y \in Y} \mathcal{L}(z,y), \tag{2.86}$$

and it follows for all $z \in Z$ and for all $y \in Y$, that

$$\mathcal{M}(z) \geq \mathcal{L}(z,y) \geq \mathcal{P}(y). \tag{2.87}$$

This indicates that the minimum of $\mathcal{M}(z)$ will never go below $\mathcal{P}(y)$ and the maximum of $\mathcal{P}(y)$ can never go above $\mathcal{M}(z)$. We conclude by presenting the weak duality statement, for all $z \in Z$, and for all $y \in Y$,

$$\min_{z \in Z} \max_{y \in Y} \mathcal{L}(z,y) \leq \max_{y \in Y} \min_{z \in Z} \mathcal{L}(z,y) \tag{2.88}$$

where for reasons of clarity we have substituted sup by max.

We now define the saddlepoint (z^*, y^*) of $\mathcal{L}(z,y)$ as

$$\mathcal{L}(z^*,y) \leq \mathcal{L}(z^*,y^*) \leq \mathcal{L}(z,y^*), \quad \forall z \in Z,\ \forall y \in Y, \tag{2.89}$$

which, in the smooth case can be calculated from the stationarity condition,

$$\frac{\partial \mathcal{L}(z, y^*)}{\partial z} = 0, \tag{2.90}$$

$$\frac{\partial \mathcal{L}(z^*, y)}{\partial y} = 0. \tag{2.91}$$

The value of our Lagrangian at the saddle point $\mathcal{L}(z^*, y^*)$ is precisely c, it corresponds to the Lagrangian $\mathcal{L}(z, y)$ being maximized with respect to y, and at the same time being minimized with respect to z. This is also obvious from Figure 2-2. Note that the existence of the saddlepoint is equivalent to a zero duality gap, that is, the constrained minimization of $\mathcal{M}(z)$ equals the maximization of $\mathcal{P}(y)$.

We now present the key idea that will lead to obtaining a lower bound to the constrained minimization solution c. From (2.83) and (2.88) we get

$$c = \min_{z \in Z} \max_{y \in Y} \mathcal{L}(z, y), \tag{2.92}$$

$$\geq \max_{y \in Y} \min_{z \in Z} \mathcal{L}(z, y). \tag{2.93}$$

Now, if we look at the unconstrained problem, that is for any value $\hat{y} \in Y$ we obtain,

$$\hat{c} \equiv \min_{z \in Z} \mathcal{L}(z, \hat{y}) \leq c. \tag{2.94}$$

When the value c is not known, then, the value $\hat{c}$ can correctly be used as a lower approximation of the value of c. Note that the closer $\hat{y}$ is to y the closer $\hat{c}$ is to c; the thickline of Figure 2-3 represents the locus of all the points of $\hat{c}$. From Figure 2-3 we see that $\hat{c}$ converges to c as $y = \hat{y} - y^*$ tend to zero where $\hat{y}$ and y^* correspond to the y coordinate of $\hat{c}$ and c, respectively. Nevertheless, if we allow all possible choices of $\hat{y}$ we may encounter situations where $\hat{c} = -\infty$. To avoid this situation and to obtain a lower bound ($\hat{c}$) which is meaningful, we restrict our choice of $\hat{y}$ to the a space defined as

$$Y_{bd} = \{y \in Y | \min_{z \in Z} \mathcal{L}(z, y) > -\infty\}. \tag{2.95}$$

In this thesis this condition is be satisfied by the appropriate construction of the Lagrange multiplier.

We now want to apply the above principles to our quadratic linear program. Our Lagrangian becomes

$$\mathcal{L}(z, y) = \mathcal{A}(z, z) - \mathcal{D}(z) + \mathcal{B}(y, z) - \mathcal{G}(y). \tag{2.96}$$

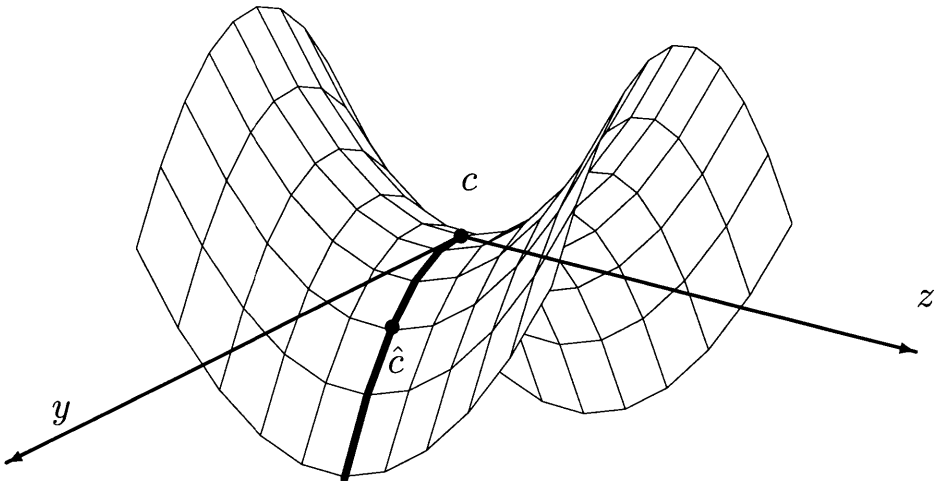

Figure 2-3: Location of the unconstrained problem solution $\hat{c}$.

Since we are in presence of a quadratic objective function with linear constraints there exists a saddle point [44]. We know where the saddle points (z^*, y^*) are positioned. Their location is given by the equilibrium equation,

$$2\mathcal{A}(z, z^*) + \mathcal{B}(y^*, z) = \mathcal{D}(z), \quad \forall z \in Z, \tag{2.97}$$

$$\mathcal{B}(y, z^*) = \mathcal{G}(y), \quad \forall y \in Y. \tag{2.98}$$

A lower value ($\hat{c} \leq c$) to this saddle point value is obtained for any choice of $\hat{y} \in Y_{bd}$. For a quadratic linear program the space Y_{bd} is defined by,

$$Y_{bd} = \{y \in Y | -\mathcal{D}(z_s) + \mathcal{B}(y, z_s) = 0\} \tag{2.99}$$

where z_s is similar to the right nullspace of linear systems,

$$\mathcal{A}(z, z_s) = 0, \quad \forall z \in Z. \tag{2.100}$$

Note that, for singular matrices, the linear terms become dominant in the Lagrangian (2.96) and can lead to infinity when minimizing or maximizing. The space Y_{bd}, defined in (2.99), ensures solvability of (2.97) and also precludes $-\infty$ since linear terms vanish when the quadratic term vanishes in the Lagrangian. In addition, we observe that for $y \in Y_{bd}$ the Lagrangian is invariant, that is,

$$\mathcal{L}(z, y) = \mathcal{L}(z + \beta z_s, y). \tag{2.101}$$

To conclude this section we make a few remarks: first, the perfect choice of the Lagrange multiplier is $\hat{y} = y^*$ for which $\hat{c} = c$; second, for a very close approximation $\hat{y} \approx y^*$ then we get a very close lower approximation $\hat{c} \approx c$; and third $y \in Y_{bd}$ is the condition for solvability of (2.97)-(2.98).

2.5 Previous Work on A Posteriori Error Estimators

Our approach to the construction of bounds (1.1) is closely related to the local Neumann subdomain problems used in *a posteriori* error estimation procedure for the finite element discretization of partial differential equations [5]. In this section we review earlier subdomain proposals which estimate the discretization error $e_H = u - u_H$ given by,

$$a(e_H, v) = a(u, v) - a(u_H, v) = \ell^N(v) - a(u_H, v), \qquad v \in X_H, \tag{2.102}$$

where u_H is the finite element approximation to (2.26). We exploit the notation introduced earlier in this Chapter.

The residual equation (2.102) can be stated equivalently as a maximization problem [3, 13], such as

$$\max_{v \in X_H} J(v) = \frac{1}{2} a(e_H, e_H), \tag{2.103}$$

where

$$J(v) \equiv -\frac{1}{2} a(v, v) + \ell^N(v) - a(v, u_H). \tag{2.104}$$

Although, problem (2.103) could be solved using a higher order discretization at a corresponding higher cost, a more practical approach is to reduce the cost by decomposing (2.103) into local problems posed over each element T_H in $\mathcal{T}_H$. That is, "fluxes" $y|_{E(\gamma_{T_H})} \in \mathcal{Q}$ are introduced on the edges of each element T_H to yield a local Neumann problem for $\hat{e}_H|_{T_H} \in Z_H(T_H)$ which is written as,

$$a_{T_H}(\hat{e}_H|_{T_H}, v) = \ell^N_{T_H}(v) - a^s_{T_H}(u_H, v) + \sum_{\gamma_{T_H} \in \mathcal{E}(\mathcal{T}_H)} \sigma^{\gamma_{T_H}}_{T_H} \int_{\gamma_{T_H}} v y|_{E(\gamma_{T_H})} \mathrm{d}s, \qquad \forall v \in Z_H(T_H), \tag{2.105}$$

where

$$Z_H(T_H) = (\mathbf{P}_1(T_H)), \tag{2.106}$$

and

$$\mathcal{Q} = \{t \in \mathcal{H}^{-1/2}(\mathcal{E}(\mathcal{T}_H))\}. \tag{2.107}$$

In a "global notation", we obtain, for $\hat{e}_H \in V_H$,

$$a(\hat{e}_H, v) = \ell^N(v) - a_{T_H}(u_H, v) + b(v, y), \qquad \forall v \in V_H, \tag{2.108}$$

where the "broken" spaces are defined by

$$V_H = \{v \in \mathcal{H}^1_*(\Omega) | v|_{T_H} \in Z_H(T_H), \forall T_H \in \mathcal{T}_H\}, \tag{2.109}$$

and

$$\mathcal{H}^1_*(\Omega) = \left\{v \in L^2(\Omega) |\ v|_{T_H} \in \mathcal{H}^1(T_H),\ \forall T_H \in \mathcal{T}_H\right\}. \tag{2.110}$$

For solvability of (2.105), we require that the boundary fluxes y satisfy the equilibrium equation condition,

$$\ell^N_{T_H}(v) - a_{T_H}(u_H, v) + \sum_{\gamma_{T_H} \in \mathcal{E}(\mathcal{T}_H)} \sigma^{\gamma_{T_H}}_{T_H} \int_{\gamma_{T_H}} vy|_{E(\gamma_{T_H})} \mathrm{d}s = 0, \quad \forall v \in Z_H(T_H). \tag{2.111}$$

Note that by addressing this reduced problem we preserve the bounding properties, that is, upper bounds on the error in the energy norm, such as

$$\frac{1}{2}(a(e_H, e_H)) \leq \frac{1}{2} a(\hat{e}_H(y), \hat{e}_H(y)). \tag{2.112}$$

To prove (2.112), a Lagrangian $J_s :\ V_H \times \mathcal{Q}$, is defined as

$$J_s(v,t) = -\frac{1}{2} a(v,v) + \ell^N(v) - a(u_H, v) + b(v,t). \tag{2.113}$$

Note that by evoking stationarity of this Lagrangian we obtain (2.105). Based on the Duality theory of Section 2.4, we write, for any $\hat{t} \in \mathcal{Q}$,

$$\max_{v \in V_H} \min_{t \in \mathcal{Q}} J_s(v,t) \leq \min_{t \in \mathcal{Q}} \max_{v \in V_H} J_s(v,t) \leq \max_{v \in V_H} J_s(v, \hat{t}). \tag{2.114}$$

The solution procedure to obtain the upper bound is, first, to calculate y from (2.111), and second, to calculate $\hat{e}_H(y)$ from (2.108). Replacing y and $\hat{e}_H(y)$ in the Lagrangian J_s we obtain

$$a(\hat{e}_H(y), \hat{e}_H(y)) = \max_{v \in V_H} J_s(v, \hat{t}), \tag{2.115}$$

and finally we prove

$$\frac{1}{2} a(e_H, e_H) \leq \frac{1}{2} a(\hat{e}_H(y), \hat{e}_H(y)), \tag{2.116}$$

as desired.

This approach proposed by Ladeveze and Leguillon [31] and generalized by Ainsworth and Oden [3] is similar to our bound procedure. In particular, we both form a Lagrangian which we minimize (or maximize) leading to the formulation of subdomain Neumann problems. The procedures addressing the equilibration problem is, in both cases, based on previous work by Ladeveze and Leguillon [31]. It is important to understand that (2.104)

only applies to error estimates of symmetric problems which are measured in the energy norm: $\|e_H\|^2 = a(e_H, e_H)$. These restrictions are intrinsically due to the choice of the Lagrangian. In contrast, our augmented Lagrangian approach is more general: we can treat nonsymmetric PDEs; furthermore, we obtain bounds not on the energy–norm, but rather on the error in the output linear–functional of engineering interest.

This important problem of *a posteriori* analysis of output linear–functionals was addressed by Becker and Rannacher [16, 17, 41]. Before we review their approach, which attempts to estimate the error directly in the output linear functional norm, we pause and introduce a simple error estimator in the energy norm.

From integration by parts of (2.102) we write, as in [3],

$$a(e_H, v) = \sum_{T_H \in \mathcal{T}_H} \left\{ \int_{T_H} rv \, \mathrm{d}A + \int_{\partial T_H} Rv \, \mathrm{d}s \right\}, \quad \forall v \in V_H, \tag{2.117}$$

where r is the interior residual,

$$r = f + \frac{\partial^2 u_H}{\partial x_i \partial x_i}, \tag{2.118}$$

and R is the boundary residual,

$$R = -\left[\frac{\partial u_H}{\partial x_i}\right], \tag{2.119}$$

where $[\cdot]$ refers to the jump across the boundary edges between two triangles. We now state the orthogonality property,

$$\sum_{T_H \in \mathcal{T}_H} \left\{ \int_{T_H} rv_h \, \mathrm{d}A + \int_{\partial T_H} Rv_h \, \mathrm{d}s \right\} = 0, \tag{2.120}$$

where $v_h \in X_H$. By adding (2.120) to (2.117), we obtain

$$a(e_H, v) = \sum_{T_H \in \mathcal{T}_H} \left\{ \int_{T_H} r(v - v_h) \, \mathrm{d}A + \int_{\partial T_H} R(v - v_h) \, \mathrm{d}s \right\}, \quad \forall v \in V_H, \tag{2.121}$$

and by applying Cauchy–Schwarz inequality to the integrals and also to the sums over all element, and from standard approximation and trace results, we rewrite

$$a(e_H, v) \leq C|v|_{\mathcal{H}^1(\Omega)} \sum_{T_H \in \mathcal{T}_H} \left(H_{T_H}^2 \|r\|_{L^2(T_H)}^2 + \frac{1}{2} H_{T_H} \|R\|_{L^2(\partial T_H)}^2 \right)^{\frac{1}{2}}, \tag{2.122}$$

where H_{T_H} is the characteristic size of the element T_H. Finally, taking $v = e_H$, and evoking $|e_H|_{\mathcal{H}^1(\Omega)} \leq \|e_H\|$, we write

$$a(e_H, e_H) \leq C\|e_H\| \sum_{T_H \in \mathcal{T}_H} \left(H_{T_H}^2 \|r\|_{L^2(T_H)}^2 + \frac{1}{2} H_{T_H} \|R\|_{L^2(\partial T_H)}^2 \right)^{\frac{1}{2}}. \tag{2.123}$$

We can now simplify $\|e_H\|$ on both sides, and then square the equation to obtain an error in the energy norm

$$\|e_H\|^2 \leq C \sum_{T_H \in \mathcal{T}_H} \eta^2_{L^2(T_H)}, \tag{2.124}$$

where $\eta^2_{L^2(T_H)}$ is a local error indicator for each T_H,

$$\eta^2_{L^2(T_H)} = H^2_{T_H} \|r\|^2_{L^2(T_H)} + \frac{1}{2} H_{T_H} \|R\|^2_{L^2(T_H)}, \tag{2.125}$$

where C is a constant. Note that this error estimator requires no regularity assumptions and that C is independent of e_H and H_{T_H}.

Returning to the approach of Becker and Rannacher, we note that it is based on introducing an auxiliary problem for $\mu \in X$,

$$a(w, \mu) = \ell^O(w), \qquad \forall w \in X. \tag{2.126}$$

The error $e_H = u - u_H$ is estimated in the norm:

$$\ell^O(e_H) = a(e_H, \mu). \tag{2.127}$$

Therefore, by replacing v by μ in (2.117), and exploiting the Galerkin orthogonality property to introduce $\bar{\mu} \in X_H$, we obtain

$$\begin{aligned} |\ell^O(e_H)| &= |a(e_H, \mu)| \\ &\leq \left| \sum_{T_H \in \mathcal{T}_H} \left\{ \int_{T_H} r(\mu - \bar{\mu}) \, \mathrm{d}A + \int_{\partial T_H} R(\mu - \bar{\mu}) \, \mathrm{d}s \right\} \right| \end{aligned} \tag{2.128}$$

and by applying Cauchy–Schwarz inequality to the integrals only, and from standard approximation and trace results, we rewrite

$$|\ell^O(e_H)| \leq C \left(\sum |\mu|_{\mathcal{H}^2(T_H)} H^2_{T_H} \|r\|^2_{L^2(T_H)} + \sum \frac{1}{2} |\mu|_{\mathcal{H}^2(\partial T_H)} H^{3/2}_{T_H} \|R\|^2_{L^2(\partial T_H)} \right). \tag{2.129}$$

To obtain (2.129) we have assumed regularity so $\mu \in \mathcal{H}^2(\Omega)$

$$\|\mu - \bar{\mu}\|_{L^2(T_H)} \leq C H^2_{T_H} |\mu|_{\mathcal{H}^2(T_H)}, \tag{2.130}$$

$$\|\mu - \bar{\mu}\|_{L^2(\partial T_H)} \leq C H^{3/2}_{T_H} |\mu|_{\mathcal{H}^2(\partial T_H)}. \tag{2.131}$$

We observe in (2.123) that $\|e_H\|_{\mathcal{H}^1}$ cancels on both sided of the equations. However, here we don't have this fortuitous cancelation and we are obliged to evaluate this new constants $|\mu|_{\mathcal{H}^2(T_H)}, |\mu|_{\mathcal{H}^2(\partial T_H)}$. This latter constants are approximated from the solution of the "dual" problem by $|\mu_H|_{\mathcal{H}^2(T_H)}, |\mu_H|_{\mathcal{H}^2(\partial T_H)}$. Although these estimators offer rapid

evaluation for adaptive refinement with application to a large class of equations including the Navier-Stokes equations, this procedure is limited to finite element approximations. In addition, in the context of validation and confirmation of ($s_H = \ell(u_H)$) it is imperative to know or to calculate all constants as to obtain rigorous quantitative estimators. In their approach, calculation of C, and $|\mu|_{\mathcal{H}^2(T_H)}, |\mu|_{\mathcal{H}^2(\partial T_H)}$, is less than trivial and therefore their approach is very difficult to apply in our design context. Our approach provides quantitative and rigorous bounds of the output of interest.

Extension of *a posteriori* error estimates from elliptic equation to the Stokes problem (2.47)-(2.48) has been performed by Verfürth [48] and successfully reconsidered by Bank and Welfred [15]. These estimates are based on the solution of local Stokes problems for all T_H in $\mathcal{T}_H$,

$$a_{T_H}(e_{iH}, v_i) - d_{i\,T_H}(v_i, E_H) = (r_i, v_i) + \sum_{\gamma_{T_H} \in \mathcal{E}(\mathcal{T}_H)} \left(\left[\hat{n}_j \frac{\partial u_{iH}^{\ell}}{\partial x_j} \right], v \right), \tag{2.132}$$

$$-d_{i\,T_H}(e_i, q) = (s, q), \quad \forall (v_1, v_2, q) (\in X_H)^2 \times Y_H, \tag{2.133}$$

where $e_{iH} = u_i - u_{iH}^{\ell}$, $E_H = p - p_H$ and u_{iH}^{ℓ} is the linear part of the mini–element discretization of the velocity u_{iH}. The quantities r_1, r_2 and s are the residuals of (2.39)-(2.41) defined as,

$$\begin{cases} r_i = f_i - \frac{\partial P_H}{\partial x_i}, & i = 1, ..., 2 \\ s = \frac{\partial u_{iH}^{\ell}}{\partial x_j}, & i, j = 1, ..., 2 \end{cases} . \tag{2.134}$$

These error estimates are based on the norm and semi norms associated with the solution of (2.132)-(2.133). The energy norms considered were:

$$N_1(u_1, u_2, p) = \left\{ \left\| \frac{\partial u_j}{\partial x_i} \right\|_{L^2(\Omega)}^2 + \|p\|_{L^2(\Omega)}^2 \right\}^{\frac{1}{2}}, \tag{2.135}$$

$$N_2(u_1, u_2, p) = \left\{ \left\| \frac{\partial u_j}{\partial x_i} \right\|_{L^2(\Omega)}^2 + \sum_{T_H \in \mathcal{T}_H} \left\| \frac{\partial p}{\partial x_i} \Big|_{T_H} \right\|_{L^2(T_H)}^2 \right\}^{\frac{1}{2}}. \tag{2.136}$$

Verfürth shows in [48] that there exists constants, only depending on geometry, for which his local estimators,

$$\eta_{T_H}^2 = area(T_H) \|r_i\|_{L^2(T_H)}^2 + \|s\|_{L^2(T_H)}^2 + \frac{1}{2}|\gamma| \left\| \left[\frac{\partial u_H^{\ell}}{\partial n} \right] \right\|_{L^2(\partial T_H)}^2 \tag{2.137}$$

are globally upper and locally lower bounds for the error of the finite element discretization. In [15], Bank and Welfred derive an estimate, bounded on both sides, which is a reasonable global estimate of the actual discretization error resulting from the uses of the mini–element [2]. A comparison of these methods found in [14] indicated that all estimates seem to be

a good indicator of the error and that they both require about a fourth of the computing time needed for the solution process.

Note that the above mentioned estimates only applies to the mini–element discretization of the Stokes problem. Assuming that the engineering interest is, as we have stated earlier, focused on the output of interest, then the norms presented in (2.136)-(2.136) are not relevant.

Less standard norms to measure the error have been proposed in [32, 4]. We first review the error estimators proposed by Ladeveze and al. which measure the error in the constitutive law of materials in the limit of incompressible solids. Note that, there is a direct analogy between an incompressible linear–elastic isotropic solid in equilibrium and an incompressible Newtonian fluid in the steady creeping limit [38]. We restate the constitutive law for linear elasticity:

$$\sigma_{ij} = \lambda_1 (\frac{\partial u_i}{\partial x_j} + \frac{\partial u_j}{\partial x_i}) + \lambda_2 \frac{\partial u_k}{\partial x_k} \delta_{ij}, \tag{2.138}$$

where σ_{ij} is the stress field, u is the displacement and λ_1, λ_2 are the Lamé constants. Introducing $\epsilon(u)$ to define the strain field associated with u and K the Hooke's operator, the constitutive law becomes

$$\sigma_{ij} = K\epsilon(u). \tag{2.139}$$

The error is measured in an energy like norm as

$$|e| = \|\hat{\sigma} - K\epsilon(\hat{u})\|, \tag{2.140}$$

where $\|\cdot\| = [\int_\Omega \mathrm{Tr}[\cdot K^{-1} \cdot] \, \mathrm{d}A]^{\frac{1}{2}}$ and Tr is the trace operator. The terms $\hat{\sigma}$ and $\hat{u}$ are calculated from the finite element approximation of the equilibrium equation. We note that the focus of their approach is to verify the kinematic constraints and the equilibrium equation rigorously contrasting with most other a *posteriori* error analysis approaches which focus on the equilibrium equation only.

Yet another estimator for the Stokes problem is found in [4], where the discretization error,

$$|||e_H, E_H||| = \left\{ \|r\|^2_{\mathcal{A}} + \|s\|^2_{\mathcal{C}} \right\}^{\frac{1}{2}} \tag{2.141}$$

is bounded from above by

$$|||e_H, E_H||| \leq \sum_{T_H \in \mathcal{T}_H} \left\{ \|r|_{T_H}\|^2_{\mathcal{A}(\mathcal{T}_\mathcal{H})} + \left\| \frac{\partial u_i}{\partial x_i} \right\|^2_{\mathcal{C}(\mathcal{T}_\mathcal{H})} \right\}. \tag{2.142}$$

where $\|\cdot\|_{\mathcal{A}}$ and $\|\cdot\|_{\mathcal{C}}$ are the norms associated with the inner products,

$$a(v,w) = \int_{\Omega} \frac{\partial v}{\partial x_i}\frac{\partial w}{\partial x_i}\,\mathrm{d}A, \qquad \forall v,w \in \mathcal{H}^1(\Omega), \tag{2.143}$$

$$c(p,q) = \int_{\Omega} pq\,\mathrm{d}A, \qquad \forall p,q \in L^2(\Omega). \tag{2.144}$$

In this approach only the calculation of r and u_H are required and can be obtain from two decoupled subdomain problems of Poisson type with Neumann data. Although this method has the advantage of being fast, it is still based on an energy norm (even though "untraditional") which is not relevant to our validation and confirmation objective in engineering design.

We remark that most of the previous work in the error estimation field is related to estimating the error for application to mesh adaptivity rather than for an engineering design framework. Therefore, we conclude that there is indeed a lack of methods for validation and confirmation which focused on rigorously quantifying the error in the outputs of interest. However, the usefulness of adaptive mesh technology is incontestable which indicated that we also should extend our technique to quantify the error locally for use in adaptive error control procedures.

Chapter 3

Bounds Formulation in One Space Dimension

3.1 Model Problem

3.1.1 Governing Equations

As our model problem we consider a second order ordinary differential equation for $u(x)$,

$$-\frac{\mathrm{d}^2 u}{\mathrm{d}x^2} + \alpha \frac{\mathrm{d}u}{\mathrm{d}x} + \beta u = f, \qquad \forall x \in \Omega, \tag{3.1}$$

$$u(0) = g_0, \; u(1) = g_1, \tag{3.2}$$

where (α, β) are positive constant coefficients and Ω is the domain $]0,1[$. Note that, for $\alpha = \frac{U}{\nu}$ and $\beta = 0$, we recognize the one–dimensional convection–diffusion problem.

The weak form of this equation is: For $f \in \mathcal{H}^{-1}(\Omega)$ find $u \in \mathcal{H}^1_D(\Omega)$ such that,

$$\int_0^1 \frac{\mathrm{d}v}{\mathrm{d}x}\frac{\mathrm{d}u}{\mathrm{d}x} + \alpha v \frac{\mathrm{d}u}{\mathrm{d}x} + \beta v u \, \mathrm{d}x = \int_0^1 v f \, \mathrm{d}x, \qquad \forall v \in \mathcal{H}^1_0(\Omega), \tag{3.3}$$

where

$$\mathcal{H}^1_D(\Omega) = \left\{ v \in \mathcal{H}^1(\Omega) |\; v(0) = g_0, \; v(1) = g_1 \right\}, \tag{3.4}$$

and

$$\mathcal{H}^1_0(\Omega) = \left\{ v \in \mathcal{H}^1(\Omega) |\; v(0) = 0, \; v(1) = 0 \right\}. \tag{3.5}$$

3.1.2 Output Linear Functionals

We shall consider three bounded and one unbounded linear–functional outputs s,

$$s^{(1)} = \ell^{(1)}(u) \quad \equiv \quad u(\overline{x}), \tag{3.6}$$

$$s^{(2)} = \ell^{(2)}(u) \equiv \int_0^1 u(x)\mathrm{d}x, \tag{3.7}$$

$$s^{(3)} = \ell^{(3)}(u) \equiv \int_0^1 \left(\frac{\mathrm{d}\mathcal{X}}{\mathrm{d}x}\frac{\mathrm{d}u}{\mathrm{d}x} + \alpha\mathcal{X}\frac{\mathrm{d}u}{\mathrm{d}x} + \beta\mathcal{X}u - \mathcal{X}f\right)\mathrm{d}x, \tag{3.8}$$

$$s^{(4)} = \ell^{(4)}(u) \equiv u_x(1), \tag{3.9}$$

where $\mathcal{X}(x)$ is any function in $\mathcal{H}^1_E(\Omega) = \{v \in \mathcal{H}^1(\Omega) |\ v(0) = 0,\ v(1) = 1\}$, and $\overline{x}$ is a particular point in $]0,1[$. The four outputs correspond to the value of $u(x)$ at $\overline{x}$, the average of $u(x)$ over Ω and the "flux" at $x = 1$ using a bounded and an unbounded linear functional, respectively. To show that $\ell^{(3)}(u) = u_x(1)$ we integrate by parts to obtain

$$\ell^{(3)}(u) = \int_0^1 \mathcal{X}\left(-\frac{\mathrm{d}}{\mathrm{d}x}\left(\frac{\mathrm{d}u}{\mathrm{d}x}\right) + \alpha\frac{\mathrm{d}u}{\mathrm{d}x} + \beta u - f\right)\mathrm{d}x + \mathcal{X}(1)u_x(1) - \mathcal{X}(0)u_x(0), \qquad \forall \mathcal{X}(x) \in \mathcal{H}^1_E(\Omega). \tag{3.10}$$

From (3.1) we see that the first term vanishes, and from the definition of the space $\mathcal{H}^1_E(\Omega)$ we recover the first derivative ("flux") at $x = 1$. Nevertheless, $\ell^{(3)}$ and $\ell^{(4)}$ are not equivalent. To show that $\ell^{(3)}$ is a bounded functional we use the Cauchy–Schwartz inequality to obtain,

$$|\ell^{(3)}(u)| \leq |\mathcal{X}|_{\mathcal{H}^1}|u|_{\mathcal{H}^1} + \alpha\|\mathcal{X}\|_{L^2}|u|_{\mathcal{H}^1} + \beta\|\mathcal{X}\|_{L^2}\|u\|_{L^2}. \tag{3.11}$$

Note that $\ell^{(3)}$ is affine therefore we only need to bound the linear part. Applying

$$|v|_{\mathcal{H}^1} \leq \|v\|_{\mathcal{H}^1} \qquad \forall v \in \mathcal{H}^1_0(\Omega), \tag{3.12}$$

$$\|v\|_{L^2} \leq \|v\|_{\mathcal{H}^1} \qquad \forall v \in \mathcal{H}^1_0(\Omega), \tag{3.13}$$

to (3.11), we finally obtain

$$|\ell^{(3)}(u)| \leq \|\mathcal{X}\|_{\mathcal{H}^1}\|u\|_{\mathcal{H}^1}, \tag{3.14}$$

and thus, $\ell^{(3)}(u)$ is bounded in $\mathcal{H}^1(\Omega)$.

In contrast, to show that $\ell^{(4)}(u)$ is unbounded, we write,

$$\ell^{(4)}(u) = \left.\frac{\mathrm{d}u}{\mathrm{d}x}\right|_{x=1} = \int_0^1 \frac{\mathrm{d}}{\mathrm{d}x}\left(\frac{\mathrm{d}u}{\mathrm{d}x}\right)\mathrm{d}x \tag{3.15}$$

and evoking the Cauchy–Schwartz inequality we see that

$$\ell^{(4)}(u) \leq |u|_{\mathcal{H}^2}\ (\geq |u|_{\mathcal{H}^1}), \tag{3.16}$$

which is clearly not bounded in $\mathcal{H}^1(\Omega)$. For example, we consider a function $u = x^{\frac{4}{3}}$ in $\mathcal{H}^1(\Omega)$ where $\Omega =]0,1[$. Now we look at square of the $\mathcal{H}^1$ seminorm of $\frac{\mathrm{d}u}{\mathrm{d}x}$, out output, and write

$$\int_0^1 \left(\frac{\mathrm{d}^2u}{\mathrm{d}x^2}\right)^2 \mathrm{d}x = \int_0^1 \frac{16}{81}x^{-\frac{4}{3}}\,\mathrm{d}x = \left[-\frac{16}{27}x^{-\frac{1}{3}}\right]_0^1 \tag{3.17}$$

which obviously in unbounded because it blows up at $x = 0$.

We conclude this section by noticing that the adjoint solution is sensitive to the choice of $\mathcal{X}$. If $\mathcal{X}$ is not smooth then we will see a jump in the adjoint derivative which may require additional mesh refinement to adequately resolve this feature. There are, in fact, many ways to choose $\mathcal{X}$ and we will discuss a few in Chapter 8. In addition, we point out that the boundary conditions on the adjoint presented here are for bounded functionals. When the output functional is not bounded, as $\ell(4)$, a different derivation must be employed, [35].

3.2 Variational Formulation

We present in this section the variational formulation for the bounds calculation in one space dimension.

3.2.1 Finite Element Approximation

We shall introduce here the general finite element ingredients required to construct the bounds.

Elements

For the one–dimensional problem we need to redefine the elemental decomposition ("triangulation"). Therefore, we define our subdomains to be all of equal length $H = 1/K$ as non–overlapping K subdomain T_H,

$$\overline{\Omega} = \bigcup_{T_H \in \mathcal{T}_H} \overline{T}_H, \tag{3.18}$$

where the overbar denotes closure. Similarly, we denote the set of all the N nodes of the triangulation by $\mathcal{M}(\mathcal{T}_H)$ where $\mathcal{T}_H$ is our subdomain discretization of Ω. Note that the nodes also correspond to the edges of the subdomain. For spatial discretization where the subdomain can include more than one element the reader should refer to [35, 46].

We next introduce the h–mesh triangulation $\mathcal{T}_h$, consisting of elements T_h of length h. Similarly, we require that $\mathcal{T}_h$ be a uniform R refinement of T_H as in (2.56) which yields R elements in each subdomain.

Bilinear and Linear Forms

We define here the bilinear and linear forms for the ordinary second order differential equations. We first define a space which permits discontinuities across edges of the h–mesh, a

"broken" $\mathcal{H}^1(\Omega)$ space, as

$$\mathcal{H}^1_*(\Omega) = \left\{ v \in L^2(\Omega) |\ v|_{T_H} \in \mathcal{H}^1(T_H),\ \forall T_H \in \mathcal{T}_H \right\}. \tag{3.19}$$

We then define the bilinear form associated with our operator as

$$a(w,v) = \sum_{T_H \in \mathcal{T}_H} a_{T_H}(w|_{T_H}, v|_{T_H}), \quad \forall w, v \in \mathcal{H}^1_*(\Omega), \tag{3.20}$$

where for all T_H in $\mathcal{T}_H$

$$a_{T_H}(w,v) = \int_{T_H} \frac{\mathrm{d}w}{\mathrm{d}x}\frac{\mathrm{d}v}{\mathrm{d}x} + \alpha w \frac{\mathrm{d}v}{\mathrm{d}x} + \beta w v \ \mathrm{d}x, \quad \forall w, v \in \mathcal{H}^1(T_H). \tag{3.21}$$

We shall also need the symmetric part of our operator,

$$a^s(w,v) = \sum_{T_H \in \mathcal{T}_H} a^s_{T_H}(w|_{T_H}, v|_{T_H}), \quad \forall w, v \in \mathcal{H}^1_*(\Omega), \tag{3.22}$$

where for all T_H in $\mathcal{T}_H$

$$a^s_{T_H}(w,v) = \int_{T_H} \frac{\mathrm{d}w}{\mathrm{d}x}\frac{\mathrm{d}v}{\mathrm{d}x} + \beta w v \ \mathrm{d}x, \quad \forall w, v \in \mathcal{H}^1(T_H). \tag{3.23}$$

Note that, for an element T_H, $a^s_{T_H}(,)$ is not the symmetric part of $a_{T_H}(,)$.

We next introduce a set of "jump" bilinear and linear forms which will be required in our variational relaxations. In particular, we define the bilinear form

$$b(v,t) = \sum_{k=2}^{K} t_k [v]_k + t_{K+1} v_{K+1} + t_1 v_1, \qquad \forall v \in \mathcal{H}^1_*(\Omega),\ t \in \mathcal{Q}, \tag{3.24}$$

where $\mathcal{Q} = \mathbf{R}^{K+1}$. Note that $[v]_k$ calculates the difference in values of the function v across the element boundaries at the interface k which is also a node. We also require the related linear functional associated with the Dirichlet conditions,

$$\ell^D(t) = \begin{cases} g_0 t_1 & x = 0 \\ g_1 t_{K+1} & x = 1 \\ 0 & \text{elsewhere} \end{cases} \qquad \forall t \in \mathcal{Q}. \tag{3.25}$$

We now introduce our linear functionals. Associated with the volumetric inhomogeneities, we have

$$\ell^N(v) = \sum_{T_H \in \mathcal{T}_H} \ell^N_{T_H}(v|_{T_H}), \quad \forall v \in \mathcal{H}^1_*(\Omega), \tag{3.26}$$

where for all T_H in $\mathcal{T}_H$

$$\ell^N_{T_H}(v) = \int_{T_H} vf \, \mathrm{d}x \quad \forall v \in \mathcal{H}^1(T_H). \tag{3.27}$$

Associated with our output functional, we have

$$\ell^O(v) = \sum_{T_H \in \mathcal{T}_H} \ell^O_{T_H}(v|_{T_H}), \quad \forall v \in \mathcal{H}^1_*(\Omega), \tag{3.28}$$

such that

$$\ell^O(v) = \ell(v), \quad \forall v \in \mathcal{H}^1(\Omega). \tag{3.29}$$

Here $\ell()$ is the formal output functional introduced in (2.49). Note that the construction (3.28)-(3.29) permits us to evaluate the output associated with a field variable which is not in $\mathcal{H}^1(\Omega)$.

Function Spaces

We first introduce the standard conforming linear approximation spaces,

$$X_\delta = \{v|_{T_\delta} \in \mathbf{P}_1(T_\delta), \forall T_\delta \in \mathcal{T}_\delta\} \bigcap \mathcal{H}^1_0(\Omega), \tag{3.30}$$

and

$$X^{D\pm}_\delta = \{v \pm u_D |\ v \in X_\delta\}, \tag{3.31}$$

where $u_D \in \mathcal{H}^1_D(\Omega)$ is any lifting of the Dirichlet boundary data, and $\mathbf{P}_1(T_\delta)$ is the space of linear polynomials over T_δ. Note that the $\pm$ in $X^{D\pm}_\delta$ refers to the Dirichlet boundary conditions on the field variable and on the adjoint. We shall need only $\delta = H$ and $\delta = h$ corresponding to our "working" and "truth" discretizations, respectively; from our refinement hypothesis, $X^{D\pm}_H \subset X^{D\pm}_h$ and $X_H \subset X_h$. Note that for the model problem described in Section 3.1 , u_D will be chosen such that $u_D|_{T_H} \in \mathbf{P}_1(T_H)$, $\forall T_H \in \mathcal{T}_H$ and u_D is the Dirichlet data g_D on Γ_D.

Finally, we introduce our subdomain–local spaces: for all T_H in $\mathcal{T}_H$,

$$Z_H(T_H) = (\mathbf{P}_1(T_H)), \tag{3.32}$$

and

$$Z_h(T_H) = \{v|_{T_H} \in \mathbf{P}_1(T_h), \forall T_h \in \mathcal{R}_{T_H}\} \bigcap \mathcal{H}^1(T_H), \tag{3.33}$$

where we recall that $\mathcal{R}_{T_H}$ is the set of h–mesh elements that constitute T_H. We can define the associated "product" spaces as

$$V_\delta = \{v_1 \in \mathcal{H}^1_*(\Omega) | v|_{T_H} \in Z_\delta(T_H), \forall T_H \in \mathcal{T}_H\}, \tag{3.34}$$

for $\delta = H$ and $\delta = h$. In essence, the $Z_\delta(T_H)$ are Neumann spaces over each T_H, for which V_δ is the corresponding global representation.

3.2.2 Construction of Augmented Lagrangian: Proof of Bounding Properties

Our approach is based on the construction of a Lagrangian with a quadratic objective function and linear constraints. From Section 2.4, it is clear that the bounds are obtained from the quadratic properties of this quadratic linear program.

We first construct the objective function of our augmented Lagrangian. For a δ–mesh, the original problem is: Find $u_\delta \in X_\delta^{D+}$ such that

$$a(v, u_\delta) = \ell^N(v), \qquad \forall v \in X_\delta. \tag{3.35}$$

By introducing any function g in X_δ^{D+} we can write

$$a(u_\delta - g, u_\delta) = \ell^N(u_\delta - g). \tag{3.36}$$

In addition, from (3.20) and (3.22), we write

$$a(u_\delta, u_\delta) = a^s(u_\delta, u_\delta) + c_\alpha, \tag{3.37}$$

where we recall that $a^s(,)$ is the symmetric part of $a(,)$. The c_α term in (3.37) arises from the convection operator which is given by $\alpha(g_1^2 - g_0^2)/2$.

Expanding (3.36), we obtain

$$a^s(u_\delta, u_\delta) + c_\alpha - \ell^N(u_\delta) - (a(g, u_\delta) - \ell^N(g)) = 0, \tag{3.38}$$

as the desired quadratic form that we want to include in our Lagrangian.

We can now express our linear–functional output $s_\delta (= \ell(u_\delta))$ — more precisely, $+s_\delta$ and $-s_\delta$ — as

$$\pm s_\delta = \mathcal{S}_\delta^\pm(u_\delta), \tag{3.39}$$

where

$$\mathcal{S}_\delta^\pm(v) = a^s(v, v) + c_\alpha - \ell^N(v) - [a(g, v) - \ell^N(g)] \pm \ell^O(v). \tag{3.40}$$

Note that, to allow for local decoupled problems we appeal to our "broken" space V_δ. We now introduce our two constraints to ensure the finite–element equilibrium equation and the intersubdomain continuity requirement which leads to the constrained minimization

problem,

$$\pm s_\delta = \min_{\left\{ v\in V_\delta \;\middle|\; \begin{array}{lll} a(w,v) & = \ell^N(w) & ,\ \forall w \in X_\delta \\ b(v,t) & = \ell^D(t) & ,\ \forall t \in \mathcal{Q} \end{array} \right\}} \mathcal{S}_\delta^\pm(v), \tag{3.41}$$

since for $v = u_\delta$ the objective reduces to $\pm\ell^O(u_\delta)$. We now form the Lagrangian associated with the constrained minimization problem: $\mathcal{L}_g^\pm : V_\delta \times X_\delta \times \mathcal{Q} \to \mathbf{R}$ as

$$\begin{aligned} \mathcal{L}_g^\pm(v,\mu',t) &= (a^s(v,v) + c_\alpha - \ell^N(v) - [a(g,v) - \ell^N(g)] \\ &\pm \ell^O(v)) + (a(\mu',v) - \ell^N(\mu')) - (b(v,t) - \ell^D(t)). \end{aligned} \tag{3.42}$$

Next, we absorb the "g" terms into the adjoint μ' to define an equivalent but simpler Lagrangian $\mathcal{L}^\pm : V_\delta \times X_\delta^{D-} \times \mathcal{Q} \to \mathbf{R}$ as

$$\begin{aligned} \mathcal{L}^\pm(v,\mu,t) &= a^s(v,v) + c_\alpha - \ell^N(v) \pm \ell^O(v) \\ &+ (a(\mu,v) - \ell^N(\mu)) - (b(v,t) - \ell^D(t)). \end{aligned} \tag{3.43}$$

Recall from (3.31) that X_δ^{D-} is a linear polynomial space with a negative translation of the Dirichlet data. One can perhaps view (3.43) as a slightly non–standard (in both form and application) augmented Lagrangian with respect to the output s_δ, [27]. Our hybridization contribution $b(v,t)$ is equivalent to the intersubdomain–continuity linear functionals of the earlier subdomain *a posteriori* procedures [3, 13, 31]. Note that, however, our objective function is different from those of previous methods and that our constraints include not only the intersubdomain continuity requirements but also the finite-element equilibrium equations.

It follows from the classical quadratic linear duality theory of Section 2.4 that

$$\pm s_\delta = \mathcal{S}_\delta^\pm(v) = \min_{v\in V_\delta} \sup_{\mu\in X_\delta^{D-},\, t\in\mathcal{Q}} \mathcal{L}^\pm(v,\mu,t) \tag{3.44}$$

$$= \max_{\mu\in X_\delta^{D-},\, t\in\mathcal{Q}} \inf_{v\in V_\delta} \mathcal{L}^\pm(v,\mu,t) \tag{3.45}$$

$$\geq \inf_{v\in V_\delta} \mathcal{L}^\pm(v,\hat{\mu},\hat{t}) \equiv \eta^\pm \tag{3.46}$$

$$\forall \hat{\mu},\hat{t} \in X_\delta^{D-} \times \mathcal{Q}.$$

Our approach to obtain bounds is to find candidate Lagrange multipliers, $\hat{\mu}$ and $\hat{t}$, and then to introduced them in (3.46). An inexpensive choice of candidate multipliers is to appeal to the H–mesh Lagrangian, $\mathcal{L}_H^\pm : V_H \times X_H^{D-} \times \mathcal{Q}$. By evoking stationarity we get

$$2a^s(w,u_H) + a(\psi_H^\pm, w) - \ell^N(w) \pm \ell^O(w) - b(w,y^\pm) = 0, \quad \forall w \in V_H, \tag{3.47}$$

$$a(w, u_H) - \ell^N(w) = 0, \quad \forall w \in X_H^{D-}, \tag{3.48}$$

$$b(u_H, \rho) - \ell^D(\rho) = 0, \quad \forall \rho \in \mathcal{Q}, \tag{3.49}$$

where $\psi_H^{\pm}$ and $y^{\pm}$ are the H–mesh Lagrange multipliers at stationarity. By constraining w to continuous spaces $X_H (\subset V_H)$ we eliminate the term $b(w, y^{\pm})$ in (3.47) because X_H is continuous and therefore has no intersubdomain jumps. We can then easily solve for $\psi_H^{\pm}$. Returning to our broken space we can use the same equation and solve for $y^{\pm}$. These H–mesh Lagrange multipliers can now serve as candidates for our h–mesh problem. Note that $X_H^{D-} \subset X_h^{D-}$ and therefore the adjoint in X_H^{D-} is a valid candidate multiplier and will yield valid bounds, $\eta^{\pm}$. The hybrid flux has no such subtleties; any choice on the H–mesh is a valid candidate on the h–mesh because both have the same number of intersubdomain edges.

3.2.3 Bound Procedure

We have seen that prior to calculating the bounds to our output of interest we need to find our Lagrange multiplier candidates: adjoint and hybrid flux. Therefore, our bounds procedure involves three steps. The first step determines the adjoint; the second step determines the hybrid flux; and the third step determines the local h–mesh solution from which we construct the bounds.

The H–Mesh Adjoint Calculation

We obtain an equation for the adjoint from a classical, albeit some what trivial, saddle problem (3.47)-(3.49) on the H–mesh. That is, once we solve for the field solution $u_H \in X_H^{D+}$ which satisfies

$$a(w, u_H) = \ell^N(w), \quad \forall w \in X_H, \tag{3.50}$$

and also directly satisfies

$$b(u_H, \rho) - \ell^D(\rho) = 0, \quad \forall \rho \in \mathcal{Q}, \tag{3.51}$$

we are able to calculate $\psi_H^{\pm} \in X_H^{D-}$ from (3.47) as,

$$a(\psi_H^{\pm}, w) = -(2a^s(w, u_H) - \ell^N(w) \pm \ell^O(w)), \quad \forall w \in X_H, \tag{3.52}$$

where all $\pm$ refer to the pair of solutions required to ultimately generate lower $(+)$ and $(-)$ bounds. By choosing the test function, w, to lie in X_H we are able to cancel the hybrid flux term in (3.47). We remark that the Dirichlet boundary conditions on the adjoint are the negative of the boundary conditions on the field solution.

We perform three system solves on the H–mesh to obtain the field solution, the adjoint

for the upper bound and the adjoint for the lower bound from (3.50)-(3.52). However, for direct strategies the work required to solve the three systems is only slightly larger that the work required to solve the single system (3.50) as we can exploit a LU decomposition; for iterative strategies, such economies of scale are more difficult to realize.

Knowing $\psi_H^{\pm}$ we are interested in rewriting (3.52) as an equation for u_H with all other terms on the right–hand side. Therefore, we rewrite (3.52) in two ways. In the first reformulation, we look for $u_H \in X_H^{D+}$ such that

$$2a^s(w, u_H) = -F^{\pm}(w; \psi_H^{\pm}), \quad \forall w \in X_H. \tag{3.53}$$

Here, for any function $\mathcal{F} \in \mathcal{H}_*^1(\Omega)$ and for all $v \in \mathcal{H}_*^1(\Omega)$ we write

$$F^{\pm}(v; \mathcal{F}) = \sum_{T_H \in \mathcal{T}_H} F_{T_H}^{\pm}(v|_{T_H}; \mathcal{F}), \quad \forall v \in \mathcal{H}_*^1(\Omega), \tag{3.54}$$

where for all T_H in $\mathcal{T}_H$

$$F_{T_H}^{\pm}(v; \mathcal{F}) = -\ell_{i\,T_H}^N(v) + a_{T_H}(\mathcal{F}|_{T_H}, v) \pm \ell_{T_H}^O(v), \quad \forall v \in \mathcal{H}_*^1(\Omega). \tag{3.55}$$

In some sense, $-F^{\pm}(v; \psi_H^{\pm})$ represents the sum of "forces" in (3.52) when solving for $u_H \in X_H^{D+}$.

In the second reformulation, we look for $u_H \in X_H^{D+}$ such that

$$B^{\pm}(w, u_H) = 0, \quad \forall w \in X_H. \tag{3.56}$$

Here, for any function $\mathcal{G} \in \mathcal{H}_*^1(\Omega)$, for all $v \in \mathcal{H}_*^1(\Omega)$

$$B^{\pm}(v; \mathcal{G}) = \sum_{T_H \in \mathcal{T}_H} B_{T_H}^{\pm}(v|_{T_H}; \mathcal{G}), \quad \forall v \in \mathcal{H}_*^1(\Omega), \tag{3.57}$$

where for all T_H in $\mathcal{T}_H$

$$B_{T_H}^{\pm}(v; \mathcal{G}) = 2a_{T_H}^s(v, \mathcal{G}|_{T_H}) + F_{T_H}^{\pm}(v, \psi_H^{\pm}), \quad \forall v \in \mathcal{H}_*^1(\Omega). \tag{3.58}$$

In effect, (3.56) is simply a restatement of equilibrium or balance.

The H–mesh Hybrid Flux Calculation

Recall that the intersubdomain continuity condition is that the values of v on each side of a subdomain boundary must be equal, $b(v, y^{\pm}) = \ell^D(y^{\pm})$, $\forall v \in X_H$. This coupling between elements can be relaxed while conserving the bounding properties of our estimators by allowing a different Lagrange multiplier (known as the hybrid flux). An inexpensive choice of

the hybrid flux is obtained by exploiting our H–mesh, in particular (3.47)-(3.49). Therefore, we look for $y^{\pm} \in \mathcal{Q}$ such that

$$b(v, y^{\pm}) = B^{\pm}(v, u_H), \qquad \forall v \in V_H, \tag{3.59}$$

which gives, for all T_H in $\mathcal{T}_H$,

$$[v]^L_{T_H} y^{\pm}|^L_{T_H} + [v]^R_{T_H} y^{\pm}|^R_{T_H} = B^{\pm}_{T_H}(v, u_H), \ \ \forall v \in Z_H(T_H), \tag{3.60}$$

where $[v]^L_{T_H}$ is the jump of v on the left side of element T_H. For implementation purposes it may be more useful to introduce two test function $(\zeta^L_{T_H}, \zeta^R_{T_H})$ such that the left and right hybrid fluxes $y^{\pm}|^L_{T_H}$ and $y^{\pm}|^R_{T_H}$ for all T_H in $\mathcal{T}_H$ are simply computed as,

$$y^{\pm}|^L_{T_H} = B^{\pm}_{T_H}(\zeta^L_{T_H}, u_H), \tag{3.61}$$

$$y^{\pm}|^R_{T_H} = -B^{\pm}_{T_H}(\zeta^R_{T_H}, u_H), \tag{3.62}$$

where $(\zeta^L_{T_H}, \zeta^R_{T_H})$ are the left and right basis function restricted to each element T_H. For our choice of subdomain — one element per subdomain — $\zeta^L_{T_H}$ is 1 and 0 respectively at the left and right ends of T_H corresponding to the left and right nodes. To demonstrate that (3.61) and (3.62) are consistent, that they yield the same hybrid flux on each side of an edge, we sum (3.61) and (3.62) over all T_H in $\mathcal{T}_H$; we obtain,

$$b(1, y^{\pm}) = B^{\pm}(1, u_H). \tag{3.63}$$

Because 1 is definitely in X_H, we get

$$b(1, y^{\pm}) = B^{\pm}(1, u_H) = 0, \tag{3.64}$$

and prove that both calculations of the hybrid flux on either side give the same result.

The h–mesh subdomain Neumann Problem

We now look for $\hat{u}^{\pm}_h \in Z_h(T_H)$, for all T_H in $\mathcal{T}_H$, such that

$$2a^s_{T_H}(w, \hat{u}^{\pm}_h) = -F^{\pm}_{T_H}(w; \psi^{\pm}_H) + [w]^L_{T_H} y^{\pm}|^L_{T_H} + [w]^R_{T_H} y^{\pm}|^R_{T_H}, \quad \forall w \in Z_h(T_H). \tag{3.65}$$

To write (3.65) in a global form we appeal to $\hat{\mathcal{U}}^{\pm}_h \in V_h$ where $\hat{\mathcal{U}}^{\pm}_h|_{T_H} = \hat{u}^{\pm}_h$, $\forall T_H \in \mathcal{T}_H$, then $\hat{\mathcal{U}}^{\pm}_h$ satisfies

$$2a^s(w, \hat{\mathcal{U}}^{\pm}_h) = -F^{\pm}(w; \psi^{\pm}_H) + b(w, y^{\pm}), \qquad \forall w \in V_h. \tag{3.66}$$

For a singular element ($a^s_{T_H}(v^s, v^s) = 0$), we require for solvability,

$$-F^{\pm}_{T_H}(v^s; \psi^{\pm}_H) + y^{\pm}|^L_{T_H} - y^{\pm}|^R_{T_H} = 0. \tag{3.67}$$

To show (3.67), we observe that $v^s = 1$ is in V_H and by summing (3.61) and (3.62) we obtain

$$y^{\pm}|^L_{T_H} - y^{\pm}|^R_{T_H} = B^{\pm}_{T_H}(v^s, u_H) = F^{\pm}_{T_H}(v^s, \psi^{\pm}_H), \tag{3.68}$$

as desired.

We make several remarks. First, note that for one dimensional problems, even if the calculation of $\hat{u}^{\pm}_h$ is performed on decoupled subdomains as K Neumann problems the cost is similar to solving the h–mesh system directly due to the tridiagonal structure of the one space dimensional finite element discretization. However, in higher dimension the work to compute the subdomain Neumann local problems is considerably less than the work to solve the global system $a(v, u_h) = \ell^N(v)$. Second, this approach imposes the Dirichlet conditions through the "equivalent" hybrid flux Lagrange multiplier on Γ_D [9]. A different procedure where the Dirichlet boundary conditions are imposed directly is presented for the one-dimensional convection diffusion problem in [35]. The advantage of the approach presented here is that all edges, including boundary edges, are treated in (almost) the same fashion. Third, as in other local–Neumann–problem *a posteriori* formulations [3, 13, 31] for equations without a positive diagonal term in the operator, e.g., βu with $\beta = 0$, we must verify that (3.65) does indeed have a solution, which in our context is equivalent to demonstrating that for the candidate Lagrangian multipliers chosen, (3.52) and (3.61)-(3.62) are in Y_{bd} defined in (2.95). We observe that the equilibration equation embedded in the space Y_{bd} is similar to the equilibration we require for solvability (3.67). In this context, we proved (3.68) because our candidates are in Y_{bd} as desired. This space corresponds to the set of functions for which the minimum of the Lagrangian is not $-\infty$.

Finally, we can now calculate the bounds as

$$(s_h)_{LB}(H) = \eta^+, \tag{3.69}$$

and

$$(s_h)_{UB}(H) = -\eta^-, \tag{3.70}$$

where

$$\eta^{\pm} = -a^s(\hat{\mathcal{U}}^{\pm}_h, \hat{\mathcal{U}}^{\pm}_h) + c_\alpha - \ell^N(\psi^{\pm}_h) + \ell^D(y^{\pm}). \tag{3.71}$$

We have seen that to calculate our bounds $\eta^{\pm}$ we minimize over all $v \in V_h$. Written in

another form, we look for,

$$\hat{\mathcal{U}}_h^{\pm} = \arg\min_{v \in V_h} \mathcal{L}^{\pm}(v, \psi_H^{\pm}, y^{\pm}), \tag{3.72}$$

such that

$$\mathcal{L}^{\pm}(\hat{\mathcal{U}}_h^{\pm}, \psi_H^{\pm} y^{\pm}) = \min_{v \in V_h} \mathcal{L}^{\pm}(v, \psi_H^{\pm}, y^{\pm}) \equiv \eta^{\pm}. \tag{3.73}$$

Recall that this problem is equivalent to solving the saddle problem for the Lagrangian defined for the h–mesh and (3.65) is in fact the first variation in w of this Lagrangian.

To show (3.72)-(3.73), we expand our Lagrangian (3.43) for $v = \hat{\mathcal{U}}_h^{\pm} + w$, $\mu = \psi_H^{\pm}$, and $t = y^{\pm}$, to obtain

$$\begin{aligned} \mathcal{L}^{\pm}(\hat{\mathcal{U}}_h^{\pm} + w, \psi_H^{\pm}, y^{\pm}) &= \mathcal{L}^{\pm}(\hat{\mathcal{U}}_h^{\pm}, \psi_H^{\pm}, y^{\pm}) \\ &\quad + 2a^s(w, \hat{\mathcal{U}}_h^{\pm}) + F^{\pm}(w, \psi_H^{\pm}) - b(w, y^{\pm}) \\ &\quad + a^s(w, w), \qquad \forall w \in V_h. \end{aligned} \tag{3.74}$$

For $\hat{\mathcal{U}}_h^{\pm}$ to be a minimum, we require that that all linear terms in w vanish, that is

$$2(w, \hat{\mathcal{U}}_h^{\pm}) = -F^{\pm}(w, \psi_H^{\pm}) + b(w, y^{\pm}), \qquad \forall w \in V_h. \tag{3.75}$$

which is therefore used to compute $\hat{\mathcal{U}}_h^{\pm}$. However this system is never formed, we use the equivalent subdomain form introduced earlier in this Section.

We close this section by summarizing some of the attributes of our technique. First, by including the equilibrium equation as a constraint in our Lagrangian — standard practice in our optimization and control applications — we "automatically" obtain the necessary error residual equation (2.102). In particular, we do not exploit orthogonality (2.52) as in Becker and Rannacher [16, 17, 41]. Neither do we use energy minimization in our variational statement as in [3, 13]. Recall the equilibrium residual method of Section 2.5, where the quadratic function (2.104) is only constructed for symmetric operators. Thus, our formulation is not specific to finite element projection, but can, in fact, be applied to any "nodal" partial–differential–equation discretization procedure.

Second, by hybridizing the finite element equations and including these conditions as constraints in our Lagrangian, only local problems are encountered on the h-mesh similar to earlier proposals which have lead to decoupled local systems (2.105). Third, by virtue of the energy equality we are able to treat general nonsymmetric systems even though only local (well–conditioned, "unsquared") symmetric problems need to be solved on the truth mesh; this symmetrization is achieved without modifying the norm of the resulting estimates. Many *a posteriori* estimation procedures originally proposed or illustrated for symmetric problems also readily extend to nonsymmetric problems [12, 8, 47]; however, most bound

techniques have been applied only to symmetric problems [3, 32]. Fourth, and perhaps most importantly, by appropriate choice of the objective function contribution to the augmented Lagrangian, we automatically generate the "inhomogeneities" required to obtain rigorous duality bounds for the linear–functional and, even more general, outputs typically of interest to engineering analysis. Fifth, a simple sign artifice $\pm s_\delta$ provides both lower and upper bounds, often an advantage in design problems with one-sided inequality constraints or Pareto preferences [29]. Sixth, thanks to the duality arguments, no *a priori* approximation or stability results are required to evaluate bounds; in contrast to [16, 17, 41], all constants are readily computed as part of the procedure and thus there is complete certainty in the final result (to within the truth assumption). Recall that in [16, 17, 41] an upper bound is obtained for the error on the output, (2.123), however this latter involves constants that are difficult to evaluate. Seventh, "good" choices for the adjoint and the hybrid flux are directly obtained from the Lagrangian saddlepoint condition on the H–mesh assuming the location of the saddlepoint on the H–mesh to be relatively close to the location of the saddlepoint of the h–mesh.

3.3 Algebraic Formulation

3.3.1 Finite Element Approximation

Discrete Equations

For purposes of simplicity we consider a linear Galerkin finite element approximation on a uniform mesh with grid-spacing δ [43, 30]. We introduce the classical continuous–piecewise–polynomial finite–element subspaces $\underline{X}_\delta \subset \mathcal{H}^1_0(\Omega)$, $\underline{X}^D_\delta \subset \mathcal{H}^1(\Omega)$, $\underline{X}^E_\delta \subset \mathcal{H}^1_0(\Omega)$, which we express in terms of the standard nodal basis,

$$\underline{X}_\delta = \text{span}\{\varphi_{\delta 2}(x), ..., \varphi_{\delta n_\delta - 1}(x)\}, \tag{3.76}$$

$$\underline{X}^{D\pm}_\delta = \{v^{D\pm}(x) = v(x) \pm g_0\varphi_{\delta 1}(x) \pm g_1\varphi_{\delta n_\delta}(x) |\ v(x) \in \underline{X}_\delta\}, \tag{3.77}$$

$$\underline{X}^E_\delta = \{v^E(x) = v(x) + \varphi_{\delta n_\delta}(x) |\ v(x) \in \underline{X}_\delta\}. \tag{3.78}$$

Here $\varphi_{\delta j}(x)$ is the piecewise–linear hat function associated with node $x_{\delta j} = (j-1)\delta$, $j = 1, ..., n_\delta$: note that $n_\delta = \delta^{-1} + 1$ is the number of nodes in Ω including the boundary nodes. We now look for $u_\delta \in \underline{X}^{D+}_\delta$ such that

$$\int_0^1 (\frac{\mathrm{d}w}{\mathrm{d}x}\frac{\mathrm{d}u_\delta}{\mathrm{d}x} + \alpha w\frac{\mathrm{d}u_\delta}{\mathrm{d}x} + \beta w u_\delta)\mathrm{d}x = \int_0^1 wf\mathrm{d}x, \quad \forall w \in \underline{X}_\delta, \tag{3.79}$$

where all the quadratures are assumed exact.

To obtain the finite element approximation of the solution $u(x)$, we expand $u_\delta(x) \in \underline{X}^{D+}_\delta$

as

$$u_\delta(x) = \sum_{j=1}^{n_\delta} (\underline{u}_\delta)_j \varphi_{\delta j}(x), \qquad (\underline{u}_\delta)_1 = g_0,\ (\underline{u}_\delta)_{n_\delta} = g_1, \tag{3.80}$$

and the test function $w(x) \in \underline{X}_\delta$,

$$w(x) = \sum_{j=1}^{n_\delta} (\underline{w}_\delta)_j \varphi_{\delta j}(x), \qquad (\underline{w}_\delta)_1 = 0,\ (\underline{w}_\delta)_{n_\delta} = 0, \tag{3.81}$$

where $(\underline{u}_\delta)_j$ and $(\underline{w}_\delta)_j$ are the j^{th} component of $\underline{u}_\delta \in \mathbf{R}^{n_\delta}$ and $\underline{w}_\delta \in \mathbf{R}^{n_\delta}$, the vector of nodal values and of the test function, respectively. We then insert the expansions (3.80)-(3.81) into the weak form (3.79) to arrive,

$$\underline{w}_\delta^T [\underline{L}_\delta \underline{u}_\delta - \underline{f}_\delta] = 0, \qquad \forall \underline{w}_\delta \in \mathcal{R}_\delta \tag{3.82}$$

where $\underline{L}_\delta \in \mathbf{R}^{n_\delta \times n_\delta}$ is the system matrix, $\underline{f}_\delta \in \mathbf{R}^{n_\delta}$ is the inhomogeneity vector and $\mathcal{R}_\delta = \{\underline{v}_\delta \in \mathbf{R}^{n_\delta} | (\underline{v}_\delta)_1 = 0,\ (\underline{v}_\delta)_{n_\delta} = 0\}$. The latter space is introduced, maybe as an abuse of notation, to remind us of the boundary condition applied when deriving the discrete system of equations. Here $()^T$ refers to algebraic transpose. We use the discrete form (3.82) extensively in this section for two reasons: first, we directly observe that the first and last row of the system $\underline{L}_\delta \underline{u}_\delta = \underline{f}_\delta$ are non admissible equations because the test function is zero for those rows; and seconds, we can relate more easily this form to the variational form (3.50). To solve for the "interior" unknowns, $\tilde{\underline{u}}_\delta = (\underline{u}_\delta)_2, ..., (\underline{u}_\delta)_{n_\delta - 1}$, that is find the discrete system of equations with corresponding boundary conditions, we take the coefficients $(\underline{w}_\delta)_i = \underline{e}_i$ for $i = 1, ..., n_\delta$ where the $\underline{e}_i$ are the unit vectors in each of the n_δ directions of R^{n_δ} and eliminate the entries $i = 1$ and $i = n_\delta$ for which $(x)_1$ and $(x)_{n_\delta}$ are the endpoints of Ω. We also need to move the first and last columns of $\underline{L}_\delta$ to the right–hand side, as usual for non-homogeneous Dirichlet boundary conditions. The resulting linear system is,

$$\tilde{\underline{L}}_\delta \tilde{\underline{u}}_\delta = \tilde{\underline{f}}_\delta - (\underline{u}_\delta)_1 (\underline{L}_\delta)_{i,1} - (\underline{u}_\delta)_{n_\delta} (\underline{L}_\delta)_{i,n_\delta}, \qquad i = 2, ..., n_\delta - 1, \tag{3.83}$$

where $\tilde{}$ represents all the values not associated with the first and last rows.

We evaluate the components in (3.82) in terms of our basis functions. In particular, the discrete operator is given by

$$(\underline{L}_\delta)_{i,j} = \int_0^1 \left(\frac{\mathrm{d}\varphi_{\delta\, i}}{\mathrm{d}x} \frac{\mathrm{d}\varphi_{\delta\, j}}{\mathrm{d}x} + \alpha \varphi_{\delta\, i} \frac{\mathrm{d}\varphi_{\delta\, j}}{\mathrm{d}x} + \beta \varphi_{\delta\, i} \varphi_{\delta\, j}\right) \mathrm{d}x, \qquad 1 \le i, j \le n_\delta, \tag{3.84}$$

where $(\underline{L}_\delta)_{i,j}$ denotes the (i, j) member of $\underline{L}_\delta$. Similarly, the inhomogeneity takes the form

$$(\underline{f}_\delta)_i = \int_0^1 \varphi_{\delta\, i} f \ \mathrm{d}x, \qquad 1 \le i \le n_\delta. \tag{3.85}$$

In the analysis that follows we shall also require a symmetric operator,

$$(\underline{A}_\delta)_{i,j} = \int_0^1 (\frac{\mathrm{d}\varphi_{\delta\, i}}{\mathrm{d}x}\frac{\mathrm{d}\varphi_{\delta\, j}}{\mathrm{d}x} + \beta\varphi_{\delta\, i}\varphi_{\delta\, j})\,\mathrm{d}x, \quad 1 \le i,j \le n_\delta. \tag{3.86}$$

where $\underline{A}_\delta$ differs from the symmetric part of $\underline{L}_\delta$ by $\pm\frac{1}{2}$ in the first and last diagonal terms. We note that, for $\beta = 0$, $(\underline{A}_\delta)$ is simply the discrete Laplacian.

To express our outputs as a discrete linear functional of the field solution $\underline{u}_\delta$, we write

$$s_\delta^{(q)} = \underline{u}_\delta^T \underline{\ell}_\delta^{(q)}, \quad q = 1, ..., 4, \tag{3.87}$$

where $\underline{\ell}_\delta^{(q)} \in \mathbf{R}^{n_\delta}$ are defined by

$$(\underline{\ell}_\delta^{(q)})_i = \ell^{(q)}(\varphi_{\delta\, i}), \quad 1 \le i \le n_\delta. \tag{3.88}$$

The output functionals have the following algebraic expressions. For the pointwise output we find

$$\underline{\ell}_\delta^{(1)} = (00 \ldots 010 \ldots)^T, \tag{3.89}$$

where the single nonzero entry is for $j = \overline{x}/\delta$, assumed integral. For the average output we simply obtain

$$\underline{\ell}_\delta^{(2)} = \delta(11 \ldots 1)^T, \tag{3.90}$$

while for our flux output we include our discrete operator $\underline{L}_\delta$ such as, for all $\mathcal{X}^T \in \underline{X}_\delta^E$

$$\underline{\ell}_\delta^{(3)} = \underline{\mathcal{X}}^T \underline{L}_\delta - \underline{\mathcal{X}}^T \underline{f}_\delta, \tag{3.91}$$

where the choice of $\underline{\mathcal{X}}$ will be discussed in Chapter 8. Note, that this functional is equivalent to the first derivative of $u(x)$ at $x = 1$. Finally, the unbounded flux functional is simply,

$$\underline{\ell}_\delta^{(4)} = \frac{1}{\delta}(0 \ldots -11)^T. \tag{3.92}$$

These discrete functionals have the same bounding and un-bounding properties as discussed in Section 3.1.2.

Domain Decomposition Formulation

We can successfully reduce the computational cost by solving the h–mesh problem on subdomains with continuity imposed at the intersubdomain boundaries. For one space dimension, this technique will decrease the computation time because the discrete operator $\underline{L}_\delta$ is tridiagonal. Nevertheless, for simplicity, the one dimension model problem is best to describe this technique.

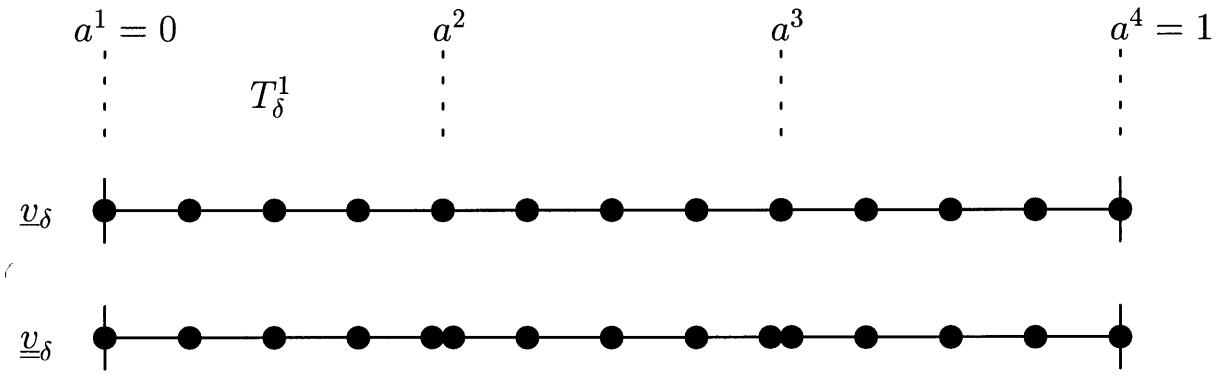

Figure 3-1: Coupled ($\underline{v}_\delta$) and decoupled ($\underline{\underline{v}}_\delta$) vectors of unknowns.

We introduce a H–mesh elemental decomposition ($\mathcal{T}_H$) of Ω consisting of K elements T_H such that,

$$\overline{\Omega} = \bigcup_{k=1}^{K} \overline{T}_H^k, \tag{3.93}$$

where $\overline{\Omega}$ is the closure of Ω.

For simplicity, we require that each subdomain T_H is of equal length $\delta = H$ and contains only one element. A similar derivation for subdomains with multiple H–mesh elements can be found in [35, 46]. We next uniformly refine our T_H element to construct the h–mesh "triangulation" $\mathcal{T}_h$, consisting of R elements T_h per subdomain, each of length $h = \frac{1}{RK}$. Therefore, the subdomain boundaries coincide with nodes, as shown in Figure 3-1. We introduce the intersubdomain node identification, J_δ^k, $k = 1, ..., K+1$, associated with the subdomain edge location a^k, $k = 1, ..., K+1$, where

$$a^1 = 0 < a^2 < ... < a^k = (k-1)H < .... < a^{K+1} = 1, \tag{3.94}$$

and

$$T_H^k =]a^k, a^{k+1}[. \tag{3.95}$$

It follows that $J_\delta^k = (k-1)n_\delta/K$, $k = 1, ..., K+1$ and the number of local nodes corresponding to each subdomain is $M_\delta = n_\delta/K + 1$. Finally, the total number of degrees–of–freedom is $\hat{n}_\delta = n_\delta + K - 1$ where the nodes on subdomain boundaries are counted twice, once for each participating subdomain. Note that when $\delta = H$, we have $M_H = 2$ and $J_H^k = k$, $k = 1, ..., K+1$. We present in Figure 3-1 vectors $\underline{v}_\delta \in \mathbf{R}^{n_\delta}$ and $\underline{\underline{v}}_\delta \in \mathbf{R}^{\hat{n}_\delta}$ which illustrates the coupled and decoupled enumeration, respectively.

Our subdomain matrix operators are then define as the appropriate restrictions of the

underlying bilinear forms to subdomain T_H^k, $k = 1, ..., K$,

$$(\underline{L}_\delta^k)_{i,j} = \int_{a^k}^{a^{k+1}} (\frac{\mathrm{d}\varphi_{\delta\, i+J_\delta^k-1}}{\mathrm{d}x}\frac{\mathrm{d}\varphi_{\delta\, j+J_\delta^k-1}}{\mathrm{d}x} + \alpha\varphi_{\delta\, i+J_\delta^k-1}\frac{\mathrm{d}\varphi_{\delta\, j+J_\delta^k-1}}{\mathrm{d}x} + \beta\varphi_{\delta\, i+J_\delta^k-1}\varphi_{\delta\, j+J_\delta^k-1})\mathrm{d}x, \quad 1 \le i,j \le M_\delta, \tag{3.96}$$

$$(\underline{A}_\delta^k)_{i,j} = \int_{a^k}^{a^{k+1}} (\frac{\mathrm{d}\varphi_{\delta\, i+J_\delta^k-1}}{\mathrm{d}x}\frac{\mathrm{d}\varphi_{\delta\, j+J_\delta^k-1}}{\mathrm{d}x} + \beta\varphi_{\delta\, i+J_\delta^k-1}\varphi_{\delta\, j+J_\delta^k-1})\mathrm{d}x, \quad 1 \le i,j \le M_\delta.$$

Note that $\underline{A}_\delta^k \neq \mathrm{sym}(\underline{L}_\delta^k)$. Similarly, the restriction of the inhomogeneity term and of the output linear functional to each subdomain is given as, for all T_H^k, $k = 1, ..., K$,

$$(\underline{f}_\delta^k)_i = \int_{a^k}^{a^{k+1}} (\varphi_{\delta\, i+J_\delta^k-1} f)\, \mathrm{d}x, \quad 1 \le i \le M_\delta, \tag{3.97}$$

and

$$(\underline{\ell}_\delta^{(q)})_i = \ell^{(q)}|_{T_H^k}. \tag{3.98}$$

For the pointwise output at $x = \overline{x}$ located at the intersubdomain we interpret any δ–function to reside equally in the two participating elements.

We next introduce two operators that will play a role in the nonconforming hybrid flux calculations: $\underline{Q}_\delta \in \mathbf{R}^{\hat{n}_\delta \times n_\delta}$ and $\underline{R}_\delta \in \mathbf{R}^{(K+1)\times \hat{n}_\delta}$ related to assembly and intersubdomain continuity, respectively. The operator $\underline{Q}_\delta$ is given by

$$(\underline{Q}_\delta)_{i,j} = \begin{cases} 1 & i = j + (k-1), J_\delta^k \le j \le J_\delta^{k+1}, k = 1, ..., K \\ 0 & \text{otherwise} \end{cases}. \tag{3.99}$$

For any $\underline{v}_\delta \in \mathbf{R}^{n_\delta}$, $\underline{Q}_\delta \underline{v}_\delta$ assigns the specified global nodal values to the nodes local to each subdomain, similarly to the "mortar" operator of [7, 18]. To be more explicit, we show $\underline{Q}_\delta$

for our $K = 3$ example in Figure 3-1,

$$\underline{Q}_\delta = \begin{pmatrix} 1 & 0 & ... & 0 & & & & & & & \\ 0 & 1 & \ddots & \vdots & & & & & & & \\ \vdots & \ddots & 1 & 0 & & & & & & & \\ 0 & ... & 0 & 1 & & & & & & & \\ & & & 1 & 0 & ... & 0 & & & & \\ & & & 0 & 1 & \ddots & \vdots & & & & \\ & & & \vdots & \ddots & 1 & 0 & & & & \\ & & & 0 & ... & 0 & 1 & & & & \\ & & & & & & 1 & 0 & ... & 0 \\ & & & & & & 0 & 1 & \ddots & \vdots \\ & & & & & & \vdots & \ddots & 1 & 0 \\ & & & & & & 0 & ... & 0 & 1 \end{pmatrix} . \tag{3.100}$$

Note that some columns have two non–zero entries associated with the decoupled intersubdomain rows.

The operator $\underline{R}_\delta$ is defined, as

$$(\underline{R}_\delta)_{i,j} = \begin{cases} 1 & j = J_\delta^k + (k-1) \\ -1 & j = J^{k+1} + (k-1) \\ 0 & \text{otherwise} \end{cases} , k \leq i \leq k+1, k = 1, ..., K \quad . \tag{3.101}$$

For our running example the operator $\underline{R}_\delta$ is

$$\underline{R}_\delta = \begin{pmatrix} 1 & 0 & ... & 0 & 0 & 0 & 0 & ... & 0 & 0 & 0 & 0 & ...0 & 0 \\ 0 & 0 & ... & 0 & -1 & 1 & 0 & ... & 0 & 0 & 0 & 0 & ...0 & 0 \\ 0 & 0 & ... & 0 & 0 & 0 & 0 & ... & 0 & -1 & 1 & 0 & ...0 & 0 \\ 0 & 0 & ... & 0 & 0 & 0 & 0 & ... & 0 & 0 & 0 & 0 & ...0 & -1 \end{pmatrix} . \tag{3.102}$$

For any $\underline{\underline{v}}_\delta \in \mathbf{R}^{\hat{n}_\delta}$, $\underline{R}_\delta \underline{\underline{v}}_\delta$ evaluates the jumps in $\underline{\underline{v}}_\delta$ across the $K-1$ subdomain boundaries and the jump at both endpoints of the domain. This operator $\underline{R}_\delta$ serves the same purpose as the hybrid flux operator (3.24) of the variational form in Section 3.2. In Figure 3-2, we present, for two different types of mesh discretizations, an illustration of these jumps occuring at the edges of the subdomains (represented by bullets). The intersubdomain continuity constraint imposed by $\underline{R}_\delta$ requires that these jumps are equal to zero. Operators analogous to $\underline{Q}_\delta$ and $\underline{R}_\delta$ are common in earlier *a posteriori* analysis [3, 5, 13].

We can now form the block–diagonal operator $\underline{\underline{L}}_\delta \in \mathbf{R}^{\hat{n}_\delta \times \hat{n}_\delta}$ and $\underline{\underline{A}}_\delta \in \mathbf{R}^{\hat{n}_\delta \times \hat{n}_\delta}$ containing

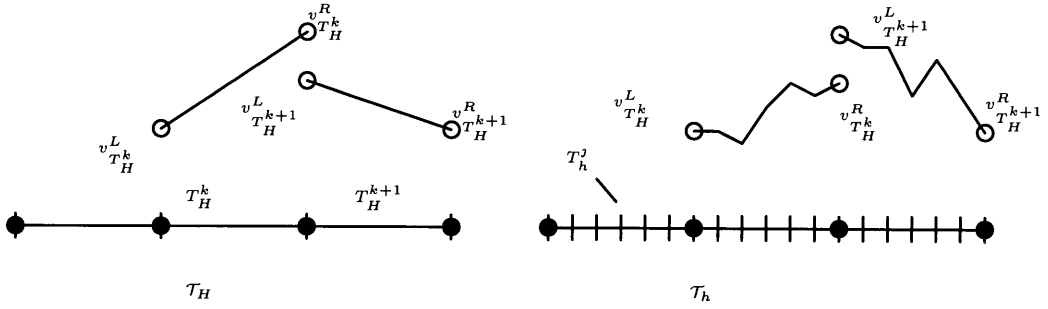

Figure 3-2: Illustration of intersubdomain $\underline{v}_\delta$ jumps.

the assembled, decoupled subdomain matrices (3.96), (3.97) as

$$(\underline{\underline{L}}_\delta)_{i,j} = \begin{cases} (\underline{\underline{L}}^k_\delta)_{i-\tilde{J}^k_\delta+1,j-J^k_\delta+1} & J^k_\delta \le i,j \le J^{k+1}_\delta,\ k=1,...,K, \\ 0 & \text{otherwise} \end{cases}, \tag{3.103}$$

and

$$(\underline{\underline{A}}_\delta)_{i,j} = \begin{cases} (\underline{\underline{A}}^k_\delta)_{i-\tilde{J}^k_\delta+1,j-J^k_\delta+1} & J^k_\delta \le i,j \le J^{k+1}_\delta,\ k=1,...,K, \\ 0 & \text{otherwise} \end{cases}, \tag{3.104}$$

respectively, and the vectors $\underline{\underline{f}}_\delta \in \mathbf{R}^{\hat{n}_\delta}$ and $\underline{\underline{\ell}}_\delta \in \mathbf{R}^{\hat{n}_\delta}$ containing the assembled inhomogeneities and linear functionals (3.97), (3.98) as

$$(\underline{\underline{f}}_\delta)_i = (\underline{\underline{f}}^k_\delta)_{i-J^k_\delta+1} \quad J^k_\delta \le i \le J^{k+1}_\delta, k=1,...,K, \tag{3.105}$$

and

$$(\underline{\underline{\ell}}_\delta)_i = (\underline{\underline{\ell}}^k_\delta)_{i-J^k_\delta+1} \quad J^k_\delta \le i \le J^{k+1}_\delta, k=1,...,K, \tag{3.106}$$

respectively. It then follows that

$$\underline{L}_\delta = \underline{Q}^T_\delta \underline{\underline{L}}_\delta \underline{Q}_\delta \tag{3.107}$$

$$\underline{A}_\delta = \underline{Q}^T_\delta \underline{\underline{A}}_\delta \underline{Q}_\delta \tag{3.108}$$

$$\underline{f}_\delta = \underline{Q}^T_\delta \underline{\underline{f}}_\delta \tag{3.109}$$

$$\underline{\ell}_\delta = \underline{Q}^T_\delta \underline{\underline{\ell}}_\delta \tag{3.110}$$

which is simply a restatement of the assembly process. In effect, the column and row summing actions of $\underline{Q}_\delta$ and $\underline{Q}^T_\delta$ corresponds to pulling together the decoupled matrix $\underline{\underline{L}}_\delta$ to its original form $\underline{L}_\delta$. This assembly process is less transparent in the variational form; it involves testing on a continuous space or on a broken space as in (3.52) and (3.59).

Finally, we remark that the unique solution $\underline{\underline{v}}_\delta \in \mathbf{R}^{\hat{n}_\delta}$ to the system

$$\underline{w}_\delta^T[\underline{Q}_\delta^T \underline{\underline{L}}_\delta \underline{\underline{v}}_\delta - \underline{f}_\delta] = 0, \quad \forall \underline{w}_\delta \in \mathcal{R}_\delta, \tag{3.111}$$

$$\underline{\rho}_\delta^T[\underline{R}_\delta \underline{\underline{v}}_\delta - \underline{d}_\delta] = , \quad \forall \underline{\rho}_\delta \in \mathbf{R}^{K+1}, \tag{3.112}$$

is $\underline{\underline{v}}_\delta = \underline{\underline{u}}_\delta$, where

$$\underline{\underline{u}}_\delta \equiv \underline{\underline{Q}}_\delta \underline{u}_\delta, \tag{3.113}$$

and

$$(\underline{d}_\delta)_i = \begin{cases} g_0 & i = 1 \\ -g_1 & i = K+1 \\ 0 & \text{otherwise} \end{cases} . \tag{3.114}$$

We write (3.111) without applying the boundary condition yet but remembering that $\mathcal{R}_\delta$ contains these conditions. This way we avoid any confusion regarding the first and last rows of $\underline{\underline{L}}_\delta$. Recall $\underline{u}_\delta$ is the solution to our original finite element system (3.82). To show that we recover the original system (3.82) , we insert (3.113) into (3.111) to obtain

$$\underline{w}_\delta^T[\underline{Q}_\delta^T \underline{\underline{L}}_\delta \underline{\underline{Q}}_\delta \underline{u}_\delta - \underline{f}_\delta] = 0, \quad \forall \underline{w}_\delta \in \mathcal{R}_\delta. \tag{3.115}$$

From (3.107) we obtain (3.82). Furthermore, we insert (3.113) into (3.112) and we write

$$\underline{\rho}_\delta^T[\underline{R}_\delta \underline{\underline{Q}}_\delta \underline{u}_\delta - \underline{d}_\delta] = 0, \quad \forall \underline{\rho}_\delta \in \mathbf{R}^{K+1}. \tag{3.116}$$

We now verify that (3.116) is satisfied. By applying the boundary conditions, for all $\underline{u}_\delta \in \underline{X}_\delta^{D+}$, we have the first and the last row equations satisfied. We then take $(\underline{t}_\delta)_i = \underline{e}_i$, for $i = 1, ..., K+1$ ($\underline{e}_i$ is the unit vector in each of the dimensions of R^{K+1}) such that (3.116) becomes

$$\underline{\tilde{R}}_\delta \underline{\tilde{Q}}_\delta \underline{\tilde{u}}_\delta = \underline{0}, \tag{3.117}$$

where $\underline{\tilde{u}}_\delta \in \mathbf{R}^{n_\delta - 2}$, is $\underline{u}_\delta$ with first and last entries eliminated, $\underline{\tilde{R}}_\delta$ is $\underline{R}_\delta$ with the first and last row eliminated and $\underline{\tilde{Q}}_\delta$ is $\underline{Q}_\delta$ with the first and last rows and columns eliminated. We observe that (3.117) is satisfied because $\underline{\tilde{Q}}_\delta$ (of rank $n_\delta - 2$) is the right nullspace of $\underline{\tilde{R}}_\delta$ (of rank $K-1$). Uniqueness of the solution to (3.111)–(3.112) then follows when $\underline{\underline{L}}_\delta$ is coercive. This system is, in some sense, "half–hybridized": we separately impose continuity on $u_h(x)$ through the jump constraint of $\underline{R}_\delta$ in (3.116), but directly impose continuity on the test function through the row–summing action of $\underline{Q}_\delta^T$ in (3.111). We can relate the row–summing action of $\underline{Q}_\delta^T$ to the variational formulation where the hybrid flux term vanishes for continuous test function $w \in X_H$ in (3.52). To fix ideas, we show in Figure 3-3 the structure of $\underline{L}_\delta$, $\underline{\underline{L}}_\delta$ and $\underline{Q}_\delta^T \underline{\underline{L}}_\delta$ for our running example.

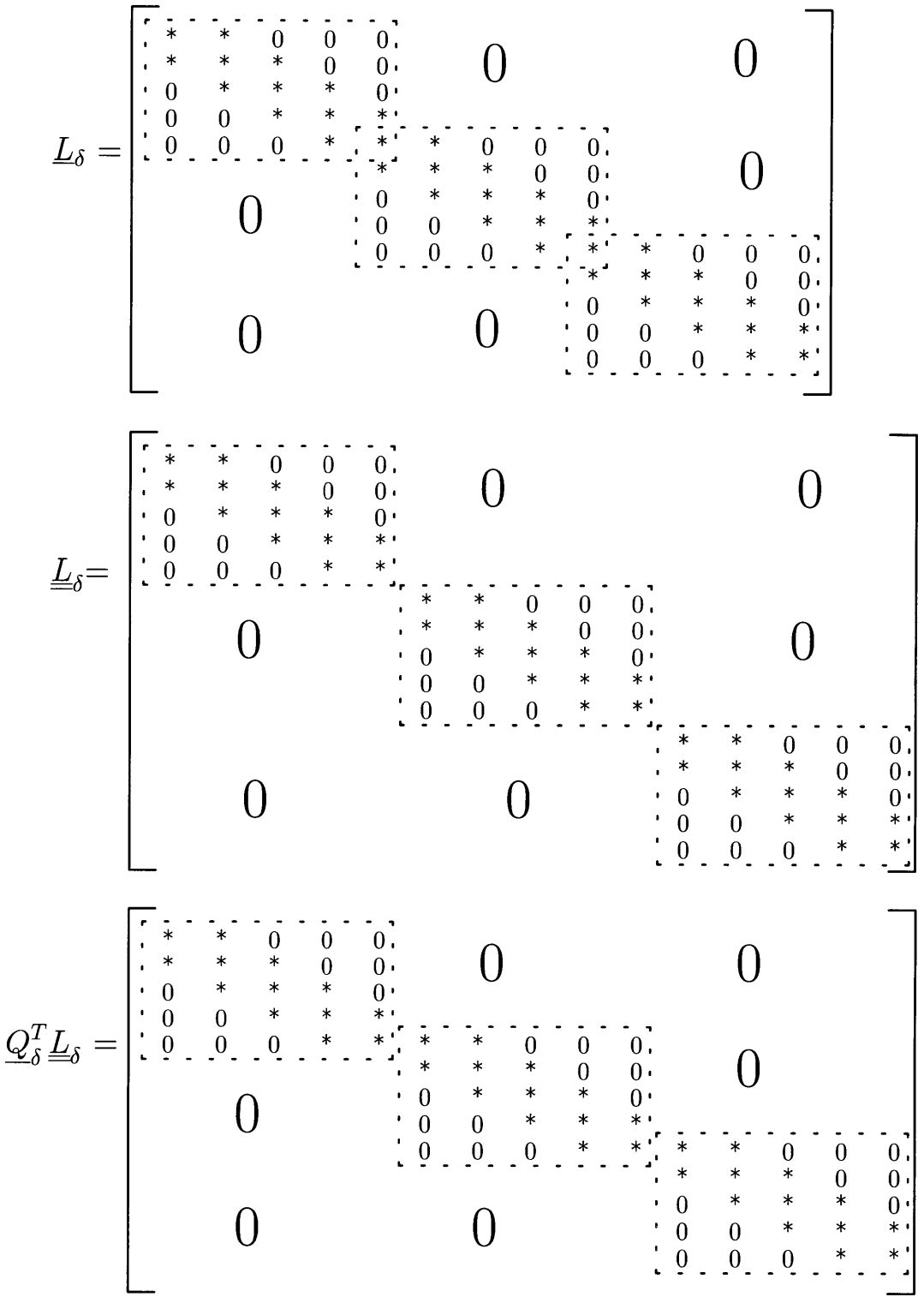

Figure 3-3: Structure of the standard ($\underline{L}_\delta$), domain–decomposition decoupled ($\underline{\underline{L}}_\delta$), and half–hybridized ($\underline{Q}_\delta^T \underline{\underline{L}}_\delta$) discrete operators for the domain decomposition of Figure 3-1: the $*$ indicate nonzero entries.

3.3.2 Construction of our Augmented Lagrangian: Proof of Bounding Properties

We proceed similarly to Section 3.2.2: first, we derive a simple energy equality; second, we construct our augmented Lagrangian; and third, we appeal to the duality results to proof our bounding properties. To begin, we multiply (3.82) by $(\underline{u}_\delta - \underline{g}_\delta)^T$ to obtain

$$(\underline{u}_\delta - \underline{g}_\delta)^T \underline{L}_\delta \underline{u}_\delta - (\underline{u}_\delta - \underline{g}_\delta)^T \underline{f}_\delta = 0. \tag{3.118}$$

Note, $\underline{u}_\delta$ satisfies (3.82) and $(\underline{u}_\delta - \underline{g}_\delta)$ is the vector of discrete component of a test function in $\underline{X}_\delta$ where $\underline{g}_\delta$ is the discrete coefficient of a function in $\underline{X}_\delta^{D^+}$. Expanding,

$$\frac{1}{2}\underline{u}_\delta^T(\underline{L}_\delta + \underline{L}_\delta^T)\underline{u}_\delta + \frac{1}{2}\underline{u}_\delta^T(\underline{L}_\delta - \underline{L}_\delta^T)\underline{u}_\delta - \underline{g}_\delta^T \underline{L}_\delta \underline{u}_\delta - \underline{u}_\delta^T \underline{f}_\delta + \underline{g}_\delta^T \underline{f}_\delta = 0, \tag{3.119}$$

and since for all real $\underline{u}_\delta$ and $\underline{L}_\delta$, we have

$$\frac{1}{2}\underline{u}_\delta^T(\underline{L}_\delta + \underline{L}_\delta^T)\underline{u}_\delta = \underline{u}_\delta^T \underline{A}_\delta \underline{u}_\delta + g_1^2\frac{\alpha}{2} - g_0^2\frac{\alpha}{2}, \tag{3.120}$$

$$\frac{1}{2}\underline{u}_\delta^T(\underline{L}_\delta - \underline{L}_\delta^T)\underline{u}_\delta = \underline{0}, \tag{3.121}$$

we thus obtain

$$\underline{u}_\delta^T \underline{A}_\delta \underline{u}_\delta + g_1^2\frac{\alpha}{2} - g_0^2\frac{\alpha}{2} - \underline{g}_\delta^T \underline{L}_\delta \underline{u}_\delta - \underline{u}_\delta^T \underline{f}_\delta + \underline{g}_\delta^T \underline{f}_\delta = 0. \tag{3.122}$$

It follows from (3.108), (3.109), and (3.113) that

$$\underline{\underline{u}}_\delta^T \underline{\underline{A}}_\delta \underline{\underline{u}}_\delta + g_1^2\frac{\alpha}{2} - g_0^2\frac{\alpha}{2} - \underline{g}_\delta^T \underline{Q}_\delta^T \underline{\underline{L}}_\delta \underline{\underline{u}}_\delta - \underline{\underline{u}}_\delta^T \underline{\underline{f}}_\delta + \underline{g}_\delta^T \underline{Q}_\delta^T \underline{\underline{f}}_\delta = 0. \tag{3.123}$$

This is our desired energy equality similar to (3.38) expressed in our discrete decoupled variables. Recall that g_0 and g_1 are the boundary conditions at $x = 0$ and $x = 1$ which are already included in the vector of unknowns $\underline{u}_\delta$. In (3.120), these boundary conditions appear in the additional constants on the right hand side. In fact, these constants are the first and last terms in our unknown vector $\underline{u}_\delta$ times the first and last diagonal terms in $\underline{L}_\delta$. Note that, all the other terms in the diagonal of the connective operator are zero.

We can now express our linear–functional output $s_\delta (= \ell(u_\delta))$,

$$\pm s_\delta = \mathcal{S}_\delta^\pm(\underline{\underline{u}}_\delta), \tag{3.124}$$

where

$$\mathcal{S}_\delta^\pm(\underline{\underline{v}}_\delta) = \underline{\underline{v}}_\delta^T \underline{\underline{A}}_\delta \underline{\underline{v}}_\delta + g_1^2\frac{\alpha}{2} - g_0^2\frac{\alpha}{2} - \underline{g}_\delta^T \underline{Q}_\delta^T \underline{\underline{L}}_\delta \underline{\underline{v}}_\delta - \underline{\underline{v}}_\delta^T \underline{\underline{f}}_\delta + \underline{g}_\delta^T \underline{Q}_\delta^T \underline{\underline{f}}_\delta \pm \underline{\underline{v}}_\delta^T \underline{\underline{\ell}}_\delta \tag{3.125}$$

is defined for any $\underline{\underline{v}}_\delta \in \mathbf{R}^{\hat{n}_\delta}$. Note that

$$\pm s_\delta = \left\{ \underline{\underline{v}}_\delta \in \mathbf{R}^{\hat{n}_\delta} \;\middle|\; \begin{array}{rcl} \min & & \\ \underline{w}_\delta^T [\underline{Q}_\delta^T \underline{\underline{L}}_\delta \underline{\underline{v}}_\delta - \underline{f}_\delta] & = & 0 \quad \forall \underline{w}_\delta \in \mathcal{R}_\delta \\ \underline{\rho}_\delta^T [\underline{R}_\delta \underline{\underline{v}}_\delta - \underline{d}_\delta] & = & 0, \quad \forall \underline{\rho}_\delta \in \mathbf{R}^{K+1} \end{array} \right\} \mathcal{S}_\delta^\pm(\underline{\underline{v}}_\delta), \tag{3.126}$$

since from (3.111)-(3.113) the constraint forces $\underline{\underline{v}}_\delta = \underline{\underline{u}}_\delta$. This rather trivial result suggest the formation of a Lagrangian,

$$\tilde{\mathcal{L}}_\delta^\pm(\underline{\underline{v}}_\delta, \tilde{\underline{\mu}}_\delta, \underline{t}_\delta) = \mathcal{S}_\delta^\pm(\underline{\underline{v}}_\delta) + \tilde{\underline{\mu}}_\delta^T (\underline{Q}_\delta^T \underline{\underline{L}}_\delta \underline{\underline{v}}_\delta - \underline{f}_\delta) + \underline{t}_\delta^T \underline{R}_\delta \underline{\underline{v}}_\delta, \tag{3.127}$$

defined for all $\underline{\underline{v}}_\delta \in \mathbf{R}^{\hat{n}_\delta}, \tilde{\underline{\mu}}_\delta \in \mathcal{R}_\delta$, and $\underline{t}_\delta \in R^{K+1}$. Note that $\tilde{\underline{\mu}}_\delta$ is the vector of discrete coefficient of a function in $\underline{X}_\delta^{D+}$. It is easy to see that we can absorb the $\underline{g}_\delta$ vector into the adjoint $\tilde{\underline{\mu}}_\delta$, ($\underline{\mu}_\delta = \tilde{\underline{\mu}}_\delta - \underline{g}_\delta$), to define an equivalent but simpler Lagrangian, $\mathcal{L}_\delta^\pm$: $\mathbf{R}^{\hat{n}_\delta} \times \mathcal{R}_\delta^* \times R^{K+1} \to \mathbf{R}$,

$$\begin{aligned} \mathcal{L}_\delta^\pm(\underline{\underline{v}}_\delta, \underline{\mu}_\delta, \underline{t}_\delta) &= \underline{\underline{v}}_\delta^T \underline{\underline{A}}_\delta \underline{\underline{v}}_\delta + g_1^2 \frac{\alpha}{2} - g_0^2 \frac{\alpha}{2} - \underline{\underline{v}}_\delta^T \underline{\underline{f}}_\delta \pm \underline{\underline{v}}_\delta^T \underline{\underline{\ell}}_\delta \\ &\quad + \underline{\mu}_\delta^T (\underline{Q}_\delta^T \underline{\underline{L}}_\delta \underline{\underline{v}}_\delta - \underline{f}_\delta) + \underline{t}_\delta^T \underline{R}_\delta \underline{\underline{v}}_\delta, \end{aligned} \tag{3.128}$$

where $\mathcal{R}_\delta^* = \{\underline{v}_\delta \in \mathbf{R}_\delta^n | \; (\underline{v}_\delta)_1 = -g_0, (\underline{v}_\delta)_{n_\delta} = -g_1 \}$. We have now directly obtained a derivation for the adjoint boundary condition where $\underline{\mu}_\delta$ is the describe coefficient of a function in $\underline{X}_\delta^{D-}$.

In summary, our augmented Lagrangian consists of a quadratic "energy" reformulation of the desired output as the objective to be minimized with respect to linear constraints which are the finite element equilibrium equation and the intersubdomain continuity conditions. Clearly the main difference is in the introduction of the hybridization operators $\underline{Q}_\delta$ and $\underline{R}_\delta$ which actually do the transformation to go from continuous spaces to our broken spaces. Notice, that the adjoint is not decoupled and our hybrid flux includes the Dirichlet boundary terms.

As $\underline{\underline{A}}_\delta$ is symmetric positive-semidefinite, (3.128) constitutes a classical quadratic–linear program. Recall, from Section 2.4, the duality result,

$$\pm s_\delta = \mathcal{S}_\delta^\pm(\underline{\underline{u}}_\delta) = \min_{\underline{\underline{v}}_\delta \in \mathbf{R}^{\hat{n}_\delta}} \sup_{\underline{\mu}_\delta \in \mathcal{R}_\delta^*, \, \underline{t}_\delta \in \mathbf{R}^{K+1}} \mathcal{L}_\delta^\pm(\underline{\underline{v}}_\delta, \underline{\mu}_\delta, \underline{t}_\delta) \tag{3.129}$$

$$= \max_{\underline{\mu}_\delta \in \mathcal{R}_\delta^*, \, \underline{t}_\delta \in \mathbf{R}^{K+1}} \inf_{\underline{\underline{v}}_\delta \in \mathbf{R}^{\hat{n}_\delta}} \mathcal{L}_\delta^\pm(\underline{\underline{v}}_\delta, \underline{\mu}_\delta, \underline{t}_\delta). \tag{3.130}$$

Bounds for our output then follow directly from (3.130): from the max min problem we see

that, for any candidate multipliers $\underline{\hat{\mu}}_\delta^\pm \in (\mathcal{R}_\delta^*)^2, \underline{\hat{t}}_\delta^\pm \in (\mathbf{R}^{K+1})^2$,

$$\inf_{\underline{\underline{v}}_\delta \in \mathbf{R}^{\hat{n}_\delta}} \mathcal{L}_\delta^\pm(\underline{\underline{v}}_\delta, \underline{\hat{\mu}}_\delta^\pm, \underline{\hat{t}}_\delta^\pm) \leq \pm s_\delta. \tag{3.131}$$

As for the variational formulation, we define $\eta^\pm$ to be

$$\eta^\pm = \mathcal{L}_\delta^\pm(\underline{\underline{\hat{u}}}_\delta^\pm, \underline{\hat{\mu}}_\delta^\pm, \underline{\hat{t}}_\delta^\pm), \tag{3.132}$$

where $\underline{\underline{\hat{u}}}_\delta^\pm$ is given by,

$$\mathcal{L}_\delta^\pm(\underline{\underline{\hat{u}}}_\delta^\pm, \underline{\hat{\mu}}_\delta^\pm, \underline{\hat{t}}_\delta^\pm) = \inf_{\underline{\underline{v}}_\delta \in \mathbf{R}^{\hat{n}_\delta}} \mathcal{L}_\delta^\pm(\underline{\underline{v}}_\delta, \underline{\hat{\mu}}_\delta^\pm, \underline{\hat{t}}_\delta^\pm). \tag{3.133}$$

We will not show here the proof of (3.133) as it follows directly the proof of (3.73) shown in Section 3.2.2 where we replace $a(v,v)$, $a^s(v,v)$ and $\ell^N(v)$ by $\underline{\underline{v}}_\delta^T \underline{\underline{L}}_\delta \underline{\underline{v}}_\delta$, $\underline{\underline{v}}_\delta^T \underline{\underline{A}}_\delta \underline{\underline{v}}_\delta$ and $\underline{\underline{v}}_\delta^T \underline{\ell}_\delta$, respectively.

We conclude that

$$\eta^+ \leq s_\delta \leq -\eta^-, \tag{3.134}$$

which is the basis for our estimators. Note that both the lower and upper bounds are obtained without evoking complementary energy arguments.

In addition to our duality results, we also know that the saddlepoint $(\underline{\underline{u}}_\delta, \underline{\psi}_\delta^\pm, \underline{y}_\delta^\pm)$ associated with (3.129)–(3.130) can be found by evoking stationarity of the Lagrangian (3.128), yielding

$$\begin{aligned}
\underline{\underline{v}}_\delta^T [2\underline{\underline{A}}_\delta \underline{\underline{u}}_\delta + \underline{\underline{L}}_\delta^T \underline{\underline{Q}}_\delta \underline{\psi}_\delta^\pm + \underline{R}_\delta^T \underline{y}_\delta^\pm - \underline{\underline{f}}_\delta \pm \underline{\underline{\ell}}_\delta] &= 0, \quad \forall \underline{\underline{v}}_\delta \in \mathbf{R}^{\hat{n}_\delta}, && (3.135)\\
\underline{\underline{w}}_\delta^T [\underline{Q}_\delta^T \underline{\underline{L}}_\delta \underline{\underline{u}}_\delta - \underline{\underline{f}}_\delta] &= 0, \quad \forall \underline{\underline{w}}_\delta \in \mathcal{R}_\delta^*, && (3.136)\\
\underline{\rho}_\delta^T [\underline{R}_\delta \underline{\underline{u}}_\delta - \underline{d}_\delta] &= 0, \quad \forall \underline{\rho}_\delta \in \mathbf{R}^{K+1}, && (3.137)
\end{aligned}$$

where (3.135), (3.136), and (3.137) correspond to variations with respect to the first, second, and third arguments of $\mathcal{L}_\delta^\pm(\cdot,\cdot,\cdot)$, respectively. Note that,

$$(\underline{\psi}_\delta^\pm, \underline{y}_\delta^\pm) = \underset{\underline{\mu}_\delta \in \mathcal{R}_\delta^*,\, \underline{t}_\delta \in \mathbf{R}^{K+1}}{\arg\max} \; [\inf_{\underline{\underline{v}}_\delta \in \mathbf{R}^{\hat{n}_\delta}} \mathcal{L}_\delta^\pm(\underline{\underline{v}}_\delta, \underline{\mu}_\delta, \underline{t}_\delta)], \tag{3.138}$$

and thus $(\underline{\psi}_\delta^\pm, \underline{y}_\delta^\pm)$ is the choice for $(\underline{\hat{\mu}}_\delta^\pm, \underline{\hat{t}}_\delta^\pm)$ which renders the bounds (3.134) exact. The system (3.135)–(3.137) is now fully hybridized: as expected from standard results in mixed methods [19] and domain decomposition approaches, $\underline{y}_\delta^\pm$ is a hybrid flux and $\underline{R}_\delta^T$ is the consistent flux "splitting" such that the original discrete equations are satisfied.

3.3.3 Bounds Procedure

To bound the "truth" output, s_h, we evoke (3.134) with $(\underline{\psi}_h^{\pm}, \underline{y}_h^{\pm})$ taken to be the interpolant of the H–mesh saddle problem solution $(\underline{\psi}_H^{\pm}, \underline{y}_H^{\pm})$. To the extent that $(\underline{\psi}_h^{\pm}, \underline{y}_h^{\pm})$ is close to $(\underline{\psi}_h^{\pm}, \underline{y}_h^{\pm})$, the bounds will be sharp. Hence, this hierarchical procedure involves calculations on both the H–mesh and the h–mesh, however, the calculations on the h-mesh are inexpensive. For purpose of solvability we require that the h–mesh is a refinement of the H–mesh, $X_H^{D\pm} \subset X_h^{D\pm}$.

To determine the $(\underline{\psi}_H^{\pm}, \underline{y}_H^{\pm})$, we solve the saddle problem (3.135)–(3.137) for $\delta = H$,

$$\underline{\underline{v}}_H^T[2\underline{\underline{A}}_H\underline{\underline{u}}_H + \underline{\underline{L}}_H^T\underline{Q}_H\underline{\psi}_H^{\pm} + \underline{R}_H^T\underline{y}_H^{\pm} - \underline{\underline{f}}_H \pm \underline{\underline{\ell}}_H] = 0, \quad \forall \underline{\underline{v}}_H \in \mathbf{R}^{\hat{n}_H}, \tag{3.139}$$

$$\underline{\underline{w}}_H^T[\underline{Q}_H^T\underline{\underline{L}}_H\underline{\underline{u}}_H - \underline{\underline{f}}_H] = 0, \quad \forall \underline{\underline{w}}_\delta \in \mathcal{R}_H^*, \tag{3.140}$$

$$\underline{\rho}_H^T[\underline{R}_H\underline{\underline{u}}_H - \underline{d}_H] = 0, \quad \forall \underline{\rho}_H \in \mathbf{R}^{K+1}. \tag{3.141}$$

Adjoint Calculation

We first find $\underline{\underline{u}}_H$ from (3.140)-(3.141), which from (3.111)-(3.113) and (3.82) can be computed as

$$\underline{\underline{w}}_H^T[\underline{\underline{L}}_H\underline{\underline{u}}_H = \underline{\underline{f}}_H], \quad \forall \underline{\underline{w}}_H \in \mathcal{R}_H^* \tag{3.142}$$

$$\underline{\underline{u}}_H = \underline{Q}_H\underline{u}_H, \tag{3.143}$$

where we need to take $\underline{\underline{w}}_H = \underline{\underline{e}}_i$, $i = 1, ..., n_H$ and then apply the corresponding boundary conditions. To calculate the adjoint $\underline{\psi}_H^{\pm}$, first we take $\underline{v}_H = \underline{e}_i$, $i = 1, ..., \hat{n}_H$ in (3.139), second, we multiply by $\underline{Q}_H^T$ and finally we evoke (3.107)-(3.110) to find

$$\underline{L}_H^T\underline{\psi}_H^{\pm} = -(\underline{A}_H\underline{u}_H + \underline{Q}_H^T\underline{R}_H^T\underline{y}_H^{\pm} - \underline{f}_H \pm \underline{\ell}_H), \tag{3.144}$$

where $\underline{Q}_H^T\underline{R}_H^T\underline{y}_H^{\pm}$ is effectively zero except on the rows corresponding to the Dirichlet boundary nodes. Recall that the boundary values of the adjoint are known, so we do not need to solve for these end nodes and therefore we only solve the following system

$$\tilde{\underline{L}}_H^T\tilde{\underline{\psi}}_H^{\pm} = -(\tilde{\underline{A}}_H\tilde{\underline{u}}_H - \tilde{\underline{f}}_H \pm \tilde{\underline{\ell}}_H) + g_0(\underline{L}_H^T)_{\imath,1} + g_1(\underline{L}_H^T)_{\imath,n_\delta}, \quad i = 2, ..., n_H - 1, \tag{3.145}$$

to obtain

$$(\underline{\psi}_H^{\pm})_i = \begin{cases} -g_0 & i = 1 \\ \tilde{\underline{\psi}}_H^{\pm} & 2 \le i \le n_H - 1 \\ -g_1 & i = n_H \end{cases}. \tag{3.146}$$

Relating back to the variational form, we have effectively solved for the adjoint on a continuous space as in (3.52).

Hybrid Flux Approximation

We see from (3.104) that (3.139) is decoupled into K systems. To calculate the values of $(\underline{y}_h^{\pm})_i,\ i = 1, ..., K+1$ we multiply each of the decoupled systems associated with T_H^k by $\underline{\zeta}_H\big|_{T_H^k}^L$ and $\underline{\zeta}_H\big|_{T_H^k}^R$ which are vectors in $\mathbf{R}^2$ equal to [1 0] and [0 1], respectively. This procedure will yield,

$$(\underline{y}_H^{\pm})_k = -(\underline{\zeta}_H\big|_{T_H^k}^L)^T(2\underline{A}_H^k\underline{u}_H^k + (\underline{L}_H^k)^T\underline{\psi}_H^{k\pm} - \underline{f}_H^k \pm \underline{\ell}_H^k) \tag{3.147}$$

$$(\underline{y}_H^{\pm})_{k+1} = (\underline{\zeta}_H\big|_{T_H^k}^R)^T(2\underline{A}_H^k\underline{u}_H^k + (\underline{L}_H^k)^T\underline{\psi}_H^{k\pm} - \underline{f}_H^k \pm \underline{\ell}_H^k) \tag{3.148}$$

where $\underline{u}_H^k$ is $\underline{u}_H$ associated with T_H^k. Note that, the values of $(\underline{y}_h^{\pm})$ at the interface of two subdomains can be computed from either sides.

Next, we need to form $\underline{\psi}_h^{\pm} \in (\mathcal{R}_h^*)^2$ and $\underline{y}_h^{\pm} \in (\mathbf{R}^{(K+1)})^2$ in order to evaluate our bounds (3.134). First, considering the adjoint $\underline{\psi}_h^{\pm}$, we form

$$(\underline{\psi}_h^{\pm})_i = \sum_{j=1}^{n_H}(\underline{\psi}_H^{\pm})_j\varphi_{Hj}(x_{hi}), \qquad 1 \le i \le n_h, \tag{3.149}$$

which is simply the h–mesh linear interpolation of the H–mesh adjoint. Second,considering the hybrid flux $\underline{y}_h^{\pm}$, we simply take $\underline{y}_H^{\pm}$ because for one–dimensional problems where only one point appears at the intersubdomain edges. Therefore,

$$\underline{y}_h^{\pm} = \underline{y}_H^{\pm}. \tag{3.150}$$

Finally, we now look for the minimizers,

$$\underline{\hat{u}}_h^{\pm} = \underset{\underline{v}_h \in \mathbf{R}^{n_h}}{\arg\min}\ \mathcal{L}_h^{\pm}(\underline{v}_h, \underline{\psi}_h^{\pm}, \underline{y}_h^{\pm}), \tag{3.151}$$

which is obtained simply by solving (3.135) with $\delta = h$ and $(\underline{\psi}_\delta^{\pm}, \underline{y}_\delta^{\pm})$, that is we look for $(\underline{\psi}_h^{\pm}, \underline{y}_h^{\pm})$ such that $\underline{\hat{u}}_h^{\pm}$ satisfies

$$2\underline{\underline{A}}_h\underline{\hat{u}}_h^{\pm} = -(\underline{L}_h^T\underline{Q}_h\underline{\psi}_h^{\pm} + \underline{R}_h^T\underline{y}_h^{\pm} - \underline{f}_h \pm \underline{\ell}_h). \tag{3.152}$$

Note that in this system there is no boundary condition to implement. This system is a fully decoupled system into all Neumann subdomain problems.

As in Section 3.2.3, we need to verify that (3.152) does have a solution for $\beta = 0$. Note that $\underline{\underline{A}}_h$ is singular. To show that (3.152) has a solution we need to show,

$$\underline{e}_h^T(\underline{L}_h^T\underline{Q}_h\underline{\psi}_h^{\pm} + \underline{R}_h^T\underline{y}_h^{\pm} - \underline{f}_h \pm \underline{\ell}_h) = 0, \tag{3.153}$$

where $\underline{e}_h$ is the unit vector. By rewriting (3.147) and (3.148) for the h–mesh and subtracting one from the other so that $\underline{\zeta}_h\Big|_{T_H^k}^L$ and $\underline{\zeta}_h\Big|_{T_H^k}^R$ construct $\underline{e}_h$ we recover (3.153). In general, for exact quadratures and (bounded) Galerkin linear functionals, solvability will not be an issue in one space dimension.

We compute our bounds for s_h as

$$\begin{aligned}
(s_h)_{LB}(H) &= \mathcal{L}_h^+(\underline{\hat{\underline{u}}}_h^+, \underline{\psi}_h^+, \underline{y}_h^+) \\
&= -\underline{\hat{\underline{u}}}_h^{+T}\underline{\underline{A}}_h\underline{\hat{\underline{u}}}_h^+ + g_1^2\frac{\alpha}{2} - g_0^2\frac{\alpha}{2} + \underline{\psi}_h^{+T}\underline{f}_h, \qquad (3.154) \\
(s_h)_{UB}(H) &= -\mathcal{L}^{\pm}(\underline{\hat{\underline{u}}}_h^-, \underline{\psi}_h^-, \underline{y}_h^-) \\
&= -\underline{\hat{\underline{u}}}_h^{+T}\underline{\underline{A}}_h\underline{\hat{\underline{u}}}_h^+ + g_1^2\frac{\alpha}{2} - g_0^2\frac{\alpha}{2} - \underline{\psi}_h^{-T}\underline{f}_h \qquad (3.155)
\end{aligned}$$

We now review the computational steps in our bounding procedure:

1. We solve the "original" problem on the H–mesh, (3.82), to determine $\underline{u}_H$.

2. We solve two adjoint problems on the H–mesh ,(3.52), to determine $\underline{\psi}_H^+$ and $\underline{\psi}_H^-$. Note that, for direct solution strategies, these adjoint calculations are of negligible additional expenses, as the LU decomposition of Step 1 can be exploited.

3. We compute, from (3.147)-(3.148), the H–mesh hybrid flux, $\underline{y}_H^{\pm}$. Note that the hybrid flux calculation does not require inversion, only local evaluation.

4. We interpolate the H–mesh adjoint and hybrid flux onto the h–mesh representation according to (3.149)-(3.150).

5. We solve the two h–mesh problems, (3.152), to determine $\underline{\hat{\underline{u}}}_h^{\pm}$; and we then evaluate, from (3.154)-(3.155), the lower and upper bounds.

Note that Step 2–5 must be repeated for each desired output.

We have made some general comments concerning the cost and some solvability issues of the bounds procedure in Section 3.2.3. In this section we review those comments in the light of our discrete formulation. Recall, that to solve $\underline{\hat{\underline{u}}}_h^{\pm}$, we require two $\underline{\underline{A}}_h$-solves. However, we see from (3.104) that $\underline{\underline{A}}_h$ can be decomposed into K decoupled symmetric systems which in addition can also be easily parallelized. In practice, of course, $\underline{\underline{A}}_h$ is never actually formed: only the $\underline{\underline{A}}_h^k$, $k = 1, ..., K$, are required. For our Galerkin linear functionals our systems are tridiagonal which indeed, does not lead to any cost reduction by domain decomposition. However, in higher spatial dimensions, the local problems enjoy a mush smaller bandwidth and a smaller value of the condition number that the original global operator, $\underline{L}_h$.

Chapter 4

Bounds Formulation for the Convection–diffusion Equation

4.1 Model Problem

4.1.1 Governing Equations

We now extend our technique to the convection–diffusion problem in two space dimensions in which we look for the field variable $u(x)$ that satisfies

$$-\frac{\partial}{\partial x_i}(\nu\frac{\partial u}{\partial x_i}) + U_i\frac{\partial u}{\partial x_i} = f \quad \text{in } \Omega,\ i = 1, ..., 2\ , \tag{4.1}$$

with boundary conditions

$$u = g_D \quad \text{on } \Gamma_D, \tag{4.2}$$

$$\frac{\partial u}{\partial n} = g_N \quad \text{on } \Gamma_N, \tag{4.3}$$

where ν is the positive viscosity and Ω is a bounded domain in $\mathbf{R}^2$ with Lipschitz boundary $\overline{\Gamma}_N \cap \overline{\Gamma}_D = \partial\Omega$ where $\overline{\Gamma}_N$ and $\overline{\Gamma}_D$ are the Dirichlet and Neumann portions of the domain boundary. We require that Γ_D be non-empty and $U_i\hat{n}_i \geq 0$ on Γ_N. The data is assumed to be smooth, i.e. $f \in \mathcal{H}^1(\Omega)$, $g_D \in \mathcal{H}^{1/2}(\Gamma_D)$, and $g_N \in \mathcal{H}^{-1/2}(\Gamma_N)$.

For our problem $x = (x_1, x_2)$, with corresponding unit vector $\hat{x}_1, \hat{x}_2$, Ω is a square domain $]0,2[\times]0,2[$, the four sides of which are denoted Γ^j, $j = 1, ..., 4$, as shown in Figure 4-1. We take the boundary data on $\Gamma_D = \Gamma^1 \cap \Gamma^2$ to be $g_D|_{\Gamma^1} = x_1/2$, $g_D|_{\Gamma^2} = 1 - x_1/2$; and on $\Gamma_D = \Gamma^3 \cap \Gamma^4$ to be $g_N|_{\Gamma^1} = 1 - x_2/2$, $g_N|_{\Gamma^2} = x_2/2$. The velocity is prescribed as $U = (-1, 1)$, which thus produces a boundary layer on the Neumann sides of the domain. We take $f = 0$ to avoid any quadrature issues. For $U = (0, 0)$ we recover the Poisson problem described in Section 2.2. In addition, treatment of nonuniform velocity fields is

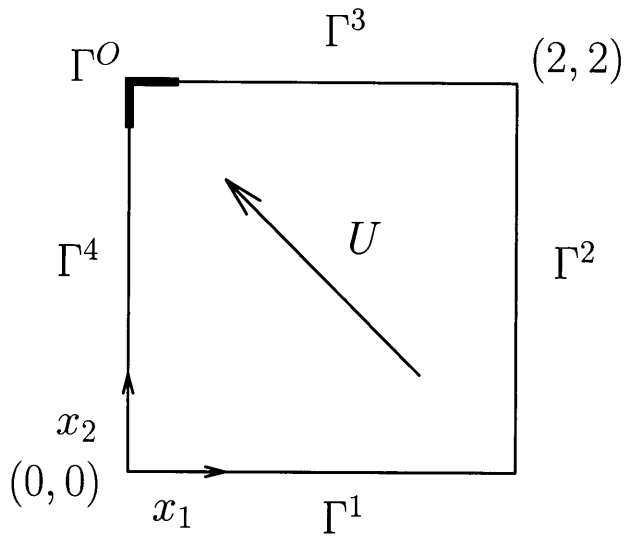

Figure 4-1: Convection-diffusion Geometry: Γ_1, and Γ_2 are Dirichlet boundaries, Γ_3 and Γ_4 are Neumann boundaries.

presented in Appendix B.

The variational form of (4.1)–(4.3) is to find $u \in \mathcal{H}^1_D(\Omega)$ such that

$$\int_\Omega \nu \frac{\partial v}{\partial x_i}\frac{\partial u}{\partial x_i} + vU_i\frac{\partial u}{\partial x_i}\,\mathrm{d}A = \int_\Omega vf\,\mathrm{d}A + \int_{\Gamma_N} vg_N\,\mathrm{d}s, \qquad \forall v \in \mathcal{H}^1_0(\Omega), \tag{4.4}$$

where $\mathrm{d}A$ is a differential area element, and $\mathrm{d}s$ is a differential line. Since $U_i\hat{n}_i \geq 0$ on the Neumann boundary Γ_N , Γ_D is non-empty, our two-dimensional bilinear form is coercive and uniqueness directly follow from the Lax–Milgram theorem. Note that if $U_i\hat{n}_i < 0$ then our bilinear form is no longer coercive and proof of uniqueness does not follow the Lax–Milgram theorem nor does the bounds technique apply.

In this section we set

$$\mathcal{H}^1_D(\Omega) = \left\{ v \in \mathcal{H}^1(\Omega) |\ v|_{\Gamma_D} = g_D \right\}, \tag{4.5}$$

and

$$\mathcal{H}^1_0(\Omega) = \left\{ v \in \mathcal{H}^1(\Omega) |\ v|_{\Gamma_D} = 0 \right\}. \tag{4.6}$$

A special case of the convection–diffusion equation is the Poisson equation for which $U = (0,0)$. We also exploit this simple Poisson problem to investigate some characteristics of the bounds for which a square domain with homogeneous Dirichlet boundary conditions is considered.

4.1.2 Output Linear Functionals

We now indicate the particular linear functionals that are investigated. We shall look at the average value of the field solution in the vicinity of the corner $(x_1,\ x_2) = (0,\ 2)$ at which we expect the maximum value to occur. In particular, for the symmetric boundary strip Γ^O identified in Figure 4-1, we define

$$s^{(5)} = \ell^{(5)}(u) = \frac{1}{|\Gamma^O|}\int_{\Gamma^O} u\mathrm{d}s, \tag{4.7}$$

where $|\Gamma^O|$ is the length of Γ^O.

We pause here and evaluate for what conditions this functional is bounded. First, we show that $\ell^{(5)}(u)$ is a bounded functional for Γ^O of non-zero measure. Considering that $\ell^{(5)}(u)$ is equivalent to inhomogeneous Neumann data in $L^2(\Gamma_N)$, we apply the Riesz representation theorem which states that there exists a unique u in $\mathcal{H}^1(\Omega)$, for this data and this $\ell^{(5)}(u)$ is bounded. Second, we show that $\ell^{(5)}(u)$ is not bounded for zero measure of Γ^O. We appeal to the Sobolev inequality stating: For any regular domain $\Omega \subset \mathbf{R}^d$, if $u \in \mathcal{H}^m(\Omega)$, $m > \frac{d}{2}$ then u is continuous. Hence, if we consider a delta–function over our two dimensional domain, then $d = 2$ and so $\frac{d}{2}$ is not strictly less that unity. Indeed, one can find functions $u \in \mathcal{H}^1(\Omega)$ which are not continuous ($m = 1 \not> 1$).

Recall that our method is also able to treat unbounded functionals. To illustrate this flexibility, we consider the corner value output of the field solution at $(x_1,\ x_2) = (0,\ 2)$, defined by

$$s^{(6)} = \ell^{(6)}(u) = u(0,\ 2). \tag{4.8}$$

Later, we will investigate the Poisson problem. As output, we will consider the average solution over the entire domain. The output is defined by

$$s^{(7)} = \ell^{(7)}(u) = \frac{1}{|\Omega|}\int_{\Omega} u\ \mathrm{d}A. \tag{4.9}$$

This output has an interesting property. It is shown in Appendix A that the H–mesh output is the same as the lower bound. We call this property *compliance* in analogy to the structural output with the same characteristics.

Lastly, we consider functionals that evaluate the "flux" on Γ^O which is a portion of a Dirichlet boundary Γ_D. We show that such functionals are unbounded unless Γ^O connects to Neumann boundaries at both ends. We study the problem in which the flux is expressed as for the one dimension problem (3.8):

$$\ell(u) = \int_{\Gamma^O} \nu\frac{\partial\mathcal{X}}{\partial x_i}\frac{\partial u}{\partial x_i} + U_i\mathcal{X}\frac{\partial u}{\partial x_i} - \mathcal{X}f\ \mathrm{d}A. \tag{4.10}$$

Note that, to evaluate the "flux" on Γ^O, $\mathcal{X}$ has to be unity on Γ^O and zero on the rest of

Γ^D. This function is not in $\mathcal{H}^{\frac{1}{2}}(\Gamma^D)$ and therefore $\ell(u)$ is unbounded.

4.2 Finite Element Approximation

4.2.1 Bilinear and Linear Forms

We define here the bilinear and linear forms for the convection–diffusion problem. We first define a space which permits discontinuities across edges of the h–mesh, "broken" $\mathcal{H}^1(\Omega)$ space, as

$$\mathcal{H}^1_*(\Omega) = \left\{ v \in \mathcal{H}^0(\Omega) |\ v|_{T_H} \in \mathcal{H}^1(T_H),\ \forall T_H \in \mathcal{T}_H \right\}. \tag{4.11}$$

Note this space is essential to decompose our global problem into subdomain problems. We then define the bilinear form associated with our operator as

$$a(w,v) = \sum_{T_H \in \mathcal{T}_H} a_{T_H}(w|_{T_H}, v|_{T_H}), \quad \forall w, v \in \mathcal{H}^1_*(\Omega), \tag{4.12}$$

where for all T_H in $\mathcal{T}_H$

$$a_{T_H}(w,v) = \int_{T_H} \nu \frac{\partial w}{\partial x_j}\frac{\partial v}{\partial x_j} + wU_j \frac{\partial v}{\partial x_j}\, \mathrm{d}A, \quad \forall w, v \in \mathcal{H}^1(T_H). \tag{4.13}$$

We shall also need the symmetric part of our operator,

$$a^s(w,v) = \sum_{T_H \in \mathcal{T}_H} a^s_{T_H}(w|_{T_H}, v|_{T_H}), \quad \forall w, v \in \mathcal{H}^1_*(\Omega), \tag{4.14}$$

where for all T_H in $\mathcal{T}_H$

$$a^s_{T_H}(w,v) = \int_{T_H} \nu \frac{\partial w}{\partial x_j}\frac{\partial v}{\partial x_j}\, \mathrm{d}A + \frac{1}{2}\int_{\partial T_H \cap \Gamma_N} wvU_j \hat{n}_j ds, \quad \forall w, v \in \mathcal{H}^1(T_H). \tag{4.15}$$

The boundary term in (4.15) arises from the convection operator and only affects the Neumann boundary. Although for problems where there are no Neumann boundaries, this term vanishes and $a^s_{T_H}(,)$ is the symmetric part of $a_{T_H}(,)$; in general $a^s_{T_H}(,)$ is not the symmetric part of $a_{T_H}(,)$.

We next introduce a set of "jump" bilinear and linear forms which will be required in our variational relaxations. We write

$$b(v,t) = \sum_{T_H \in \mathcal{T}_H} \sum_{\gamma_{T_H} \in \mathcal{E}(T_H)} \sigma^{\gamma_{T_H}}_{T_H} \int_{\gamma_{T_H}} v|_{T_H} t|_{E(\gamma_{T_H})} \mathrm{d}s, \quad \forall v \in \mathcal{H}^1_*(\Omega), \forall t \in \mathcal{Q}, \tag{4.16}$$

where $v|_{T_H}$ is to be interpreted as the trace of $v|_{T_H}$ on γ_{T_H} and $\mathcal{Q} = \{t \in \mathcal{H}^{-1/2}(\mathcal{E}(\mathcal{T}_H)) |\ t|_{\Gamma_N} = 0\}$. (More strictly, the L^2 inner products in (4.16) should be replaced by the duality pairing

between $\mathcal{H}^{-\frac{1}{2}}(\Omega)$ and $\mathcal{H}^{\frac{1}{2}}(\Omega)$ defined in (2.15).) Note that t is defined only over the edges of the triangulation and may, of course, be discontinuous; t may also be defined as the flux associated with a function $\mathcal{Q}$ in $\mathcal{H}(\mathrm{div},\Omega)$ [5]. Effectively, (4.16) computes the moments of the jumps in v over integral edges, and the moments of v over boundary edges. Similarly, we also require the related linear functional associated with the Dirichlet conditions,

$$\ell^D(y) = \sum_{T_H \in \mathcal{T}_H} \sum_{\gamma_{T_H} \in \mathcal{E}(T_H)} \sigma_{T_H}^{\gamma_{T_H}} \int_{\gamma_{T_H} \cap \Gamma_D} g_D \; y|_{E(\gamma_{T_H})} \, \mathrm{d}s, \quad \forall y \in \mathcal{Q}, \tag{4.17}$$

which computes the moments of the imposed boundary conditions on Γ_D.

We now introduce our linear functionals. Associated with the volumetric inhomogeneities, we have

$$\ell^N(v) = \sum_{T_H \in \mathcal{T}_H} \ell^N_{T_H}(v|_{T_H}), \quad \forall v \in \mathcal{H}^1_*(\Omega), \tag{4.18}$$

where for all T_H in $\mathcal{T}_H$

$$\ell^N_{T_H}(v) = \int_{T_H} v f dx + \int_{\partial T_H \cap \Gamma_N} v g_N \, \mathrm{d}s, \quad \forall v \in \mathcal{H}^1(T_H). \tag{4.19}$$

Associated with our output functional, we introduce

$$\ell^O(v) = \sum_{T_H \in \mathcal{T}_H} \ell^O_{T_H}(v|_{T_H}), \quad \forall v \in \mathcal{H}^1_*(\Omega), \tag{4.20}$$

such that

$$\ell^O(v) = \ell(v), \quad \forall v \in \mathcal{H}^1(\Omega). \tag{4.21}$$

Here $\ell()$ is the formal output functional introduced in (2.49). Note that the construction (4.20)-(4.21) permits us to evaluate the output associated with a field variable which is not in $\mathcal{H}^1(\Omega)$.

4.2.2 Function Spaces

Our function spaces are defined using the same notation as in the one–dimensional problem. We believe, however, that there will be no confusion and that the context will clearly indicate the dimensionality of the problem.

We first introduce the standard conforming linear approximation spaces,

$$X_\delta = \{v|_{T_\delta} \in \mathbf{P}_1(T_\delta), \forall T_\delta \in \mathcal{T}_\delta\} \bigcap \mathcal{H}^1_0(\Omega), \tag{4.22}$$

and

$$X_\delta^{D\pm} = \{v \pm u_D |\; v \in X_\delta\}, \tag{4.23}$$

where $u_D \in \mathcal{H}^1_D(\Omega)$ is any lifting of the Dirichlet boundary data, and $\mathbf{P}_1(T_\delta)$ is the space

of linear polynomials over T_δ. We shall need only $\delta = H$ and $\delta = h$ which corresponds to our "working" and "truth" discretizations, respectively: from our refinement hypothesis, $X_H^{D^\pm} \subset X_h^{D^\pm}$ and $X_H \subset X_h$. Note that, for the problems described in Section 8, u_D will be chosen such that $u_D|_{T_H} \in \mathbf{P}_1(T_\delta)$, $\forall T_H \in \mathcal{T}_H$ and u_D is the Dirichlet data g_D on Γ_D.

We next introduce standard *nonconforming* linear spaces [19, 42],

$$\overline{X}_H^D = \{v|_{T_H} \in \mathbf{P}_1(T_H), \forall T_H \in \mathcal{T}_H | b(v,t) = \ell^D(t), \forall t \in \mathcal{Q}\}, \tag{4.24}$$

$$\overline{X}_H = \{v|_{T_H} \in \mathbf{P}_1(T_H), \forall T_H \in \mathcal{T}_H | b(v,t) = 0, \forall t \in \mathcal{Q}\}, \tag{4.25}$$

where

$$Q_k = \{y|_\gamma \in \mathbf{P}_k(\gamma), \forall \gamma \in \mathcal{E}(\mathcal{T}_H), y|_{\Gamma_N} = 0\}. \tag{4.26}$$

The nonconforming space requires that the jumps in v over internal edges be orthogonal to zero order polynomials which implies that members of this space need only be continuous at the midpoints of the edges. Note that, in addition to weakly imposing the continuity requirements, (4.24) and (4.25) also weakly impose the Dirichlet conditions.

Finally, we introduce our subdomain–local spaces: for all T_H in $\mathcal{T}_H$,

$$Z_H(T_H) = (\mathbf{P}_1(T_H)), \tag{4.27}$$

and

$$Z_h(T_H) = \{v|_{T_H} \in \mathbf{P}_1(T_h), \forall T_h \in \mathcal{R}_{T_H}\} \bigcap \mathcal{H}^1(T_H), \tag{4.28}$$

where we recall that $\mathcal{R}_{T_H}$ is the set of h–mesh elements that constitute T_H. We can define the associated "product" spaces as

$$V_\delta = \{v_1 \in \mathcal{H}^1_*(\Omega) | v|_{T_H} \in Z_\delta(T_H), \forall T_H \in \mathcal{T}_H\}, \tag{4.29}$$

for $\delta = H$ and $\delta = h$. In essence, the $Z_\delta(T_H)$ are Neumann spaces over each T_H, for which V_δ is the corresponding global representation.

4.3 Bound Procedure

The procedure to calculate the bounds is similar to the one-dimensional case; we need to find an adjoint and a hybrid flux, our two Lagrange multipliers. Therefore, our bounds procedure involves the same three steps: first, determination of the adjoint; second, calculation of the hybrid flux; and third, solving the local h–mesh solution from which we construct the bounds. The main difference is in the calculation of the hybrid flux where in one–dimension the interface is only one point where as in two–dimensions the intersubdomain condition is computed for line elements.

4.3.1 The H–Mesh Adjoint Calculation

As in Section 3.2.3, we look for $u_H \in X_H^{D+}$ and $\psi_H^{\pm} \in X_H^{D-}$ such that

$$a(w, u_H) = \ell^N(w), \qquad \forall w \in X_H, \tag{4.30}$$

and

$$a(\psi_H^{\pm}, w) = -(2a^s(w, u_H) - \ell^N(w) \pm \ell^O(w)), \qquad \forall w \in X_H. \tag{4.31}$$

We observe that in the latter equation the flow is "reversed", nevertheless the system is still well–posed, as the Neumann condition is transformed into a weak Dirichlet requirement. To expose this fact, we integrate by parts the left–hand side of (4.31),

$$\int_\Omega \nu \frac{\partial w}{\partial x_i} \frac{\partial \psi_H^{\pm}}{\partial x_i} - U_i w \frac{\partial \psi_H^{\pm}}{\partial x_i} \, \mathrm{d}A + \int_{\Gamma_N} w \psi_H^{\pm} U_i \hat{n}_i \, \mathrm{d}s, \qquad \forall w \in X_H. \tag{4.32}$$

Because (4.32) applies for all w in X_H it follows that $\psi_H^{\pm}$ must equilibrate the right–hand side associated with the Neumann boundary. This in some sorts is similar to imposing $\psi_H^{\pm}$ to be equal to Dirichlet data. For example when the output functional on the Neumann boundary is zero, then $\psi_H^{\pm}$ must be zero as well. We also remark, as for the one space dimension, that the Dirichlet boundary conditions on the adjoint are the negative of the boundary conditions on the field solution (for our choice of Lagrangian).

We rewrite (4.31) in two ways similarly to (3.53) and (3.56). In the first reformulation, we look for $u_H \in X_H^{D+}$ such that

$$2a^s(w, u_H) = -F^{\pm}(w; \psi_H^{\pm}), \qquad \forall w \in X_H. \tag{4.33}$$

Here, for any function $\mathcal{F}$ in $\mathcal{H}^1_*(\Omega)$ and for all $v \in \mathcal{H}^1_*(\Omega)$,

$$F^{\pm}(v; \mathcal{F}) = \sum_{T_H \in \mathcal{T}_H} F^{\pm}_{T_H}(v|_{T_H}; \mathcal{F}), \qquad \forall v \in \mathcal{H}^1_*(\Omega), \tag{4.34}$$

where for all T_H in $\mathcal{T}_H$

$$F^{\pm}_{T_H}(v; \mathcal{F}) = -\ell^N_{i\,T_H}(v) + a_{T_H}(\mathcal{F}|_{T_H}, v) \pm \ell^O_{T_H}(v), \qquad \forall v \in \mathcal{H}^1_*(\Omega). \tag{4.35}$$

In some sense, $-F^{\pm}(v; \psi_H^{\pm})$ represents the sum of the "forces" in (4.31) when solving for $u_H \in X_H^{D+}$. In the second reformulation, we look for $u_H \in X_H^{D+}$ such that

$$B^{\pm}(w, u_H) = 0, \qquad \forall w \in X_H. \tag{4.36}$$

Here, for any function $\mathcal{G}$ in $\mathcal{H}^1_*(\Omega)$, for all $v \in \mathcal{H}^1_*(\Omega)$,

$$B^{\pm}(v;\mathcal{G}) = \sum_{T_H \in \mathcal{T}_H} b^{\pm}_{T_H}(v|_{T_H};\mathcal{G}), \quad \forall v \in \mathcal{H}^1_*(\Omega), \tag{4.37}$$

where for all T_H in $\mathcal{T}_H$

$$B^{\pm}_{T_H}(v;\mathcal{G}) = 2a^s_{T_H}(v,\mathcal{F}|_{T_H}) + F^{\pm}_{T_H}(v,\psi^{\pm}_H), \quad \forall v \in \mathcal{H}^1_*(\Omega). \tag{4.38}$$

4.3.2 The H–mesh Hybrid Flux Calculation

To compute the hybrid flux, we look for $y^{\pm} \in \mathcal{Q}_1 \subset \mathcal{Q}$ such that

$$b(v,y^{\pm}) = B^{\pm}(v,u_H), \quad \forall v \in V_H, \tag{4.39}$$

which gives, for all T_H in $\mathcal{T}_H$,

$$\sum_{\gamma_{T_H} \in \mathcal{E}(\mathcal{T}_H)} \sigma^{\gamma_{T_H}}_{T_H} \int_{\gamma_{T_H}} v y^{\pm}|_{E(\gamma_{T_H})} \, \mathrm{d}s = B^{\pm}_{T_H}(v,u_H), \ \forall v \in Z_H(T_H). \tag{4.40}$$

Note that both terms on each side of (4.40) would be zero if the test function v would be in X_h, then the hybrid flux could be calculated exactly. Our goal, however, is to obtain fast bounds. To obtain this result, we have introduced a "broken" space to decouple the global system into local problems. In some sense, the information from neighboring subdomains will come from the approximate hybrid flux. In Chapter 6 we present different approaches we have considered. In particular, we use a two step procedure where we calculate a first initial approximation $\bar{y}^{\pm}$ and then correct it with $\hat{y}^{\pm}$ to ensure that (4.39) is equilibrated.

4.3.3 The h–mesh subdomain Neumann Problem

We now look for $\hat{u}^{\pm}_{T_H} \in Z_h(T_H)$, for all T_H in $\mathcal{T}_H$, such that

$$2a^s_{T_H}(w,\hat{u}^{\pm}_{T_H}) = -F^{\pm}_{T_H}(w;\psi^{\pm}_H) + \sum_{\gamma_{T_H} \in \mathcal{E}(\mathcal{T}_H)} \sigma^{\gamma_{T_H}}_{T_H} \int_{\gamma_{T_H}} w y^{\pm}|_{E(\gamma_{T_H})} \, \mathrm{d}s, \ \forall w \in Z_h(T_H). \tag{4.41}$$

To write (4.41) in a global form, we introduce the variable $\hat{\mathcal{U}}^{\pm}_h \in V_h$ such that $\hat{\mathcal{U}}^{\pm}_h|_{T_H} = \hat{u}^{\pm}_{T_H}, \forall T_H \in \mathcal{T}_H$, then $\hat{\mathcal{U}}^{\pm}_h$ satisfies

$$2a^s(w,\hat{\mathcal{U}}^{\pm}_h) = -F^{\pm}(w;\psi^{\pm}_H) + b(w,y^{\pm}), \quad \forall w \in V_h. \tag{4.42}$$

The hybrid flux in (4.41)–(4.42) may be calculated by any of the procedures described in Chapter 6. Note that for singular elements T_H, which has $a^s_{T_H}(v^s,\hat{u}^{\pm}_{T_H}) = 0$, we require for

solvability that

$$-F_{T_H}^{\pm}(v^s;\psi_H^{\pm}) + \sum_{\gamma_{T_H}\in\mathcal{E}(\mathcal{T}_H)} \sigma_{T_H}^{\gamma_{T_H}} \int_{\gamma_{T_H}} v^s y^{\pm}|_{E(\gamma_{T_H})}\,\mathrm{d}s = 0. \tag{4.43}$$

From (4.40) and the fact that $v^s \in Z_h(T_H)$ we prove (4.43).

We make several remarks. First, this approach imposes the Dirichlet conditions through the "equivalent" hybrid flux Lagrange multiplier on Γ_D [9]. A different procedure where the Dirichlet boundary conditions are imposed directly is presented for the one-dimensional convection–diffusion problem in [35]. The advantages of this approach are that: all edges, including boundary edges, are treated in (almost) the same fashion and elements with edges on Γ_D support the boundary condition such that to avoid any ambiguity with any elements that have only one node on the boundary. Second, we note that (4.41) constitutes a set of decoupled Neumann problems, except for elements with an edge on Γ_N which produce mixed Neumann-Robin problems. Thanks to our equilibration procedure, the pure Neumann problems are solvable. Consequently, these systems have solutions determined up to an arbitrary constant. Note that the "level" of the solution for each element is chosen arbitrarily; the particular choice will be presented in Section 8.2. Third, we note that the K systems for the $\hat{u}_{T_H}^{\pm}$ are completely decoupled, leading to very efficient inversion compared to the original h–mesh original problem $a(v,u_h) = \ell^N(v)$. It is clear that in higher dimensions the matrices become sparse and more expensive to compute. Therefore, this domain decomposition method is very attractive: in direct strategies, the bandwidth is greatly reduced; in iterative strategies, the condition number is greatly reduced; in both cases, the h–mesh problem is now symmetric, and "embarrassingly" parallel [23]. Indeed, the h–mesh work to compute $\hat{\mathcal{U}}_h^{\pm}$ will typically be much less than the H–mesh work required to compute the adjoints and hybrid fluxes.

Finally, we can now calculate the bounds as

$$(s_h)_{LB}(H) = \eta^+, \tag{4.44}$$

and

$$(s_h)_{UB}(H) = -\eta^-, \tag{4.45}$$

where

$$\eta^{\pm} = -a^s(\hat{\mathcal{U}}_h^{\pm},\hat{\mathcal{U}}_h^{\pm}) + c_U - \ell^N(\psi_h^{\pm}) + \ell^D(y^{\pm}), \tag{4.46}$$

and

$$c_U = \frac{1}{2}\int_{\Gamma_D} g_D^2 U_i \hat{n}_i\,\mathrm{d}s. \tag{4.47}$$

(For the Poisson problem, $c_U = 0$.) Note that the particular choice of level of the solution $\hat{\mathcal{U}}_h^{\pm}$ does not affect lower and upper bound values because $a^s(,)$ has a nullspace of unity.

We now prove that the bounds are indeed bounds to the output of interest as summarized in (1.1).

4.4 Proof of Bounding Properties

To begin, we present a simple energy equality that will provide the stabilization in our Lagrangian. It is derive similarly to the one space dimension of Section 3.2.2, thus we obtain

$$a^s(u_h, u_h) + c_U - \ell^N(u_h) - [a(g, u_h) - \ell^N(g)] = 0, \tag{4.48}$$

where g is any function in X_h^{D+}.

We now introduce the set of functions $\mathcal{S}$,

$$\mathcal{S} = \left\{ v \in X_h^{D+} \;\middle|\; \begin{array}{ll} a(w, v) = \ell^N(w), & \forall w \in X_h, \\ b(v, t) = \ell^D(t), & \forall t \in \mathcal{Q}, \end{array} \right\}. \tag{4.49}$$

It is clear that this set of functions is not particularly interesting, consisting only of the singleton $v = u_h$. Continuing with trivialities, it thus follows that

$$\pm s_h = \min_{v \in \mathcal{S}} (a^s(v, v) + c_U - \ell^N(v) - [a(g, v) - \ell^N(g)] \pm \ell^O(v)), \tag{4.50}$$

since for $v = u_H$ the objective reduces to $\pm \ell^O(u_h)$.

This constrained minimization problem leads to the construction of a Lagrangian, $\mathcal{L}_g^{\pm}$: $V_h \times X_h \times \mathcal{Q} \rightarrow \mathbf{R}$, as

$$\mathcal{L}_g^{\pm}(v, \mu', t) = (a^s(v, v) + c_U - \ell^N(v) - [a(g, v) - \ell^N(g)] \pm \ell^O(v)) + (a(\mu', v) - \ell^N(\mu')) - (b(v, t) - \ell^D(t)). \tag{4.51}$$

where we recall that $Q = \{t \in \mathcal{H}^{-1/2}(\mathcal{E}(\mathcal{T}_H)) |\ t|_{\Gamma_N} = 0\}$ (that vanish on the Neumann boundaries). We next absorbed the "g" terms into the adjoint μ' to define an equivalent but simpler Lagrangian, $\mathcal{L}^{\pm} : V_h \times X_h^{D-} \times \mathcal{Q} \rightarrow \mathbf{R}$ as

$$\mathcal{L}^{\pm}(v, \mu, t) = (a^s(v, v) + c_U - \ell^N(v) \pm \ell^O(v)) + (a(\mu, v) - \ell^N(\mu)) - (b(v, t) - \ell^D(t)). \tag{4.52}$$

Finally, it shall prove convenient to write (4.52) as

$$\mathcal{L}^{\pm}(v, \mu, t) = [-a^s(v, v) + c_U - \ell^N(v) + \ell^D(t)] + [2a^s(v, v) - F^{\pm}(v; \mu) - b(v, t)]. \tag{4.53}$$

for $F^{\pm}(v; \mu)$ as defined in(4.34)-(4.35).

We now show that $\eta^{\pm}$ of (4.44)–(4.45) can be expressed as

$$\eta^{\pm} = \mathcal{L}^{\pm}(\hat{\mathcal{U}}_h^{\pm}, \psi_H^{\pm}, y^{\pm}), \tag{4.54}$$

where we simply set $v = \hat{\mathcal{U}}_h^{\pm}$, $\mu = \psi_H^{\pm}$, and $t = y^{\pm}$ in $\mathcal{L}^{\pm}(v, \mu, t)$ of (4.53), and evoke (4.42); note that, due to weak imposition of the Dirichlet conditions, all the subdomain problems in (4.41)-(4.42) are *natural*, and thus $v = \hat{\mathcal{U}}_h^{\pm}$ is an admissible test function. Moreover we have

$$\mathcal{L}^{\pm}(\hat{\mathcal{U}}_h^{\pm}, \psi_H^{\pm}, y^{\pm}) = \min_{v \in V_h} \mathcal{L}^{\pm}(v, \psi_H^{\pm}, y^{\pm}). \tag{4.55}$$

To demonstrate (4.55), we expand out Lagrangian (4.53) for $v = \hat{\mathcal{U}}_h^{\pm} + w, \mu = \psi_H^{\pm}, t = y^{\pm}$ to obtain

$$\begin{aligned} \mathcal{L}^{\pm}(\hat{\mathcal{U}}_h^{\pm} + w, \psi_H^{\pm}, y^{\pm}) &= \mathcal{L}^{\pm}(\hat{\mathcal{U}}_h^{\pm}, \psi_H^{\pm}, y^{\pm}) \\ &+ 2a^s(w, \hat{\mathcal{U}}_h^{\pm}) + F^{\pm}(w; \psi_H^{\pm}) - b(w, y^{\pm}) \\ &+ a^s(w, w), \quad \forall w \in V_h. \end{aligned} \tag{4.56}$$

From (4.42), we observe that the terms linear in w collectively vanish, and thus (4.55) directly follows since $a^s(,)$ is positive semi-definite over V_h.

Recall from (2.94) that for any choice of Lagrange multipliers we obtain a lower bound for s_h. The only requirement is that our adjoint and hybrid flux candidates $(\psi_H^{\pm}, y^{\pm})$ lie in $X_h^{D-} \times \mathcal{Q}$. It is clear that $y^{\pm} \in \mathcal{Q}_1 \subset \mathcal{Q}$ but it is not so clear that $\psi_H^{\pm} \in X_h^{D-}$. From our refinement hypothesis that $\mathcal{T}_h$ is a refinement of $\mathcal{T}_H$ it follows that $X_H^{D-} \in X_h^{D-}$, so $\psi_H^{\pm}$ is also in X_h^{D-}. In practice, this leads to a linear interpolation of $\psi_H^{\pm}$ on the h–mesh. We conclude that

$$\eta^{\pm} \leq \pm s_h, \tag{4.57}$$

and thus

$$\eta^{+} \leq s_h \leq -\eta^{-}. \tag{4.58}$$

We close this section with two remarks. First, we note that solvability is essential in the construction of the bounds [5]: without solvability, in a "singular" element T_H, $F_{T_H}^{\pm}(cv^s; \psi_H^{\pm}) - b(c\mathcal{P}v^s, y^{\pm}) \rightarrow -\infty$ for either $c \rightarrow \infty$ or $c \rightarrow -\infty$; since $a_{T_H}^s(cv^s, cv^s) = 0$,

$$\min_{v \in V_h} \mathcal{L}^{\pm}(v, \psi_H^{\pm}, y^{\pm}) = -\infty, \tag{4.59}$$

and the resulting bounds are meaningless. Solvability ensures that, in a singular element T_H, we satisfy

$$F_{T_H}^{\pm}(v^s; \psi_H^{\pm}) - b(\mathcal{P}v^s, y^{\pm}) = 0. \tag{4.60}$$

Recall, from the definition of Y_{bd} in (2.99), that candidate Lagrange multipliers must satisfy a equilibrium equation. The definition of that space Y_{bd} is similar to having our adjoint and hybrid flux satisfy (4.60). From (4.42) and from $v^s = 1$ being a valid test function it follows that (4.60), is indeed, satisfied. Thus, the modes not controlled by the quadratic

stabilization term cannot contribute to the value of the Lagrangian. As anticipated, the choice of the *level* of $\hat{\mathcal{U}}_h^{\pm}$ is, of course, irrelevant. Second, we note that we have proven here only that $(s_h)_{LB}$ and $(s_h)_{UB}$ are bounds for s_h; we expect to obtain *good* bounds since $\psi_H^{\pm}$ and $y^{\pm}$ are the saddlepoint of the H–mesh Lagrangian which should be a good approximation to the h–mesh Lagrangian.

Chapter 5

Bounds Formulation for the Incompressible Stokes Problem

5.1 Model Problem

5.1.1 Governing Equations

We consider the steady creeping flow of an incompressible (ρ = constant) Newtonian fluid with constant dynamic viscosity, μ, between two plates with a rectangle obstacle in the center. This geometry is presented in Figure 5-1 where (x_1, x_2) denotes the coordinate system, with corresponding unit vectors $\hat{x}_1$, $\hat{x}_2$; Ω is the domain; Γ_j, $j = 1, .., 5$ are the domain boundary. The flow is driven by the forcing term which can be seen as a pressure gradient $\Delta P/L$ in the x_1 direction. The velocity and pressure perturbations are periodic in the x_1 direction.

To describe this flow we use the "Laplacian" form of the incompressible Stokes equations. We present these equations in indicial notation,

$$-\frac{\partial^2 u_i}{\partial x_j x_j} + \frac{\partial p}{\partial x_i} = f_i, \quad \text{in} \quad \Omega, \qquad i = \{1, 2\}, \tag{5.1}$$

$$-\frac{\partial u_i}{\partial x_i} = 0, \quad \text{in} \quad \Omega, \tag{5.2}$$

with no–slip Dirichlet and periodic boundary conditions,

$$u = 0 \text{ on } \Gamma_i, \; i = \{1, 3, 5\}, \tag{5.3}$$

$$u|_{\Gamma_2} = u|_{\Gamma_4}, \tag{5.4}$$

where (u_1, u_2) are the velocity components, p is the periodic perturbation of pressure divided by viscosity and (f_1, f_2) are the components of the volumetric force divided by viscosity.

Since adding a constant to the periodic pressure solution yields another solution we

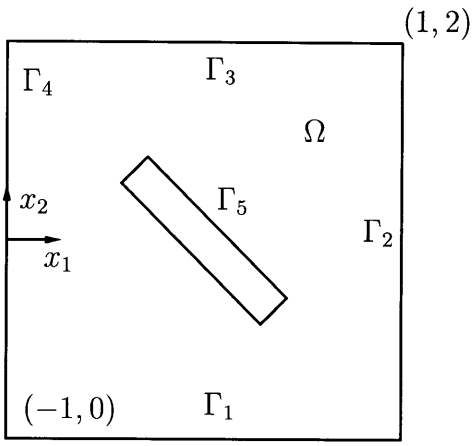

Figure 5-1: Geometry: Γ_1, Γ_3 and Γ_5 are homogeneous Dirichlet boundaries, Γ_4 and Γ_2 are periodic boundaries.

require, for uniqueness, that

$$\int_\Omega p \, \mathrm{d}A = 0. \tag{5.5}$$

Recall that p is the pressure perturbation and therefore the integral over the domain of this perturbations is zero.

The variational form of (5.1)-(5.2) is: Given $(f_1, f_2) \in (\mathcal{H}^{-1}(\Omega))^2$, find $(u_1, u_2) \in (\mathcal{H}^1_0(\Omega))^2$ and $p \in L^2_0(\Omega)$ such that

$$\int_\Omega \frac{\partial v_i}{\partial x_j}\frac{\partial u_i}{\partial x_j} - \frac{\partial v_i}{\partial x_i}p - v_i f_i \, \mathrm{d}A = 0 \quad \forall (v_1, v_2) \in (\mathcal{H}^1_0(\Omega))^2, \tag{5.6}$$

$$-\int_\Omega \frac{\partial u_i}{\partial x_i} q \, \mathrm{d}A = 0 \quad \forall q \in L^2_0(\Omega), \tag{5.7}$$

where $\mathrm{d}A$ is a differential area element. Here, we define

$$\mathcal{H}^1_0(\Omega) = \{v \in \mathcal{H}^1(\Omega) |\ v|_{\Gamma_2} = v|_{\Gamma_4},\ v|_{\Gamma_i} = 0,\ i = \{1,3,5\}\}, \tag{5.8}$$

$$L^2_0(\Omega) = \{q \in L^2(\Omega) |\ q|_{\Gamma_2} = q|_{\Gamma_4}, \int_\Omega q \, \mathrm{d}A = 0\}. \tag{5.9}$$

5.1.2 Output Linear Functionals

We assume that our output s may be expressed as a linear functional of the velocity components u_i and of pressure p, that is $s = \ell(u_1, u_2, p) = \ell^V_i(u_i) + \ell^P(p)$ where

$$\ell \ : (\mathcal{H}^1_0(\Omega))^2 \times L^2(\Omega) \to \mathbf{R}, \tag{5.10}$$

or

$$\ell^V_i \ : \mathcal{H}^1_0(\Omega) \to \mathbf{R}, \quad i = \{1,2\}, \tag{5.11}$$

$$\ell^P \quad : L^2(\Omega) \to \mathbf{R}.$$

Equivalently ℓ is a linear functional on the product space $(\mathcal{H}_0^1(\Omega))^2 \times L^2(\Omega)$. On physical grounds, $\ell^P(1) = 0$, since the pressure is arbitrary, and thus should not affect the output. The mathematical ramification are given later.

Examples of possible linear functionals include the flowrate or the lift force acting on a body immersed in the fluid. The particular linear functional for the flowrate (output $s^{(8)}$) between two parallel plates is defined as

$$\begin{aligned} \ell_1^V(v) &= \frac{L}{\Omega}\int_\Omega v \, \mathrm{d}A, \\ \ell_2^V(v) &= 0, \\ \ell^P(q) &= 0, \end{aligned} \tag{5.12}$$

where L is the height between the plates. Note that these output functionals are bounded for all v in $\mathcal{H}^1(\Omega)$. Another important engineering output of interest ($s^{(9)}$) is the lift force acting on a body. We evaluate this force with the following functionals:

$$\begin{aligned} \ell_1^V(u) &= \int_\Omega \frac{\partial \mathcal{X}_1}{\partial x_j}\frac{\partial u_1}{\partial x_j} - \mathcal{X}_1 f_1 \, \mathrm{d}A, \\ \ell_2^V(u) &= \int_\Omega \frac{\partial \mathcal{X}_2}{\partial x_j}\frac{\partial u_2}{\partial x_j} - \mathcal{X}_2 f_2 \, \mathrm{d}A, \\ \ell^P(p) &= -\int_\Omega p(\frac{\partial \mathcal{X}_1}{\partial x_1} + \frac{\partial \mathcal{X}_2}{\partial x_2}) \, \mathrm{d}A, \end{aligned} \tag{5.13}$$

or equivalently

$$s^{(9)} = \int_\Omega \frac{\partial \mathcal{X}_i}{\partial x_j}\frac{\partial u_i}{\partial x_j} - p\frac{\partial \mathcal{X}_i}{\partial x_i} - \mathcal{X}_i f_i \, \mathrm{d}A, \tag{5.14}$$

where $\mathcal{X} = (\mathcal{X}_1, \mathcal{X}_2)$ is any pair of continuous functions in $(\mathcal{H}^1(\Omega))^2$ such that $\mathcal{X}_1 = 0, \mathcal{X}_2 = 1$ on Γ^5 and $\mathcal{X}_1 = 0, \mathcal{X}_2 = 0$ on the other non–periodic boundaries. Note that, if we choose $\mathcal{X}$ to be an incompressible field then the pressure part of the functional ($\ell^P(p)$) becomes zero. To show that these choices are compatible with the incompressibility constraint we refer to Gauss' theorem

$$\int_\Omega \frac{\partial \mathcal{X}_i}{\partial x_i} \, \mathrm{d}A = \int_{\partial\Omega} \mathcal{X}_i \hat{n}_i \, \mathrm{d}s = \int_{\Gamma_5} \mathcal{X}_i \hat{n}_i \, \mathrm{d}s = 0. \tag{5.15}$$

Note that Γ_5 is a close boundary contour, and that $\mathcal{X}_1 = 0, \mathcal{X}_2 = 1$ on Γ^5, which directly leads to our result in (5.15). In Chapter 8 two particular choices of $\mathcal{X}$ will be described and tested.

The motivation behind this choice of functional is once again to obtain bounded functionals as we can predict specific convergence properties for $\ell_i^V \in \mathcal{H}^{-1}(\Omega)$ and $\ell^P \in L^2(\Omega)$. To show that this functional is bounded, we only require to bound the linear part in u_i and

in p. Since $\mathcal{X} \in (\mathcal{H}^1(\Omega))^2$ one can write

$$\begin{aligned} |s^{(9)}| &\leq |\mathcal{X}_1|_{\mathcal{H}^1}|u_1|_{\mathcal{H}^1} + |\mathcal{X}_2|_{\mathcal{H}^1}|u_2|_{\mathcal{H}^1} + \\ &\quad \|p\|_{L^2}|\mathcal{X}_1|_{\mathcal{H}^1} + \|p\|_{L^2}|\mathcal{X}_2|_{\mathcal{H}^1}, \qquad (5.16) \\ &\leq \|\mathcal{X}_1\|_{\mathcal{H}^1}\|u_1\|_{\mathcal{H}^1} + \|\mathcal{X}_2\|_{\mathcal{H}^1}\|u_2\|_{\mathcal{H}^1} + \\ &\quad \|p\|_{L^2}\|\mathcal{X}_1\|_{\mathcal{H}^1} + \|p\|_{L^2}\|\mathcal{X}_2\|_{\mathcal{H}^1}, \qquad (5.17) \\ &\leq \|\mathcal{X}\|_{\mathcal{H}^1}\|u\|_{\mathcal{H}^1} + \|\mathcal{X}\|_{\mathcal{H}^1}\|p\|_{\mathcal{H}^1}. \qquad (5.18) \end{aligned}$$

Therefore, $s^{(9)}$ is bounded.

To demonstrate that (5.13) corresponds to the lift force, we first integrate by parts (5.14),

$$s^{(9)} = \int_\Omega \frac{\partial}{\partial x_j}(\mathcal{X}_i \frac{\partial u_i}{\partial x_j}) - \mathcal{X}_i \frac{\partial^2 u_i}{\partial x_j\, \partial x_j} - \frac{\partial}{\partial x_i}(p\mathcal{X}_i) + \mathcal{X}_i \frac{\partial p}{\partial x_i} - \mathcal{X}_i f_i \, \mathrm{d}A. \qquad (5.19)$$

We now regroup terms,

$$s^{(9)} = \int_\Omega \mathcal{X}_i(-\frac{\partial^2 u_i}{\partial x_j\, \partial x_j} + \frac{\partial p}{\partial x_i} - f_i) \, \mathrm{d}A + \int_\Omega \frac{\partial}{\partial x_j}(\mathcal{X}_i \frac{\partial u_i}{\partial x_j} - p\mathcal{X}_i\delta_{ij}) \, \mathrm{d}A. \qquad (5.20)$$

Second, by appealing to the equilibrium statement (5.1) the first integral vanishes. We can add $\frac{\partial}{\partial x_j}(\frac{\partial u_j}{\partial x_i}) = 0$ and obtain

$$s^{(9)} = \int_\Omega \frac{\partial}{\partial x_j}(\mathcal{X}_i \frac{\partial u_i}{\partial x_j} + \mathcal{X}_i \frac{\partial u_j}{\partial x_i} - p\mathcal{X}_i\delta_{ij}) - \frac{\partial \mathcal{X}_i}{\partial x_j}\frac{\partial u_j}{\partial x_i} \, \mathrm{d}A. \qquad (5.21)$$

We now want to show that the term $\int_\Omega \frac{\partial \mathcal{X}_i}{\partial x_j}\frac{\partial u_j}{\partial x_i} \, \mathrm{d}A$ vanishes. Using integration by parts and knowing that $\frac{\partial}{\partial x_j}(\frac{\partial u_j}{\partial x_i}) = 0$ for our field solution we obtain

$$\int_\Omega \frac{\partial}{\partial x_j}(\mathcal{X}_i \frac{\partial u_j}{\partial x_i}) \, \mathrm{d}A = \int_\Omega \frac{\partial \mathcal{X}_i}{\partial x_j}\frac{\partial u_j}{\partial x_i} \, \mathrm{d}A, \qquad (5.22)$$

which then becomes for our model problem

$$\int_{\Gamma^5} \mathcal{X}_i \frac{\partial u_j}{\partial x_i} n_j \, \mathrm{d}s. \qquad (5.23)$$

Based on our choice of $\mathcal{X}$, in particular that $\mathcal{X}_1 = 0$ and $\mathcal{X}_2 = 1$ on Γ^5 then (5.23) becomes

$$\int_{\Gamma^5} \frac{\partial u_j}{\partial x_2} n_j \, \mathrm{d}s \equiv 0. \qquad (5.24)$$

We consider two cases, first, on a straight edge boundary we know from the no slip

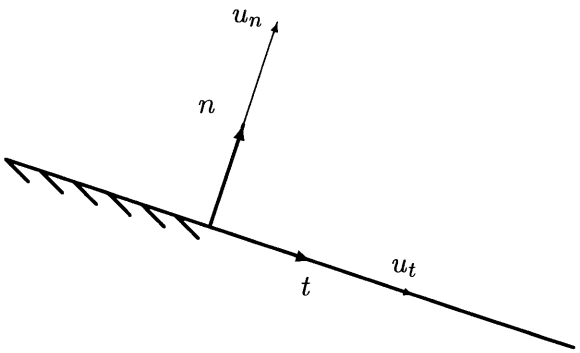

Figure 5-2: Wall normal and tangential components of velocity.

boundary condition on the wall that

$$\frac{\partial u_n}{\partial t} = 0, \tag{5.25}$$

$$\frac{\partial u_t}{\partial t} = 0, \tag{5.26}$$

where u_n and u_t are respectively the wall normal and tangential components of velocity, presented in Figure 5-2. From continuity,

$$\frac{\partial u_n}{\partial n} + \frac{\partial u_t}{\partial t} = 0, \tag{5.27}$$

we conclude that

$$\frac{\partial u_n}{\partial n} = 0. \tag{5.28}$$

From (5.28) and (5.26), it follows that

$$\frac{\partial u_n}{\partial x_2} = 0, \tag{5.29}$$

and therefore,

$$\frac{\partial u_j}{\partial x_2} n_j = \frac{\partial u_n}{\partial x_2} = 0, \tag{5.30}$$

which proves that (5.24) is satisfied on a straight line. Note that the above holds for a smooth curved line which can be approximated as infinitely small lines segments.

Second, we consider a corner such as illustrated in Figure 5-3. It appears that at the corner we can directly satisfy

$$\frac{\partial u_n}{\partial n} = \frac{\partial u_n}{\partial t} = 0, \tag{5.31}$$

to obtain (5.30) but this may not be rigorously exact. At the corner there exists a jump in

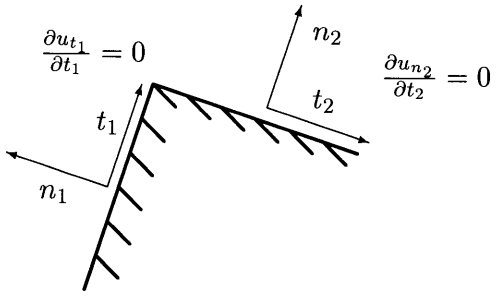

Figure 5-3: Corner normal and tangential vectors.

velocity derivatives in both directions, t_1 and t_2. However, we assume this singularity to be small enough so that it may be considered negligible. Results obtain for the lift output, $s^{(9)}$, where we have not eliminated the term $\int_\Omega \frac{\partial \mathcal{X}_i}{\partial x_j}\frac{\partial u_j}{\partial x_i}\,\mathrm{d}A$ are presented in [37]; in particular, in [37] we redefine $s^{(9)}$ as,

$$s^{(9)} = \int_\Omega \frac{\partial \mathcal{X}_i}{\partial x_j}\left(\frac{\partial u_i}{\partial x_j} + \frac{\partial u_j}{\partial x_i}\right) - p\frac{\partial \mathcal{X}_i}{\partial x_i} - \mathcal{X}_i f_i \,\mathrm{d}A. \tag{5.32}$$

Finally, we identify the stress tensor (σ_{ij}) divided by viscosity in (5.21) and we write

$$s^{(9)} = \int_\Omega \mathcal{X}_i \sigma_{ij}\hat{n}_j \,\mathrm{d}s, \tag{5.33}$$

where $\hat{n}_j$ is the normal outward vector. We see that if we impose on Γ_5 (the obstacle) $\mathcal{X}_j$ to be equal to $+1$ only in the x_2 direction and that vanishes to zero on the other boundaries we then obtain the force on the fluid in the x_2 direction. To obtain the lift force we just need to invert the signs. (Note that we can also calculate the drag force acting on the body by choosing a set of functions $\mathcal{X} = (\mathcal{X}_1, \mathcal{X}_2)$ such that $\mathcal{X}_1 = 1$ on Γ_5 and any continuous function that vanishes on the boundary.) Finally, from (5.12) and (5.13) we then compute our desired output as $s = \ell_i^V(u_i) + \ell^P(p)$.

5.2 Finite Element Discretization

The general finite element ingredients such as the bilinear and linear forms and the function spaces are introduced in this section. The general triangulation introduced in Section 2.3.1 is exploited here. Note, that in this case we are only in the presence of Dirichlet edges and periodic edges but no Neumann boundaries.

5.2.1 Bilinear and Linear Forms

We define here the bilinear and linear forms for Stokes problem. Similarly, we need to define a "broken" space which has no continuity required on the interior triangles. This space is used to define functions on the local subdomains. We denote

$$\mathcal{H}^1_*(\Omega) = \{v \in L^2(\Omega) |\ v|_{T_H} \in \mathcal{H}^1(T_H),\ \forall T_H \in \mathcal{T}_H\}. \tag{5.34}$$

Now, we define the bilinear form associated with our operator as

$$a(w,v) = \sum_{T_H \in \mathcal{T}_H} a_{T_H}(w|_{T_H}, v|_{T_H}), \qquad \forall (w,v) \in (\mathcal{H}^1_*(\Omega))^2, \tag{5.35}$$

where for all T_H in $\mathcal{T}_H$

$$a_{T_H}(w,v) = \int_{T_H} \nabla w \cdot \nabla v \ \mathrm{d}A, \qquad \forall (w,v) \in (\mathcal{H}^1(T_H))^2. \tag{5.36}$$

Similarly,

$$d_i(w,q) = \sum_{T_H \in \mathcal{T}_H} d_{iT_H}(w|_{T_H}, q|_{T_H}), \qquad \forall (w,q) \in \mathcal{H}^1_*(\Omega) \times L^2(T_H), \tag{5.37}$$

where for all T_H in $\mathcal{T}_H$

$$d_{i\,T_H}(w,q) = \int_{T_H} q \frac{\partial w}{\partial x_i} \ \mathrm{d}A, \qquad \forall (w,q) \in \mathcal{H}^1(T_H) \times L^2(\Omega). \tag{5.38}$$

We next introduce a set of "jump" bilinear and linear forms required in our variational relaxations. These forms will be apply in a scalar fashion to each component of velocity. In particular, we define the bilinear from

$$\begin{aligned} b(w,t) \quad = \quad & \sum_{T_H \in \mathcal{T}_H} \sum_{\gamma_{T_H} \in \mathcal{E}(T_H)} \sigma_H^{\gamma_{T_H}} \int_{\gamma_{T_H}} w|_{T_H}\ t|_{E(\gamma_{T_H})} \ \mathrm{d}s, \\ & \forall (w,t) \in \mathcal{H}^1_*(\Omega) \times \mathcal{Q}, \end{aligned} \tag{5.39}$$

where $w|_{T_H}$ is to be interpreted as the trace of $w|_{T_H}$ on γ_{T_H} and $\mathcal{Q} = \{t \in \mathcal{H}^{-1/2}(\mathcal{E}(\mathcal{T}_H)) |\ t|_{\Gamma_N} = 0\}$. Note that t is defined only over the edges of the triangulation. Effectively, (5.39) computes the moments of the jumps in w over integral edges, and the moments of w over boundary edges.

We now introduce our linear functionals. Associated with the volumetric inhomogeneities, we have

$$\ell_i^N(w) = \sum_{T_H \in \mathcal{T}_H} \ell_{i\,T_H}^N(w|_{T_H}), \quad \forall w \in \mathcal{H}^1_*(\Omega), \tag{5.40}$$

where for all T_H in $\mathcal{T}_H$

$$\ell_{i\,T_H}^N(w) = \int_{T_H} w f_i \, \mathrm{d}A, \quad \forall w \in \mathcal{H}^1(T_H). \tag{5.41}$$

Associated with our output functional, we introduce

$$\ell_i^{O^v}(w) = \sum_{T_H \in \mathcal{T}_H} \ell_{i\,T_H}^{O^v}(w|_{T_H}), \quad \forall w \in \mathcal{H}_*^1(\Omega), \tag{5.42}$$

such that

$$\ell_i^{O^v}(w) = \ell_i^V(w), \quad \forall w \in \mathcal{H}^1(\Omega). \tag{5.43}$$

Similarly we can introduce linear functional for pressure,

$$\ell^{O^p}(q) = \sum_{T_H \in \mathcal{T}_H} q|_{T_H} \ell^{O^p}(,) \quad \forall q \in L_0^2(\Omega), \tag{5.44}$$

such that

$$\ell^{O^p}(q) = \ell^P(q), \quad \forall q \in L_0^2(\Omega). \tag{5.45}$$

Here $\ell^{V,P}()$ is the formal output functional introduced in (5.11).

5.2.2 Function Spaces

We consider two different spatial discretizations; $\delta = H$ and $\delta = h$ which corresponds respectively to our "working" and "truth" discretizations. We use here the Crouzeix–Raviart approximation spaces as previously described in Section 2.3.4 and in Appendix C. For components of velocity, we identify

$$X_\delta = \{v|_{T_\delta} \in \mathbf{P}_2^+(T_\delta), \ \forall T_\delta \in \mathcal{T}_\delta\} \bigcap \mathcal{H}_0^1(\Omega), \tag{5.46}$$

where $\mathbf{P}_2^+(T_\delta) = \{\mathbf{P}_2(T_\delta) + \alpha_{T_H} \xi_1 \xi_2 \xi_3, \ \alpha_{T_H} \in \mathbf{R}\}$ is the space of quadratic polynomials enhanced by a "bubble" function over T_δ. The barycentric coordinates (ξ_1, ξ_2, ξ_3) define the "bubble" function.

For pressure, we identify

$$Y_\delta = \{q|_{T_\delta} \in \mathbf{P}_1(T_\delta), \ \forall T_\delta \in \mathcal{T}_\delta\} \bigcap L_0^2(\Omega). \tag{5.47}$$

We next introduce spaces of polynomial functions defined on the edges only,

$$\mathcal{Q}_k = \{t|_\delta \in \mathbf{P_k}(\gamma), \forall \gamma \in \mathcal{E}(\mathcal{T}_H)\} \bigcap \mathcal{Q}. \tag{5.48}$$

Let's now define two subdomain local spaces. First, for velocity, the subdomain local spaces

is given as

$$Z_H(T_H) = (\mathbf{P}_2^+(T_H)), \tag{5.49}$$

and

$$Z_h(T_H) = \{v|_{T_h} \in \mathbf{P}_2^+(T_h),\ \forall T_h \in \mathcal{R}_{T_H},\} \bigcap \mathcal{H}_0^1(T_H), \tag{5.50}$$

where we recall that $\mathcal{R}_{T_H}$ is the set of h–mesh elements that constitute T_H. Associated with these spaces we add an incompressibility constraint for velocity and define the spaces

$$D_\delta(T_H) = \{(v_1, v_2) \in (Z_\delta(T_H))^2, d_{i\,T_H}(v_i, q) = 0,\ \forall q \in L^2(T_H)\}. \tag{5.51}$$

Second, for pressure, the subdomain local spaces is given as

$$M_H(T_H) = (\mathbf{P}_1(T_H)), \tag{5.52}$$

and

$$M_h(T_H) = \{q|_{T_H} \in \mathbf{P}_1(T_h),\ \forall T_h \in \mathcal{R}_{T_H}\} \bigcap L^2(T_H). \tag{5.53}$$

We can define the associated "product" spaces with and without incompressibility constraint as

$$V_\delta \quad = \quad \{v \in \mathcal{H}_*^1(\Omega)|\ v|_{T_H} \in Z_\delta(T_H),\ \forall q \in M_\delta(T_H)\}, \tag{5.54}$$

and

$$U_\delta = \{(v_1, v_2) \in (\mathcal{H}_*^1(\Omega))^2|\ (v_1|_{T_H}, v_2|_{T_H}) \in D_\delta(T_H),\ \forall T_H \in \mathcal{T}_H\}, \tag{5.55}$$

for $\delta = H$ and $\delta = h$. In essence, the $D_\delta(T_H)$ are Neumann spaces over each T_H, for which U_δ is the corresponding global representation. Note that these spaces impose local or global incompressibility on the velocity.

5.3 Bound Procedure

The bound procedure is based on choosing an approximation to the h–mesh Lagrange multipliers. Recall that the adjoint enforces the equilibrium equations and the hybrid flux enforces the intersubdomain continuity conditions. We use a hierarchical approach, that is we initially calculate our candidate Lagrange multipliers on the H–mesh that we then "interpolate" on the h–mesh.

5.3.1 The H–Mesh Adjoint Calculation

First, we solve the Stokes Problem (5.1). We look for $(u_{1\,H}, u_{2\,H}, p_H) \in (X_H)^2 \times Y_H$ such that

$$\begin{aligned} a(w_i, u_{i\,H}) - d_i(w_i, p_H) &= \ell_i^N(w_i), \qquad \forall (w_1, w_2) \in (X_H)^2, & (5.56)\\ -d_i(u_{i\,H}, q) &= 0, \qquad \forall q \in Y_H. & (5.57) \end{aligned}$$

Second we solve for the adjoint. We look for $(\psi_{1H}^{\pm}, \psi_{2H}^{\pm}, \Lambda_H^{\pm}) \in (X_H)^2 \times Y_H$ such that

$$\begin{aligned} a(\psi_{iH}^{\pm}, w_i) - d_i(w_i, \Lambda_H^{\pm}) &= -(\pm\ \ell_i^{O^v}(w_i)) + 2a(w_i, u_{iH}) - \ell_i^N(w_i)), & (5.58)\\ -d_i(\psi_{iH}^{\pm}, q) &= -(\pm \ell_i^{O^p}(q)), \quad \forall (w_1, w_2, q) \in (X_H)^2 \times Y_H. & (5.59) \end{aligned}$$

It is required that $\ell^P(1) = 0$ to avoid any forcing term which is not equilibrated when v^s is the nullspace of the divergence operator. This condition is required for solvability reasons because the pressure functional appears on the right hand side of (5.59). Physically, this condition is required because the pressure level is arbitrary and our output (5.10)-(5.11) should not depend on the pressure level, it should be uniquely determined.

In fact, (5.56)-(5.59) are obtained from stationarity of the saddle problem associated with our Lagrangian. In (5.58)-(5.59) the hybrid flux vanishes because the velocity space is continuous, (X_H). Note that, (5.58)-(5.59) need to be solved twice, once for each bound; $\pm$ refers to the *pair* of solutions required for the lower $(+)$ and upper $(-)$ bounds. If a direct solver is used only one LU factorization is required which can also be used to solve (5.1)-(5.2). The Stokes operator is in fact the same and only the right hand side of the equations changes. Recall that we have used Crouzeix–Raviart elements, presented in Section 2.3.4, to avoid the calculation of a hybrid flux calculation for the pressure. These elements satisfy the *inf–sup* condition which is necessary to ensure that we have a stable discretization [19].

We now define a function $F_i^{\pm}(v; \mathcal{F}, \mathcal{P})$ which in some sense represents the forcing term and the pressure term in each of the momentum equations of (5.58). This function is introduced mainly to simplify the notation. Therefore, for any function $\mathcal{F}$ in $\mathcal{H}^1_*(\Omega)$ and $\mathcal{P}$ in $L^2_0(\Omega)$, we write

$$F_i^{\pm}(v; \mathcal{F}, \mathcal{P}) = \sum_{T_H \in \mathcal{T}_H} F_{i\,T_H}^{\pm}(v|_{T_H}; \mathcal{F}, \mathcal{P}), \quad \forall v \in \mathcal{H}^1_*(\Omega), \tag{5.60}$$

where for all T_H in $\mathcal{T}_H$,

$$F_{i\,T_H}^{\pm}(v|_{T_H}; \mathcal{F}, \mathcal{P}) = \pm\ \ell_{i\,T_H}^{O^v}(v) + a_{T_H}(\mathcal{F}|_{T_H}, v) - \ell_{i\,T_H}^N(v) - d_{i\,T_H}(v, \mathcal{P}). \tag{5.61}$$

We rewrite the momentum equations of (5.58) where we look for $(u_{1H}, u_{2H}) \in (X_H)^2$, such that

$$2a(w_i, u_{iH}) = -F_i^{\pm}(w_i, \psi_{iH}^{\pm}, \Lambda_H^{\pm}). \tag{5.62}$$

We can also introduce a second way in which to re–express (5.62) where we look for $(u_{H1}, u_{H2}) \in (X_H)^2$ such that

$$B_i^{\pm}(v, u_{iH}) = 0, \ \ \forall v \in X_H, \ i = \{1, 2\}. \tag{5.63}$$

Here, for any function $\mathcal{G}$ in $\mathcal{H}_*^1(\Omega)$

$$B_i^{\pm}(v, \mathcal{G}) = \sum_{T_H \in \mathcal{T}_H} B_{i\,T_H}^{\pm}(v|_{T_H}, \mathcal{G}), \quad \forall v \in \mathcal{H}_*^1(\Omega), \tag{5.64}$$

where for all T_H in $\mathcal{T}_H$,

$$B_{i\,T_H}^{\pm}(w, \mathcal{G}) = 2a_{T_H}(w, \mathcal{G}|_{T_H}) + F_{i\,T_H}^{\pm}(w; \psi_{iH}^{\pm}, \Lambda_H^{\pm}), \quad \forall w \in \mathcal{H}_*^1(T_H). \tag{5.65}$$

5.3.2 The H–Mesh Hybrid Flux Calculation

The hybrid flux will appear in our Lagrangian as a Lagrange multiplier that enforces the subdomain continuity constraints. Recall that, for the Crouzeix–Raviart elements we only need to impose continuity for the velocity components. Our procedure here is to calculate the hybrid flux by appealing to the broken space. We now have, for each component of velocity, the full equilibration equation that needs to be satisfied,

$$b(v, y_i^{\pm}) = B_i^{\pm}(v, u_{Hi}), \qquad \forall v \in V_H, \tag{5.66}$$

which then becomes, for all T_H in $\mathcal{T}_H$,

$$\sum_{\gamma_{T_H} \in \mathcal{E}(T_H)} \sigma_{T_H}^{\gamma_{T_H}} \int_{\gamma_{T_H}} v y_i^{\pm}|_{E(\gamma_{T_H})} \, \mathrm{d}s = B_{i\,T_H}^{\pm}(v, u_{iH}), \qquad \forall v \in Z_H(T_H). \tag{5.67}$$

In Chapter 6 we will present two different approaches to approximate the hybrid flux for quadratic elements. All are based on an initial approximation which is corrected with a $\mathbf{P}_1$ term to ensure solvability. In addition, we add a higher order term to improve accuracy. The latter is not required but should give sharper bounds.

5.3.3 The h–Mesh Subdomain Neumann Problem

Before we solve the subdomain problem, we compute the adjoint $(\hat{\psi}_{ih}^{\pm})$ on the h–mesh. For all T_H in $\mathcal{T}_H$, the adjoint $(\hat{\psi}_{ih}^{\pm})$ needs to be continuous to be a valid Lagrange multiplier and it requires to satisfy an equilibration equation to obtain meaningful bounds as we will

discuss below. We satisfy these conditions for all T_H in $\mathcal{T}_H$ by solving the system to find $\hat{\psi}_{ih}^{\pm} \in (Z_h^D(T_H))^2$, such that

$$a_{T_H}(v_i, \hat{\psi}_{ih}^{\pm} - \psi_{iH}^{\pm}) - d_{i\,T_H}(v_i, \tilde{p}_h) = 0, \quad \forall (v_1, v_2) \in (Z_h(T_H))^2, \tag{5.68}$$

$$-d_{i\,T_H}(\hat{\psi}_{ih}^{\pm}, q) = -(\pm \ell_{T_H}^{Op}(q)) \quad \forall q \in M_h(T_H), \tag{5.69}$$

where

$$Z_h^D(T_H) = \{v|_{T_H} \in Z_h(T_H) |\ v|_{\gamma_{T_H}} = \psi_{iH}^{\pm}|_{\gamma_{T_H}},\ \forall \gamma \in \mathcal{E}(T_H)\}. \tag{5.70}$$

In effect, (5.70) is simply a space which imposes the H–mesh adjoint values ($\psi_{iH}^{\pm}$) at the nodes on the boundary of the T_H and it is important to note that for ∂T_H and ∂T_h the bubble vanish so that the trace of $\psi_H^{\pm}$ on ∂T_H is in $Z_h(T_H)$ — the h–mesh subdomain space. The term $\tilde{p}_h$ in (5.68) is a "dummy" variable which is not used in the rest of this work. The equilibration between $d_{iT_H}(\hat{\psi}_{ih}^{\pm}, q)$ and $\pm \ell^{Op}(q)$ is required in addition to the above Dirichlet boundaries to impose some compatibility constraints. Note that, if $q = 1$ in (5.69) and since 1 is in the X_H then,

$$d_{i\,T_H}(\hat{\psi}_{ih}^{\pm}, 1) = \int_{\partial\Omega} \psi_{iH}^{\pm} \hat{n}_i^{\gamma_{T_H}}\, \mathrm{d}s = d_{i\,T_H}(\psi_{iH}^{\pm}, 1) = \pm\, \ell_{T_H}^{Op}(1). \tag{5.71}$$

where $\hat{n}_i^{\gamma_{T_H}}$ is the outward normal on γ_{T_H} with respect to T_H. Physically, this means that for incompressible fluids we can not have any change in mass inside any element. The issue of solvability of (5.68)-(5.69) needs not be considered here because we do not have any singular elements — all boundaries are Dirichlet.

For the local subdomain problem, we now look for $(\hat{u}_{1\,T_H}^{\pm}, \hat{u}_{2\,T_H}^{\pm}) \in D_h(T_H)$, for all T_H in $\mathcal{T}_H$, such that

$$\begin{aligned} 2a_{T_H}(w_i, \hat{u}_{i\,T_H}^{\pm}) - d_{i\,T_H}(w_i, \bar{\tau}_h^{\pm}) &= -(\pm\, \ell_{i\,T_H}^{Ov}(w_i) - \ell_{i\,T_H}^{N}(w_i) + a_{T_H}(\hat{\psi}_{ih}^{\pm}, w_i) \\ -d_{i\,T_H}(w_i, \Lambda_h^{\pm}) &- \sum_{\gamma_{T_H} \in \mathcal{E}(T_H)} \sigma_{T_H}^{\gamma_{T_H}} \int_{\gamma_{T_H}} w_i y_i^{\pm}|_{E(\gamma_{T_H})} \mathrm{d}s), \qquad (5.72) \\ -d_{i\,T_H}(\hat{u}_{i\,T_H}^{\pm}, q) &= 0, \quad \forall (w_1, w_2, q) \in (Z_h(T_H))^2 \times M_h(T_H). \qquad (5.73) \end{aligned}$$

To check solvability, we appeal to (5.63) where we replace v by v^s which is a function for which our bilinear form $a_{T_H}(,)$ is singular. From this we prove that the right hand side of (5.72) vanishes. Note that the construction of $\hat{\psi}_{ih}^{\pm}$ is also essential for solvability. The issue is that the equilibrium equation (5.66) includes $\psi_{iH}^{\pm}$, but in (5.73) $\hat{\psi}_{ih}^{\pm}$ appears. However, since $a(\hat{\psi}_{ih}^{\pm}, 1) = a(\psi_{iH}^{\pm}, 1) = 0$, we are able to satisfy solvability.

In a more compact notation, we can introduce functions $(\hat{\mathcal{U}}_{1h}^{\pm}, \hat{\mathcal{U}}_{2h}^{\pm}) \in U_h$ such that

$\hat{\mathcal{U}}_{ih}^{\pm}|_{T_H} = \hat{u}_{i\,T_H}^{\pm}$, $\forall T_H \in \mathcal{T}_H$, where $(\hat{\mathcal{U}}_{1h}^{\pm}, \hat{\mathcal{U}}_{2h}^{\pm})$ satisfies

$$2a(w_i, \hat{\mathcal{U}}_{ih}^{\pm}) - d_i(w_i, \bar{\tau}_h^{\pm}) = -F_i^{\pm}(w_i, \hat{\psi}_{ih}^{\pm}, \Lambda_H^{\pm}) + b(w_i, y_i^{\pm}), \tag{5.74}$$

$$-d_i(\hat{\mathcal{U}}_{ih}^{\pm}, q) = 0, \quad \forall (w_1, w_2, q) \in (V_h)^2 \times M_h. \tag{5.75}$$

We make several remarks. First, we note that the K systems for $\hat{u}_{i\,T_H}^{\pm}$ are completely decoupled leading to very efficient inversion compared to the original h–mesh problem of (5.6)-(5.7). This cost reduction is considerable especially when decoupling the Stokes problem which is a larger system with a larger bandwidth than for the elliptic problems. An additional advantage is that each of these subdomain problems may be easily solved in parallel. Second, we have introduce an additional constraint on the subdomain problems. We have imposed a local incompressibility constraint for $\hat{\mathcal{U}}_{ih}^{\pm}$. This is not required by the bound theory however we expect that it does improve the accuracy of the bounds. This approach leads to solutions of local Stokes problems instead of two local conduction problems. It would be interesting to compare our results with the results of this latter cheaper approach. Third, note that we solve two (one for each bounds) local Stokes problem to interpolate the adjoint on the h–mesh. The cost of this additional solve is small specially if we decide to use direct solves in which case only one LU decomposition is necessary for both the adjoint and the velocity calculations.

Finally, we make a few implementation remarks. If $(\mathcal{X}_1, \mathcal{X}_2)$ is chosen to be incompressible, then a Stokes problem on the H–mesh is initially solved given the approximate boundary conditions appropriate to obtain the output of interested. Therefore, we look for $(\mathcal{X}_{1H}, \mathcal{X}_{2H}) \in (X_H^*)^2$ such that

$$a(w_i, \mathcal{X}_{i\,H}) - d_i(w_i, \tilde{p}_H) = \ell_i^N(w_i), \qquad \forall (w_1, w_2) \in (X_H^*)^2, \tag{5.76}$$

$$-d_i(u_{i\,H}, q) = 0, \qquad \forall q \in Y_H, \tag{5.77}$$

where $\tilde{p}_H$ is a "dummy" variable and $X_H^* = \{v|_{T_\delta} \in \mathbf{P}_2^+(T_\delta),\ \forall T_\delta \in \mathcal{T}_\delta\ v|_{\partial\Omega\setminus\Gamma_5} = 0,\ v|_{\Gamma_5} = g^*\} \bigcap \mathcal{H}^1(\Omega)$ with $g^* = 0$ and $g^* = 1$ corresponding to Dirichlet data of each component of $\mathcal{X}$ ($\mathcal{X}_1$ and $\mathcal{X}_2$), respectively. When we arrive at the h–mesh problem we then project locally $(\mathcal{X}_{1H}, \mathcal{X}_{2H})$ on the h–mesh. We proceed element by element and solve for $(\mathcal{X}_{1h}, \mathcal{X}_{2h})$ by calculating a local Stokes problems for $(\mathcal{X}_{1h}, \mathcal{X}_{2h})$. This procedure is similar to projecting $\psi_{iH}^{\pm}$ to obtain $\hat{\psi}_{ih}^{\pm}$ in (5.68)-(5.69). However, if $(\mathcal{X}_1, \mathcal{X}_2)$ is chosen not to be incompressible then the incompressibility constraints is not required, hence, only two symmetric problems need to be solved for each element.

Finally, we can now calculate the bounds as

$$(s_h)_{LB}(H) = \eta^+, \tag{5.78}$$

and

$$(s_h)_{UB}(H) = -\eta^-, \tag{5.79}$$

where

$$\eta^{\pm} = -a(\hat{\mathcal{U}}_{ih}^{\pm}, \hat{\mathcal{U}}_{ih}^{\pm}) - \ell_i^N(\hat{\psi}_{ih}^{\pm}). \tag{5.80}$$

Note that the upper bounds is only obtain by solving the same problem as the lower bound but where the output is multiplied by -1. This technique is similar to the optimal stabilization parameter artifice presented in Chapter 7.

5.4 Proof of Bounding Properties

The proof of the bounding properties of $\eta^{\pm}$ is based on the classical quadratic duality theory [44, 35]. The key feature of our approach is to construct a Lagrangian which must have a quadratic objective function and linear constraints such that at stationarity this Lagrangian is equal to the output of interest. Therefore, we derive an "energy" equality that provides the stabilization in our Lagrangian. Note that it is the energy term which allows us to have candidate Lagrange multipliers and still provide non–infinite bounds. We take the test function to be the solution to (5.1)-(5.2), $(u_{1\,h}^{\pm}, u_{2\,h}^{\pm}, p_h)$ which is inserted in our weak form of the Stokes equations to obtain

$$\begin{aligned} a(u_{ih}, u_{ih}) - d_i(u_{ih}, p_h) &= \ell_i^N(u_{ih}), & (5.81)\\ d_i(u_{ih}, q) &= 0, \qquad \forall q \in Y_h. & (5.82) \end{aligned}$$

Note that (5.81)-(5.82) reduces to a quadratic form in each of the components u_{ih} because the term $d_i(u_{ih}, p_h)$ is effectively zero. For inhomogeneous Dirichlet boundary conditions, a boundary function would be introduced as in Section 4.4 to directly obtain boundary conditions for the adjoint.

By adding the output functional to the quadratic form (5.81) for all $v_i \in (X_h)^2$, we get a function that would reduce to $s_h = \ell_i^{O^v}(u_{ih}) + \ell^{O^p}(p_h)$ when $(v_i = u_{ih},\ q = p_h)$, that is

$$\pm s_h = \min_{(v_1,v_2,q)\in S} \left(\pm \ell_i^{O^v}(v_i) \pm \ell^{O^p}(q) + a(v_i, v_i) - \ell_i^N(v_i) \right), \tag{5.83}$$

where

$$\mathcal{S} = \left\{ (v_1, v_2, q) \in U_h \times Y_h \;\middle|\; \begin{array}{l} a(w_i, v_i) - d_i(w_i, q) = \ell_i^N(w_i), \\ d_i(\mu_i, \lambda) = 0,\ \forall (\mu_1, \mu_2, \lambda) \in (X_h)^2 \times Y_h, \\ b(w_i, t_i) = 0,\ \forall (t_1, t_2) \in (\mathcal{Q})^2 \end{array} \right\} \tag{5.84}$$

This set of functions $\mathcal{S}$ is a singleton $(v_i = u_{hi},\ q = p_h)$ equivalent to the solution of the Stokes equations (5.1)-(5.2).

From a mathematical point of view, the solution to (5.83) is equivalent to finding the saddlepoint of a Lagrangian, $\mathcal{L}^{\pm} : (v_1, v_2, q, \mu_1, \mu_2, \lambda, t_1, t_2) \in U_h \times Y_h \times (X_h)^2 \times Y_h \times (\mathcal{Q})^2$

$$\begin{aligned} \mathcal{L}^{\pm}(v_1, v_2, q, \mu_1, \mu_2, \lambda, t_1, t_2) &= \pm \ell_i^{O^v}(v_i) \pm \ell^{O^p}(q) \\ +a(v_i, v_i) - \ell_i^N(v_i) &+ a(\mu_i, v_i) - d_i(\mu_i, q) - \ell_i^N(\mu_i) \\ &- d_i(v_i, \lambda) - b(v_i, t_i). \end{aligned} \tag{5.85}$$

We have decomposed the spaces product $V_h \times V_h$ of globally smooth functions into functions belonging to space U_h and hence, we have decoupled (5.72)-(5.72) into (5.74)-(5.75). The introduction of intersubdomain continuity requirement may be regarded as a constraint on the edged imposed by the hybrid flux.

Inserting $F_i^{\pm}(v_i; \mu_i, \lambda)$ from (5.61) and regrouping terms so that subsequent simplifications are more obvious, we rewrite (5.85) as

$$\begin{aligned} \mathcal{L}^{\pm}(v_1, v_2, q, \mu_1, \mu_2, \lambda, t_1, t_2) &= \left[-a(v_i, v_i) - \ell_i^N(\mu_i)\right] \\ &+ \left[2a(v_i, v_i) + F_i^{\pm}(v_i; \mu_i, \lambda) - b(v_i, t_i)\right] \\ &+ \left[-d_i(\mu_i, q) \pm \ell^{O^p}(q)\right]. \end{aligned} \tag{5.86}$$

Our goal is to show that (5.86) equals $\eta^{\pm}$ calculated in (5.80) when $(v_1, v_2, q, \mu_1, \mu_2, \lambda, t_1, t_2) = (\hat{\mathcal{U}}_{1h}^{\pm}, \hat{\mathcal{U}}_{2h}^{\pm}, \cdot, \hat{\psi}_{1h}^{\pm}, \hat{\psi}_{2h}^{\pm}, \Lambda_h^{\pm}, y_1^{\pm}, y_2^{\pm})$, where the "$\cdot$" represents any value in Y_h. The Lagrangian becomes

$$\begin{aligned} \mathcal{L}^{\pm}(\hat{\mathcal{U}}_{1h}^{\pm}, \hat{\mathcal{U}}_{2h}^{\pm}, \cdot, \hat{\psi}_{1h}^{\pm}, \hat{\psi}_{2h}^{\pm}, \Lambda_h^{\pm}, y_1^{\pm}, y_2^{\pm}) &= \left[-a(\hat{\mathcal{U}}_{ih}^{\pm}, \hat{\mathcal{U}}_{ih}^{\pm}) - \ell_i^N(\hat{\psi}_{ih}^{\pm})\right] \\ &+ \left[2a(\hat{\mathcal{U}}_{ih}^{\pm}, \hat{\mathcal{U}}_{ih}^{\pm}) + F_i^{\pm}(\hat{\mathcal{U}}_{ih}^{\pm}; \hat{\psi}_{ih}^{\pm}, \Lambda_h^{\pm}) - b(\hat{\mathcal{U}}_{ih}^{\pm}, y_i^{\pm})\right] \\ &+ \left[-d_i(\hat{\psi}_{ih}^{\pm}, \cdot) \pm \ell^{O^p}(\cdot)\right]. \end{aligned} \tag{5.87}$$

Note that the first bracket of (5.86) equals $\eta^{\pm}$, we recall that

$$\eta^{\pm} = -a(\hat{\mathcal{U}}_{ih}^{\pm}, \hat{\mathcal{U}}_{ih}^{\pm}) - \ell_i^N(\hat{\psi}_{ih}^{\pm}). \tag{5.88}$$

It remains to show that all the other terms in (5.87) vanish. We observe that the second bracket in (5.87) equals $d_i(\hat{\mathcal{U}}_{ih}^{\pm}, \cdot)$ which is zero from (5.75). Finally, the last bracket terms in (5.87) vanishes due to the construction of the adjoint in which we have imposed $-d_i(\mu_i, \cdot) \pm \ell^{O^p}(\cdot) = 0$.

We now write

$$\eta^{\pm} = \mathcal{L}^{\pm}(\hat{\mathcal{U}}_{1h}^{\pm}, \hat{\mathcal{U}}_{2h}^{\pm}, \cdot, \hat{\psi}_{1h}^{\pm}, \hat{\psi}_{2h}^{\pm}, \Lambda_h^{\pm}, y_1^{\pm}, y_2^{\pm}). \tag{5.89}$$

It then follows from the classical quadratic linear duality theory that

$$\eta^{\pm} \leq \pm s_h \Rightarrow \eta^{+} \leq s_h \leq -\eta^{-} \tag{5.90}$$

if

$$\mathcal{L}^{\pm}(\hat{\mathcal{U}}_{1h}^{\pm}, \hat{\mathcal{U}}_{2h}^{\pm}, \cdot, \hat{\psi}_{1h}^{\pm}, \hat{\psi}_{2h}^{\pm}, \Lambda_h^{\pm}, y_1^{\pm}, y_2^{\pm}) = \min_{(v_1,v_2)\in U_h} \mathcal{L}^{\pm}(v_1, v_2, \cdot, \hat{\psi}_{1h}^{\pm}, \hat{\psi}_{2h}^{\pm}, \Lambda_h^{\pm}, y_1^{\pm}, y_2^{\pm}). \tag{5.91}$$

To demonstrate (5.91), we expand our Lagrangian (5.85) for $v_i = \hat{\mathcal{U}}_{1h}^{\pm} + w_i,\ q,\ \mu_i = \hat{\psi}_{ih}^{\pm},\ \lambda = \Lambda_h^{\pm},\ t_i = y_i^{\pm}$ to obtain,

$$\begin{aligned} \mathcal{L}^{\pm}(\hat{\mathcal{U}}_{1h}^{\pm} + w_1, \hat{\mathcal{U}}_{2h}^{\pm} + w_2, \cdot, \hat{\psi}_{1h}^{\pm}, \hat{\psi}_{2h}^{\pm}, \Lambda_h^{\pm}, y_1^{\pm}, y_2^{\pm}) &= \mathcal{L}^{\pm}(\hat{\mathcal{U}}_{1h}^{\pm}, \hat{\mathcal{U}}_{2h}^{\pm}, \cdot, \hat{\psi}_{1h}^{\pm}, \hat{\psi}_{2h}^{\pm}, \Lambda_h^{\pm}, y_1^{\pm}, y_2^{\pm}) \\ + \left[2a(w_i, \hat{\mathcal{U}}_{ih}^{\pm}) + F_i^{\pm}(w_i; \hat{\psi}_{ih}^{\pm}, \Lambda_h^{\pm}) - b(w_i, y_i^{\pm})\right] &+ \left[-d_i(\hat{\psi}_{ih}^{\pm}, \cdot) \pm \ell^{Op}(\cdot)\right] \\ &+ a(w_i, w_i), \quad \forall (w_1, w_2) \in U_h. \end{aligned} \tag{5.92}$$

We observe that the terms linear in w_i (first bracket) equal to $d_i(w_i, \cdot)$ which vanishes from (5.75) because $(w_1, w_2) \in U_h$ is incompressible. The terms, $-d_i(\hat{\psi}_{ih}^{\pm}, \cdot) \pm \ell^{Op}(\cdot)$ (second bracket), also vanish by construction of the adjoint (5.68)-(5.69) and the remaining are positives semi–definite terms $a(,)$ which thus proves (5.91).

To avoid meaningless bounds we need to check that when minimizing our augmented Lagrangian we do not obtain $-\infty$. To this end, two main concerns must be addressed. First, solvability of (5.74)-(5.75) is essential. Without solvability the terms on the right hand side could tend to infinity if the test function tends to infinity. Second, equilibration between $-d_i(\hat{\psi}_{ih}^{\pm}, q)$ and $\pm\ell^{op}(q)$ is also essential because these terms are not controlled by any quadratic stabilization. Because the above conditions are satisfied we are guaranteed non-infinite bounds. However, there is nothing in the theory that indicated that the bounds should be sharp. For the moment, we can suggest that $\Psi_{iH}^{\pm}, \Lambda_H^{\pm}$ and $y_i^{\pm}$ are the saddlepoints of the H–mesh approximation to our Lagrangian which are close enough to the h–mesh to give good bounds.

To decrease the cost we have reduced the global problem (5.6)-(5.7) into a sequence of independent problems posed locally over each element. We can observe from the proof that substituting the continuous spaces $(X_h \times X_h)$ with the "broken" spaces (U_h) preserving the inequality (5.90) and thereby guaranteeing rigorous bounds.

Chapter 6

The Hybrid Flux Approximation

In this Chapter we consider different approaches for the calculations of the hybrid flux approximation. This approximation to the true hybrid flux on the intersubdomain boundaries plays an important role in the sharpness of the bounds and is essential for the consistency of the bounding properties. Recall that to ensure finite and acceptable bounds, we are required to satisfy the equilibration equations, (3.59)-(3.60) for one space dimension, (4.39)-(4.40) for two space dimensions, and (5.66)-(5.67) for the Stokes problem.

In one space dimension, this equilibration is straightforward and was already presented in Section 3.2.3. We focus here on two space dimensions problems and consider a few different approaches. In Section 6.1 we present a nonconforming approach which is based on a standard linear nonconforming approximation. In Section 6.2 we describe two conforming approximations: a strong conforming and a gradient forced conforming. We end this Chapter with Section 6.3 where we extend the two conforming approaches to higher order spatial discretizations.

For clarity we present these approaches using the notation for scalar field variables introduced in Section 4 where the convection-diffusion equations were treated. Nevertheless, to apply the following procedures to the Stokes problem, we only replace the definition of $F^{\pm}$ and $B^{\pm}$ with the corresponding Stokes definitions (5.61) and (5.65) respectively and apply the procedure for each component of velocity.

6.1 Nonconforming Approach

To start, we look for a new field variable $\overline{u}_H^{\pm} \in \overline{X}_H$ which is a solution to (4.30), such that

$$2a^s(w, \overline{u}_H^{\pm}) = -F^{\pm}(w, \psi_H^{\pm}) \quad \forall w \in \overline{X}_H, \tag{6.1}$$

or equivalently,

$$B^{\pm}(w, \overline{u}_H^{\pm}) = 0 \quad \forall w \in \overline{X}_H. \tag{6.2}$$

This problem represents a standard linear nonconforming discretization associated with the space $\overline{X}_H$ defined in (4.25). Recall that $F^{\pm}(w, \psi_H^{\pm})$ and $B^{\pm}(w, \overline{u}_H^{\pm})$ are defined in (4.35) and (4.38), respectively. The numerical solution of (6.1) requires two "inversions" of the symmetric nonconforming stiffness matrix $\underline{A}_H^*$, one for $\overline{u}_H^+$ and $\overline{u}_H^-$. For iterative strategies, inspection of (6.1) and (6.2) indicated that $\overline{u}_H^{\pm}$ and u_H are, respectively, conforming and nonconforming approximations of the same quantity; u_H can thus serve as a good initial iterate for $\overline{u}_H^{\pm}$.

We recall that subdomain problems will require us to test on $v \in V_H$, not on $v \in \overline{X}_H$, leading to the introduction of the $b(v, y^{\pm})$ term. Therefore, we look for $y^{\pm} \in \mathcal{Q}_0$, the edge function space defined in 4.26, such that

$$b(v, y^{\pm}) = B^{\pm}(v, \overline{u}_H^{\pm}) \quad \forall v \in V_H. \tag{6.3}$$

Assuming that (6.3) has a solution, we directly obtain the important property that, for all T_H in $\mathcal{T}_H$,

$$\sum_{\gamma_{T_H} \in \mathcal{E}(\mathcal{T}_H)} \sigma_{T_H}^{\gamma_{T_H}} \int_{\gamma_{T_H}} v y^{\pm}|_{E(\gamma_{T_H})} \, \mathrm{d}s = B_{T_H}^{\pm}(v, \overline{u}_H^{\pm}), \quad \forall v \in Z_H(T_H). \tag{6.4}$$

The condition (6.4) will ensure solvability of the subsequent-local truth calculations. In particular, (6.4) applies to all those cases $v = v^s = 1$ for which our bilinear form $a_{T_H}^s(,)$ is singular for non–diagonal terms giving

$$\sum_{\gamma_{T_H} \in \mathcal{E}(\mathcal{T}_H)} \sigma_{T_H}^{\gamma_{T_H}} \int_{\gamma_{T_H}} v^s y^{\pm}|_{E(\gamma_{T_H})} \, \mathrm{d}s = F_{T_H}^{\pm}(v^s, \psi_H^{\pm}). \tag{6.5}$$

Note that, for the "Robin" boundary term in (4.15), $a_{T_H}^s(,)$ is not singular for the convection–diffusion problem in those elements T_H with a edge on Γ_N for which $U_i \hat{n}_i$.

It remains to show that (6.4) does, indeed, have a solution. In fact, the left nullspace of (6.4) is rather large, however the system is solvable, and the solution is unique; the latter follows from the fact that the *inf–sup* condition is satisfied for the associated hybrid discretization [19, 42]. To demonstrate this less abstractly, we simply construct the solution following the standard nonconforming postprocessing treatment [42].

We first consider the case of an interior edge, $\gamma \in \mathcal{E}_{int}(\mathcal{T}_H)$ and use the "nonconforming" basis functions,$\zeta_{T_H}^{\gamma_{T_H}}$ defined in Section 2.3.3. Given the orthogonality property (2.68) and our requirement that $y^{\pm} \in \mathcal{Q}_0$, it is clear that the two equations for $y^{\pm}|_{\gamma}$ are

$$y^{\pm}|_{\gamma} = \sigma_{T_H}^{\gamma_{T_H}} \frac{1}{|\gamma|} B_{T_H}^{\pm}(\zeta_{T_H}^{\gamma_{T_H}}, \overline{u}_H^{\pm}), \tag{6.6}$$

and

$$y^{\pm}|_{\gamma} = \sigma_{T'_H}^{\gamma_{T'_H}} \frac{1}{|\gamma|} B_{T_H}^{\pm}(\zeta_{T'_H}^{\gamma_{T'_H}}, \overline{u}_H^{\pm}), \tag{6.7}$$

where $E(\gamma_{T_H}) = E(\gamma_{T'_H}) = \gamma$, and $|\gamma|$ is the length of γ. Hence this choice of nonconforming basis functions is critical. We see that for $y^{\pm} \in \mathcal{Q}_0$ ("constant"),

$$\int_{\gamma_{T_H}} \zeta_{T_H}^{\gamma_{T_H}} y^{\pm}|_{E(\gamma_{T_H})} \, \mathrm{d}s = 0 \tag{6.8}$$

on two of the three edges of T_H. This allows us to isolate one edge and calculate the corresponding hybrid flux. To demonstrate that (6.6) and (6.7) are consistent, we first introduce the function $\xi^{\gamma} = \mathcal{P}\xi_{T_H}^{\gamma_{T_H}} + \mathcal{P}\xi_{T'_H}^{\gamma_{T'_H}}$, where for any domain $\mathcal{D} \subset \Omega$, and $\mathcal{F} : \mathcal{D} \to \mathbf{R}$, $\mathcal{P}\mathcal{F} : \Omega \to \mathbf{R}$ is the extension of $\mathcal{F}$ defined by

$$\mathcal{P}\mathcal{F} = \begin{cases} \mathcal{F} & \text{in } \mathcal{D} \\ 0 & \text{in } \Omega \backslash \mathcal{D} \end{cases} . \tag{6.9}$$

We now subtract (6.6) from (6.7) to obtain the consistency condition

$$B^{\pm}(\xi^{\gamma}, \overline{u}_H^{\pm}) = 0. \tag{6.10}$$

It is clear, from our orthogonality condition (2.68), from the fact that ξ^{γ} is a member of $\overline{X}_H$, and from the equilibrium requirement, (6.2), (6.10) is satisfied. We can thus choose either (6.6) or (6.7), or

$$y^{\pm}|_{\gamma} = \frac{1}{2|\gamma|}(\sigma_{T_H}^{\gamma_{T_H}} B_{T_H}^{\pm}(\zeta_{T_H}^{\gamma_{T_H}}, \overline{u}_H^{\pm}) + \sigma_{T'_H}^{\gamma_{T'_H}} B_{T_H}^{\pm}(\zeta_{T'_H}^{\gamma_{T'_H}}, \overline{u}_H^{\pm})), \tag{6.11}$$

which is an equivalent average flux. Recall that, in one dimension, (3.61) and (3.62) were used to calculate the hybrid fluxes for the two sides of one element. Here, (6.6) and (6.7) are used to calculate the fluxes from either side of and edge. However, these equations are essentially the same. Note that, for one dimension, hybrid fluxes fluxes calculated on both sides give the same result.

We next consider the case in which γ is an edge $\partial\Omega$. In this case, (6.4) yields only a single equation, say (6.6). However, we see from the definition of $\mathcal{Q}$ in (4.26) that, if γ is in $\mathcal{E}_N(\mathcal{T}_H)$ there are additional "boundary" conditions that must be satisfied. It can readily be shown that this requirement is, in fact, consistent. For example, $\gamma \in \mathcal{E}_N(\mathcal{T}_H)$ such that $\gamma = E(\gamma_{T_H})$, $\xi_{T_H}^{\gamma_{T_H}}$ is clearly a member of $\overline{X}_H$, and $B^{\pm}(\xi_{T_H}^{\gamma_{T_H}}, \overline{u}_H^{\pm}) = 0$. We may therefore write our edge hybrid fluxes as

$$y^{\pm} = \begin{cases} \sigma_{T_H}^{\gamma_{T_H}} \frac{1}{|\gamma|} B_{T_H}^{\pm}(\zeta_{T'_H}^{\gamma_{T'_H}}, u_H)) & \gamma \in \mathcal{E}_D(\mathcal{T}_H) \\ 0 & \gamma \in \mathcal{E}_N(\mathcal{T}_H) \end{cases} . \tag{6.12}$$

We close this section by summarizing the advantage and disadvantages of this approach. The advantage are that, first, we obtain a uniquely defined hybrid flux, and second, the associated procedure is relatively simply to implement. The disadvantage are that, first we must perform additional global solves on the H–mesh, and second, for such problems as the linear elasticity problem [36], the coercivity of the nonconforming system (6.1) is not guaranteed [19]. In addition, extension to nonconforming $\mathbf{P}_1$ approximation to the hybrid flux seems impossible [24] to construct. The difficulty appears to be in the nodal structure of the underlying elements. The fact is that these nodes lie on an ellipse and that there exists a second–degree polynomial which vanishes at all these nodes.

6.2 Conforming Approach

To address some of the disadvantages described in the previous Section, a conforming approach is presented which computes the hybrid fluxes directly from the considered solution, u_H. This approach is based on decomposing the hybrid flux in two contributions: $\mathbf{P}_0$ and $\mathbf{P}_1$ polynomial contributions. To start, we present our strong conforming approach which uses a nonconforming initial approximation as the initial approximation, $\mathbf{P}_0$ contribution. As an alternative, we describe a gradient forced conforming approach where the initial approximation is based on a gradient evaluation.

6.2.1 Strong Conforming

We look for $y^{\pm} \in \mathcal{Q}_1$, such that

$$b(v, y^{\pm}) = B^{\pm}(v, u_H), \qquad \forall v \in V_H, \tag{6.13}$$

which then gives, for all T_H in $\mathcal{T}_H$,

$$\sum_{\gamma_{T_H} \in \mathcal{E}(\mathcal{T}_H)} \sigma_{T_H}^{\gamma_{T_H}} \int_{\gamma_{T_H}} v y^{\pm}|_{E(\gamma_{T_H})} \mathrm{d}s = B_{T_H}^{\pm}(v, u_H), \ \ \forall v \in Z_H(T_H). \tag{6.14}$$

In particular, (6.14) applies for the singular modes of $a_{T_H}^s(,)$, which thus yields for $v^s = 1$,

$$\sum_{\gamma_{T_H} \in \mathcal{E}(\mathcal{T}_H)} \sigma_{T_H}^{\gamma_{T_H}} \int_{\gamma_{T_H}} v^s y^{\pm}|_{E(\gamma_{T_H})} \mathrm{d}s = F_{T_H}^{\pm}(v^s, \psi_H^{\pm}), \tag{6.15}$$

For $y^{\pm} \in \mathcal{Q}_1$ the system (6.13) becomes singular but solvable. However, unlike our nonconforming system (6.3), (6.13) will not yield a unique solution. To treat this indeterminacy we write

$$y^{\pm} = \bar{y}^{\pm} + \hat{y}^{\pm} \tag{6.16}$$

where $\bar{y}^{\pm} \in \mathcal{Q}_0$ and $\hat{y}^{\pm} \in \mathcal{Q}_1$ and we assume that $\bar{y}^{\pm}$ is, in fact, a good approximation, and look for that solution $y^{\pm}$ for which $\hat{y}^{\pm}$ is as small as possible. The initial $\mathbf{P}_0$ approximation is therefore computed as

$$\bar{y}^{\pm}|_{\gamma} = \frac{1}{2|\gamma|}(\sigma_{T_H}^{\gamma_{T_H}} B_{T_H}^{\pm}(\zeta_{T_H}^{\gamma_{T_H}}, u_H) + \sigma_{T'_H}^{\gamma_{T'_H}} B_{T_H}^{\pm}(\zeta_{T'_H}^{\gamma_{T'_H}}, u_H)), \tag{6.17}$$

for any interior edge $\gamma \in \mathcal{E}_{int}(\mathcal{T}_H)$ such that $E(\gamma_{T_H}) = E(\gamma_{T'_H}) = \gamma$. Similarly, for edges γ on the boundary $\partial\Omega$ we write

$$\bar{y}^{\pm} = \begin{cases} \sigma_{T_H}^{\gamma_{T_H}} \frac{1}{|\gamma|} B_{T_H}^{\pm}(\zeta_{T_H}^{\gamma_{T_H}}, u_H)) & \gamma \in \mathcal{E}_D(\mathcal{T}_H) \\ 0 & \gamma \in \mathcal{E}_N(\mathcal{T}_H) \end{cases} . \tag{6.18}$$

We expect that, in analogy to the corresponding nonconforming (6.11) and (6.12), (6.17) and (6.18) should give a good approximation to the hybrid flux. However, unlike ((6.11) and (6.12), (6.17) and (6.18)) will not lead to solvability in the subsequent subdomain–local truth calculations: u_h is not equilibrated in the nonconforming sense. For example, for the singular mode v^s, the average in (6.17) brings into element T_H information that is "slightly" inconsistent with the force balance.

In the nonconforming case, we seek to satisfy the condition (6.3) for each element by solving over the nodes of that element. Here, we are looking to construct the linear term of the hybrid flux, $\hat{y}$, (for simplicity we have removed $\pm$) such that we satisfy the condition for each node by solving over the elements containing the node.

Then, for any edge γ in $\mathcal{E}(\mathcal{T}_H)$, we write for $\hat{y}$,

$$\hat{y}|\gamma = \alpha_n^{\gamma}\theta_n^{\gamma}(x) + \alpha_m^{\gamma}\theta_m^{\gamma}(x), \tag{6.19}$$

where x_n, x_m are the nodes of $\mathcal{T}_H$ which define γ; α_n^{γ} and α_m^{γ} are real coefficients to be determined. The linear functions $(\theta_n^{\gamma}, \theta_m^{\gamma})$ defined on γ are constructed to be bi–orthogonal to $(\varphi_{T_H}^n|_{\gamma}, \varphi_{T_H}^m|_{\gamma})$ for any element T_H for which there is an edge $\gamma_{T_H} \in \mathcal{E}(T_H)$ such that $\gamma = E(\gamma_{T_H})$ [31, 13]. More precisely,

$$\int_{\gamma} \theta_m^{\gamma}\varphi_{T_H}^n|_{\gamma} \mathrm{d}s = |\gamma|\delta_{mn}, \tag{6.20}$$

where δ_{mn} is the Kronecker-delta symbol. Based on this definition we can show that

$$\theta_n^{\gamma} = 4\xi_n^{\gamma} - 2\xi_m^{\gamma}, \tag{6.21}$$

where $\xi_n^{\gamma}, \xi_m^{\gamma}$ are the usual linear basis function associated with side γ which are equal to $+1$ (0) at node n (m) and 0 ($+1$) at node m (n). In Figure 6-1 we represent the $\alpha_n^{\gamma}\theta_n^{\gamma}(x)$ component of the hybrid flux associated with node n.

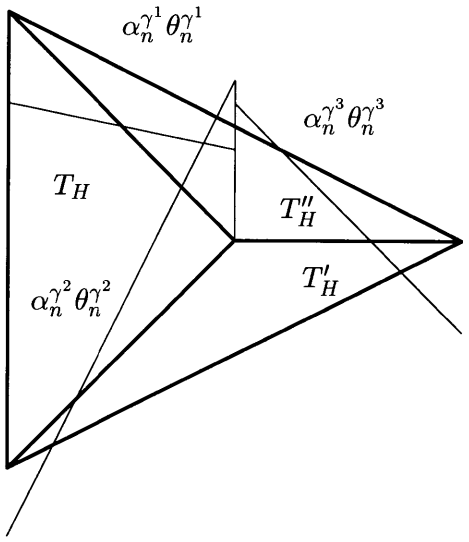

Figure 6-1: Representation of $\alpha_n^{\gamma^1}\theta_n^{\gamma^1}$, $\alpha_n^{\gamma^2}\theta_n^{\gamma^2}$ and $\alpha_n^{\gamma^3}\theta_n^{\gamma^3}$.

By virtue of the bi–orthogonality, for each side connected to node n, we have

$$\int_\gamma (\alpha_n^\gamma \theta_n^\gamma(x) + \alpha_m^\gamma \theta_m^\gamma(x))\varphi_{T_H}^n|_\gamma \mathrm{d}s = \alpha_n^\gamma |\gamma|. \tag{6.22}$$

Therefore, the determination of the α_n^γ reduces to N smaller systems, one for each node of $\mathcal{T}_H$. For an interior node x_n with element multiplicity M_n, the local system of size M_n, is given by (for simplicity, for the case $M_n = 3$)

$$\begin{bmatrix} \sigma_{T_H}^{\gamma^1_{T_H}}|\gamma^1| & \sigma_{T_H}^{\gamma^2_{T_H}}|\gamma^2| & 0 \\ 0 & \sigma_{T'_H}^{\gamma^1_{T'_H}}|\gamma^2| & \sigma_{T'_H}^{\gamma^2_{T'_H}}|\gamma^3| \\ \sigma_{T''_H}^{\gamma^2_{T''_H}}|\gamma^1| & 0 & \sigma_{T''_H}^{\gamma^1_{T''_H}}|\gamma^3| \end{bmatrix} \begin{bmatrix} \alpha_n^{\gamma^1} + \frac{1}{2}\bar{y}|_{\gamma^1} \\ \alpha_n^{\gamma^2} + \frac{1}{2}\bar{y}|_{\gamma^2} \\ \alpha_n^{\gamma^3} + \frac{1}{2}\bar{y}|_{\gamma^3} \end{bmatrix} = \begin{bmatrix} B_{T_H}(\varphi_{T_H}^n, u_H) \\ B_{T_H}(\varphi_{T'_H}^n, u_H) \\ B_{T_H}(\varphi_{T''_H}^n, u_H) \end{bmatrix}, \tag{6.23}$$

as is readily derived from (6.13). In Figure 6-2, we present the basis functions that intervene in the calculation of $\alpha_n^{\gamma^1}$, $\alpha_n^{\gamma^2}$ and $\alpha_n^{\gamma^3}$ associated with each edge connected to node n. From our bi–orthogonal property (6.20), we can see how by taking these basis, $\varphi_{T_H}^n$, $\varphi_{T'_H}^n$ and $\varphi_{T''_H}^n$, the other nodes don't interact. Here T_H, T'_H, T''_H and $\gamma^1, \gamma^2, \gamma^3$ are, respectively, the $M_n = 3$ elements and $M_n = 3$ edges which share x_n; furthermore, $\gamma^1 = E(\gamma_{T_H}^1) = E(\gamma_{T''_H}^2), \gamma^2 = E(\gamma_{T'_H}^1) = E(\gamma_{T_H}^2), \gamma^3 = E(\gamma_{T''_H}^1) = E(\gamma_{T'_H}^2)$. Recall this system is singular but solvable. To demonstrate, we see from the definition of $\sigma_{T_H}^{\gamma_{T_H}}$ in (2.54) and also from Figure 6-3 where the sign pairings on each side of an edge are presented, that the left nullspace of

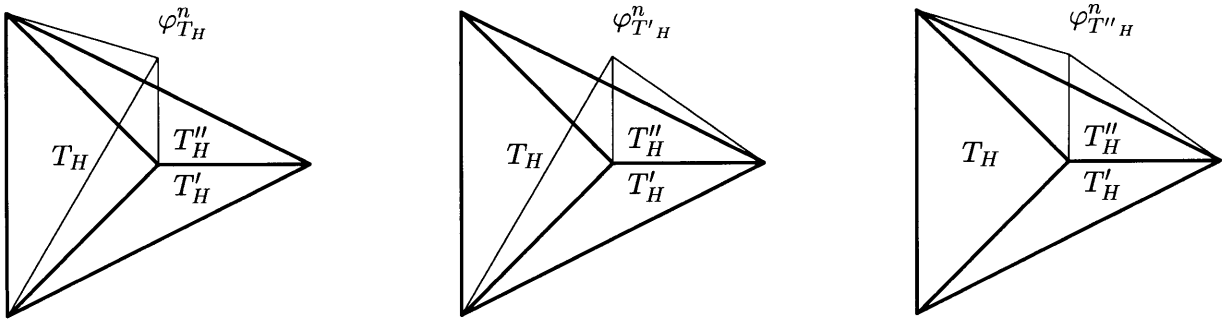

Figure 6-2: Representation of $\varphi^n_{T_H}$,$\varphi^n_{T'_H}$ and $\varphi^n_{T''_H}$.

the coefficient matrix in (6.23) is $(1,1,1)$. However, the function $\mathcal{P}\varphi^n_{T_H} + \mathcal{P}\varphi^n_{T'_H} + \mathcal{P}\varphi^n_{T''_H}$ is clearly in X_H; recall the definition of $\mathcal{P}$ in (6.9). Thus from equilibrium, (4.36), the right-hand side of (6.23) is orthogonal to $(1,1,1)$, and the system is therefore solvable. Finally, since by assumption $\hat{y}$ is a correction to $\bar{y}$; we take the pseudoinverse in (6.23) to control the size of the α^γ_n [31, 32].

We now consider nodes x_n on the boundary $\partial\Omega$. The local system will now be of size $M_n \times (M_n + 1)$, as the edge multiplicity will be greater that the element multiplicity. For simplicity, we consider the case $M_n = 2$ the local system which comprises the first two equation of (6.23),

$$\begin{bmatrix} \sigma^{\gamma^1_{T_H}}_{T_H}|\gamma^1| & \sigma^{\gamma^2_{T_H}}_{T_H}|\gamma^2| & 0 \\ 0 & \sigma^{\gamma^1_{T'_H}}_{T'_H}|\gamma^2| & \sigma^{\gamma^2_{T'_H}}_{T'_H}|\gamma^3| \end{bmatrix} \begin{bmatrix} \alpha^{\gamma^1}_n + \frac{1}{2}\bar{y}|_{\gamma^1} \\ \alpha^{\gamma^2}_n + \frac{1}{2}\bar{y}|_{\gamma^2} \\ \alpha^{\gamma^3}_n + \frac{1}{2}\bar{y}|_{\gamma^3} \end{bmatrix} = \begin{bmatrix} B_{T_H}(\varphi^n_{T_H}, u_H) \\ B_{T_H}(\varphi^n_{T'_H}, u_H) \end{bmatrix}, \tag{6.24}$$

where we assume that γ^1 and γ^3 are on $\partial\Omega$, and $\gamma^2 \in \mathcal{E}_{int}(\mathcal{T}_H)$. We first address the situation in which γ^1 and γ^3 are both in $\mathcal{E}_D(\mathcal{T}_H)$. In this case, there are no boundary conditions to be satisfied; furthermore, the left nullspace, is now empty, and solvability is, thus, not an issue. The indeterminacy in the α^γ_n is "removed", as before, by application of the pseudoinverse. Next, we address the situation in which $\gamma^1 \in \mathcal{E}_N(\mathcal{T}_H)$ and $\gamma^3 \in \mathcal{E}_D(\mathcal{T}_H)$. Now, to honor the boundary conditions on y, we set $\alpha^{\gamma^1}_n = 0$; it is clear that the coefficients $\alpha^{\gamma^2}_n, \alpha^{\gamma^3}_n$ are then uniquely determined, where the system becomes

$$\begin{bmatrix} \sigma^{\gamma^2_{T_H}}_{T_H}|\gamma^2| & 0 \\ \sigma^{\gamma^1_{T'_H}}_{T'_H}|\gamma^2| & \sigma^{\gamma^2_{T'_H}}_{T'_H}|\gamma^3| \end{bmatrix} \begin{bmatrix} \alpha^{\gamma^2}_n + \frac{1}{2}\bar{y}|_{\gamma^2} \\ \alpha^{\gamma^3}_n + \frac{1}{2}\bar{y}|_{\gamma^3} \end{bmatrix} = \begin{bmatrix} B_{T_H}(\varphi^n_{T_H}, u_H) \\ B_{T_H}(\varphi^n_{T'_H}, u_H) \end{bmatrix}. \tag{6.25}$$

Finally, we address the situation in which both γ^1 and γ^3 are in $\mathcal{E}_N(\mathcal{T}_H)$. We must now set

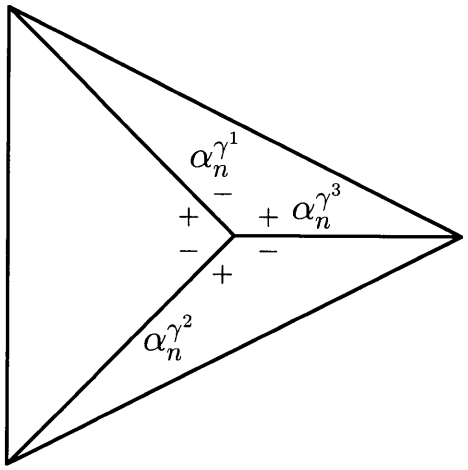

Figure 6-3: Sign convention around a node.

$\alpha_n^{\gamma^1} = \alpha_n^{\gamma^3} = 0$ to honor the boundary conditions. Fortunately, the remaining $M_n \times (M_n - 1)$ system

$$\begin{bmatrix} \sigma_{T_H}^{\gamma^2_{T_H}} |\gamma^2| \\ \sigma_{T'_H}^{\gamma^1_{T'_H}} |\gamma^2| \end{bmatrix} \left[\alpha_n^{\gamma^2} + \tfrac{1}{2}\bar{y}|_{\gamma^2} \right] = \begin{bmatrix} B_{T_H}(\varphi^n_{T_H}, u_H) \\ B_{T_H}(\varphi^n_{T'_H}, u_H) \end{bmatrix}, \tag{6.26}$$

is solvable. Indeed, equilibrium, (4.36), applies at a boundary node x_n with two Neumann edges, and thus the right–hand side of (6.26) will be orthogonal to $(1, 1)$, the left nullspace of the coefficient matrix. It follows that $\alpha_n^{\gamma^2}$ may be uniquely determined.

6.2.2 Gradient Forced Conforming

This procedure is very close to those originally proposed in [31], [13] and [3]. The main difference is that, for our complex Lagrangian, the hybrid flux contains more that simply the gradient of u_H — there are boundary terms that arise due to the $a_{T_H}(\psi_H^{\pm}, v)$ contribution.

To start, we rewrite our elemental equilibrium equation (4.37) to separate the edge and the interior contributions. Applying integration by parts for each T_H in $\mathcal{T}_H$ gives

$$\begin{aligned} B^{\pm}_{T_H}(v,u) - \sum_{\gamma_{T_H} \in \mathcal{E}(\mathcal{T}_H)} \sigma_{T_H}^{\gamma_{T_H}} \int_{\gamma_{T_H}} vy|_{E(\gamma_{T_H})} \mathrm{d}s &= \int_{T_H} -v(2\frac{\partial}{\partial x_i}(\nu \frac{\partial u}{\partial x_i})) - \frac{\partial}{\partial x_i}(\nu \frac{\partial \psi}{\partial x_i}) \\ &+ U_i \frac{\partial \psi}{\partial x_i} \, \mathrm{d}A - \ell^N_{T_H}(v) \pm \ell^O_{T_H}(v) \end{aligned}$$

$$+ \int_{\partial T_H} v(2\nu\hat{n}_i \frac{\partial u}{\partial x_i} + \nu\hat{n}_i \frac{\partial \psi}{\partial x_i} + \psi v U_i \hat{n}_i) \mathrm{d}s$$

$$- \sum_{\gamma_{T_H} \in \mathcal{E}(\mathcal{T}_H)} \sigma_{T_H}^{\gamma_{T_H}} \int_{\gamma_{T_H}} vy|_{E(\gamma_{T_H})} \mathrm{d}s \quad (6.27)$$

$$= 0. \quad (6.28)$$

To satisfy (6.28) we need to equilibrate the terms on the edges and thus obtain our initial approximation of the hybrid flux,

$$\sigma_{T_H}^{\gamma_{T_H}} y^{\pm} = 2\nu\hat{n}_i \frac{\partial u}{\partial x_i} + \nu\hat{n}_i \frac{\partial \psi}{\partial x_i} + \psi v U_i \hat{n}_i \, . \quad (6.29)$$

Note that (6.28) is equilibrated in the interior of the element which leads to elimination of the first integral in (6.28). This initial approximation will not lead to solvability of (6.13). It is then required to calculate a $\mathbf{P}_1$ correction based on the same procedure as in the previous Section.

6.3 Extension to Higher Order Spatial Discretization

Higher order spatial discretization is often needed to improve the convergence properties but also required in some cases like the Stokes problem where for "efficiency" reasons the the velocity space must be one degree higher than the pressure space. Therefore, the problem that arises is to satisfy the equilibrium equation,

$$\sum_{\gamma_{T_H} \in \mathcal{E}(T_H)} \sigma_{T_H}^{\gamma_{T_H}} \int_{\gamma_{T_H}} vy|_{E(\gamma_{T_H})} \, \mathrm{d}s = B_{T_H}(v, u_H) \quad \forall v \in Z_H(T_H), \quad (6.30)$$

for higher order basis functions. In this section we propose two methods to calculate y that satisfies (6.30) for the finite element subspace based on polynomials of degree two.

6.3.1 $\mathbf{P}_0$ Initial Approximation

This first step is to find a constant approximation on each edge γ, therefore $\bar{y} \in \mathcal{Q}_0$ is obtained from

$$\bar{y}|_\gamma = \frac{1}{2|\gamma|} \left(\sigma_{T_H}^{\gamma_{T_H}} B_{T_H}(\zeta_{T_H}^{\gamma_{T_H}}, u_H) + \sigma_{T'_H}^{\gamma_{T'_H}} B_{T'_H}(\zeta_{T'_H}^{\gamma_{T'_H}}, u_H) \right), \quad (6.31)$$

for any interior edge $\gamma \in \mathcal{E}(\mathcal{T}_H)$ such that $\gamma = E(\gamma_{T_H}) = E(\gamma_{T'_H})$. Similarly, for edges γ on the boundary $\partial\Omega$, we write,

$$\bar{y} = \sigma_{T_H}^{\gamma_{T_H}} \frac{1}{|\gamma|} B_{T_H}(\zeta_{T_H}^{\gamma_{T_H}}, u_H) \quad \gamma \in \mathcal{E}_D(\mathcal{T}_H), \quad (6.32)$$

where $\zeta_{T_H}^{\gamma_{T_H}}$ is the "nonconforming" basis function for $\mathbf{P_1}(T_H)$ defined in Section 2.3.3.

We expect that, in analogy to the corresponding nonconforming results presented in Section 6.1, (6.31)–(6.32) should give a good approximation to the hybrid flux. However, the system (6.31)-(6.32) will not lead to solvability in the subdomain–local calculations. To this end we introduce a linear contribution to the hybrid flux as in the previous Section. In addition, we hope to improve accuracy and convergence of the bounds by adding a quadratic contribution.

We thus look for $\bar{y} \in \mathcal{Q}_0$, $\hat{y} \in \mathcal{Q}_1$ and $\tilde{y} \in \mathcal{Q}_2$ and in particular we write

$$y = \bar{y} + \hat{y} + \tilde{y}. \tag{6.33}$$

We then require that

$$b(v, y) = B(v, u_H), \qquad \forall v \in V_H, \tag{6.34}$$

which then gives, for all T_H in $\mathcal{T}_H$,

$$\sum_{\gamma_{T_H} \in \mathcal{E}(T_H)} \sigma_{T_H}^{\gamma_{T_H}} \int_{\gamma_{T_H}} vy|_{E(\gamma_{T_H})} \, \mathrm{d}s = B_{T_H}(v, u_H), \qquad \forall v \in Z_H(T_H). \tag{6.35}$$

Our goal is to show how to calculate all these terms in the hybrid flux. We will proceed step by step, but beforehand, we define the quadratic approximation of the hybrid flux,

$$\tilde{y} = \beta_\gamma \rho_\gamma, \tag{6.36}$$

where $\rho_\gamma : \gamma \to \mathbf{R}$ is the quadratic function uniquely defined by the conditions:

$$\int_\gamma \rho_\gamma \varphi_{T_H}^n \, \mathrm{d}s = 0, \tag{6.37}$$

and

$$\int_\gamma \rho_\gamma^2 \, \mathrm{d}s = |\gamma|, \tag{6.38}$$

where n refers to the vertices of the γ and $\varphi_{T_H}^n$ is the linear basis function associated with node n of element T_H.

Proceeding as in Section 6.2.1, we calculate a first approximation to the Hybrid flux, $\bar{y} \in \mathcal{Q}_0$ given by,

$$\bar{y}|_\gamma = \frac{1}{2|\gamma|}(\sigma_{T_H}^{\gamma_{T_H}} B_{T_H}(\zeta_{T_H}^{\gamma_{T_H}}, u_H) + \sigma_{T'_H}^{\gamma_{T'_H}} B_{T_H}(\zeta_{T'_H}^{\gamma_{T'_H}}, u_H)), \tag{6.39}$$

for edges in the interior. For edges γ on the boundary $\partial\Omega$ we use

$$\bar{y} = \begin{cases} \sigma_{T_H}^{\gamma_{T_H}} \frac{1}{|\gamma|} B_{T_H}(\zeta_{T_H}^{\gamma_{T_H}}, u_H)) & \gamma \in \mathcal{E}_D(\mathcal{T}_H) \\ 0 & \gamma \in \mathcal{E}_N(\mathcal{T}_H) \end{cases} . \tag{6.40}$$

Second, we calculate a correction $\hat{y}$,

$$\hat{y}|\gamma = \alpha_n^\gamma \theta_n^\gamma(x) + \alpha_m^\gamma \theta_m^\gamma(x), \tag{6.41}$$

where α_n^γ are calculates by solving for example (6.23), for each node. Note that when we integrate over an edge γ we obtain

$$\int_\gamma \varphi_{T_H}^n(\bar{y} + \hat{y} + \tilde{y})\mathrm{d}s = \int_\gamma \varphi_{T_H}^n(\bar{y} + \alpha_n^\gamma \theta_n^\gamma(x) + \alpha_m^\gamma \theta_m^\gamma(x) + \beta_\gamma \rho_\gamma)\mathrm{d}s = (\frac{1}{2}\bar{y} + \alpha_n^\gamma)|\gamma|, \tag{6.42}$$

where the quadratic function ρ_γ is orthogonal to the linear functions $\varphi_{T_H}^n$ which ensure that $\tilde{y}$ does not affect $\hat{y}$ or $\overline{y}$.

Finally, we describe the higher order equilibration procedure for $\tilde{y}^\pm$ [5]. The constant β_γ is calculated to satisfy the equilibrium equation (4.36). It can readily be shown that, by introducing a standard quadratic basis function $\tilde{\varphi}_{T_H}^p$, we obtain

$$\int_\gamma \tilde{\varphi}_{T_H}^p(\bar{y}|_\gamma + \hat{y}|_\gamma) \ \mathrm{d}s = \frac{2}{3}|\gamma|(\bar{y}|_\gamma + \alpha_n^\gamma + \alpha_m^\gamma) \tag{6.43}$$

where p refers to the node number at the middle of each edge and not the vertices of the triangle, that is $\tilde{\varphi}_{T_H}^p$ is quadratic basis function defined for the reference element by any of the equations (C.4)-(C.6), depending on which side we refer to. We now show that the span$(\varphi_{T_H}^n, \tilde{\varphi}_{T_H}^p) = \mathbf{P}_2$ required because $v \in Z_H(T_H)$. Recall that $\tilde{\varphi}_{T_H}^p$ is the usual quadratic basis function associated with the side only. Knowing that any quadratic function can be represented as a linear combination of linear basis functions defined at the vertices, here $\varphi_{T_H}^n$ and a quadratic bubble function, here $\tilde{\varphi}_{T_H}^p$ we therefore span $\mathbf{P}_2$. It follows that when $v = \tilde{\varphi}_{T_H}^p$, equation (6.35) becomes,

$$\sigma_{T_H}^{\gamma_{T_H}} \int_\gamma \tilde{\varphi}_{T_H}^p \tilde{y} \ \mathrm{d}s = B_{T_H}(\tilde{\varphi}_{T_H}^p, u_H) - \frac{2}{3}\sigma_{T_H}^{\gamma_{T_H}} |\gamma|(\bar{y}|_\gamma + \alpha_n^\gamma + \alpha_m^\gamma), \tag{6.44}$$

and finally,

$$\beta_\gamma = \frac{15}{2\sqrt{5}} \left(\frac{2}{3}(\bar{y}|_\gamma + \alpha_n^\gamma + \alpha_m^\gamma) - \frac{\sigma_{T_H}^{\gamma_{T_H}}}{|\gamma|} B_{T_H}(\tilde{\varphi}_{T_H}^p, u_H) \right). \tag{6.45}$$

This equation can be solved on either element for all edge γ in $\mathcal{E}_{int}(\mathcal{T}_H)$. To prove, we

calculate the difference of (6.45) from each side of an edge and we obtain

$$B_{T_H}(\mathcal{P}\tilde{\varphi}^{p}_{T_H} + \mathcal{P}\tilde{\varphi}^{p'}_{T'_H}, u_H) = 0 \tag{6.46}$$

where $\mathcal{P}$ is defined in (6.9). By evoking equilibrium (4.36), we prove that the solutions to (6.45) are consistent. For the edges that lie on the boundary, we directly apply (6.45). To summarize the above, first, we solve for the non–conforming approximation to the hybrid flux. However, this approximation does not lead to solvability of the equilibrium equation (4.36). Therefore to ensure solvability, we solve N local systems, one for each node of $\mathcal{T}_H$ to determine the α^{γ}_{n} constants of the linear contribution to $\hat{y}$. Finally, we look for a quadratic contribution, so we solve (6.45) for each side. An alternative approach could be to calculate the first order gradient approximation of the hybrid flux are presented next.

6.3.2 $\mathbf{P}_1$ Initial Approximation

Applying the procedure of Section 6.2.2 yields an initial approximation for the hybrid flux,

$$\sigma^{\gamma_{T_H}}_{T_H}\bar{y} = 2\nu\hat{n}_i\frac{\partial u_H}{\partial x_i} + \nu\hat{n}_i\frac{\partial \psi_H}{\partial x_i} + \psi_H U_i\hat{n}_i. \tag{6.47}$$

Note that, u_H and ψ_H are $\mathbf{P}_2$ approximations of the field solution and upper bound adjoint and therefore $\bar{y}$ becomes an $\mathbf{P}_1$ approximation which can be written as

$$\bar{y} = \pi^{\gamma}_{n}\xi^{n}_{\gamma} + \pi^{\gamma}_{m}\xi^{m}_{\gamma}. \tag{6.48}$$

Note that $\pi^{\gamma}_{n}, \pi^{\gamma}_{m}$ are calculated directly from (6.47). It is easy to show that for a side γ,

$$\int_{\gamma}\bar{y}^{\pm}\varphi^{n}_{T_H}\,\mathrm{d}s = \frac{\pi^{\gamma}_{n}}{3} + \frac{\pi^{\gamma}_{m}}{6}. \tag{6.49}$$

We proceed by calculating the $\hat{y}$ contribution to the hybrid flux. The procedure as is previously described in Section 6.3.1. For each T_H in $\mathcal{T}_H$, if we take the test function to be $\varphi^{n}_{T_H}$ we obtain,

$$\sum_{\gamma_{T_H}\in\mathcal{E}(\mathcal{T}_H)}\sigma^{\gamma_{T_H}}_{T_H}\int_{\gamma_{T_H}}\varphi^{n}_{T_H}(\bar{y}|_{E(\gamma_{T_H})} + \hat{y}|_{E(\gamma_{T_H})} + \tilde{y}|_{E(\gamma_{T_H})})\mathrm{d}s = B_{T_H}(v, u_H) \tag{6.50}$$

$$\sum_{\gamma_{T_H}\in\mathcal{E}(\mathcal{T}_H)}\sigma^{\gamma_{T_H}}_{T_H}\int_{\gamma_{T_H}}\varphi^{n}_{T_H}\hat{y}|_{E(\gamma_{T_H})}\mathrm{d}s = B_{T_H}(v, u_H)$$

$$-\sigma^{\gamma^1_{T_H}}_{T_H}(\frac{\pi^{n}_{\gamma^1}}{3} + \frac{\pi^{m}_{\gamma^1}}{6}) - \sigma^{\gamma^2_{T_H}}_{T_H}(\frac{\pi^{n}_{\gamma^2}}{3} + \frac{\pi^{m'}_{\gamma^2}}{6}), \tag{6.51}$$

where γ^1 and γ^2 are the two sides of the T_H that touch node n and end in nodes m and m', respectively. We calculate the coefficients α^{γ}_{n} and α^{γ}_{m} by solving for each node a

system similar to (6.23). Note that we again take advantage of orthogonality properties, $\int_\gamma \varphi^n_{T_H} \tilde{y}\, \mathrm{d}s = 0$, which allows us to separate the calculation of the $\hat{y}$ contribution from the calculation of the $\tilde{y}$ contribution.

Finally, we calculate the coefficient of the edge bubble function β_γ which follows as,

$$\beta_\gamma = \frac{15}{2\sqrt{5}} \left(\frac{2}{3}(\alpha^\gamma_n + \alpha^\gamma_m) + \frac{1}{3}(\pi^\gamma_n + \pi^\gamma_m) - \frac{\sigma^{\gamma_{T_H}}_{T_H}}{|\gamma|} B_{T_H}(\tilde{\varphi}^p_{T_H}, u_{iH}) \right). \tag{6.52}$$

Recall that $\tilde{\varphi}^p_{T_H}$ is the usual quadratic basis function, defined for the reference element by any — depending on which side — (C.4)-(C.6) associated with the mid node of each edge γ.

Chapter 7

Optimal Stabilization Parameter

In this section we present a procedure by which we improve the sharpness of the bounds by maximizing our lower bound and minimizing our upper bound. To this end, we introduce a positive real number, κ, to scale our output s and we look for the bounds to this scaled output. It is obvious that when dividing the final bounding inequality by κ we obtain our usual bounds (1.1). Therefore for any κ real we obtain bounds. We are now looking for the optimal κ that will yield the sharpest bounds. A κ optimization procedure is presented for the convection diffusion model problem and the Stokes problem in Section 7.1 and in Section 7.2, respectively. A different but equivalent approach where we scale the entire energy equality (4.48) or (5.81)-(5.82) is presented in $\mathbf{R}^1$ in [35, 46].

7.1 Output Scaling for the Convection–Diffusion Problem

The strategy is to write all variables as linear functions in κ and then derive the bounds as a function in κ. This procedure does not change the bounding theory and our bounds remain rigorous. Our choices of Lagrange candidates is still valid even if the adjoint and the hybrid flux are divided into different terms. The key is that these candidates have to remain in the appropriate spaces, so some attention must be given to the boundary conditions.

To begin, we decompose $\psi_H^{\pm}$ as

$$\psi_H^{\pm} = \psi_H^{0\pm} + \kappa\psi_H^{1\pm}, \tag{7.1}$$

where

$$\begin{aligned} a(\psi_H^{0\pm}, w) &= -(2a^s(w, u_H^{\pm}) - \ell^N(w)), \quad \forall w \in X_H, & (7.2)\\ a(\psi_H^{1\pm}, w) &= -(\pm\ell^O(w)), \quad \forall w \in X_H. & (7.3) \end{aligned}$$

The boundary condition on $\psi_H^{0\pm}$ and $\psi_H^{1\pm}$ are respectively $(-g_D)$ Dirichlet and homo-

geneous Dirichlet. The boundary condition derivation follows as in Section 4.4 where a "lifting" function g is introduced in the energy equality and then absorbed in the adjoint. We now present the decomposition of the hybrid flux. First, we need to define the function $F^{0\pm}(v;\mathcal{F})$ and $F^{1\pm}(v;\mathcal{F})$ such that for any function $\mathcal{F}$ in $\mathcal{H}^1_*(\Omega)$ and for all $v \in \mathcal{H}^1_*(\Omega)$

$$F^{0\pm}(v;\mathcal{F}) = \sum_{T_H \in \mathcal{T}_H} F^{0\pm}_{T_H}(v|_{T_H};\mathcal{F}), \quad \forall v \in \mathcal{H}^1_*(\Omega), \tag{7.4}$$

$$F^{1\pm}(v;\mathcal{F}) = \sum_{T_H \in \mathcal{T}_H} F^{1\pm}_{T_H}(v|_{T_H};\mathcal{F}) \quad \forall v \in \mathcal{H}^1_*(\Omega), \tag{7.5}$$

where for all T_H in $\mathcal{T}_H$

$$F^{0\pm}_{T_H}(v;\mathcal{F}) = a_{T_H}(\mathcal{F}|_{T_H}, v) - \ell^N_{T_H}(v), \quad \forall v \in \mathcal{H}^1_*(\Omega), \tag{7.6}$$

$$F^{1\pm}_{T_H}(v;\mathcal{F}) = a_{T_H}(\mathcal{F}|_{T_H}, v) \pm \ell^0_{T_H}(v), \quad \forall v \in \mathcal{H}^1_*(\Omega). \tag{7.7}$$

In continuation, we write the hybrid flux

$$y^{\pm} = y^{0\pm} + \kappa y^{1\pm}, \tag{7.8}$$

which is derived as in Chapter 6. That is we solve for all T_H in $\mathcal{T}_H$

$$\sum_{\gamma_{T_H} \in \mathcal{E}(\mathcal{T}_H)} \sigma^{\gamma_{T_H}}_{T_H} \int_{\gamma_{T_H}} v y^{0\pm}|_{E(\gamma_{T_H})}\, \mathrm{d}s = 2a_{T_H}(v, u^{\pm}_H) - F^{0\pm}_{T_H}(v;\psi^{0\pm}_H), \ \forall v \in Z_H(T_H) \tag{7.9}$$

$$\sum_{\gamma_{T_H} \in \mathcal{E}(\mathcal{T}_H)} \sigma^{\gamma_{T_H}}_{T_H} \int_{\gamma_{T_H}} v y^{1\pm}|_{E(\gamma_{T_H})}\, \mathrm{d}s = -F^{1\pm}_{T_H}(v;\psi^{1\pm}_H) \quad \forall v \in Z_H(T_H). \tag{7.10}$$

We now look at the h–mesh subdomain solves. We solve for $\hat{u}^{0\pm}_h$ and $\hat{u}^{1\pm}_h$ such that $\hat{\mathcal{U}}^{\pm}_h = \hat{u}^{0\pm}_h + \kappa \hat{u}^{1\pm}_h$. The equation are,

$$2a(w, \hat{u}^{0\pm}_h) = -F^{0\pm}(w;\psi^{0\pm}_H) + b(w, y^{0\pm}) \quad \forall w \in V_H, \tag{7.11}$$

$$2a(w, \hat{u}^{1\pm}_h) = -F^{1\pm}_i(w;\psi^{1\pm}_H) + b(w, y^{1\pm}) \quad \forall w \in V_H. \tag{7.12}$$

Solvability of (7.11)-(7.12) requires that

$$0 = -F^{0\pm}(1;\psi^{0\pm}_H) + b(1, y^{0\pm}), \tag{7.13}$$

$$0 = -F^{1\pm}_i(1;\psi^{1\pm}_H) + b(1, y^{1\pm}), \tag{7.14}$$

which is satisfied from (7.9)-(7.10) and the fact that 1 is in V_H.

For simplicity of notation, we denote our bounds as

$$\eta^+(\kappa) \equiv (s_h)_{LB}, \tag{7.15}$$

$$-\eta^-(\kappa) \equiv (s_h)_{UB}. \tag{7.16}$$

Recall that our procedure is to scale the output which yield scaled bounds that we scale back to obtain bounds on our original output. Therefore, our scaled bounds can be expressed as

$$\begin{aligned}
\kappa\eta^{\pm}(\kappa) &= -a^s(\hat{u}_h^{0\pm} + \kappa\hat{u}_h^{1\pm}, \hat{u}_h^{0\pm} + \kappa\hat{u}_h^{1\pm}) + c_U \\
&\quad -\ell^N(\psi_H^{0\pm} + \kappa\psi_H^{1\pm}) + \ell^D(y^{0\pm} + \kappa y^{1\pm}) \qquad (7.17)\\
\eta^{\pm}(\kappa) &= -\frac{1}{\kappa}a^s(\hat{u}_h^{0\pm}, \hat{u}_h^{0\pm}) - 2a^s(\hat{u}_h^{0\pm}, \hat{u}_h^{1\pm}) - \kappa a^s(\hat{u}_h^{1\pm}, \hat{u}_h^{1\pm}) + \frac{1}{\kappa}c_U \qquad (7.18)\\
&\quad -\frac{1}{\kappa}\ell^N(\psi_H^{0\pm}) - \ell^N(\psi_H^{1\pm}) + \frac{1}{\kappa}\ell^D(y^{0\pm}) + \ell^D(y^{1\pm}).
\end{aligned}$$

Differentiating with respect to κ, we find

$$\begin{aligned}
\eta_\kappa^{\pm}(\kappa) &= \frac{1}{\kappa^2}a^s(\hat{u}_h^{0\pm}, \hat{u}_h^{0\pm}) - \frac{1}{\kappa^2}c_U - a^s(\hat{u}_h^{1\pm}, \hat{u}_h^{1\pm}) + \frac{1}{\kappa^2}\ell^N(\psi_H^{0\pm}) + \frac{1}{\kappa^2}\ell^D(y^{0\pm}), \qquad (7.19)\\
\eta_{\kappa\kappa}^{\pm}(\kappa) &= -\frac{2}{\kappa^3}\left(a^s(\hat{u}_h^{0\pm}, \hat{u}_h^{0\pm}) - c_U + \ell^N(\psi_H^{0\pm}) - \ell^D(y^{0\pm})\right). \qquad (7.20)
\end{aligned}$$

To optimize our bounds we require $\eta_\kappa^{\pm}(\kappa^{*\pm}) = 0$, which yields,

$$\kappa^{*\pm} = \sqrt{\frac{a^s(\hat{u}_h^{0\pm}, \hat{u}_h^{0\pm}) - c_U + \ell^N(\psi_H^{0\pm}) - \ell^D(y^{0\pm})}{a^s(\hat{u}_h^{1\pm}, \hat{u}_h^{1\pm})}}. \tag{7.21}$$

We first want to show from second derivatives considerations, (7.20), that $\eta\pm(\kappa^*)$ is a maximum. We know that, for all values of κ positive, $\eta^{\pm}(\kappa^*) \leq s_h$. It follows that the terms in $\frac{1}{k^2}$ in (7.19) which are the same as the parenthesis term of (7.20) must be positive — otherwise the lower bound goes to $+\infty$ as κ decreases. Therefore we conclude that $\eta^{\pm}(\kappa^*)$ is indeed a maximum.

We now show that computational effort on the h–mesh requires only two subdomain solves and not four, as it appears. From (7.2)–(7.3), we observe that $\psi_H^{0+} = \psi_H^{0-}$ and $\psi_H^{1+} = -\psi_H^{1-}$. It follows that $\hat{u}_h^{0+} = \hat{u}_h^{0-}$ and $\hat{u}_h^{1+} = -\hat{u}_h^{1-}$. Furthermore, because a^s is symmetric positive semidefinite then $a^s(u_h^{1+}, u_h^{1+}) = a^s(u_h^{1-}, u_h^{1-})$. From the above arguments, we obtain that $\kappa^{*+} = \kappa^{*-} \equiv \kappa^*$. It follows that, in fact, we only need to perform two subdomain solves to compute our optimized bounds, just as in the non-optimized case.

We also remark that κ^* will be a function of H, as will, of course, the optimal bounds, $(s_h)_{LB}(H) = \eta^+(\kappa^*, H), (s_h)_{UB}(H) = -\eta^-(\kappa^*, H)$. For $H \to h$ our bounds must be independent of κ, which implies from (7.21) that both the numerator and the denominator of (7.21) vanish. It follows that $\lim_{H\to h}\kappa^*$ may be zero, finite, or infinite. Hence, in some special circumstances the maximum occurs on the "boundary" for $\kappa^{*\pm} = 0$ [46]. Another pathological case is when the output value is zero then $\kappa^{*\pm} = 0$ for all H. A discrete presentation of the optimal stabilization parameter is presented for the one–dimensional model

problem in [35, 46].

7.2 Output Scaling for the Stokes Problem

Our procedure here is the same as in Section 7.1. We write our candidates as linear function in κ.

Similarly, we decompose $\psi_{iH}^{\pm}$ and $\Lambda_H^{\pm}$ as

$$\psi_{iH}^{\pm} = \psi_{iH}^{0\pm} + \kappa\psi_{iH}^{1\pm}, \tag{7.22}$$

$$\Lambda_H^{\pm} = \Lambda_H^{0\pm} + \kappa\Lambda_H^{1\pm}, \tag{7.23}$$

where

$$a(\psi_{iH}^{0\pm}, w_i) - d_i(w_i, \Lambda_H^{0\pm}) = -(2a(w_i, u_{iH}) - \ell_i^N(w_i)), \quad \forall (w_1, w_2) \in (X_H)^2, \tag{7.24}$$

$$-d_i(\psi_{iH}^{0\pm}, q) = 0, \quad \forall q \in Y_H, \tag{7.25}$$

and

$$a(\psi_{iH}^{1\pm}, w_i) - d_i(w_i, \Lambda_H^{1\pm}) = -(\pm\ell_i^{O^v}(w_i)), \quad \forall (w_1, w_2) \in (X_H)^2, \tag{7.26}$$

$$-d_i(\psi_{iH}^{1\pm}, q) = -(\pm\ell^{O^p}(q)), \quad \forall q \in Y_H. \tag{7.27}$$

Note that, u_{iH} is the solution to (5.1) and only appears on the right hand side of the equation. In fact in both equations the operator is identical and we can take advantage of direct solvers. We now write $\psi_{ih}^{\pm}$ as

$$\psi_{ih}^{\pm} = \psi_{ih}^{0\pm} + \kappa\psi_{ih}^{1\pm}, \tag{7.28}$$

which needs to satisfy for each element T_H on the h–mesh,

$$a_{T_H}(w_i, \psi_{ih}^{0\pm} - \psi_{iH}^{0\pm}) - d_{iT_H}(w_i, \tilde{p}_h^0) = 0, \quad \forall (w_1, w_2) \in (X_H)^2, \tag{7.29}$$

$$-d_{iT_H}(\psi_{ih}^{0\pm}, q) = 0, \quad \forall q \in Y_H, \tag{7.30}$$

and

$$a_{T_H}(w_i, \psi_{ih}^{1\pm} - \psi_{iH}^{1\pm}) - d_{iT_H}(w_i, \tilde{p}_h^1) = 0 \quad \forall (w_1, w_2) \in (X_H)^2, \tag{7.31}$$

$$-d_{iT_H}(\psi_{ih}^{1\pm}, q) = -(\pm\ell_{T_H}^{O^p}(q)), \quad \forall q \in Y_H. \tag{7.32}$$

Bases on similar arguments as in Section 5.4, the boundary condition for $\psi_{ih}^{0\pm}$ and $\psi_{ih}^{1\pm}$ are $(-g_D)$ Dirichlet and homogeneous Dirichlet, respectively. These two set of equations are similar to (5.68)-(5.68) in all respects; for forcing continuity of the adjoint across the

subdomain boundaries and for imposing an incompressibility constraint in the interior of each subdomain.

We now present the κ decomposition of the hybrid flux. First, we need to define functions $F_i^{0\pm}(v;\mathcal{F},\mathcal{P})$ and $F_i^{1\pm}(v;\mathcal{F},\mathcal{P})$. Therefor, for any function $\mathcal{F}$ and $\mathcal{P}$ in $\mathcal{H}^1_*(\Omega)$ and $L^2(\Omega)$, we define respectively, and for all $v \in \mathcal{H}^1_*(\Omega)$

$$F_i^{0\pm}(v;\mathcal{F},\mathcal{P}) = \sum_{T_H\in\mathcal{T}_H} F_{iT_H}^{0\pm}(v|_{T_H};\mathcal{F},\mathcal{P}) \tag{7.33}$$

$$F_i^{1\pm}(v;\mathcal{F},\mathcal{P}) = \sum_{T_H\in\mathcal{T}_H} F_{iT_H}^{1\pm}(v|_{T_H};\mathcal{F},\mathcal{P}) \tag{7.34}$$

where

$$F_{iT_H}^{0\pm}(v;\mathcal{F},\mathcal{P}) = a_{T_H}(\mathcal{F}_{T_H},v) - d_{i\,T_H}(v,\mathcal{P}) - \ell_{i\,T_H}^{N}(v), \tag{7.35}$$

$$F_{iT_H}^{1\pm}(v;\mathcal{F},\mathcal{P}) = a_{T_H}(\mathcal{F}_{T_H},v) - d_{i\,T_H}(v,\mathcal{P}) \pm \ell_{i\,T_H}^{O^v}(v). \tag{7.36}$$

Finally, we write

$$y_i^{\pm} = y_i^{0\pm} + \kappa y_i^{1\pm} \tag{7.37}$$

which is derived as in Section 6. That is, we solve for all T_H in $\mathcal{T}_H$ the following equations

$$\sum_{\gamma_{T_H}\in\mathcal{E}(\mathcal{T}_H)} \sigma_{T_H}^{\gamma_{T_H}} \int_{\gamma_{T_H}} v y_i^{0\pm}|_{E(\gamma_{T_H})}\,\mathrm{d}s = 2a_{T_H}(v,u_{iH}^{\pm}) - F_{iT_H}^{0\pm}(w;\psi_{iH}^{0\pm},\Lambda_H^{0\pm}), \tag{7.38}$$

$$\forall v \in Z_H(T_H),$$

$$\sum_{\gamma_{T_H}\in\mathcal{E}(\mathcal{T}_H)} \sigma_{T_H}^{\gamma_{T_H}} \int_{\gamma_{T_H}} v y_i^{1\pm}|_{E(\gamma_{T_H})}\,\mathrm{d}s = -F_{iT_H}^{1\pm}(v;\psi_{iH}^{1\pm},\Lambda_H^{1\pm}), \quad \forall v \in Z_H(T_H). \tag{7.39}$$

We can now solve the h–mesh problems,

$$2a(w_i,\hat{u}_{ih}^{0\pm}) - d_i(w_i,\hat{m}^{0\pm}) = -F_i^{0\pm}(w_i;\psi_{ih}^{0\pm},\Lambda_h^{0\pm}) + b(w_i,y_i^{0\pm}), \tag{7.40}$$

$$-d_i(\hat{u}_{ih}^{0\pm},q) = 0, \quad \forall (w_1,w_2,q) \in (X_H)^2 \times Y_H. \tag{7.41}$$

and

$$2a(w_i,\hat{u}_{ih}^{1\pm}) - d_i(w_i,\hat{m}^{1\pm}) = -F_i^{1\pm}(w_i;\psi_{ih}^{1\pm},\Lambda_h^{1\pm}) + b(w_i,y_i^{1\pm}), \tag{7.42}$$

$$-d_i(\hat{u}_{ih}^{1\pm},q) = 0, \quad \forall (w_1,w_2,q) \in (X_H)^2 \times Y_H. \tag{7.43}$$

We will not address solvability of (7.40)-(7.41) and (7.42)-(7.43) as it follows our usual proof (see Section 5.3.3).

Using the same derivation as in (5.80) the bounds can be expressed as

$$\eta^{\pm}(\kappa) = -\frac{1}{\kappa}\left(a(\hat{u}_{ih}^{0\pm} + \kappa\hat{u}_{ih}^{1\pm}, \hat{u}_{ih}^{0\pm} + \kappa\hat{u}_{ih}^{1\pm}) + \ell^N(\psi_{ih}^{0\pm} + \kappa\psi_{ih}^{1\pm})\right) \tag{7.44}$$

$$= -\frac{1}{\kappa}\left(a(\hat{u}_{ih}^{0\pm}, \hat{u}_{ih}^{0\pm}) + \ell^N(\psi_{ih}^{0\pm})\right)$$
$$-2a(\hat{u}_{ih}^{0\pm}, \hat{u}_{ih}^{1\pm}) - \ell^N(\psi_{ih}^{1\pm}) - \kappa(a(\hat{u}_{ih}^{0\pm}, \hat{u}_{ih}^{0\pm}). \tag{7.45}$$

Differentiating with respect to κ, we find

$$\eta_{\kappa}^{\pm}(\kappa) = \frac{1}{\kappa^2}\left(a(\hat{u}_{ih}^{0\pm}, \hat{u}_{ih}^{0\pm}) + \ell^N(\psi_{ih}^{0\pm}) - a(\hat{u}_{ih}^{1\pm}, \hat{u}_{ih}^{1\pm})\right), \tag{7.46}$$

$$\eta_{\kappa\kappa}^{\pm}(\kappa) = -\frac{2}{\kappa^3}\left(a(\hat{u}_{ih}^{0\pm}, \hat{u}_{ih}^{0\pm}) + \ell^N(\psi_{ih}^{0\pm})\right). \tag{7.47}$$

To optimize our bounds we require $\eta_{\kappa}^{\pm}(\kappa^{*\pm}) = 0$, which yields,

$$\kappa^{*\pm} = \sqrt{\frac{a(\hat{u}_{ih}^{0\pm}, \hat{u}_{ih}^{0\pm}) + \ell^N(\psi_{ih}^{0\pm})}{a(\hat{u}_{ih}^{1\pm}, \hat{u}_{ih}^{1\pm})}}, \tag{7.48}$$

To prove that κ is a maximum, we use the same arguments as in Section 7.1. We note that $\eta^{\pm}$ is a lower bound to s_h. It follows that the terms in $\frac{1}{k^2}$ must be positive such that our lower bound does not go to $+\infty$ as κ decreases. These terms also enter in the second derivative making the second derivative negative for all positive values of κ. Finally, it follows that$\eta^{\pm}(\kappa^{*\pm})$ is, indeed, a maximum.

We will make some remarks concerning computational cost, that is, we want to show that we need only two subdomain solves rather than four to calculate the bounds for the optimal stabilization parameter κ^*. In this case, it is obvious that the numerator is the same in both the upper and the lower bound calculation because it does not depend on the output functional. In addition, we can show from (7.31) that $\psi_{ih}^{1+} = -\psi_{ih}^{1-}$; the forcing term changes signs and the boundary condition is homogeneous Dirichlet. Furthermore, we note that the right hand side of the (7.42) only differs by the sign when replacing ψ_{ih}^{1+} by $-\psi_{ih}^{1-}$ which leads to $\hat{u}_{ih}^{1+} = -\hat{u}_{ih}^{1-}$. Finally, because a is symmetric positive semidefinite then $a(\hat{u}_{ih}^{1+}, \hat{u}_{ih}^{1+}) = a(\hat{u}_{ih}^{1-}, \hat{u}_{ih}^{1-})$ and the denominator of (7.48) is the same for both the upper and the lower bounds. From the above arguments, we obtain that $\kappa^{*+} = \kappa^{*-} \equiv \kappa^*$. It follows that, in fact, we only need to perform two subdomain solves to compute our optimized bounds, just as in the non-optimized case.

For clarity we summarize the above identities:

$$\hat{u}_{ih}^{0+} = \hat{u}_{ih}^{0-} \tag{7.49}$$

$$\hat{u}_{ih}^{1+} = -\hat{u}_{ih}^{1-} \tag{7.50}$$

$$\psi_{0h}^{1+} = -\psi_{ih}^{0-} \tag{7.51}$$

$$\psi_{ih}^{1+} = -\psi_{ih}^{1-}. \tag{7.52}$$

These identities lead to an interesting property that the average of the bounds is not affected by κ. The average of the bounds is given by

$$\begin{aligned}\frac{1}{2}(\eta^+ - \eta^-) = & -\frac{1}{2\kappa}\Big(a(\hat{u}_{ih}^{0+}, \hat{u}_{ih}^{0+}) + \ell^N(\psi_{ih}^{0+}) \\ & -a(\hat{u}_{ih}^{0-}, \hat{u}_{ih}^{0-}) - \ell^N(\psi_{ih}^{0-})\Big) \\ & -a(\hat{u}_{ih}^{0+}, \hat{u}_{ih}^{1+}) + a(\hat{u}_{ih}^{0-}, \hat{u}_{ih}^{1-}) \\ & -\frac{1}{2}\ell^N(\psi_{ih}^{1+}) + \frac{1}{2}\ell^N(\psi_{ih}^{1-}) \\ & -\frac{k}{2}\Big(a(\hat{u}_{ih}^{1+}, \hat{u}_{ih}^{1+}) - a(\hat{u}_{ih}^{1-}, \hat{u}_{ih}^{1-})\Big). \end{aligned} \tag{7.53}$$

From (7.49)-(7.51) we observe that the terms in $\frac{1}{2k}$ vanish. From (7.50) we see that the terms in $\frac{k}{2}$ vanish as well. After, replacing the remaining $\hat{u}_{ih}^{1-}$ and ψ_{ih}^{1-} by their equivalent functions, we obtain

$$\frac{1}{2}(\eta^+ - \eta^-) = -2a(\hat{u}_{ih}^{1+}, \hat{u}_{ih}^{1+}) - \ell^N(\psi_{ih}^{1-}). \tag{7.54}$$

Indeed, the average of the bounds does not depend on κ.

Chapter 8

Numerical Results

In this chapter we present bounds for outputs of equations of increasing difficulty. In Section 8.1 we illustrate our bound procedure for a one–dimensional convection–diffusion equation and the four linear–functional outputs (3.6)-(3.9). In Section 8.2 we consider a two–dimensional convection–diffusion equation. We compare results for the different approaches to calculate the hybrid flux. In this case, the output of interest is the average value (4.7) and the point value at the corner (4.8). In Section 8.3 we analyze results for our Poisson equation where we investigate the bounding procedure for $\mathbf{P}_2$ spatial discretizations. Finally, in Section 8.4 we present results for the incompressible Stokes Problem.

As discussed previously, the purpose of the bounds is to capture the engineering output of interest, s, to within some acceptable accuracy. This accuracy mainly depends on the H–mesh exploited in the calculation. Therefore, we are interested in establishing, through the intermediary of the H–mesh discretization, inexpensive yet sharp lower and upper bounds, $(s_h)^*_{LB}$ and $(s_h)_{UB}$, for the output of the "truth" mesh, s_h. Recall from the motivation and the description of our procedure that the bounds offer a fast and reliable design environment. In fact, the scenario described in Section 1.1 will become more obvious in the sense that the reader may start to understand the difference between, s_h, the output on the "truth" mesh, s_H, the output on the H–mesh, $(s_h)_{LB}$ and $(s_h)_{UB}$, the bounds, and $(s_h)^*_{pre}$, the average of the bounds, as defined in (1.2). In particular we investigate how the bounds vary as a function of the H–mesh exploited in the calculations.

8.1 Convection–Diffusion Equation in One Space Dimension

In the example presented here, $f = 0$ (which avoids all quadrature problems), $\alpha = \frac{U}{\nu}$, $\beta = 0$ in (3.1), where $\nu = .1$, $U = 1$. Related to the mesh, we have $h = .001, h \leq H \leq .1$, and $K = H^{-1}$ (similar results are also obtained for domains decomposed in one subdomain or in ten subdomains [35, 46]). Although for purposes of illustration we have selected a small h–mesh grid Peclet number, $h/\nu = .01$, similar bound performance is observed for h/ν of

order unity. Note that resolution is an important issue because for the adjoint the flow is reversed and new boundary layers are introduced at $x = 0$ (not present in $u(x) \sim e^{(x-1)/\nu}$); furthermore, for the pointwise–value output, the adjoint suffers an internal layer at $x = \overline{x}$ associated with the jump in the derivative.

The bounds presented here reflect the optimal scaling κ^* described in Section 7. For the bounded flux output ($s^{(3)}$) and for the average output ($s^{(2)}$), $\kappa = 1$ for all $H > h$, and for $s^{(1)}$, κ^* approaches 1.12 as $H \to h$ and for $s^{(4)}$, κ^* approaches ∞ as $H \to h$. Results that illustrate the improvement brought by the optimum stabilization parameter are presented for Ω in [46] and in Section 8.2 for the corner output.

To begin, we show in Figure 8-1a, 8-1b, 8-1c and 8-1d, $(s_h)^*_{UB}/s_h, (s_h)^*_{LB}/s_h, (s_h)^*_{pre}/s_h$, and s_H/s_h as a function of H for the pointwise-value output $s^{(1)}$ (for $\overline{x} = .9$), the solution-average output $s^{(2)}$, the bounded flux output $s^{(3)}$ and the unbounded flux output $s^{(4)}$, respectively. In addition, we present in Figure 8-2a, 8-2b, 8-2c, and 8-2d, $\log|(s_h)^*_{UB} - s_h|, \log|(s_h)^*_{LB} - s_h|, \log|(s_h)^*_{pre} - s_h|$, and $\log|s_H - s_h|$ as a function of $\log H$ for the pointwise-value output $s^{(1)}$ (for $\overline{x} = .9$), the solution-average output $s^{(2)}$, the bounded flux output $s^{(3)}$ and the unbounded flux output $s^{(4)}$, respectively. We observe that, in general, the bounds are quite accurate, and that $(s_h)_{pre}$ is the most accurate estimator of the truth output s_h, in fact more accurate than s_H. Furthermore, we see that $(s_h)^*_{pre}, (s_h)^*_{UB}, (s_h)^*_{LB}$, and s_H converge to s_h as H^2 for our three bounded output, which is optimal given our piecewise–linear approximation space. The convergence rates of the unbounded flux are less impressive; we obtain $H^{1.65}$ for $(s_h)^*_{pre}, (s_h)^*_{UB}, (s_h)^*_{LB}$ and H^1 for s_H.

The bound–based predictors $(s_h)^*_{pre}$ are appealing, however, we can only rigorously bound the errors in these predictors by $((s_h)^*_{LB} - (s_h)^*_{pre}) \leq (s_h - (s_h)^*_{pre}) \leq ((s_h)^*_{UB} - (s_h)^*_{pre})$. For the average ($s^{(2)}$) and the bounded flux ($s^{(3)}$) outputs there is clearly fortuitous cancellation in the evaluation of $\ell(u_H)$ such that s_H is accurate even at $H = .1$ for which $u_H(x)$ is a very crude approximation of $u(x)$. This cancellation also appears in $(s_h)^*_{pre}$ because of the symmetry of the upper and lower bounds, where the latter are relatively inaccurate estimators of s_h. However, for the pointwise output ($s^{(1)}$), in which no such cancellation occurs, not only is $|(s_h)^*_{pre} - s_h| < |s_H - s_h|$, but $|(s_h)^*_{LB} - s_h| \approx |s_H - s_h|$, and $|(s_h)^*_{UB} - s_h| < |s_H - s_h|$. Similar conclusions can be drawn for the unbounded flux output ($s^{(4)}$) where the bounds $(s_h)^*_{LB}$ and $(s_h)^*_{UB}$ provide better prediction than s_H. In fact, s_H is an inaccurate approximation of s_h which illustrates the added value of having bounded functionals. We also observe, in this case, that the bounds are very sharp and give a much better "approximation" of s_h than s_H.

In an engineering design application, four values can be obtained from the bounds procedure: the two bounds, the average of the bounds and the H–mesh output. Note that the bounds do not give any indication about the accuracy of s_H but instead relate to s_h; therefore increasing the reliability of the design framework.

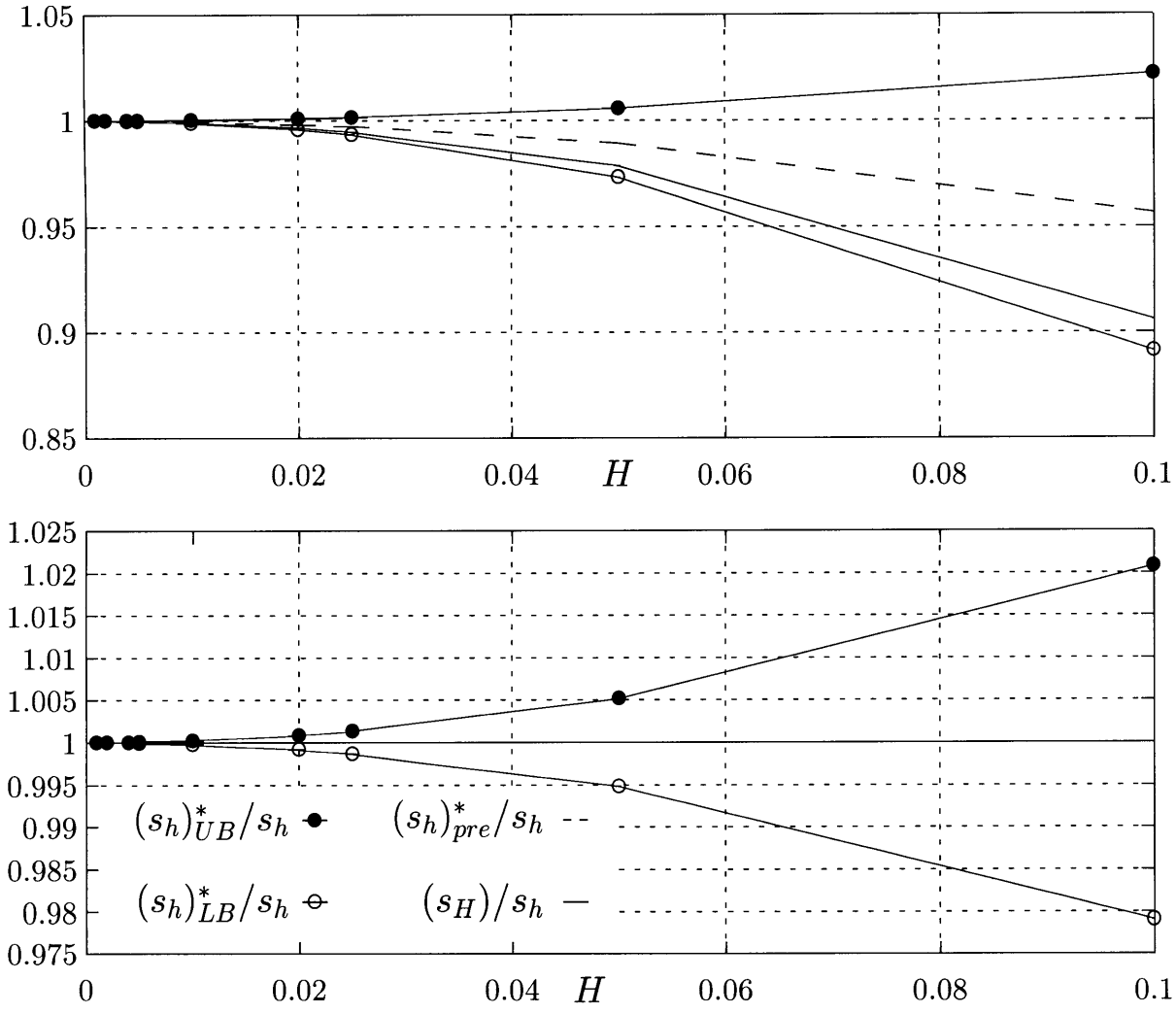

Figure 8-1: Plots of $(s_h)^*_{UB}/s_h$, $(s_h)^*_{pre}/s_h$, $(s_h)^*_{LB}/s_h$, and s_H/s_h as a function of (effective) H for (a, top) $s^{(1)}$, the pointwise–value output, (b, bottom) $s^{(2)}$, the solution–average output.

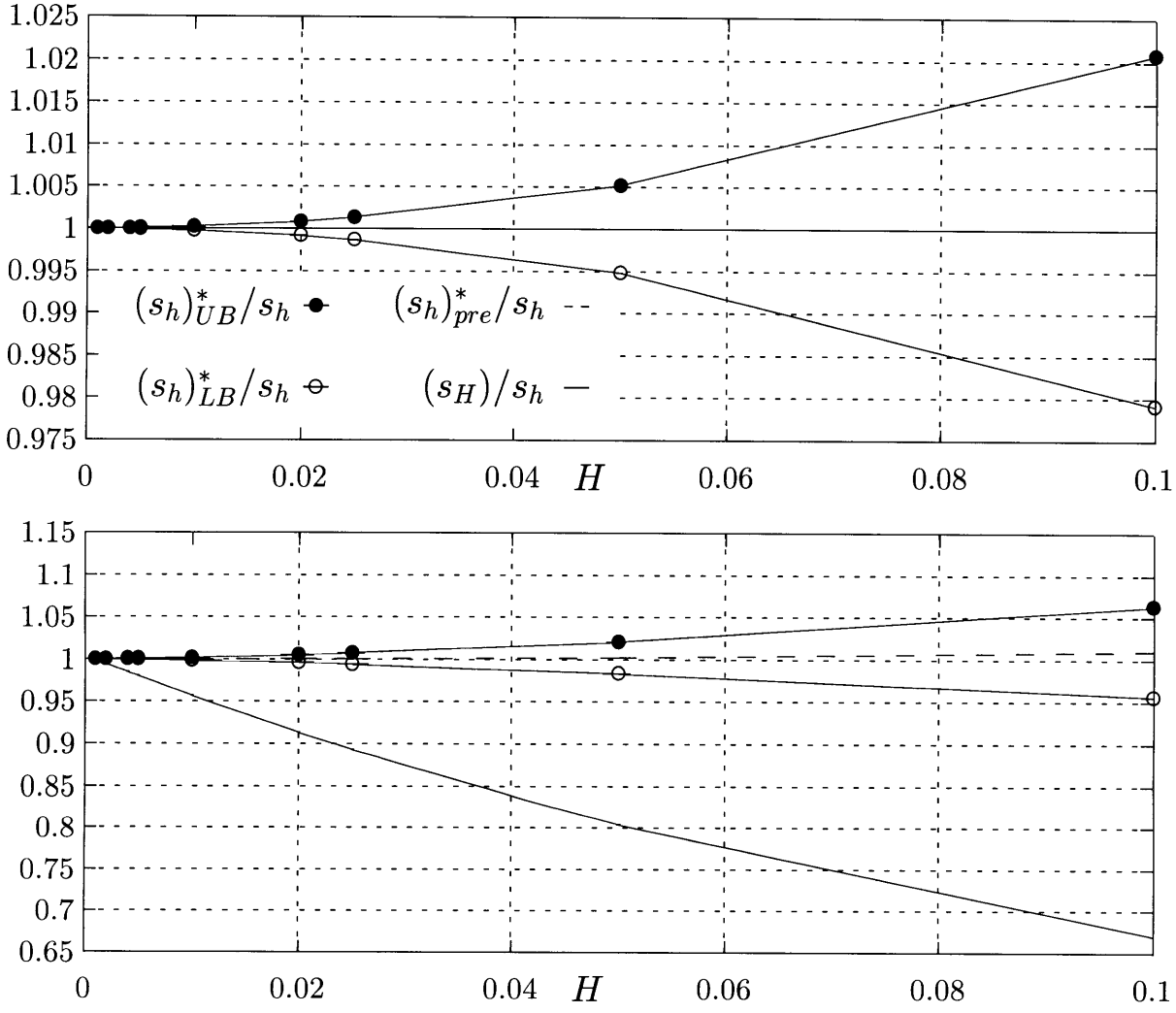

Figure 8-1: Plots of $(s_h)^*_{UB}/s_h$, $(s_h)^*_{pre}/s_h$, $(s_h)^*_{LB}/s_h$, and s_H/s_h as a function of (effective) H for (c, top) $s^{(3)}$, the bounded flux output, (d, bottom) $s^{(4)}$, the unbounded flux output.

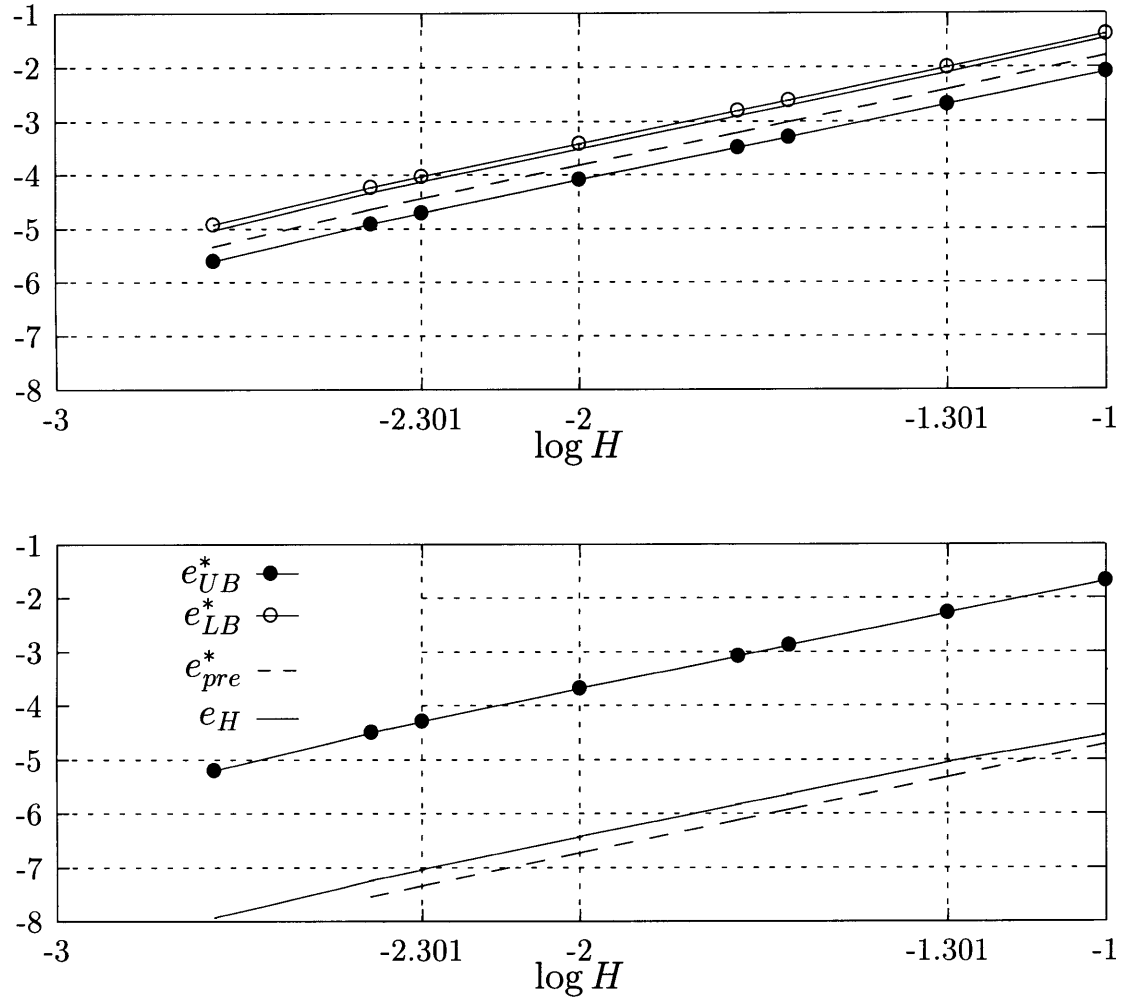

Figure 8-2: Plots of $e^*_{UB} = \log|(s_h)^*_{UB} - s_h|$, $e^*_{LB} = \log|(s_h)^*_{LB} - s_h|$, $e^*_{pre} = \log|(s_h)^*_{pre} - s_h|$, and $e_H = \log|s_H - s_h|$ as a function of $\log H$ for (a, top) $s^{(1)}$, the pointwise–value output , (b, top) $s^{(2)}$, the solution–average output.

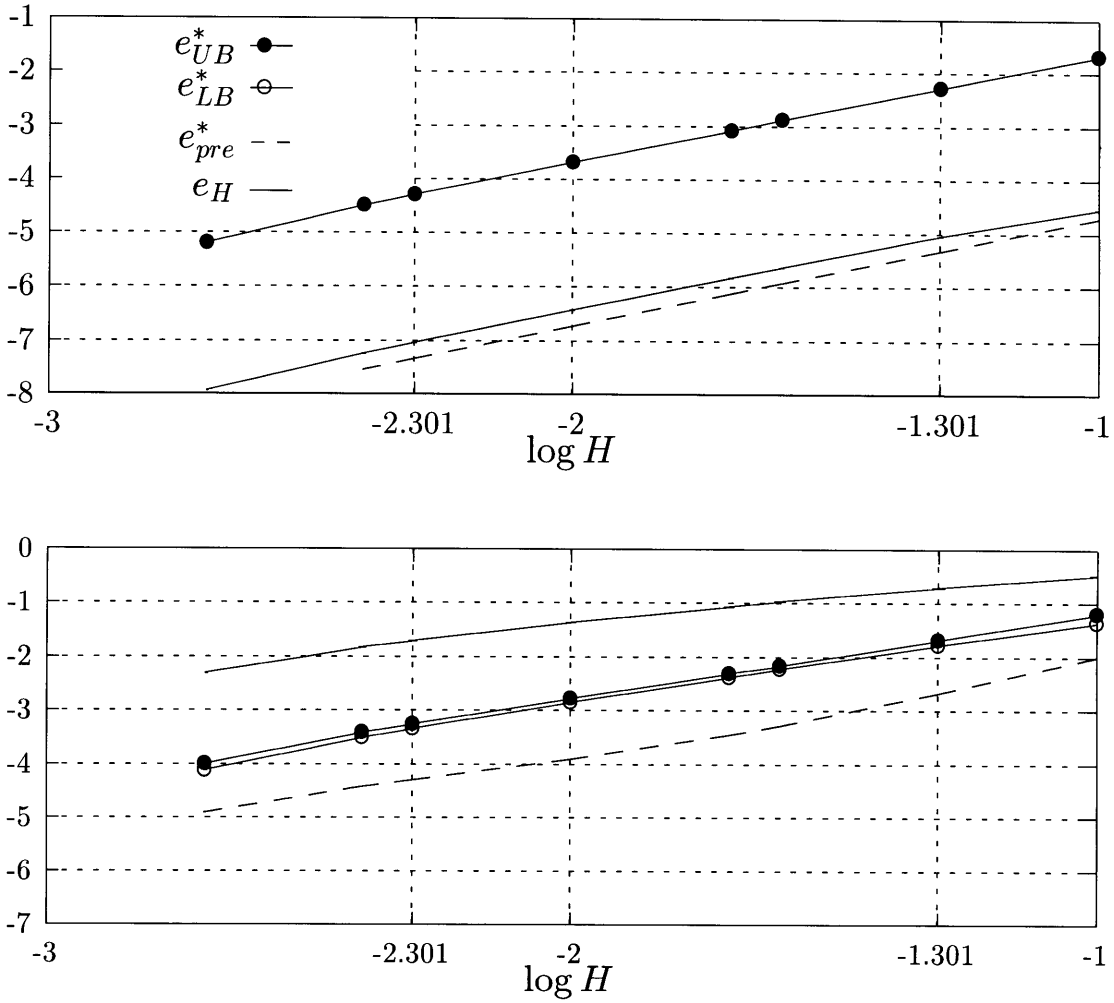

Figure 8-2: Plots of $e^*_{UB} = \log|(s_h)^*_{UB} - s_h|$, $e^*_{LB} = \log|(s_h)^*_{LB} - s_h|$, $e^*_{pre} = \log|(s_h)^*_{pre} - s_h|$, and $e_H = \log|s_H - s_h|$ as a function of $\log H$ for (c, top) $s^{(3)}$, the bounded flux output , (d, bottom) $s^{(4)}$,the unbounded flux output.

8.2 Convection–Diffusion Equation in Two Space Dimensions

In this Section we present results for the convection–diffusion equation, for $\nu = .1$, and for two outputs: the average solution on the segment Γ^O shown in Figure 4-1, (4.7), and the value at the corner (4.8). We compare three different hybrid flux formulations for the $\mathbf{P}_1$ finite element discretization: the *nonconforming* formulation presented in Section 6.1, the *strong conforming* formulation and the *gradient forced conforming* formulation presented in Section 6.2.

The triangulation, $\mathcal{T}_{(H_o,R)}$, is investigated to evaluate the H–mesh influence on the bounds. It consists of uniform refinements of the coarsest mesh $\mathcal{T}_{(H_o,1)}$. The H–meshes, $\mathcal{T}_H$, correspond to $\mathcal{T}_{(H_o,R)}$, $R = 1, 2, 3, 4, 6$ and the truth h–mesh corresponds to $\mathcal{T}_h = \mathcal{T}_{(H_o,12)}$; $\mathcal{T}_{(H_o,1)}$ and $\mathcal{T}_h$ are shown in Figures 8-3a and 8-3b, respectively. Note that, for different refinement values of R, we satisfy $X_H \subset X_h$ as required by the theory. We shall denote the effective working–approximation element size associated with triangulation $\mathcal{T}_H = \mathcal{T}_{(H_o,R)}$ as $H \equiv 1/R$. In all the meshes $\mathcal{T}_{(H_o,R)}$, elements are concentrated near the domain boundary walls in anticipation of the boundary layers that will form on the "left" and "top" walls but also in anticipation of the boundary layers in the adjoint, $\psi_H^{\pm}(x)$, for which the flow is reversed. It is clear that this "bottom" and "right" wall refinement is not required for the original problem, and is thus a "hidden" cost associated with the bound procedure.

We plot in Figure 8-4a, 8-4b, and 8-4c, $(s_h)^*_{UB}/s_h, (s_h)^*_{LB}/s_h, (s_h)^*_{pre}/s_h$, and s_H/s_h as a function of H for the three different hybrid flux formulations considered: nonconforming, strong conforming and gradient forced conforming, respectively. Here, the output of interest, s_h, is the average boundary values near the top left corner, (4.7). The bounds presented reflect the optimal scaling κ^* described in Section 7 where κ^* approaches 0.93 for the nonconforming formulation, κ^* approaches 1.16 for the strong conforming formulation and κ^* approaches 1.18 for the gradient forced formulation as $H \to h$.

From the nonconforming formulation results, we see that the most accurate estimator of the true output, s_h, is s_H, followed by $(s_h)^*_{pre}, (s_h)^*_{UB}$, and $(s_h)^*_{LB}$. We contend that the degradation in the accuracy of $(s_h)^*_{LB}$ and $(s_h)^*_{UB}$ is more than balanced by the certainty that these quantities bounds s_h from below and above; no such two–sided, or even one–sided, assurances are associated with either s_H or $(s_h)_{pre}$. Nevertheless, as an error estimator for s_h, the bounds are less than impressive. Recall, that in our engineering design scenario, the bounds do not serve as estimators but more as "verificators" of s_h.

We observe that in the conforming case we have considerably improved the lower bound $(s_h)^*_{LB}$ and therefore $(s_h)^*_{pre}$ is now the most accurate estimator for the true output, s_h, followed by $s_H, (s_h)^*_{UB}$, and $(s_h)^*_{LB}$. The accuracy of $(s_h)^*_{LB}$ and $(s_h)^*_{UB}$ is not yet impressive but has improved and is within reasonable engineering values. For our coarsest mesh calculations, we obtain bounds on the output within $\pm 12\%$ and for calculations on $\mathcal{T}_{(H_o,2)}$

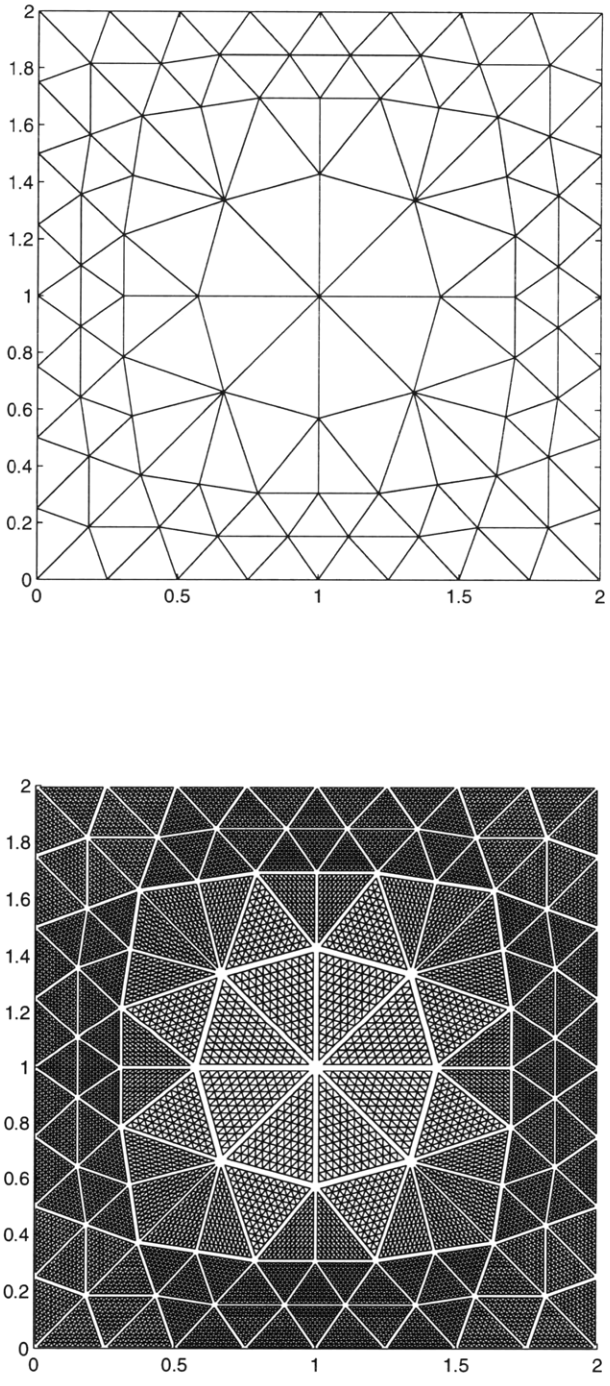

Figure 8-3: (a) Coarsest working mesh $\mathcal{T}_H = \mathcal{T}_{(H_o,1)}$, and (b) truth mesh $\mathcal{T}_H = \mathcal{T}_{(H_o,12)}$.

we are well within $\pm 5\%$ of s_h.

Recall that the only difference in the gradient forced and strong conforming formulations is the approach to calculate the initial approximation for the hybrid flux. We note, from Figure 8-4b and 8-4c that the gradient based hybrid flux initial approximation is almost as good as the strong initial approximation of the conforming formulation. However, the accuracy of $(s_h)^*_{pre}$ in the strong conforming formulation is slightly better that $(s_h)^*_{pre}$ for the gradient based calculations.

In Figure 8-5a, 8-5b, and 8-5c we present $\log|(s_h)^*_{UB} - s_h|$, $\log|(s_h)^*_{LB} - s_h|$, $\log|(s_h)^*_{pre} - s_h|$, and $\log|s_H - s_h|$ as a function of $\log H$ for the same three hybrid flux formulations. As expected, we observe that $s_H, (s_h)^*_{LB}$, and $(s_h)^*_{UB}$ all converge to s_h as $O(H^2)$ in all three cases.

The reconstructed solution $\hat{\mathcal{U}}^{\pm}_h$ illustrates the bounds sharpness. It is clear that, if the bounds are tight, the approximation $\hat{\mathcal{U}}^{\pm}_h$ must be close to u_h. We compare in Figure 8-6, 8-7, 8-8, and 8-9, $\hat{\mathcal{U}}^{+}_h$ for the nonconforming formulation, the strong conforming formulation and the gradient forced conforming formulation associated with the working mesh $\mathcal{T}_H = \mathcal{T}_{(H_o,3)}$, and u_h for the truth mesh $\mathcal{T}_H = \mathcal{T}_{(H_o,12)}$, respectively. In order to render visual comparison more transparent we choose the level of $\hat{\mathcal{U}}^{+}_h$ in all singular domains T_H so that $\hat{\mathcal{U}}^{+}_h$ and u_H agree at one vertex of T_H. We observe the small discontinuities in $\hat{\mathcal{U}}^{+}_h$ across subdomains boundaries which are an indication of the accuracy of the method used in the hybrid flux approximation. Indeed, $\hat{\mathcal{U}}^{+}_h$ is quite close to u_h for the working mesh $\mathcal{T}_{(H_o,3)}$. This is not always the case as for the working approximation $\mathcal{T}_H = \mathcal{T}_{(H_o,1)}$ (Figure 8-10) where we clearly see that $\hat{\mathcal{U}}^{+}_h$ is not close to u_h. For this coarsest H–mesh the grid Peclet number is "supercritical"; the resulting oscillations are also responsible for the poor quality of the bounds for $H = 1$. We believe that stabilization techniques applied on the H–mesh should improve the bounds for large H.

The increased sharpness observed for the lower bound of the strong conforming formulation discussed above is also apparent on the reconstructed solution $\hat{\mathcal{U}}^{\pm}_h$ presented in Figure 8-7. We observe that the small discontinuities in $\hat{\mathcal{U}}^{+}_h$ across subdomains boundaries are almost not visible which is not the case for the nonconforming formulation of Figure 8-6. This suggests that the strong conforming approach to the hybrid flux approximation is more accurate. Similarly, we observe, for the forced approximation, that the discontinuities in $\hat{\mathcal{U}}^{+}_h$ across subdomains boundaries are also very small. The discontinuities appear to be of equivalent size as in the strong conforming approach.

We conclude the analysis of the different types of hybrid flux approximations with a few remarks. First, it seems — at least for this model problem — that both conforming approaches give similar results, slightly better in the strong conforming approach but nothing really significant. We should point out that the latter approach has the advantage of being easier to implement. Second, for all our corner average values output results, the

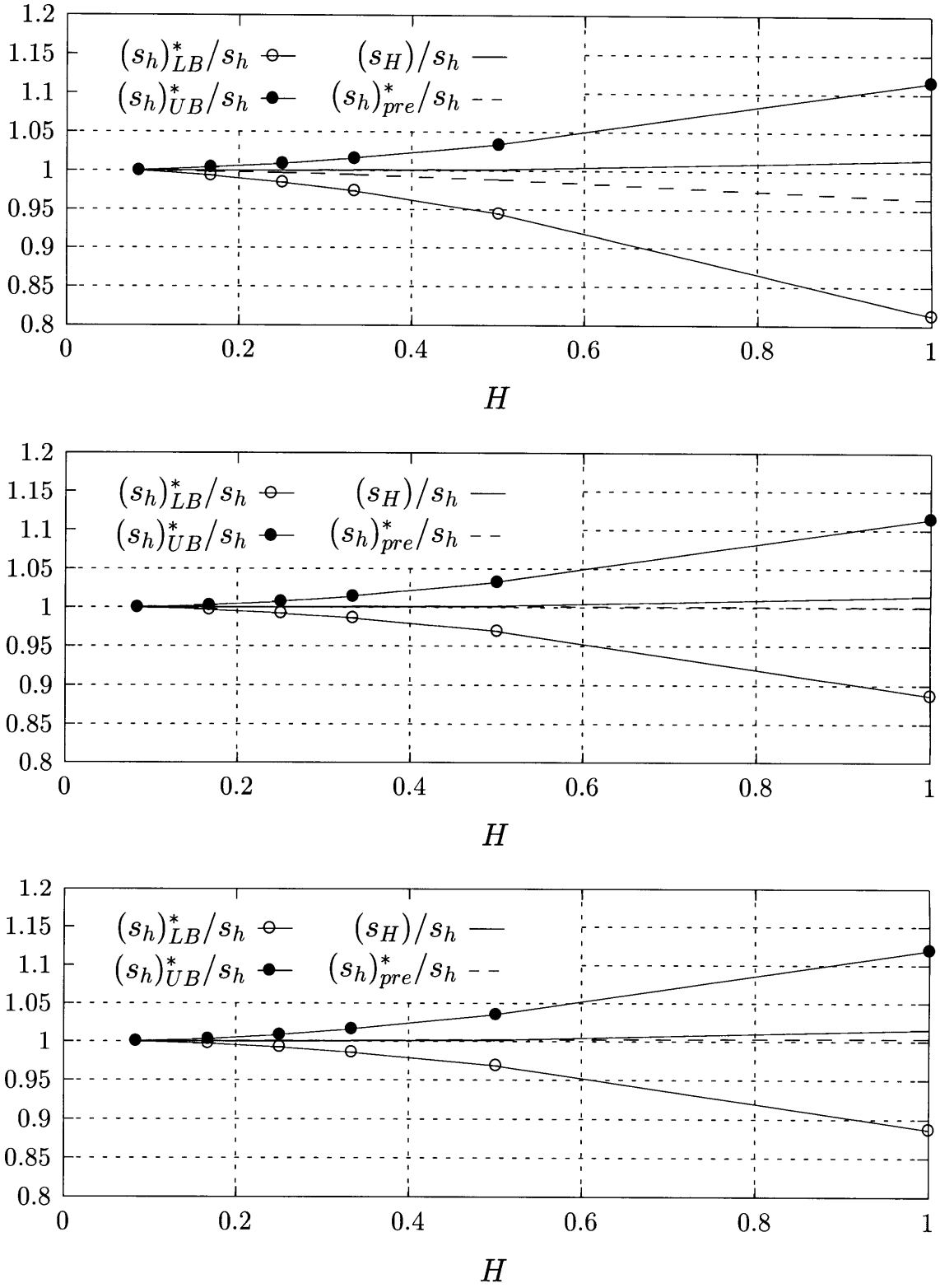

Figure 8-4: Plots of $(s_h)^*_{UB}/s_h$, $(s_h)^*_{pre}/s_h$, $(s_h)^*_{LB}/s_h$, and s_H/s_h as a function of (effective) H for (a, top) for nonconforming hybrid flux, (b, middle) for strong conforming hybrid flux, and (c, bottom) for gradient forced conforming hybrid flux.

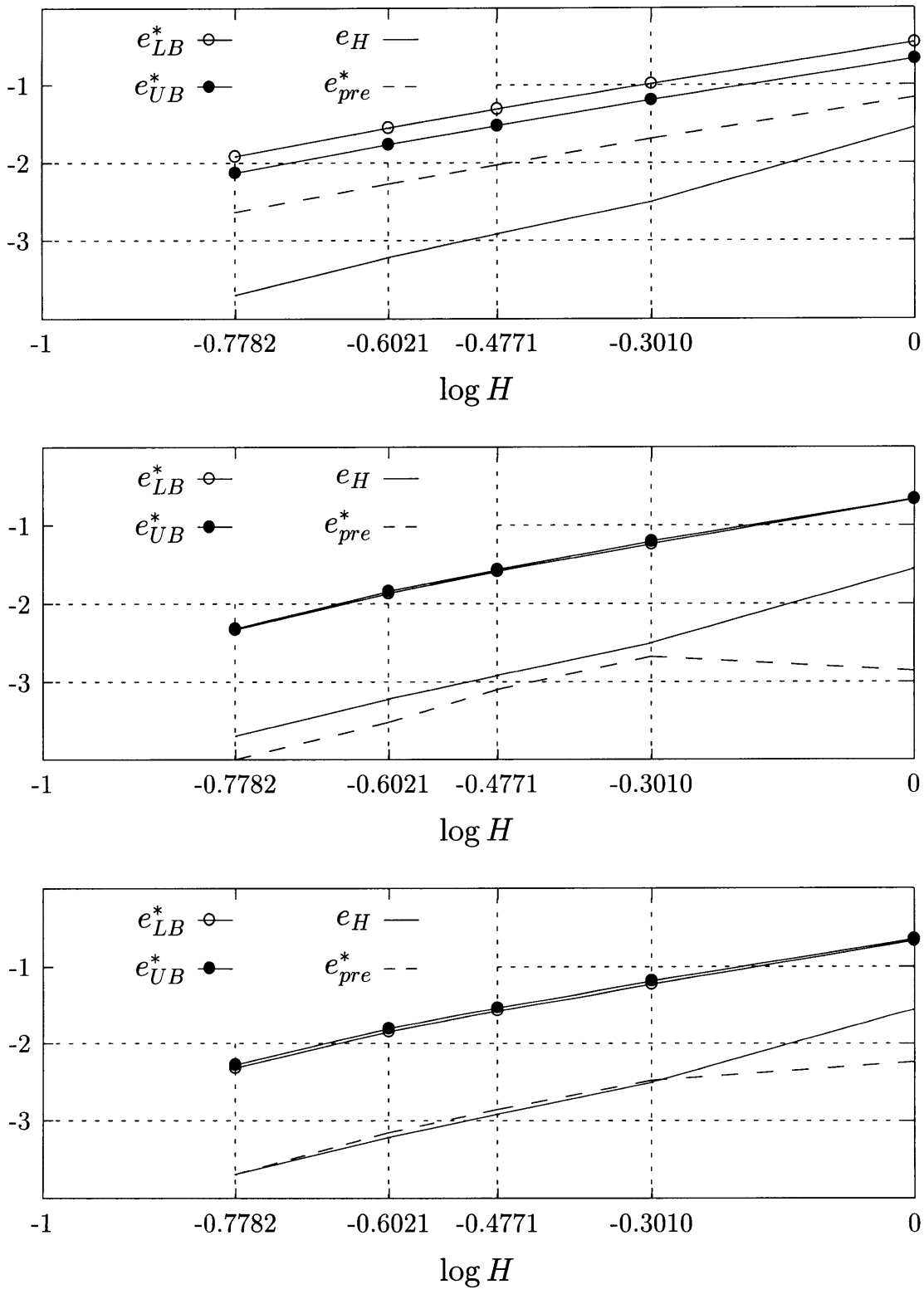

Figure 8-5: Plots of $e^*_{UB} = \log|(s_h)^*_{UB} - s_h|$, $e^*_{LB} = \log|(s_h)^*_{LB} - s_h|$, $e^*_{pre} = \log|(s_h)^*_{pre} - s_h|$, and $e_H = \log|s_H - s_h|$ as a function of $\log H$ for (a, top) for nonconforming hybrid flux, (b, middle) for strong conforming hybrid flux, and (c, bottom) s, for gradient forced conforming hybrid flux.

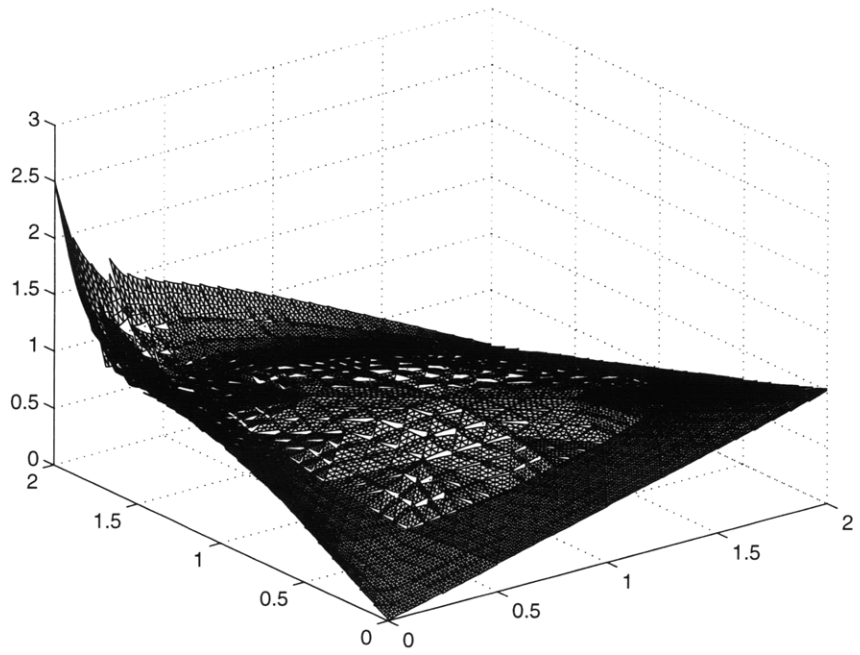

Figure 8-6: Plot of $\hat{\mathcal{U}}_h^+$ for $\mathcal{T}_H = \mathcal{T}_{(H_o,3)}$ using a nonconforming formulation to calculate the hybrid flux.

stabilization parameter is of order unity and therefore just slightly improves the bounds. Nevertheless, there exist outputs where the use of the stabilization parameter is essential, for example the corner value output which will be presented next. In fact this stabilization parameter is more often essential that not; other examples include the Stokes problem lift output of Section 8.4 and the nonuniform velocity field of the convection–diffusion problem introduced in Appendix B. Finally, the bounds are relatively sharp and converge to s_h at least as fast as s_H converges to s_h as $H \to h$.

The output $s^{(6)}$ is now considered. Recall that this output functional is unbounded. In this example, the strong conforming formulation is employed in the bounds calculations. Our goal in presenting results for this output is twofold: first, to show how one unbounded functional performs in two space dimensions and second, to demonstrate the need of the optimal output procedure.

We plot in Figure 8-11, $(s_h)^*_{UB}/s_h, (s_h)^*_{LB}/s_h, (s_h)^*_{pre}/s_h, (s_h)_{UB}/s_h, (s_h)_{LB}/s_h, (s_h)_{pre}/s_h$, and s_H/s_h as a function of H for the corner pointwise value. The superscript $*$ refers to the optimal bounds. Both optimal scaling κ^* and non optimal scaling $\kappa = 1$ are presented for comparison. Note that $(s_h)^*_{pre}$ and $(s_h)_{pre}$ is in both cases the same. The effect κ^* is uniquely the reduction of the gap between the bounds as proved in Section 7.2. For our optimal scalarization parameter κ^* approaches 0.04 as $H \to h$. It is clear from the small value of κ^* that the stabilization parameter is essential as seen in Figure 8-11.

In Figure 8-12, we present $\log|(s_h)^*_{UB} - s_h|, \log|(s_h)^*_{LB} - s_h|, \log|(s_h)^*_{pre} - s_h|, \log|(s_h)_{UB} -$

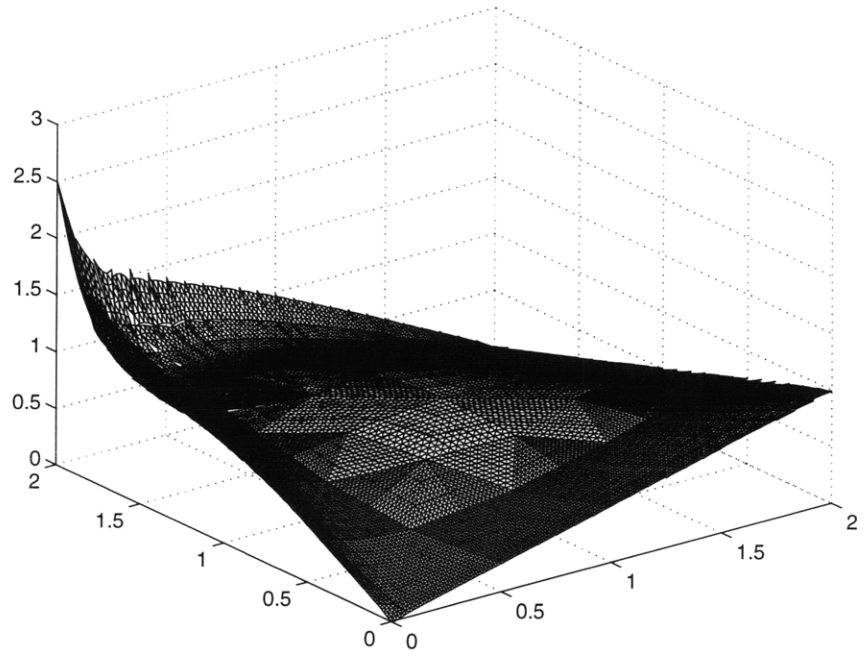

Figure 8-7: Plot of $\hat{\mathcal{U}}_h^+$ for $\mathcal{T}_H = \mathcal{T}_{(H_o,3)}$ using a strong conforming formulation to calculate the hybrid flux.

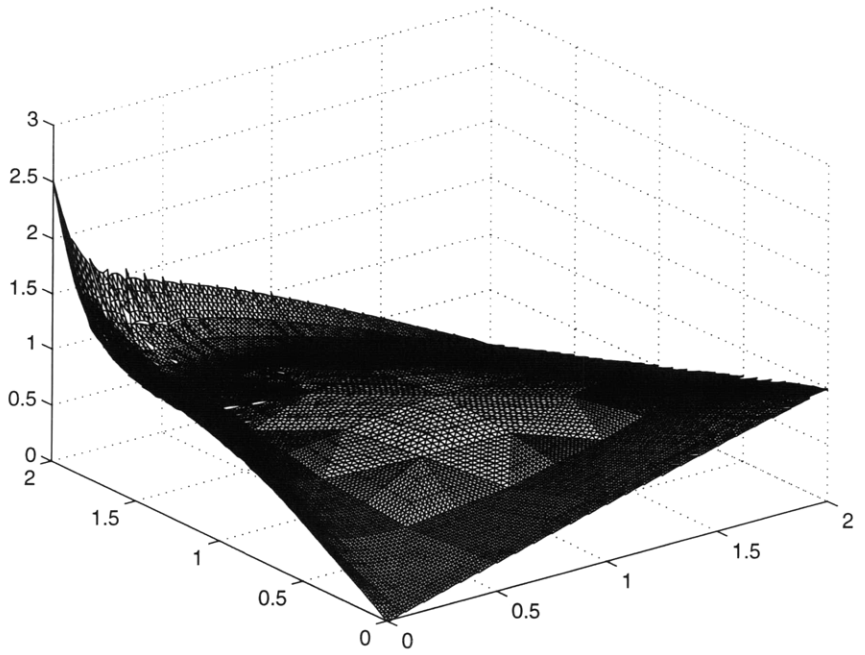

Figure 8-8: Plot of $\hat{\mathcal{U}}_h^+$ for $\mathcal{T}_H = \mathcal{T}_{(H_o,3)}$ using a gradient forced conforming formulation to calculate the hybrid flux.

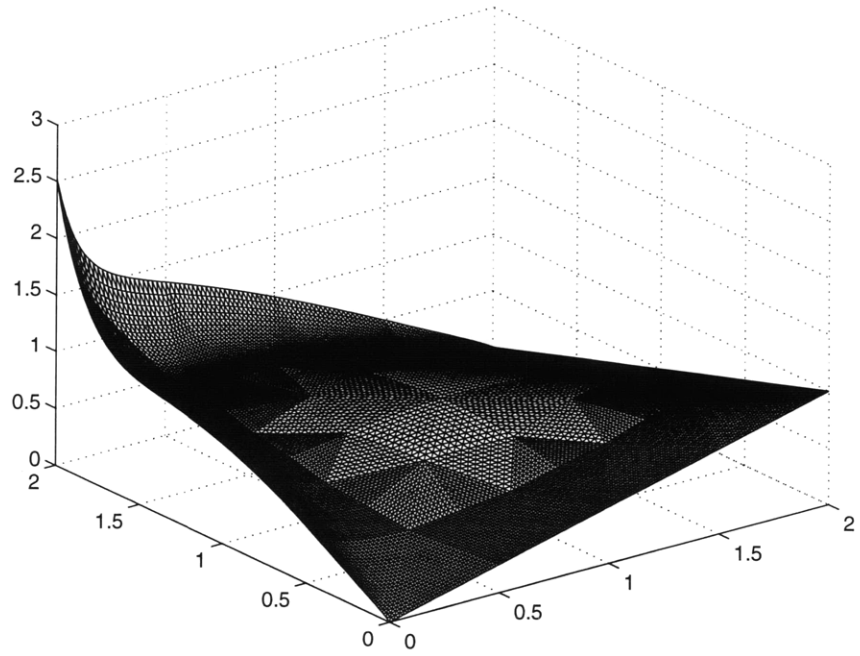

Figure 8-9: Plot of u_h for $\mathcal{T}_H = \mathcal{T}_{(H_o,12)}$.

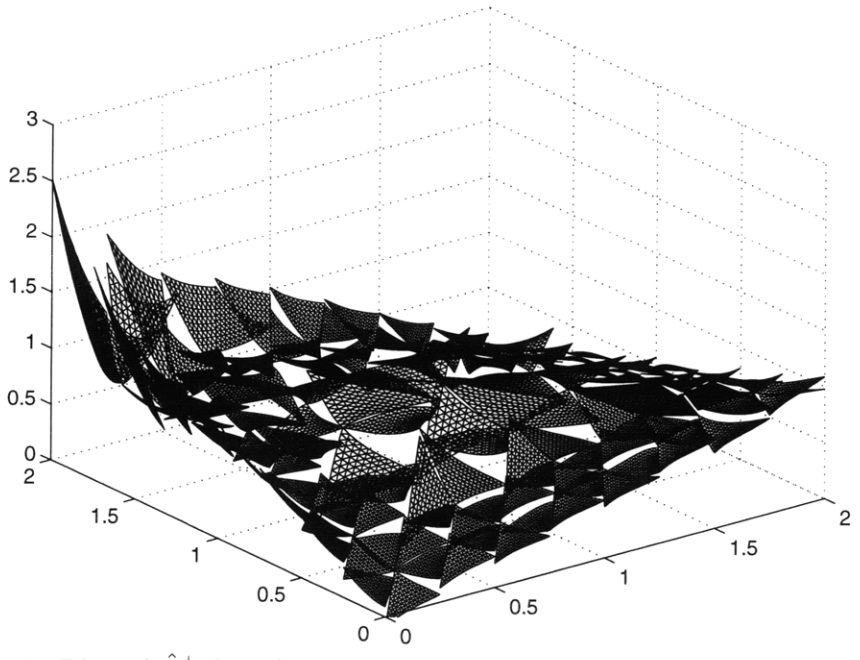

Figure 8-10: Plot of $\hat{\mathcal{U}}_h^+$ for $\mathcal{T}_H = \mathcal{T}_{(H_o,1)}$ using a nonconforming formulation to calculate the hybrid flux.

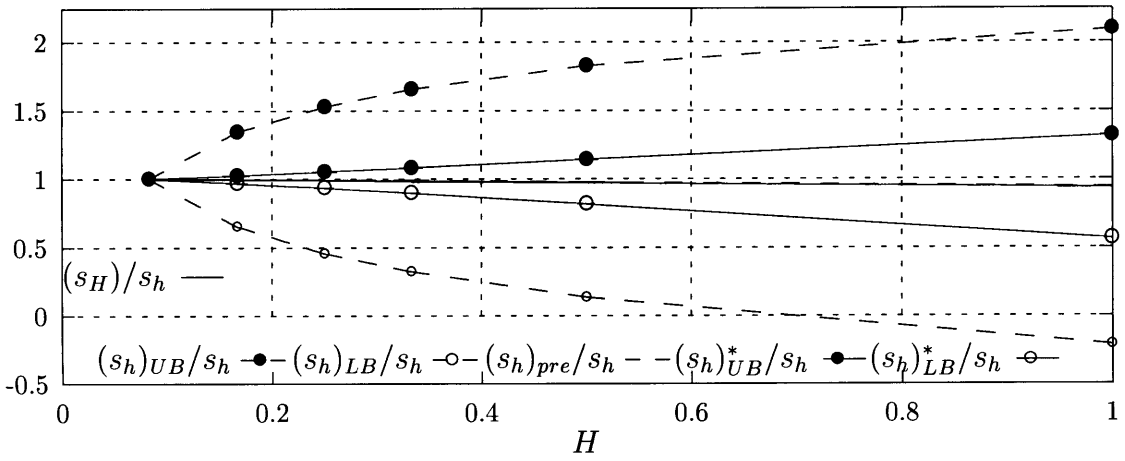

Figure 8-11: Plots of $(s_h)_{UB}/s_h$, $(s_h)_{LB}/s_h$, (non optimal bounds) $(s_h)^*_{UB}/s_h$, $(s_h)^*_{LB}/s_h$, (optimal bounds) $(s_h)^*_{pre}/s_h$, and s_H/s_h as a function of (effective) H for the corner value output, $s^{(6)}$.

$s_h|, \log|(s_h)_{LB} - s_h|, \log|(s_h)_{pre} - s_h|$, and $\log|s_H - s_h|$ as a function of $\log H$ to illustrate the convergence results for both optimal and non-optimal scaling parameter κ. We note a large improvement in convergence rates for the optimal κ^*. For $\kappa = 1$ both bounds, $(s_h)_{LB}$, $(s_h)_{UB}$, converge to s_h as $H^{0.65}$ while $(s_h)_{pre}$, s_H converge to s_h as $H^{1.85}$ and $H^{1.56}$, respectively. When we optimize κ not only the bounds are more accurate but the convergence rate of $(s_h)^*_{LB}$, $(s_h)^*_{UB}$ increases to $O(H^{1.5})$.

From the reconstructed solution $\hat{\mathcal{U}}_h^+$ and $\hat{\mathcal{U}}_h^-$ for the optimal κ^* presented in Figure 8-13 and 8-14 (zoom in near the corner) we clearly see the deformation of the element at the point of interest. We observe how the elements is flipped down and up for the lower bound result and the upper bound result, respectively. This effect is directly related to the output functional ℓ^O which acts as a Neumann source at the corner. In fact, the lower bound output is essentially a sink, pulling down the values of $\hat{\mathcal{U}}_h^+$ and the upper bounds output is a source, pushing up the values of $\hat{\mathcal{U}}_h^-$.

8.3 Poisson Equation in Two Space Dimensions with Higher Order Spatial Discretization

The Poisson equation on a square domain with homogeneous Dirichlet boundary conditions and a forcing term equal to unity is considered here. For this problem our finite element space is enriched to pursue second order interpolants, that is we use $\mathbf{P}_2$ triangular elements. This configuration has a slight singularity at the corner; the boundary condition impose the

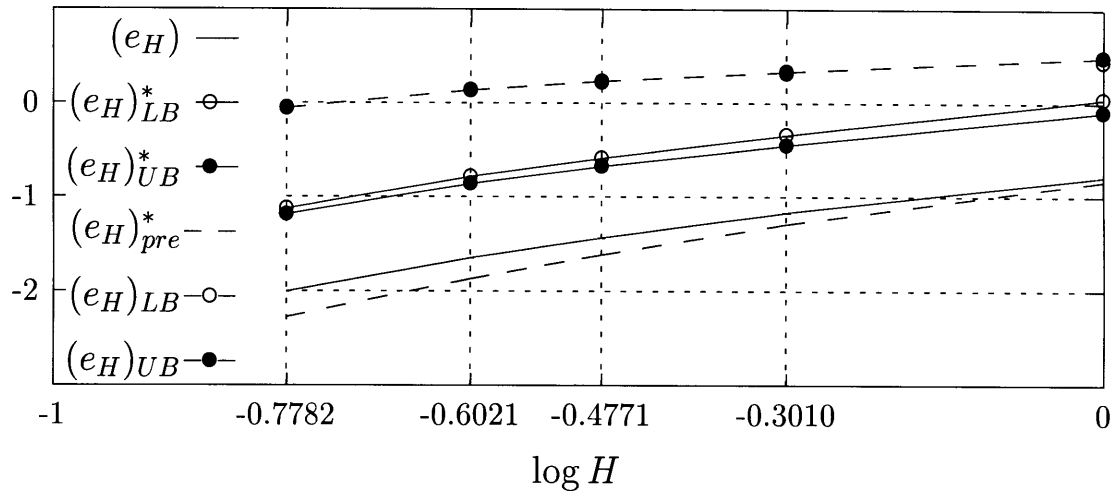

Figure 8-12: Plots of $e_{UB} = \log|(s_h)_{UB} - s_h|$, $e_{LB} = \log|(s_h)_{LB} - s_h|$ (error for non optimal bounds) , $e^*_{UB} = \log|(s_h)^*_{UB} - s_h|$, $e^*_{LB} = \log|(s_h)^*_{LB} - s_h|$ (error for optimal bounds) , $e^*_{pre} = \log|(s_h)^*_{pre} - s_h|$, and $e_H = \log|s_H - s_h|$ as a function of $\log H$ for the corner value output, $s^{(6)}$.

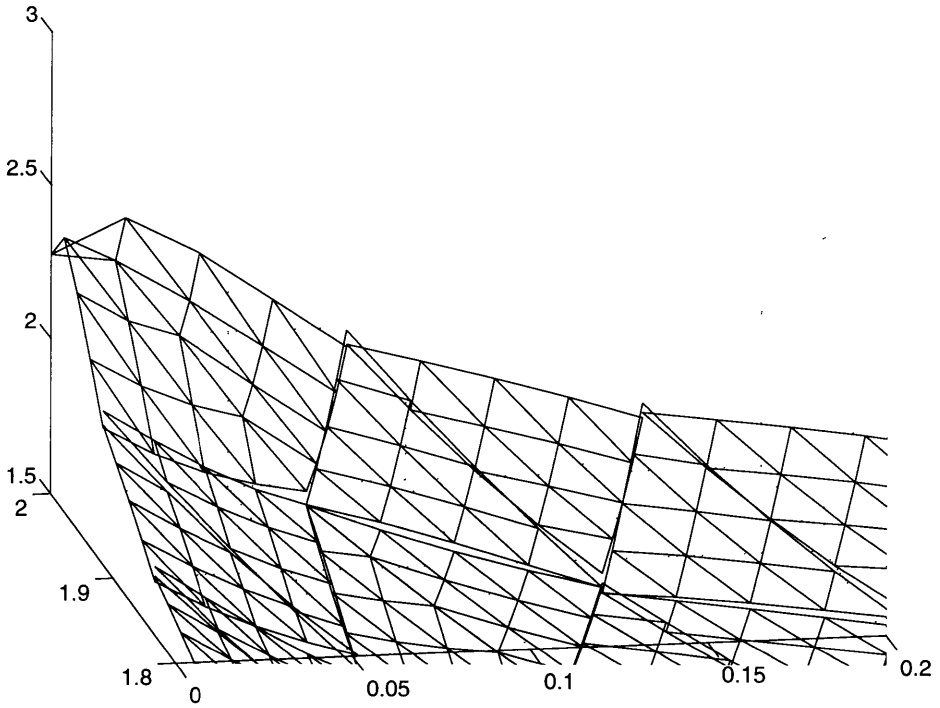

Figure 8-13: Plot of $\hat{\mathcal{U}}^+_h$ for $\mathcal{T}_H = \mathcal{T}_{(H_o,3)}$ for the corner value output, $s^{(6)}$.

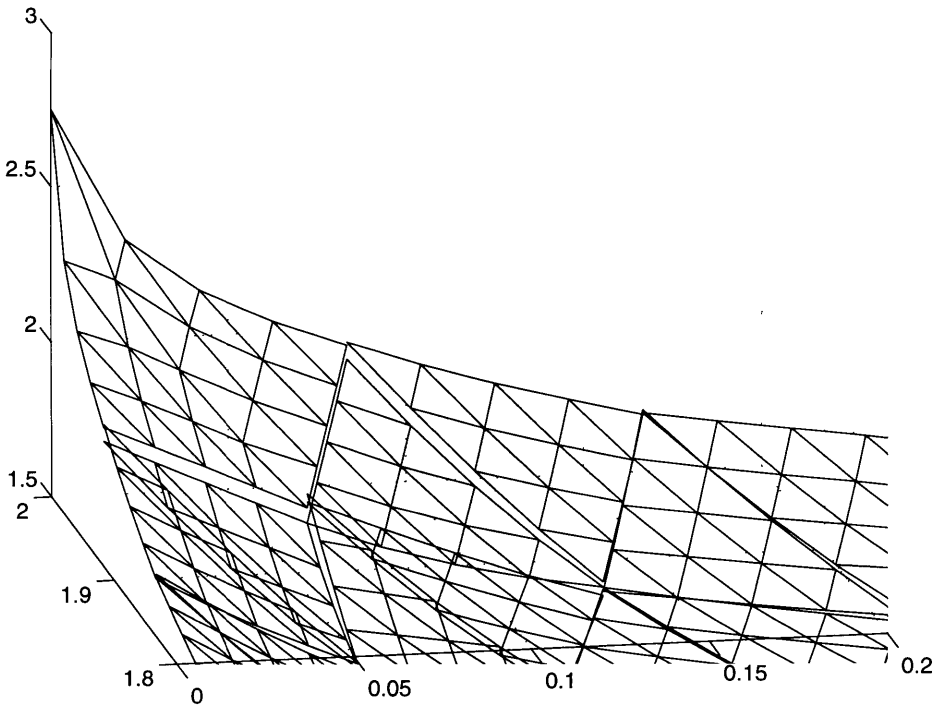

Figure 8-14: Plot of $\hat{\mathcal{U}}_h^-$ for $\mathcal{T}_H = \mathcal{T}_{(H_o,3)}$ for the corner value output, $s^{(6)}$.

Laplacian to be zero but the forcing term imposes the Lagrangian to be equal to one.

The triangulations investigated, $\mathcal{T}_{(H_o,R)}$, are uniform refinements of the coarsest mesh $\mathcal{T}_{(H_o,1)}$. The H–meshes, $\mathcal{T}_H$, correspond to $\mathcal{T}_{(H_o,R)}$, $R = 1, 2, 4$ and the truth h–mesh corresponds to $\mathcal{T}_h = \mathcal{T}_{(H_o,8)}$; $\mathcal{T}_h$. Note that, the triangulation is structured and that for different refinement values of R, we satisfy $X_H \subset X_h$ as required by the theory. As before, we shall denote the effective working–approximation element size associated with triangulation $\mathcal{T}_H = \mathcal{T}_{(H_o,R)}$ as $H \equiv 1/R$.

We investigate here two types of higher order hybrid flux formulations presented in Section 6, that is, the nonconforming $\mathbf{P}_0$ initial approximation (strong conforming, approach A) and the gradient based $\mathbf{P}_1$ initial approximation (gradient forced conforming, approach B). Here, we only present the convergence plots in Figure 8-15a and 8-15b, $\log|(s_h)_{UB} - s_h|, \log|(s_h)_{LB} - s_h|, \log|(s_h)_{pre} - s_h|$, and $\log|s_H - s_h|$ as a function of $\log H$ for the solution average over the entire domain calculated with approach A and with approach B, respectively. For the results presented here we do not optimize with respect to output scaling κ^*. Our results are obtained for $\kappa = 1$. Recall, from Section 6.1 that $\mathbf{P}_1$ nonconforming initial approximation does not allow the required orthogonality construction and cannot be implemented.

We consider here the average solution output, $s^{(7)}$ of equation (4.9). We show in Appendix A that this output is a "compliance", $(s_h)_{LB} = s_H$. In Figure 8-15a and 8-15b we see that both $(s_h)_{LB}$ and s_H are superposed as indicated by the theory. In such "variationally

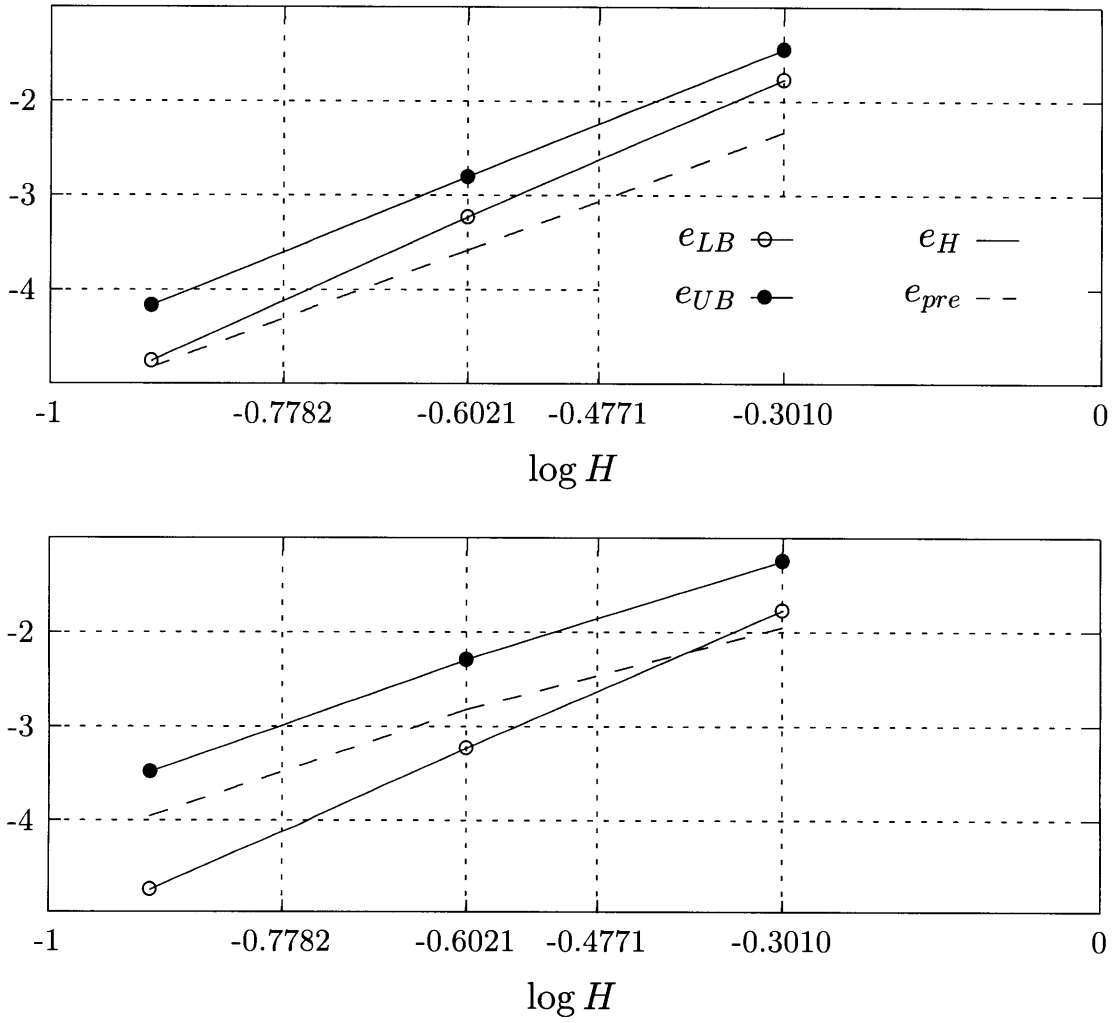

Figure 8-15: Plots of $e_{UB} = \log|(s_h)_{UB} - s_h|$, $e_{LB} = \log|(s_h)_{LB} - s_h|$, $e_{pre} = \log|(s_h)_{pre} - s_h|$, and $e_H = \log|s_H - s_h|$ as a function of $\log H$ for (a, top) the $\mathbf{P}_0$ initial approximation, and (b, bottom) the $\mathbf{P}_1$ initial approximation.

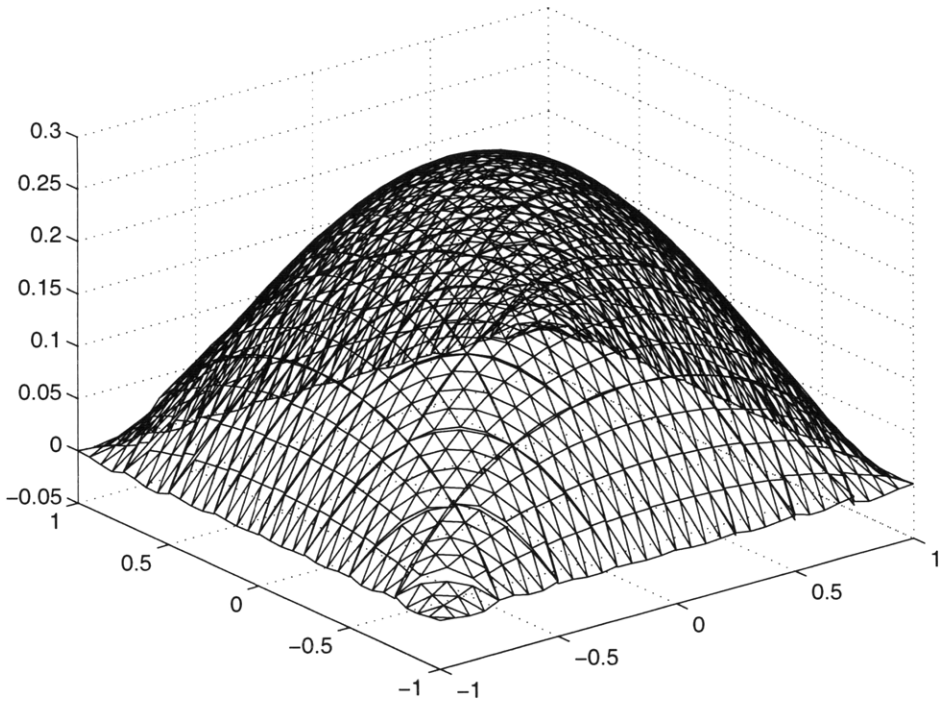

Figure 8-16: Plot of $\hat{\mathcal{U}}_h^-$ for $\mathcal{T}_H = \mathcal{T}_{(H_o,2)}$ for $\mathbf{P}_0$ initial approximation.

(very) special" circumstances — a symmetric problem and energy output — our new bound procedure is less compelling: the only advantage is that upper bounds for the output may be readily obtained (without recourse to complementary energy principles). Unfortunately, or fortunately, most problems and outputs are less accommodating than the compliance.

Three observation can be drawn from the upper bounds analysis of the convergence. First, we note that in both approaches $(s_h)_{UB}$ convergences to s_h slower that $(s_h)_{LB}$ which converges to s_h as $O(H^{3.7})$. For smooth data the convergence rate should be $O(H^4)$ but the singularity reduces slightly. The convergence rates for the upper bounds are $O(H^{3.4})$ and $O(H^{2.7})$ for approach A and for approach B, respectively. Second, the convergence rate of $(s_h)_{UB}$ for approach A is higher than for approach B. We would expect the opposite because approach B is based on a higher order initial approximation for the hybrid flux. Third, we observe that even for the coarsest mesh the upper bound $(s_h)_{UB}$ is more accurate in approach A than in approach B. These results are not yet well understood and require future work.

The reconstructed solution $\hat{\mathcal{U}}_h^+$ are presented for both cases in Figure 8-16 and 8-17 for the working mesh $\mathcal{T}_H = \mathcal{T}_{(H_o,3)}$. We observe that the small discontinuities in $\hat{\mathcal{U}}_h^+$ across subdomains boundaries are indistinguishable to the naked eye.

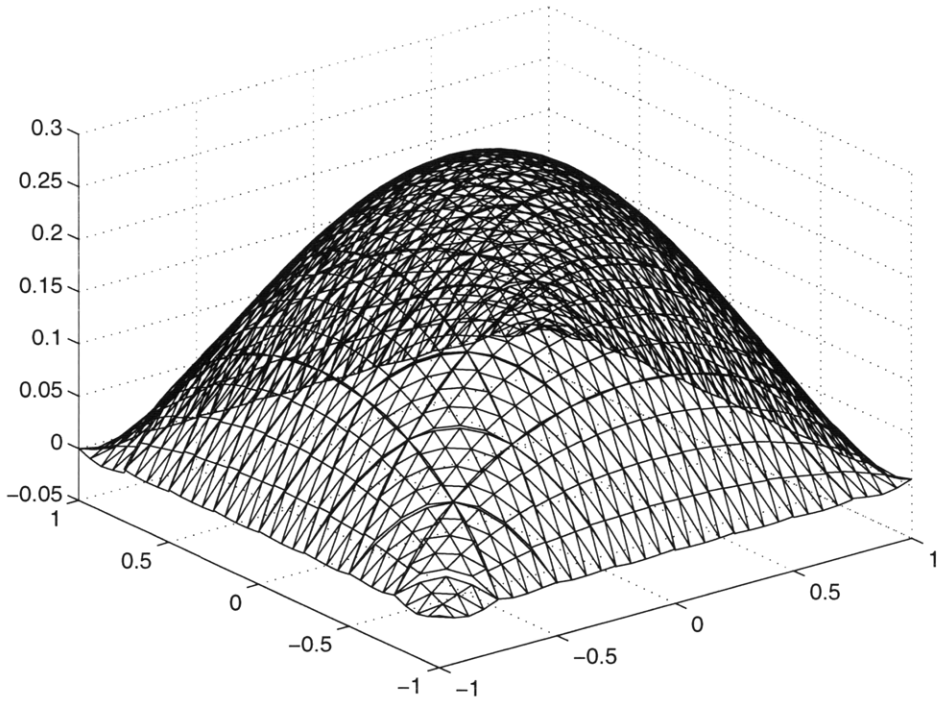

Figure 8-17: Plot of $\hat{\mathcal{U}}_h^-$ for $\mathcal{T}_H = \mathcal{T}_{(H_o,2)}$ for $\mathbf{P}_1$ initial approximation.

8.4 Stokes Problem

We present results for the Stokes problem for a periodic domain (Figure 5-1) where the flow is driven by a pressure gradient. For this model problem the pressure gradient divided by viscosity equals to 1. A velocity field solution of this problem is shown in Figure 8-18. The triangulation investigated, $\mathcal{T}_{(H_o,R)}$, are uniform refinements of the coarsest mesh $\mathcal{T}_{(H_o,1)}$ shown in Figure 8-19a. The H–meshes, $\mathcal{T}_H$, correspond to $\mathcal{T}_{(H_o,R)}$, $R = 1, 2, 3, 4, 6$ and the truth h–mesh corresponds to $\mathcal{T}_h = \mathcal{T}_{(H_o,12)}$; $\mathcal{T}_h$ is shown in Figure 8-19b. Note that, for different refinement values of R, we satisfy $X_H \subset X_h$ as required by the theory. We shall denote the effective working–approximation element size associated with triangulation $\mathcal{T}_H = \mathcal{T}_{(H_o,R)}$ as $H \equiv 1/R$.

Three outputs are investigated as defined generically in (5.10): the flowrate, $s^{(8)}$, the lift force on the body, $s^{(9)}$, calculated with an incompressible test function $\mathcal{X}^a$ and the lift force, $s^{(9)}$, calculated with a test function $\mathcal{X}^b$ defined as:

$$\begin{aligned} \mathcal{X}_1^b &= 0, \quad \text{in} \quad \Omega \setminus \Omega', \\ \mathcal{X}_2^b &= 0, \quad \text{in} \quad \Omega \setminus \Omega', \\ \mathcal{X}_1^b &= 0, \quad \text{on} \quad \Gamma_i,\ i = \{1, 2, 3, 4, 5\}, \end{aligned} \tag{8.1}$$

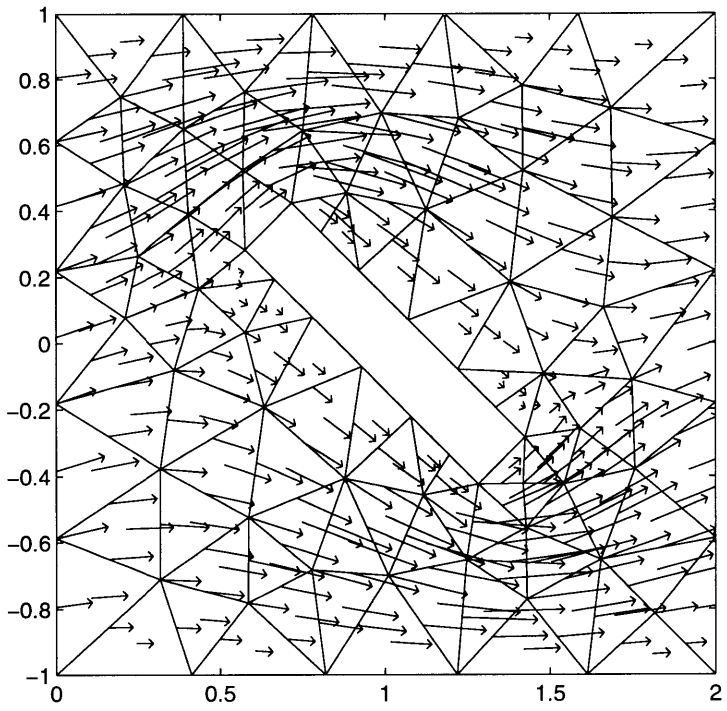

Figure 8-18: Velocity field solution for $\mathcal{T}_H = \mathcal{T}_{(H_o,1)}$.

$$\mathcal{X}_2^b = 0, \quad \text{on} \quad \Gamma_i, \; i = \{1,2,3,4\},$$
$$\mathcal{X}_2^b = 1, \quad \text{on} \quad \Gamma_5,$$

where Ω' contains all the elements of $\mathcal{T}_{(H_o,1)}$ that have an edge on Γ_5. Both choices of $\mathcal{X}$ are valid choices to obtain the lift, however their cost and effect on the bound calculations is very different. The incompressible $\mathcal{X}^a$ is calculated on the H–mesh and necessitates additional local solves to project on the h–mesh, while for $\mathcal{X}^b$, we just use the definition (8.1). Furthermore, the former forces the $\ell^{Op}()$ term to vanish in the output functional and therefore the output is only a function of the velocity components. The latter, $\mathcal{X}^b$, does indeed have a pressure contribution to the output which needs an equilibration when solving for the adjoint on the h–mesh (5.68)-(5.69). Note also that for both choices ($\mathcal{X}^a$, $\mathcal{X}^b$) the condition (5.15) is satisfied because the inhomogeneous Dirichlet boundary conditions integrate to zero.

The objective to calculate bounds is to evaluate the output associated with $\mathcal{T}_{(H_o,12)}$ by calculating rigorous bounds of that output s_h. To this end, different H–mesh can be exploited. It is obvious that the cost of the bound calculations increase as a finer H–mesh is used, that is as R increases for $\mathcal{T}_{(H_o,R)}$. This also leads to sharper bounds because the adjoint and the hybrid flux are more accurately approximated.

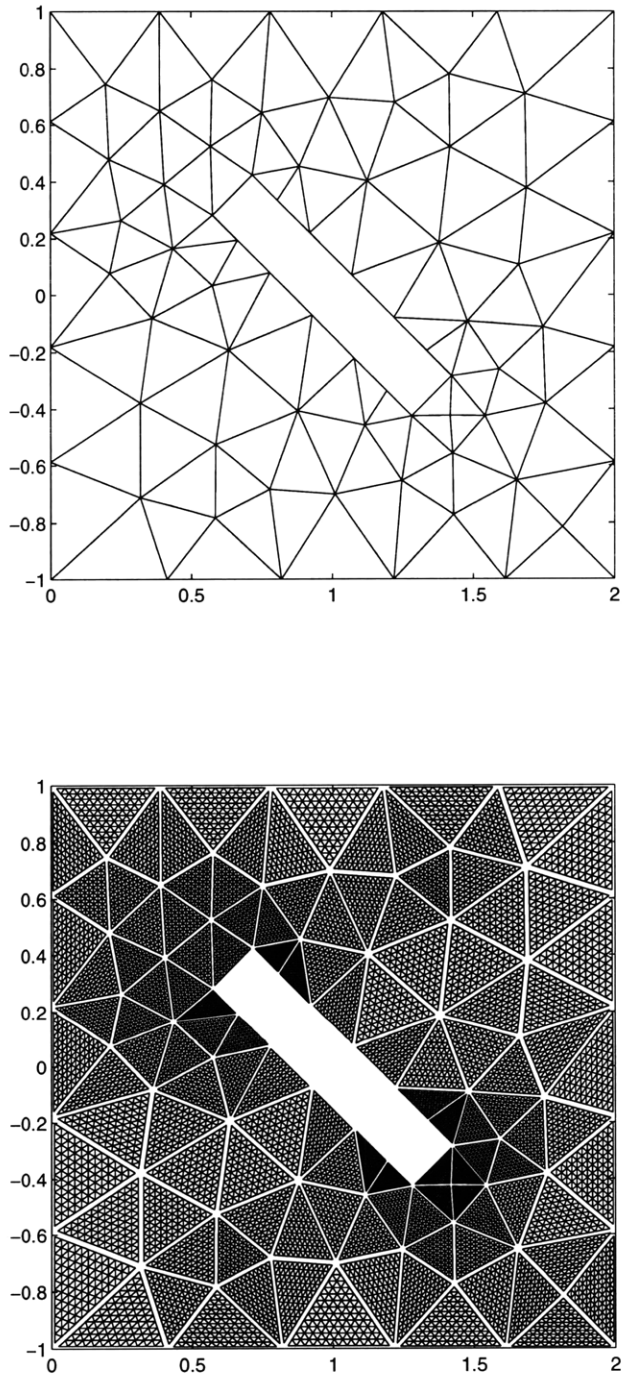

Figure 8-19: (a) Coarsest working mesh $\mathcal{T}_H = \mathcal{T}_{(H_o,1)}$, and (b) truth mesh $\mathcal{T}_H = \mathcal{T}_{(H_o,12)}$.

We plot in Figure 8-20a, 8-20b, and 8-20c, $(s_h)^*_{UB}/s_h$, $(s_h)^*_{pre}/s_h$, $(s_h)^*_{LB}/s_h$, and s^*_H/s_h as a function of (effective) H for, respectively, $s^{(8)}$ (flowrate), $s^{(9)}$ (lift force) for both choices of $\mathcal{X}$. For the coarsest mesh, we observe that the upper bounds for all outputs are within +15%. The accuracy of the lower bounds depend on the output considered. For the lift output, $s^{(8)}$, the lower bounds are within -5% and almost equal to the s_H; in fact in this case we have a "weak" compliance. For $s^{(9)}$, the lower bounds are -20% from s_h. We also observe, for a refinement of two, these bounds are well within $\pm 10\%$. Recall that one of main advantages of the bounds is the certainty that s_h lies within their values. In practice, the "working" mesh should be picked sufficiently accurate; assuming such an approach we expect very sharp bounds.

In Figure 8-21a, 8-21b, and 8-21c, we plot $e_{UB} = \log|(s_h)^*_{UB} - s_h|$, $e_{LB} = \log|(s_h)^*_{LB} - s_h|$, $e_{pre} = \log|(s_h)^*_{pre} - s_h|$, and $e_H = \log|s_H - s_h|$ as a function of $\log H$ for respectively, $s^{(8)}$, $s^{(9)}$. For $s^{(8)}$, $(s_h)^*_{LB}$ and s_H appear to converge to s_h as $O(H^{1.5})$ as $H \to h$. We would expect, for smooth solution, s_H to converge as $O(H^2)$. The corner singularities is most probably the reason why s_H converges to s_h as $O(H^{1.5})$ and not $O(H^2)$. Note that from our "weak" compliance analysis in Appendix A the hybrid fluxes are zero and therefore rule out any error contribution form that calculation. Compliance also confirms that we should expect and we do obtain the same convergence rates for both the $(s_h)_{LB}$ and s_H.

Now, if we consider the convergence of $(s_h)_{UB}$ we note that it is slightly less, $O(H^{1.3})$ compare to $O(H^{1.5})$ for $(s_h)_{LB}$. We believe that this may be caused by the hybrid flux approximation — maybe the $\mathbf{P}_0$ initial approximation. Considering $s^{(9)}$ the quantities, $(s_h)_{UB}$, $(s_h)_{LB}$ and $(s_h)_{pre}$ converge at the previous lower rate, $O(H^{1.3})$, and s_H converges at the same rate as before, $O(H^{1.5})$. The same comments regarding the convergence rate can also be expressed for the lift output, $s^{(9)}$.

The bounds presented here reflect the use of the scaling parameter κ described in Section 7.2. For the flowrate output $\kappa = 1$ is optimal for all H and for the lift output κ^* tend to 0.0886 as R increases. We also note that the choice of $\mathcal{X}$ does not influence significantly the accuracy and convergence of the bounds. This conclusion indicates that $\mathcal{X}^b$ should always be chosen because it is the least computationally expensive.

It is clear that, if the bounds are tight, the approximations $\hat{\mathcal{U}}^-_{ih}$ must be close to u_{ih}. We show, in Figure 8-22a and 8-22b, $\hat{\mathcal{U}}^-_{1h}$ and $\hat{\mathcal{U}}^-_{2h}$ associated with the flowrate for the working mesh $\mathcal{T}_H = \mathcal{T}_{(H_o,3)}$. (In order to render visualization comparison more transparent, we choose the level of $\hat{\mathcal{U}}^-_{ih}$ in all subdomain T_H so that $\hat{\mathcal{U}}^-_{ih}$ and u_{ih} agree at one vertex of T_H.) We observe that both $\hat{\mathcal{U}}^-_{ih}$ are quite smooth. The lack of small discontinuities in $\hat{\mathcal{U}}^-_{ih}$ across subdomain boundaries is an indication of the accuracy of the hybrid fluxes. Note that, near singularities (corners of Γ_5) the approximation is less accurate. We believe that this behavior contributes significantly to the gap between the upper and lower bounds. However, in practice a different H–mesh, refined in the vicinity of the singularities, would be used.

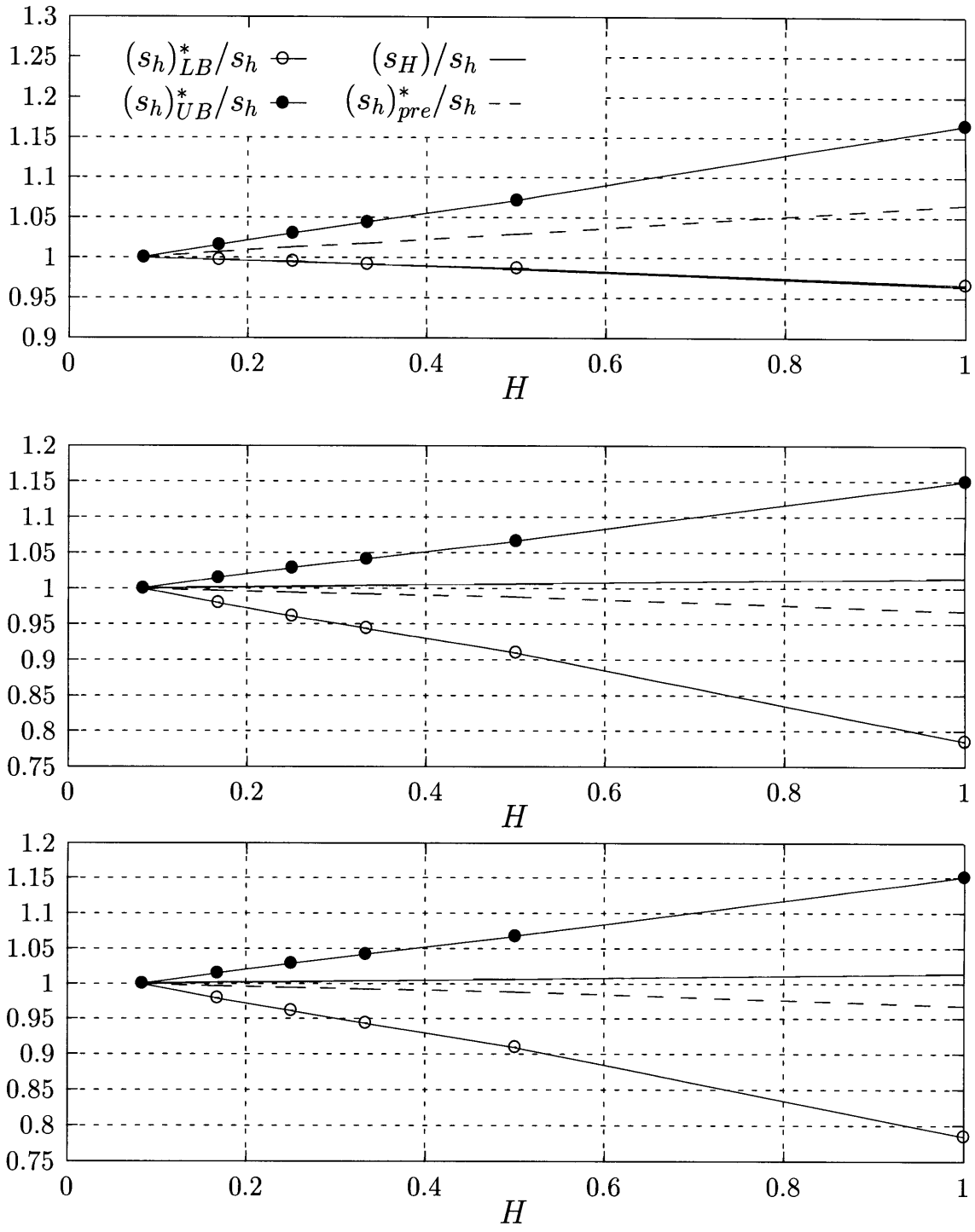

Figure 8-20: Plots of $(s_h)^*_{UB}/s_h$, $(s_h)^*_{pre}/s_h$, $(s_h)^*_{LB}/s_h$, and s_H/s_h as a function of (effective) H for (a, top) $s^{(8)}$, the flow rate, (b, middle) $s^{(9)}$, the lift force calculated using $\mathcal{X}^a$, (c, bottom) $s^{(9)}$, the lift force calculated using $\mathcal{X}^b$.

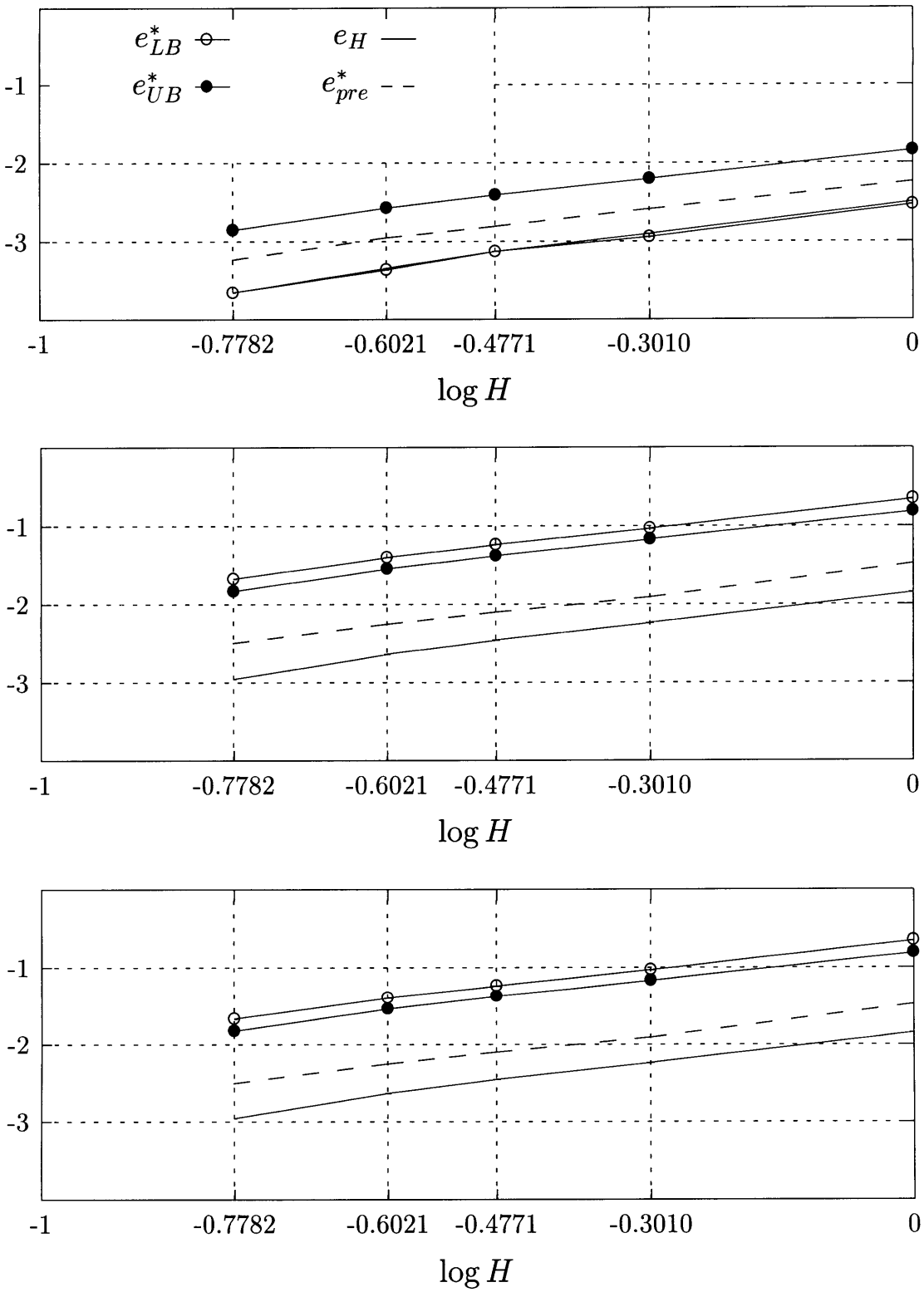

Figure 8-21: Plots of $e^*_{UB} = \log|(s_h)^*_{UB} - s_h|$, $e^*_{LB} = \log|(s_h)^*_{LB} - s_h|$, $e^*_{pre} = \log|(s_h)^*_{pre} - s_h|$, and $e_H = \log|s_H - s_h|$ as a function of $\log H$ for (a, top) $s^{(8)}$ the flowrate, (b, middle) $s^{(9)}$ the lift calculated using $\mathcal{X}^a$, and (c, bottom) $s^{(9)}$ the lift force calculated using $\mathcal{X}^b$.

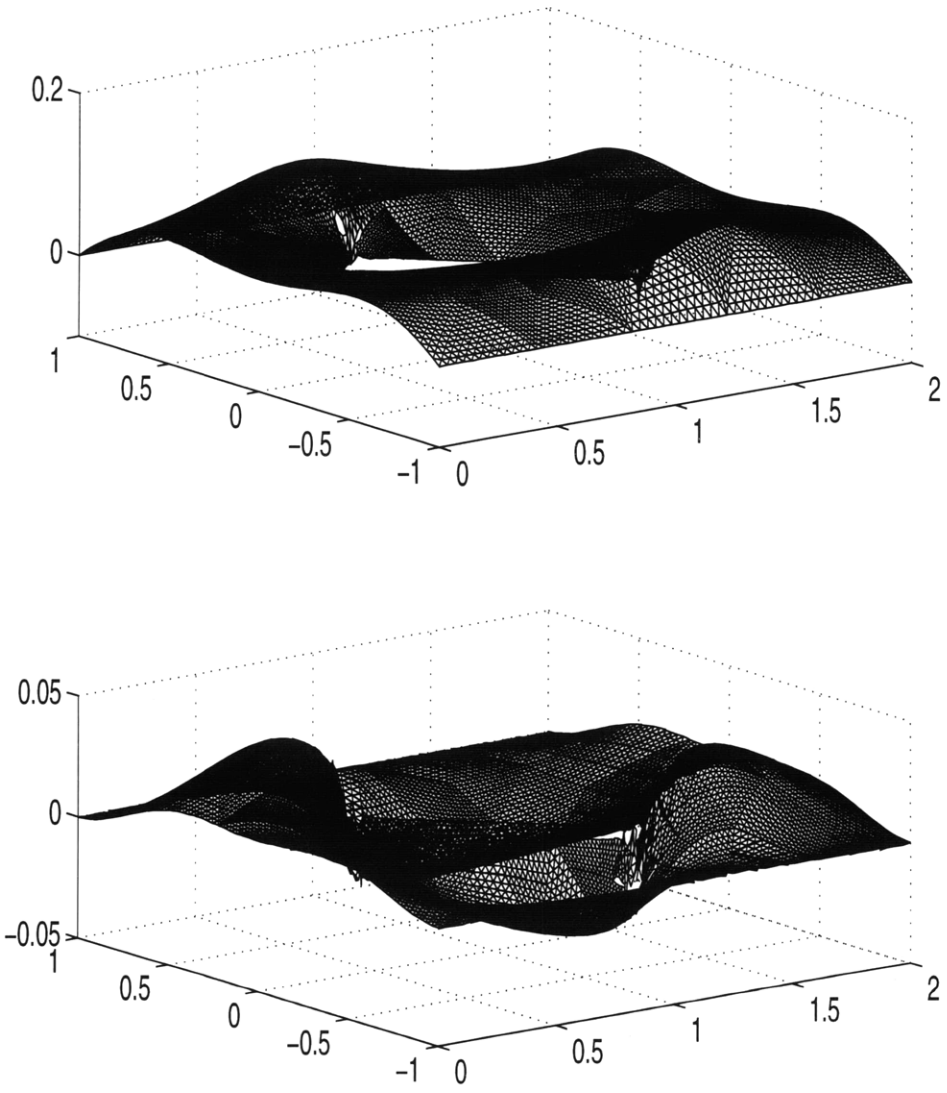

Figure 8-22: Plots for the working mesh $\mathcal{T}_H = \mathcal{T}_{(H_o,3)}$ of (a) $\hat{\mathcal{U}}_{1h}^-$, and (b) $\hat{\mathcal{U}}_{2h}^-$.

Chapter 9

Conclusion

9.1 Summary and Limitations

In this thesis we have presented an inexpensive procedure that calculates bounds to outputs of interest at a fraction of the cost of performing the "truth" mesh calculations. The outputs considered are linear functionals of the field variable which characterized the system under investigation (such as drag, average heat flux and many others).

In engineering design, outputs are introduced in the objective functions used in the optimization framework. Our approach will provide bounds to such outputs as an inexpensive alternative. The bounding procedure gives not only an estimate of the required output but also a certainty of where the "truth" output would actually lie. Recall that by "truth" we refer to a very accurate approximation of the field solution and associated output. The implication of this procedure on the design framework is mainly twofold. First, reduced computation time by allowing the use of a fast but only relatively accurate working mesh. Second, improved reliability, where we obtain for the "working" mesh a "truth" mesh certainty with respect to the output of interest.

This method is based on two key concepts: the construction of an augmented Lagrangian and the use of quadratic–linear duality theory. In essence this Lagrangian is a quadratic "energy" reformulation of the desired output, and the constraints are the finite element equilibrium equations and the intersubdomain continuity requirement. From quadratic–linear duality theory we have shown that our augmented Lagrangian leads to bounds for any chosen candidate Lagrange multipliers. Finally, through domain decomposition and "hybridization" of the intersubdomain condition we obtain decoupled Neumann subdomain calculations of the bounds. Note that this procedure also allows for different discretizations types such as finite difference and finite volumes.

The engineering relevance of the results presented in this thesis should be clear by the choice of outputs we have considered. The problems we have treated are not necessary relevant to the entire engineering community but illustrate some specific issues: nonsym-

metric operators presented in the convection–diffusion equation, incompressibility constraint treated in the Stokes problem. The bounds for the specific outputs considered are rigorous, quantitative and relatively sharp.

For the "working" H–mesh considered, which are in general not so accurate in two space dimensions, we obtain bounds within $\pm 20\%$ for a refinement value of $R = 12$. Note that for such a refinement every element is subdivided into 144 elements. In general, the average of the bounds, $(s_h)_{pre}$, is very close to s_h and may be used as a very accurate estimator of s_h. We also observe that in most cases studied to date, we find that the bounds converge to s_h at least as fast as s_H converges to s_h as $H \to h$. The only exception would be the convergence rate for the outputs of the Stokes problem.

We address now some of the limitation of our bounds procedure. Based on our computational experimentation, we came to the conclusion that bound optimization is essential in many cases. In particular, when the output is localized to a region, a line or a point, bounds without bound optimization are useless.

We also believe that the coarse mesh is of determinative practical importance. The gap of the bounds is in some sense based on how well this "working" mesh resolves some of the "hidden" adjoint features. Recall that the adjoint equation has the output as a forcing term which makes it very difficult to construct an adequate "working" mesh. It is obvious that an ideal procedure would be to have an automatic adaptive mesh that would control both the solution error and the adjoint error.

The hybrid flux calculation is another important parameter that affect the sharpness of the bounds. For higher order spatial discretisation, convergence rates of the bounds should be higher if we would have developing an initial nonconforming $\mathbf{P}_1$ approximation instead of our actual initial approximations discussed in Section 6.2.2. However, it seems impossible [24] to construct such higher order nonconforming approximation to the flux. The difficulty appears in the nodal structure of the underlying elements. The fact is that these nodes lie on an ellipse and that there exists a second–degree polynomial which vanishes at these nodes.

Furthermore, this approach is not suited to analyze the details of field solutions; it has been developed with design as a focus. Recall that our goal is to bound outputs which are linear functions of field solutions. Though, even if we obtain a reconstructed field solution, the bounds on the output are the only values we can depend on. The reconstructed field solution is more for illustrative purposes.

Many other limitations to fully utilize our technique in a design framework exist at this point in time; nevertheless these limitations will soon be addressed and therefore are discussed as future work.

9.2 Future Work

To fully exploit all the reach of this approach much work remains to be done. We briefly itemize here some of the targets that could be tackled.

On extensions to different problems: For time–dependent problems initial work has already been performed. The framework has been developed for ODEs and is now being expanded to PDEs [45]. Similarly, initial results for a nonlinear case for ODEs is already available but full treatment of the nonlinear terms still remains to be developed. In [39], a non linear conduction problem in $\mathbf{R}^1$ is presented for the flux, pointvalue and the average values outputs. A most critical issue is the extension to noncoercive operators, even for linear operators. We remind the reader that stability terms in the Lagrangian are important and allows us to bound from below the value of the Lagrangian at the saddlepoint even for candidate Lagrange multipliers which are not exact. Thus, the "energy" equality, in particular the quadratic term in this equality, is essential for stability.

On extensions within the finite element method: The results presented here are obtained for subparametric elements and exact integrations (computed analytically). Extension to treat isoparametric elements and quadratures is required to address more accurately curved geometries. Analysis these variational "crimes" should also be developed.

On extensions to different numerical formulation: Our Lagrangian formulation permits us to treat much more general discretizations, not only the finite element method. We recall from Chapter 3, that the discretized form is applicable to other finite discretization. A mix between methods is also possible. For example, having a stabilized Galerkin method for the H–mesh to improve stability of the solution and a standard method for solving the h–mesh subdomain problems. However, we do not claim that this extension is trivial, in particular concerning boundary conditions and hybrid flux approximations in two space dimensions.

On extensions to adaptive error control: The bounds procedure gives no information regarding the contribution of each element to the error. An interesting research direction would be the development of a method that would, for a given number of elements, control the errors of the elements distribution in such a way that the output of interest is more accurate. Adaptivity for the adjoint problem is also an important issue as previously discussed. The goal is to reduce the gap between the bounds by a better approximation of the adjoint on the H–mesh.

On parallel implementation: Our approach decouples directly the matrix system into subdomains; parallelization is therefore straightforward. Note also that the hybrid flux calculation, even if not very resource intensive, may be directly solved in parallel. In addition, these problems are fully independent, not just decoupled spatially, but allow concurrent processing. The only additional work required to parallelize the entire procedure is to parallelize the initial H–mesh problem and the adjoint problem. Parallelization of these

two solution strategies can be performed using existing parallelization algorithms.

On extension to larger classes of output functionals: We have considered in this thesis bounded and unbounded linear–functionals of the field variables as output. We can easily extend our approach to convex functionals of the field variables. However, many other types of outputs exist.

On extension to three space dimension: The critical ingredient should be to generate the hybrid flux in this higher dimension. Recall that going from one space to two space dimensions introduces additional complexity in the hybrid flux calculations such as the equilibrium procedure required for each node. This remains to be done in three–dimensions where we have not only elements connecting at each node but also on line segments.

On the theoretical extension: For all the results presented we have drawn the convergence plots. There exist ways to estimate *a priori* the convergence rates of the bounds. The development of such procedure adds certainty because the designer could exploit the convergence rate information and select a design mesh that yields the desired bounds accuracy.

Bibliography

[1] R.A. Adams, *Sobolev Spaces*, Academic Press, New York, 1975.

[2] D.N. Arnold, F. Brezzi, and M. Fortin, *A stable finite element for the Stokes Equations*, Calcolo, 21(1984), pp. 337-344.

[3] M. Ainsworth and J.T. Oden, *A unified approach to a posteriori error estimation using element residual methods*, Numer. Math., **65** (1993), pp. 23–50.

[4] M. Ainsworth and J.T. Oden, *A posteriori error estimates for Stokes' and Oseen's equations*, SIAM J. Numer. Anal., To Appear.

[5] M. Ainsworth and J.T. Oden, *A posteriorierror estimation in finite element analysis*, TICAM Report 96–19, 1996.

[6] M. Alexandrov and J.E Dennis, Jr., R.M. Lewis, and V. Torczon, *A trust region framework for managing the use of approximation models in optimization*, in preparation.

[7] G. Anagnoustou, Y. Maday, C. Mavriplis, and A.T. Patera, *On the mortar element method: generalizations and implementation*, in Proc, 3^{rd} INt. Symp. Domain Decomposition Methods for Partial Differential Equations, SIAM, Philadelphia, 1990, pp. 157–173.

[8] M. Azaiez, C. Bernardi, and Y. Maday, *Some tools for adaptivity in the spectral element method*, Publication du Laboratoire d'Analyse Numérique R 95037, Université Pierre et Marie Curie, Paris, 1996.

[9] I. Babuška, *The finite element method with Lagrangian multipliers*, Numer. Math. 20 (1973), pp. 179–192.

[10] I. Babuška and W.C. Rheinboldt, *A posteriori error estimates for the finite element method*, Int. J. Numeri. Methods Engrg., **12** (1978), pp. 1597–1615.

[11] I. Babuška, T. Strooubolis, C.S. Upadhyay and S.K. Gangaraj, *A posteriori and adaptive control of the pollution error in the h–version of the finite element method*, Int. J. Numer. Methods Engrg. 38 (1995), pp. 4207–4235.

[12] R.E. Bank, *Analysis of a local a posteriori error estimate for elliptic equations*, in Accuracy Estimates and Adaptive Refinements in Finite Element Computations (eds: I. Babuška, O.C. Zienkiewics, J. Gago, E.R. de A. Oliveira), John Wiley, New York, 1986, pp. 119–128.

[13] R.E. Bank and A. Weiser, *Some a posteriori error estimators for elliptic partial differential equations*, Math. Comp., **44**:170(1985), pp. 283–301.

[14] R.E. Bank and B.D. Welfert, *A Posteriori error estimates for the Stokes problem: a comparison* Math. Comput. 82 (1990), pp. 323–340.

[15] R.E. Bank and B.D. Welfert, *A posteriori error estimates for the Stokes problem*, SIAM J. Numer. Anal., **28** (1991), pp. 591–623.

[16] R. Becker and R. Rannacher, *Weighted a posteriori error control in finite element methods*, IWR Preprint 96–1 (SFB 359), Heidelberg, 1996.

[17] R. Becker and R. Rannacher, *A feedback approach to error control in finite element methods: basic analysis and examples*, IWR Preprint 96–52 (SFB 359), Heidelberg, 1996.

[18] C. Bernardi, Y. Maday, and A.T. Patera, *A new nonconforming approach to domain decomposition: the mortar element method*, College de France Seminar **XI** (eds: H. Brezis and J.-L. Lions), Pitman, 1994.

[19] F. Brezzi and M. Fortin, *Mixed and Hybrid Finite Element Methods*, Springer–Verlag, New York, 1991.

[20] M. Crouzeix and P.-A. Raviart, *Conforming and non–conforming finite elements methods for solving the stationary Stokes equation*, RAIRO Anal. Numer. 7:33–76, 1973.

[21] M.E. Cruz, *A Parallel Monte–Carlo Partial–Differential–Equation Procedure for the Analysis of Multicomponent Random Media*, Ph.D. Thesis, Department of Mechanical Engineering, M.I.T., 1993.

[22] K. Eriksson and C. Johnson, *An adaptive finite element method for linear elliptic problems*, Math. Comput. 50 (1988), pp. 361–383.

[23] P.F. Fischer and A.T. Patera, *Parallel simulation of viscous incompressible flows*, Annu. Rev. Fluid Mech. 26 (1994), pp. 483–527.

[24] M. Fortin and M. Soulie, *A non–conforming piecewise quadratic finite element on triangles*, Int. J. Numer. Methods Engrg., **19** (1983), pp. 505–520.

[25] V. Girault and P.-A. Raviart, *Finite Element Methods for the Navier–Stokes Equations: Theory and Algorithms*, Apringer–Verlag, Berlin.

[26] C.K. Ghaddar, *Parallel Analytico–Computational Methods for Multicomponents Media: Application to Thermal Composites and Porous-Media Flows*, Ph.D. Thesis, Department of Mechanical Engineering, M.I.T., 1995.

[27] R. Glowinski and P. Le Tallec, *Augmented Lagrangian and Operators–Splitting Methods in Nonlinear Mechanics*, SIAM, Philadelphia, 1989.

[28] P. Grisvard, *Elliptic Problems in Nonsmooth Domains*, Pitman Publication, Boston, 1985.

[29] M. E. Kambourides, S. Yeşilyurt, and A. T. Patera, *Nonparametric–validated computer–simulation surrogates: A Pareto formulation*, Int. J. Numeri. Methods Engrg., to appear.

[30] N. Kikuchi, *Finite element Methods in Mechanics*, Cambrige University Press, Cambridge, 1986.

[31] P. Ladeveze and D. Leguillon, *Error estimation procedures in the finite element method and applications*, SIAM J. Numer. Anal., **20** (1983), pp. 485–509.

[32] P. Ladeveze, P. Marin, J.P. Pelle, and Gastine, *Accuracy and optimal meshes in finite element computation for nearly incompressible materials*, Comp. Meth. Appl. Mech Engrg, **94**:3 (1992), pp. 303–315.

[33] M.V.S. Martins, *Schwarz Preconditioners for Elliptic Problems with Discontinuous Coefficients Using Conforming and Non–Conforming Elements*, Ph.D. Thesis, Department of Mathematics, New York University, 1994.

[34] J. Nečas, *Les Méthodes Directes en Théorie des Equations Elliptiques.* Academia, Prague, 1967.

[35] M. Paraschivoiu, and A. T. Patera, *A hierarchical duality approach to bounds for the outputs of Partial Differential Equations*, Comp. Methods Appl. Mech. Engrg., to appear.

[36] M. Paraschivoiu, J. Peraire, and A. T. Patera, *A posteriori finite element bounds for linear–functional outputs of elliptic Partial Differential Equations*, Comp. Methods Appl. Mech. Engrg., to appear.

[37] M. Paraschivoiu and A.T. Patera *A posteriori finite element bounds for linear–functional outputs of the Stokes problem*, in preparation.

[38] A.T. Patera and E.M Ronquist, *Introduction to Finite Element Methods: Application to Incompressible Fluid Flow and Heat Transfer*, Lecture Notes from course 2.274 held at the Massachusetts Institute of Technology.

[39] A.T. Patera, M. Paraschivoiu, J. Peraire, and Y. Maday, *Fast bounds for Partial Differential Equation outputs*, in preparation.

[40] M. Pedercini, *A Posteriori Variational–Bound Finite–Element Methods for Three–Dimensional Low–Reynolds–Number Porous Media and Sedimentation Flows*, S.M. Thesis, Department of Mechanical Engineering, M.I.T., 1995.

[41] R.Rannacher and F.-T. Suttmeier, *A feedback approach to error control in finite element methods: application to linear elasticity*, IWR Preprint 96–42 (SFB 359), Heidelberg, 1996.

[42] J.E. Roberts and J.-M. Thomas, *Mixed and hybrid methods*, in: P.G. Ciarlet and J.L. Lions, eds., Handbook of Numerical Analysis, Volume II: Finite Element Methods (Part 1) (North–Holland, Amsterdam, 1991).

[43] G. Strang and G.J. Fix, *An Analysis of the Finite Element Method*, Prentice–Hall, Englewood Cliffs, New Jersey, 1973.

[44] G. Strang, *Introduction to Applied Mathematics*, Wellesley–Cambridge Press, Wellesley, Massachusetts, 1986.

[45] J. Teichman, S.M. Thesis, Department of Mechanical Engineering, M.I.T., in progess.

[46] H. Vailong, *A Posteriori Bounds for Linear–Functional Outputs of Hyperbolic Partial Differential Equations*, S.M. Thesis, Department of Aeronautics and Astronautics, M.I.T., 1997.

[47] R. Verfürth, *A posteriori error estimation and adaptive mesh–refinement techniques*, J. Comp. Appl. Math., **50** (1994), pp. 67–83.

[48] R. Verfürth, *A posteriori error estimators for the Stokes equations*, Numer. Math., **55** (1989), pp. 309–325.

[49] S. Yeşilyurt and A.T. Patera, *Surrogates for numerical simulations; optimization of eddy–promoters heat exchangers*, Comput. Methods Appl. Mech. Engrg 121 (1995), pp. 231–257.

Appendix A

Compliance

By compliance we identify the property of our finite element bound technique for which the linear functional output calculated on the H–mesh is equal to the lower bound,

$$(s_h)_{LB} = \eta^+ = s_H. \tag{A.1}$$

This property is not general — otherwise we would no need to calculate the lower bound — it only exist in some specific situation. In particular, compliance exists when the following conditions are united:

- the inhomogeneity of the weak from equals the output functional, $\ell^N(v) = \ell^0(v)$,
- boundary conditions are homogeneous Dirichlet,
- the operator of the problem considered is symmetric.

To be more precise we will consider the Poisson problem — convection–diffusion of Section 4.1 with $U = 0$. The variational form is: Find $u_H \in X_H$ such that,

$$a^s(v, u_H) = \ell^N(v), \quad \forall v \in X_H. \tag{A.2}$$

The output of interest becomes,

$$s = \ell^O(u_H), \tag{A.3}$$

and from (4.53) the output can also be written as,

$$s_H = -a^s(u_H, u_H) + c_U - \ell^N(u_H) + \ell^D(u_H). \tag{A.4}$$

Now, we examine the lower bound, $(+)$ superscript. We first analyze the adjoint equation (4.31), and rewrite it for the lower bound,

$$a^s(\psi_H^+, w) = -(2a^s(w, u_H) - \ell^N(w) + \ell^O(w)), \quad \forall w \in X_H. \tag{A.5}$$

We observe, that for $\ell^N(w) = \ell^O(w)$, $\forall w \in X_H$, that (A.5) reduces to

$$a^s(\psi_H^+, w) = -2a^s(w, u_H), \qquad \forall w \in X_H. \tag{A.6}$$

It follows that the resulting adjoint, ψ_H^+, is then precisely twice the negative of the solution, u_H,

$$\psi_H^+ = -2u_H. \tag{A.7}$$

The boundary condition for the adjoint ψ_H^+ have to be consistent with the solution u_H boundary condition; therefore, only homogeneous Dirichlet boundary conditions can exist.

We now examine the hybrid flux calculation. The term $B^+(v, u_H)$, given in (4.36), equals zero. Therefore, the equilibrium equation is directly satisfied, the hybrid flux is zero and no hybrid flux calculations are required.

Using the above candidates in the Lagrange multipliers, we now solve the h–mesh problem (4.39) for $\hat{\mathcal{U}}_h^+$ which becomes,

$$2a^s(w, \hat{\mathcal{U}}_h^+) = 2a^s(w, u_H). \tag{A.8}$$

It is clear that our h–mesh solution is nothing else that the "energy" norm projection of our H–mesh solution. We then conclude that our lower bound is the same as s_H,

$$\eta^+ = -a^s(u_H, u_H) + c_U - \ell^N(u_H) + \ell^D(u_H) = s_H. \tag{A.9}$$

Results for our outputs $s^{(7)}$ and $s^{(8)}$ illustrate this property for the Poisson problem and the Stokes problem, respectively. Compliance for the Stokes problem is not as exact as in the Poisson problem. The equalities are only approximate. Nevertheless, the ideas are similar to that of the Poisson problem but have to be applied to each component of velocity. Therefore, both velocity components need to satisfy the three condition necessary for compliance. In our model problem, the momentum equation in the x direction, has a forcing term of one and the output is the average solution. For the y direction momentum equation, there is no forcing nor is there any velocity in this direction included in the output functional. In both cases we have homogeneous Dirichlet boundary conditions on Γ_1, Γ_3, and Γ_5 for each component of velocity and periodic boundaries on Γ_2 and Γ_4. Note that the periodic boundaries are also consistent with (A.7). The proof of compliance for the Stokes problem differs, it is not rigorous due to the adjoint projection from the H–mesh to the h–mesh, (5.68)-(5.69). It also differs by the treatment of the divergence operator which remains part of the equations and only vanishes at the end. At the beginning, we obtain,

$$\begin{aligned} a^s(\psi_{iH}^+, w_i) - d_i(w_i, \Lambda_H^+) &= -2a^s(w_i, u_{iH}), \qquad \forall (w_1, w_2) \in (X_H)^2, \\ -d_i(\psi_{iH}^+, q) &= -(\ell_i^{Op}(q)) \qquad \forall q \in Y_H. \end{aligned} \tag{A.10}$$

and based on the same arguments as earlier — zero hybrid flux for both component of velocity — we arrive at,

$$\begin{aligned} 2a(w_i, \hat{\mathcal{U}}_{ih}^{+}) - d_i(w_i, \bar{\tau}_h^{+}) &\approx 2a^s(w_i, u_{iH}) - d_i(w_i, \Lambda_H^{+}), \qquad \forall (w_1, w_2) \in (V_h)^2, \\ -d_{i\,T_H}(\hat{\mathcal{U}}_{ih}^{\pm}, q) &\approx 0 \quad \forall q \in M_h. \end{aligned} \tag{A.11}$$

We conclude that $\hat{\mathcal{U}}_{ih}^{+}$ is the energy projection of u_{iH} on the h–mesh which yields the desired compliance result.

Appendix B

Variable Velocity

We now extend the formulation of the convection–diffusion problem to include a variable velocity field, $U(x)$. We consider the convection–diffusion equation (4.1)-(4.3) where the velocity field $U(x)$ is assumed to have the properties:

- Incompressible field
$$\frac{\partial U_i}{\partial x_i} = 0. \tag{B.1}$$
- No flow through $\partial\Omega$,
$$U_i \cdot \hat{n}_j = 0 \quad \text{on} \quad \partial\Omega. \tag{B.2}$$

In such a context, we consider a generic square domain Ω problem with four sides denoted by Γ_j, $j = 1, ..., 4$ having both Dirichlet and Neumann boundary conditions. Assuming we are given a velocity field (U_1^E, U_2^E) either from another simulation or as an explicit function, we require to solve the incompressible projection on our H–mesh. The projected field (U_1, U_2) is obtained by solving,

$$\begin{aligned} a^s(U_i - U_i^E, v_i) - d_i(v_i, \tilde{p}) &= 0, \quad \forall v_1, v_2 \in (X_H)^2, & \text{(B.3)} \\ -d_i(v_i, q) &= 0, \quad \forall q \in Y_H & \text{(B.4)} \end{aligned}$$

where (U_1, U_2) is in $(X_H)^2$ where X_H and Y_H are defined in (5.46)-(5.47).

Given our assumptions on (U_1, U_2), the variational form of (4.1)-(4.3) is: Find $u \in \mathcal{H}_D^1(\Omega)$ such that,

$$\int_\Omega \nu \frac{\partial v}{\partial x_i}\frac{\partial u}{\partial x_i} + vU_i\frac{\partial u}{\partial x_i} + \frac{1}{2}vu\frac{\partial U_i}{\partial x_i}\,\mathrm{d}A = \int_\Omega vf\,\mathrm{d}A + \int_{\Gamma_N} vg_N\,\mathrm{d}s, \quad \forall v \in \mathcal{H}_0^1(\Omega). \tag{B.5}$$

We have introduced $\int_\Omega \frac{1}{2}vu\frac{\partial U_i}{\partial x_i}\,\mathrm{d}A$ in (B.5) because the U_i calculated in (B.3)-(B.4) does not exactly satisfy (B.1), so we need to make sure there are no sourcess.

In this variable velocity context the bilinear operators defined in (4.13)-(4.15), need to be modified to take into account the non–zero partial derivative of the velocity field. We write

$$a_{T_H}(w,v) = \int_{T_H} \nu \frac{\partial w}{\partial x_j}\frac{\partial v}{\partial x_j} + wU_j\frac{\partial v}{\partial x_j} + \frac{1}{2}wv\frac{\partial U_i}{\partial x_i}\,\mathrm{d}A, \quad \forall w,v \in \mathcal{H}^1(T_H), \tag{B.6}$$

and

$$a^s_{T_H}(w,v) = \int_{T_H} \nu \frac{\partial w}{\partial x_j}\frac{\partial v}{\partial x_j}\,\mathrm{d}A + \frac{1}{2}\int_{\partial T_H \cap \Gamma_N} wvU_j\hat{n}_j\,\mathrm{d}s, \quad \forall w,v \in \mathcal{H}^1(T_H). \tag{B.7}$$

Note that, the last two terms in (B.6) lead to the last term in (B.7) for $w = v$. To show (B.7) we write,

$$\begin{aligned}\int_{T_H} vU_j\frac{\partial v}{\partial x_j}\,\mathrm{d}A &= \frac{1}{2}\int_{T_H}\frac{\partial v^2U_j}{\partial x_j}\,\mathrm{d}A - \frac{1}{2}\int_{T_H} v^2\frac{\partial U_j}{\partial x_j}\,\mathrm{d}A &\text{(B.8)}\\ &= \frac{1}{2}\int_{\partial T_H\cap\Gamma_N} v^2U_j\hat{n}_j\,\mathrm{d}s - \frac{1}{2}\int_{T_H} v^2\frac{\partial U_j}{\partial x_j}\,\mathrm{d}A &\text{(B.9)}\end{aligned}$$

The bound procedure of Section 4.3 applies directly after substituting the new definitions for $a_{T_H}(,)$ and $a^s_{T_H}(,)$.

To complete the description of this variable velocity formulation, we need to prove solvability of (4.42). The issue is to show that the equilibration equation (4.36) also applies on the h–mesh for $v^s = 1$, The right nullspace of $a^s(,)$. Again, we examine a singular element T_H, which has $a^s_{T_H}(v^s, \hat{u}^{\pm}_{T_H}) = 0$, and for solvability we require that

$$-F^{\pm}_{T_H}(v^s,\psi^{\pm}_H) + \sum_{\gamma_{T_H}\in\mathcal{E}(\mathcal{T}_H)} \sigma^{\gamma_{T_H}}_{T_H}\int_{\gamma_{T_H}} vy^{\pm}|_{E(\gamma_{T_H})}\,\mathrm{d}s = 0 \tag{B.10}$$

where $F^{\pm}_{T_H}$ is defined in (4.35). We note that, from our refinement condition $X^{D\pm}_H \subset X^{D\pm}_h$, from our linear approximation space, X_h, for which $v^s \in X_h$, and from our exact quadrature requirement, all terms in (B.10) are equivalent on both the H–mesh and the h–mesh except one: the term,

$$\frac{1}{2}\int_{T_H}\psi^{\pm}_H v^s\frac{\partial U_j}{\partial x_j}\,\mathrm{d}A, \tag{B.11}$$

appearing in $a_{T_H}(\psi^{\pm}_H, v^s)$. We require that this term is precisely zero for both meshes. In fact, we know from (B.4) that

$$\int_{T_H} q\frac{\partial U_j}{\partial x_j}\,\mathrm{d}A = 0, \quad \forall q \in \mathbf{P}_1(T_H). \tag{B.12}$$

Because $\psi_H^{\pm}$ is in $\mathbf{P}_1(T_H)$ then we satisfy for all T_H in $\mathcal{T}_H$,

$$\frac{1}{2}\int_{T_H} \psi_H^{\pm} \frac{\partial U_j}{\partial x_j}\, \mathrm{d}A = 0, \tag{B.13}$$

which for exact quadrature holds also for both meshes. It follows that (4.42) is indeed solvable.

Lets pause here and make some comments on quadrature. Solving (B.3)-(B.4) with the Crouzeix–Raviart elements implies that the velocity field, U, is given by a quadratic–cubic (bubble function) approximation. Therefore, if implementing quadratures, the integral in (B.13) must be exact for $\mathbf{P}_2$ approximation and not only the $\mathbf{P}_1$ approximation of u or $\psi_H^{\pm}$.

Finally, it is important to notice that the velocity field, U, is only defined on the H–mesh. The bounds of the h–mesh output $s_h(u_h)$ are therefore related to the H–mesh velocity field, (U_1, U_2). In fact, the ultimate approach would be to include both the convection–diffusion equation and the incompressible projection equation in our Lagrangian take into account the effect of the velocity field on the h–mesh.

Appendix C

Basis Functions for the Crouzeix–Raviart Element

In this appendix we introduce the reference element basis functions for both the velocity and the pressure approximation of the Crouzeix–Raviart element. We map the elements in $\mathbf{R}^2$ to the standard reference element $\hat{\Omega}$ defined in the barycentric coordinates system $\underline{\xi} = (\xi_1, \xi_2, \xi_3)$.

For velocity, seven nodes located and numbered as presented in Figure C-1 are introduced. The shape functions corresponding to this $\mathbf{P}_2^+$ element are,

$$\phi_1^V = \xi_1(-1 + 2\xi_1) , \tag{C.1}$$
$$\phi_2^V = \xi_2(-1 + 2\xi_2) , \tag{C.2}$$
$$\phi_3^V = (1 - \xi_1 - \xi_2)(1 - 2\xi_1 - 2\xi_2) , \tag{C.3}$$
$$\phi_4^V = 4\xi_1\xi_2 , \tag{C.4}$$
$$\phi_5^V = 4\xi_2(1 - \xi_1 - \xi_2) , \tag{C.5}$$
$$\phi_6^V = 4\xi_1(1 - \xi_1 - \xi_2) , \tag{C.6}$$
$$\phi_7^V = \xi_1\xi_2(1 - \xi_1 - \xi_2) . \tag{C.7}$$

Note that the first six bases are the usual quadratic bases and the seventh is the bubble basis. As you may observe, this set of basis is not nodal. The value at the centroid (seventh node) is given by $\hat{v}(1/3, 1/3, 1/3) = \hat{v}_7/27 - (\hat{v}_1 + \hat{v}_2 + \hat{v}_3)/9 + 4(\hat{v}_4 + \hat{v}_5 + \hat{v}_6)/9$.

The pressure bases are supported by three independent nodes for each triangle located at their vertices. The shapes functions associated with pressure are

$$\phi_1^P = \xi_1 , \tag{C.8}$$
$$\phi_2^P = \xi_2 , \tag{C.9}$$
$$\phi_3^P = 1 - \xi_1 - \xi_2 . \tag{C.10}$$

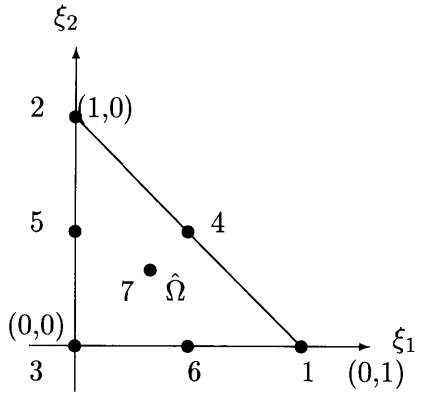

Figure C-1: Reference Crouzeix–Raviart element for velocity.

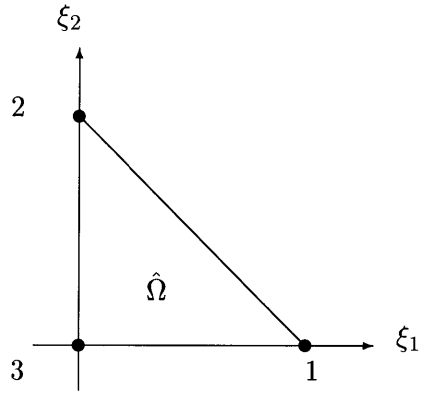

Figure C-2: Reference Crouzeix–Raviart element for pressure.

Finally, the reference element spaces are given by,

$$\hat{X} = \text{span}\{\phi_j^V, j = 1, ..., 7\}, \tag{C.11}$$

$$\hat{X} = \text{span}\{\phi_j^P, j = 1, ..., 3\}. \tag{C.12}$$